Improving the safety and function of pluripotent stem cell-derived neural transplants for the treatment of Parkinson's disease

Isabelle Rose de Luzy
0000-0003-0672-0829

February 2019

Florey Institute of Neuroscience and Mental Health
The University of Melbourne, Australia.

Submitted in total fulfilment of the requirements of the
Doctor of Philosophy

Abstract

Clinical trials using fetal tissue have provided the necessary proof-of-principle evidence that transplanted dopamine neurons can appropriately integrate into the brain and alleviate motor symptoms in Parkinson's disease patients for > 20 years. Pluripotent stem cells (PSCs), are now being pursued as an alternative cell source, circumventing ethical and availability issues, given their competent self-renewal and differentiation capabilities. Despite rapid progress in the field over the past decade, and recent advancement of these cells into clinical trials (Japan October 2018), we recognise a number of short-comings that require further attention.

Despite the existence of efficient protocols for the directed differentiation of human PSC into ventral midbrain (VM) progenitors (i.e. cells capable of maturing into dopamine neurons and amenable to transplantation), a small proportion (10%) of cells in culture remain incorrectly specified. These cells are capable of significant expansion after transplantation, such that grafts commonly contain <5% dopamine neurons when examined after many months. These highly proliferative cells not only present an evident risk of neural overgrowth, but there also remains little knowledge of the identity these cells become and the impact they may have on the graft and patient.

For these reasons, strategies have been pursued to improve the purity of donor tissue for grafting. However, to date, cell sorting approaches, to select for correctly patterned human PSC-derived cells prior to implantation have been suboptimal. In chapter 3 of the thesis we employ two human PSC reporter lines to demonstrate that the isolation of vm progenitors, but not vm precursors, results in viable cell grafts that are more predictable in their composition, retain integration and functional capacity to restore motor deficits in Parkinsonian rats, and importantly eliminate highly proliferative cells and populations known to contribute to graft-induced dyskinesias.

An alternative safeguarding approach for transplantation studies is to employ suicide gene therapy – targeted at eliminating unwanted cells after transplantation. In Chapter 4, we employ a human PSC line carrying a suicide gene (thymidine kinase) that can be activated by administration of a prodrug (ganciclovir), to enable remote killing of proliferating cells within the transplant. We demonstrate that the timely activation of this 'suicide switch' can prevent excessive expansion of undesirable cells in the graft whilst preserving DA integrity -

yet surprisingly, a small proportion of persistent dividing cells remained. We speculate that this was a result of suboptimal delivery of ganciclovir caused by insufficient vascularisation of dopamine grafts.

In a third approach to improve graft outcomes, we address the impact of human PSC-derived VM progenitor donor age (Chapter 5). Despite historical efforts to understand the impact of different aged VM fetal tissue on graft survival, dopamine contribution and functional integration, there remains no comparable assessment of human PSC-derived vm progenitor age. While the current clinical trial in Japan has elected to use late stage human PSC-derived VM progenitors, in Chapter 5 we surprisingly show that VM-specified early-stage progenitors generated the most homogeneous DA grafts, containing a considerably lower component of unwanted, off-target cells than grafts derived from older progenitors. Importantly we demonstrated that while this effect was extremely consistent within human PSC lines, considerable inter-line variability was evident, highlighting the need for rigorous assessment on a line to line basis, prior to translation.

In summary, the work provided within this thesis provides significant new insight into strategies to standardize human PSC-derived transplantation for Parkinson's disease – importantly addressing the need to consider graft survival, proportion of dopamine neurons and their function, as well as the critical requirement to eliminate unwanted cell types to ensure maximal safety.

Declaration

This is to certify that:

i) this thesis comprises only my original work towards the PhD, except where otherwise indicated in the preface.

ii) due acknowledgement has been made in the text to all other material used.

iii) this thesis is fewer than 100,000 words in length, exclusive of tables, maps, bibliographies and appendices.

Isabelle de Luzy

Preface

I acknowledge that the work presented here is a collaborative effort. My contribution to this thesis is the following:

Chapter 3 – LMX1A sorting improves vmDA transplantation

Published. Relative contribution by de Luzy – 80%

Isolation of LMX1a ventral midbrain progenitors improves the safety and predictability of human pluripotent stem cell-derived neural transplants in Parkinsonian Disease. *JNeuroscience*. *2019*; 39(48):9521-9531. Co-authored with Jonathan C Niclis, Carlos W Gantner, Jessica A Kauhausen, Colin Pouton, Cameron Hunt, Lachlan H Thompson, Clare L Parish.

Contributions: CLP, JN, IDL contributed to experimental design. IDL, JCN, CWG, JAK, CME, CH, LHT, CLP performed experiments and data analysis. CWP, LHT, CLP provided reagents. CLP and IDL – manuscript writing and editing. CLP provided funding.

IDL Contributions: Involvement in experimental design, performed all *in vitro* maintenance and differentiation, immunocytochemistry, cell sorting/FACS, behavioural testing, histology and microscopy. IDL was the primary person responsible for data analysis, statistical assessment, consolidation and interpretation. She wrote the first draft of this chapter and edited together with CP.

Chapter 4 – Suicide transgene activation improves stem cell graft safety

Relative contribution by de Luzy - 80%.

A version of this chapter will be submitted for publication to *Cell Reports*, Anticipated submission date - March 2020. Co-authored with Kevin Law, Jennifer C Hollands, Carlos W Gantner, Nathalie Payne, Lachlan H Thompson, Andras Nagy and Clare L Parish.

Contributions: CLP, IDL contributed to experimental design. IDL, KL, JCH, CWG LHT, CLP performed experiments and data analysis. NP, LHT, AN, CLP provided reagents. CLP and IDL – manuscript writing and editing. CLP provided funding.

IDL Contributions: Involvement in experimental design, performed all *in vitro* maintenance, differentiation and elimination assays, immunocytochemistry, behavioural testing, intraperitoneal GCV injections, histology and microscopy. IDL was the primary

person responsible for data analysis, statistical assessment, consolidation and interpretation. She wrote the first draft of this chapter and edited together with CP.

Chapter 5 – Impact of donor age on transplantation

Relative contribution by de Luzy - 80%.

A version of this chapter has been submitted for publication to *Stem Cell Reports*, February 2020. Co-authored with Cameron Hunt, Carlos Gantner, Niamh Moriarty, Jon Niclis, Lachlan Thompson and Clare Parish. JN and CP contributed to experimental design.

Contributions: CLP, IDL contributed to experimental design. IDL, CH, CWG, NM, CLP – performed experiments and contributed to data analysis. LHT and CLP provided reagents. CLP and IDL – manuscript writing and editing. CLP provided funding.

IDL Contributions: Involvement in experimental design, performed all *in vitro* maintenance and differentiation, immunocytochemistry, histology and microscopy. IDL was the primary person responsible for data analysis, statistical assessment, consolidation and interpretation. She wrote the first draft of this chapter and edited together with CP.

Appendix 1 – Generation of regional neuronal populations from murine PSCs

Published. Relative contribution by de Luzy - 30%.

W.F. Alsanie, J.C. Niclis, C.P. Hunt, I.R. de Luzy, V. Penna, C.R. Bye, C.W. Pouton, J. Haynes, J. Firas, L.H. Thompson, C.L. Parish. Specification of murine ground state pluripotent stem cells to regional neuronal populations. *Scientific Reports* (2017) Nov 22;7(1):16001. doi: 10.1038/s41598-017-16248-x. IDL contribution: Performed cell culture, PCR, contributed to data collection and editing of the manuscript.

Appendix 2 – Human-specific transcriptional analysis

Published. Relative contribution by de Luzy - 20%.

C.R. Bye, V. Penna, I.R. de Luzy, C.W. Gantner, C.P.J. Hunt, L.H. Thompson, C.L. Parish. Transcriptional profiling of xenogeneic transplants: examining human pluripotent stem cell-derived grafts in the rodent brain. *Stem Cell Reports* (2019) 2019 Oct 22. pii: S2213-6711(19)30362-5. doi: 10.1016/j.stemcr.2019.10.001. IDL contribution: Conducted cell culture including data collection and interpretation, manuscript preparation.

Appendix 3 – GDNF improves DA graft function

Published. Relative contribution by de Luzy - 30%.

C.W Gantner, I.R de Luzy, J.A Kauhausen, N. Moriarty, J.C Niclis, V. Penna, C.P. Hunt, C.R Bye, C.M Ermine, C.W Pouton, D. Kirik, L.H Thompson, C. L Parish. Viral delivery of GDNF improves the functional integration of human pluripotent stem cell-derived dopamine grafts in rodent models of Parkinson's disease. *BioRxiv* doi: https://doi.org/10.1101/870725, *Cell Stem Cell* (2020) April 2; 26, 1-16. IDL contribution: Conducted cell culture including data collection and interpretation, behavioural studies, manuscript preparation.

Appendix 4 - Functionalised hydrogels support dopamine grafts in PD

Relative contribution by de Luzy - 20%.

A version of this chapter has been submitted for publication to *Nature Biomedical Engineering*, February 2020.

V Penna, CW Gantner, Y Wang, I.R de Luzy, N Moriarty, LH Thompson, DR Nisbet, CL Parish. Tissue-specific hydrogels, prolonging GDNF delivery, improve functional integration of human stem cell-derived progenitor grafts in Parkinsonian rats. IDL contribution: Conducted cell culture including data collection and interpretation, behavioural studies, manuscript preparation.

Presentations

de Luzy IR, Hunt CP, Gantner CW, Moriarty N, Niclis JC, Thompson LH and Parish CL. Identifying the optimal age of human stem cell-derived dopaminergic progenitors for transplantation in Parkinson's disease. ISSCR annual meeting, Los Angeles, USA (June, 2019). Poster presentation.

de Luzy IR, Gantner CW, Niclis JC, Kauhausen JA, Thompson LH and Parish CL. Advancing stem cell treatments for Parkinson's disease (invited speaker). Stem Cells Australia Meeting, Melbourne, Australia (March, 2019). Oral Presentation

de Luzy IR, Niclis JC, Gantner CW, Kauhausen JA, Hunt CPJ, Ermine C, Pouton CW, Thompson LH and Parish CL. Isolation of LMX1a ventral midbrain progenitors improves the safety and predictability of human pluripotent stem cell-derived neural transplants in Parkinson's Disease (abstract selected). ISSCR annual meeting, Melbourne, Australia (June 2018). Oral presentation.

de Luzy IR, Niclis JC, Gantner CW, Kauhausen JA, Hunt CPJ, Ermine C, Pouton CW, Thompson LH and Parish CL. Isolation of LMX1A ventral midbrain progenitors, but not PITX3 ventral midrain precursors improve transplantion in Parkinson's disease. Students of Brain Research (SOBR) Conference, Melbourne, Australia (Oct 2017). Poster presentation.

de Luzy IR, Niclis JC, Gantner CW, Kauhausen JA, Hunt CPJ, Ermine C, Pouton CW, Thompson LH and Parish CL. Isolation of LMX1A ventral midbrain progenitors, but not PITX3 ventral midrain precursors improve transplantion in Parkinson's disease. 14th INTR meeting, Port Douglas, Australia (Sep, 2017). Oral presentation.

de Luzy IR, Niclis JC, Pouton CW, Thompson LH and Parish CL. Isolation and transplantation of human pluripotent stem cell-derived midbrain dopaminergic progenitors into Parkinsonian mice. Stem Cells Australia Annual Meeting, Gold Coast, Australia (June 2017). Poster presentation.

de Luzy IR, Niclis JC, Pouton CW, Thompson LH and Parish CL. Isolation and transplantation of human pluripotent stem cell-derived midbrain dopaminergic progenitors into Parkinsonian mice. 26th Annual NECTAR meeting, Cambridge, UK (Dec 2016). Oral presentation.

Awards and Schools

Zhongmei Chen Yong Travel Award for Scientific Excellence (2018)

Neural Stem Cells: Development and Brain Repair course at the Neuroscience School of Advanced Studies, Tuscany, Italy (June, 2017). Intensive advanced neuroscience course given by several highly successful neuroscientists that focused on developmental biology and cellular therapeutics for regenerative medicine.

Acknowledgements

This thesis would not have been possible without the love, care and guidance of many people, to whom I owe my sincere thanks.

First and foremost, I would like to personally thank my supervisor Clare, who has gone above and beyond in all aspects of my journey. I've never known her door not to be open or a silly question to ask. Her belief in me, and constant support throughout has been imperative. She has been an amazing mentor, supervisor and lab 'mama', but most of all a continued inspiration for science.

To my co-supervisor Lachlan, who originally agreed to let me come and do an internship in the lab, that ended in me staying on to do a PhD in Melbourne. Thank you for your invaluable scientific insight and critique. I wish to also thank my PhD advisory committee - Jason Howitt, Andrew Lawrence and Ed Stanley, for the excellent feedback and guidance.

To all the members of the lab (past and present), thank you for making this journey such an enjoyable one and for all the help along the way. A special mention to the Stem Cell team, it has been a pleasure to work in such close proximity together. Thank you for the support and encouragement during numerous stem cell battles. I was also like to acknowledge Jonathan Niclis, whose training at the beginning of the PhD was instrumental, and the continued mentorship that he has provided throughout has been invaluable.

I wish to also thank the groups I have been a part of, and friends I have made, whilst at the Florey Institute of Neuroscience and Mental Health. It has been a fantastic working and social environment, and a pleasure to be surrounded by so many other inspiring scientists.

A special mention to all my friends, both in Australia and back in the UK. I've been extremely fortunate to be surrounded by positive, like-minded and brilliant people, who have provided endless support and enthusiasm during this journey.

To my wonderful family, your support from overseas has been unbelievable. Specifically, to my mum, who has been present through all of my education endeavours, I could not have got this far without your love and reassurance.

Finally, to my boyfriend Will, who has been my biggest support throughout this voyage. Thank you for believing in me every step of the way and I am so grateful for your patience, enthusiasm and constant encouragement.
#doperthandopamine

Table of Contents

Chapter 2: Materials and Methods

Chapter 3: Isolation of LMX1A ventral midbrain progenitors improves the safety and predictability of human pluripotent stem-cell derived transplants in Parkinsonian rodents

Abbreviations

5HT	Serotonin
6-OHDA	6-hydroxydopamine
A9/A10	Midbrain dopamine neuron subtypes (A9/A10)
AA	Ascorbic acid
APC	Adenomatous polyposis coli
BDNF	Brain derived neurotrophic factor
BMP	Bone morphogenetic protein
CALB	Calbindin
CDK1	Cyclin dependent kinase 1
ChAT	Choline acetyltransferase
dCPU	Dorsal caudate-putamen
DAn	Dopamine neurons
DAPI	4'-6-Diamidino-2-Phenylindole
DAPT	N-[N-(3,5-Difluorophenacetyl)-L-alanyl]-S-phenylglycine t-butyl ester
DBH	Dopamine beta-hydroxylase
dCAMP	Dibutyryl cyclic AMP
DCX	Doublecortin
DIV	Days *in vitro*
eGFP	Enhanced green fluorescent protein
EN1	Engrailed 1
FACS	Fluorescence-activated cell sorting
FOXA2	Forkhead box A2
GABA	Gamma-aminobutyric acid
GDNF	Glial cell line-derived neurotrophic factor
GFAP	Glial fibrillary acidic protein
GID	Graft-induced dyskinesia
GIRK2	G-protein-gated inwardly rectifying K channel subunit 2
GCV	Ganciclovir
hESC	Human embryonic stem cell
hiPSC	Human-induced pluripotent stem cell
hPSC	Human pluripotent stem cell
HNA	Human nuclear antigen

HP	Hippocampus
HSV-TK	Herpes simplex virus thymidine kinase
iCas9	Inducible caspase-9
ITS-A	Insulin-transferrin-selenium-sodium pyruvate
KO	Knock out
LRTM1	Leucine-rich repeats and transmembrane dopamine 1
LMX1A	LIM homeobox transcription factor 1A
MAP2B	Microtubule-associated protein 2
mDA	Midbrain dopamine
NeuN	Hexaribonucleotide binding protein-3
NCAM	Neural cell adhesion molecule
NPC	Neural progenitor cell
NURR1	Nuclear receptor subfamily 4 group A member 2
OTX2	Orthodenticle homeobox 2
PD	Parkinson's disease
PFA	Paraformaldehyde
PFC	Pre-frontal cortex
PH3	Phosphohistone 3
PITX3	Paired-like homeodomain 3
PM	Purmorphamine
PSA-NCAM	Polysialic acid neural cell adhesion molecule
PVTN	Periventricular thalamic nucleus
RECA	Rat endothelial cell antigen-1
ROCKi	Rho Kinase Inhibitor Y-27632
SHH	Sonic hedgehog
SOX2	Sry box 2
SPRY1	Sprouty homolog 1
STN	Subthalamic nuclei
TGFβ	Transforming growth factor β
TH	Tyrosine hydroxylase
TK	Thymidine kinase
US	Unsorted
vm	Ventral midbrain
vmDA	Ventral midbrain dopamine

Table of figures

Table of tables

Chapter 1.

Introduction

1.1 Cellular Replacement Therapy for Parkinson's Disease

1.1.1 Parkinson's Disease

Within the midbrain, dopamine (DA) neurons reside in three anatomically and functionally distinct compartments; designated as A8, A9 and A10 neurons, that play a role in the regulation of voluntary movement, emotion and reward (German and Manaye., 1993). Crucially the A9 DA neurons, found in the pars compacta of the substantia nigra (SNpc), are responsible for co-ordinating fine motor control, and project via the nigrostriatal pathway (NSP) to innervate the caudate-putamen in primates, or equivalent striatum in rodents (Prakash and Wurst, 2006) (Figure 1.1A). Whilst, the A8 and A10 DA neurons, develop in the retrorubal field (RRF) and ventral tegmental area (VTA) respectively, are responsible for risk-reward, emotion and cognitive related behaviours, and project via the mesocorticolimbic system to innervate the ventral striatum and prefrontal cortex (Hegarty *et al*, 2013, Prakash and Wurst, 2006).

In Parkinson's Disease (PD) patients, progressive, and irreversible degeneration of A9 midbrain dopaminergic (mDA) neurons in the SNpc and loss of striatal innervation, leads to the primary hallmarks of the disease; namely rigidity, tremor at rest, bradykinesia, gait disturbances and loss of postural reflex (Jenner *et al*., 1992). These symptoms typically arise when ~60% SNpc dopaminergic neurons have degenerated (Dauer *et al.*, 2003; Jenner, 1992). It is worth noting that PD encompasses a widespread of pathologies, not limited to the SNpc, recognising non-dopaminergic degeneration in other brain areas, that can lead to additional motor symptoms and a wide myriad of non-motor manifestations (Dickson *et al.,* 2009), however these non-dopaminergic associated pathologies will not be the main focus of this thesis.

Currently there are no proven disease-modifying treatments for PD, and management typically relies on dopaminergic pharmacotherapies (commonly Levodopa, L-dopa) (Stoker *et al.*, 2018). Whilst effective for symptomatic relief, these medications ultimately depend on remaining dopaminergic neurons for efficacy and are riddled by adverse side effects related

to systemic delivery and non-physiological activation of dopamine receptors (Stoker *et al.*, 2018). Surgical options, such as deep brain stimulation (DBS), whilst an effective treatment option for some patients, can also result in troubling adverse effects (Hartmann *et al*., 2019). Despite these options successfully managing the motor symptoms of the disease, their waning efficacy and problematic side effects highlight that there is still significant scope for improvement.

1.1.2 Cellular replacement therapy

With the clear limitations of currently available therapeutics for patients, attention still remains on developing a new, more promising therapy for PD. One such option is cell replacement therapy, whereby dopamine-producing cells can be delivered directly into the diseased brain, given 1) that the disease-causing motor symptoms are underpinned by a localised pathological loss of a single defined cell type at relatively low numbers, 2) focal, controlled delivery of DA can be achieved and 3) proof-of-principle evidence exists for DA cell replacement strategies in PD patients (Barker *et al.*, 2015).

1.1.3 Pre-clinical dopamine transplantation

The earliest report of transplanting fetal brain cells into the adult central nervous system was conducted by Thompson in the late 19th century. It was not until 30 years later, after many attempts, that these embryonic-derived allografts had the capacity to survive, proliferate and exhibit fibre outgrowths (Dunn, 1917).

Building upon earlier work and focusing on engraftment of a defined cellular population, Olson and Seiger (1972) transplanted rodent embryonic ventral midbrain/mesencephalic (VM) tissue (the region of the developing brain containing immature dopamine progenitors that give rise to mDA neurons), as a whole tissue piece, demonstrating that these embryonic cells could survive and innervate the surrounding host tissue, which could be enhanced by co-grafting neurotrophic factors or other tissues (Olson and Seiger, 1972, 1973, 1975).

The excitement that developmental mDA neurons could survive and send projections in a hostile adult environment, raised the potential for cell replacement therapy (CRT) as a treatment option for Parkinson's disease, but assessment of functionality was needed. This was revolutionised by the now heavily implemented 6-hydroxydopamine (6-OHDA) lesioned rodent model of PD, first generated by Ungerstedt and colleagues in the late 1960s

(Ungerstedt, 1968). 6-OHDA is a catecholamine-selective neurotoxin, that when delivered directly into the ventral midbrain (i.e. the SNpc) or indirectly into the median forebrain bundle (an axon bundle containing DA fibre projections from the SNpc), causes selective and irreversible loss of the DA neurons and forebrain (striatal/caudate putamen) dopaminergic innervation (Ungerstedt *et al*., 1968, 1974; Ungerstedt and Arbuthnott 1970). This model of dopamine depletion, provides a means to investigate restoration of dopaminergic activity at a functional level after transplantation. For the purpose of studying CRT, the model is commonly induced unilaterally, creating motor asymmetry that can be restored through graft integration. Figure 1.1 below provides a schematic and histochemical representation of the midbrain dopamine system in the rodent brain (Figure 1.1A) and the effect of 6OHDA lesioning (Figure 1.1B).

Utilising this preclinical rodent model of PD, the first breakthrough studies to demonstrate successful functional replacement by rodent fVM tissue were conducted by Bjorklund and Stenevi (1979) and Perlow *et al* (1979) collectively. These two independent groups, were able to demonstrate rodent embryonic vm tissue transplanted into the striatum of 6-OHDA-induced parkinsonian rodents, could directly replace lost cells, elicit neurotransmitter-specific re-innervation of the host tissue and display robust amelioration of PD-induced motor deficits (Bjorklund and Stenevi 1979; Perlow *et al.,* 1979). Importantly, behavioural recovery was directly underpinned by the extent of dopaminergic striatal reinnervation (Bjorklund *et al.,* 1980). Later refinements to surgical procedures to deliver fVM transplants as a dissociated cellular suspension, instead of dissected whole tissue pieces, provided more widespread and extensive re-innervation of the host striatum (Bjorklund *et al.,* 1983). Figure 1.1C provides an example of a dissociated fVM transplant into the 6OHDA rodent brain, noting the capacity to reinnervate the host striatum.

Similar results were attained with human fVM tissue, and additional studies highlighted that graft-derived DA neurons have the capacity to both receive and make synaptic contact with the host striatum (Brundin *et al.,* 1988; Clarke *et al.,* 1988). Pre-clinical investigations also recognised appropriate dissection landmarks, the optimal donor tissue age and a suitable clinical immunosuppression regime, all collectively essential for clinical translation (Brundin *et al.*, 1986, 1988; Clarke *et al.,* 1988). Figure 1.1 provides a schematic overview of the 6OHDA PD rodent model commonly employed in transplantation studies and the approach adopted to implant new replacement cells.

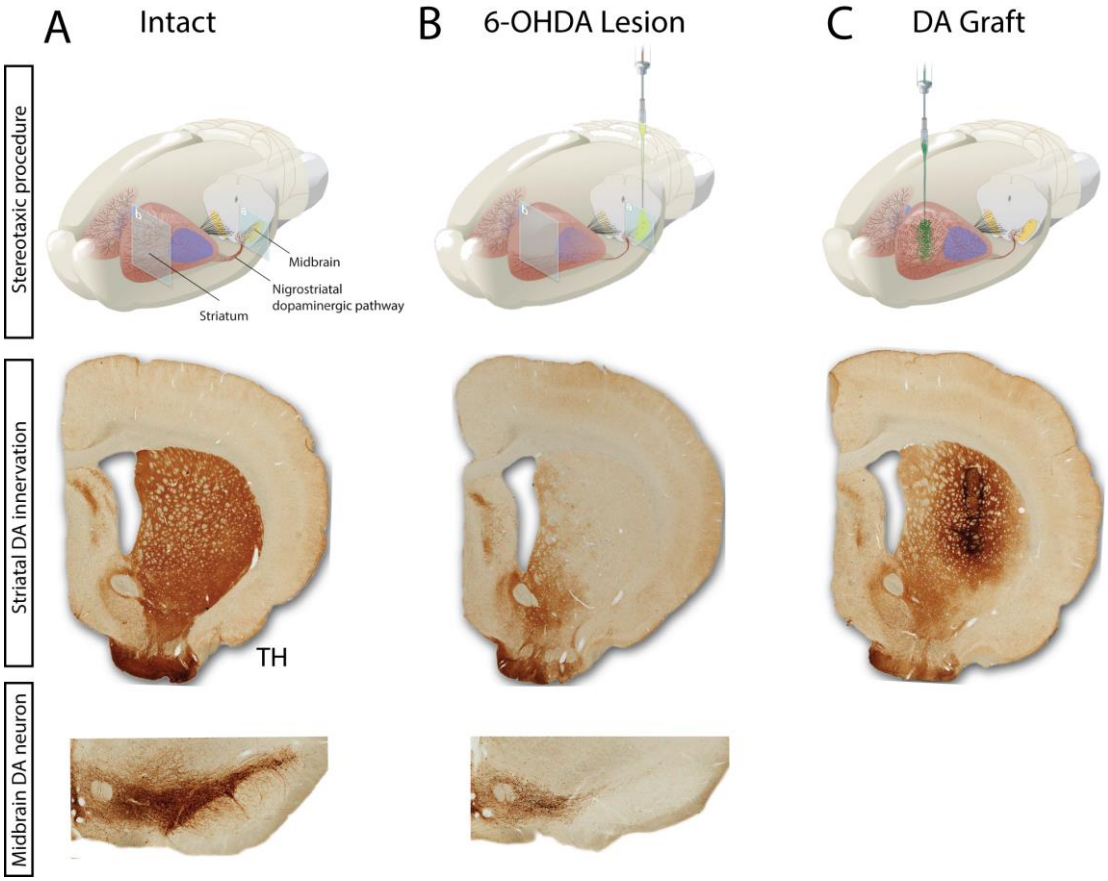

Figure 1.1 Cellular replacement therapy in a preclinical rodent model of Parkinson's disease
(A) Dopaminergic neurons lost in Parkinson's disease, identified by tyrosine hydroxylase immunoreactivity, reside in the substantia nigra pars compacta and send projections to the striatum forming the nigrostriatal pathway in the rodent **(B)** 6-OHDA administration into the median forebrain bundle leads to irreversible ablation of mDA neurons and subsequent loss of DA fibre terminals in the rodent striatum **(C)** Transplanted fVM cells injected ectopically into the striatum survive and re-innervate the host striatum. 6-OHDA; 6-hydroxydopmaine, mDA; midbrain dopamine, fVM; fetal ventral mesencephalic. Figure adapted from Parish and Thompson (2014).

1.1.4 Intrastriatal transplantation of VM fetal tissue into PD patients

Promising results from a decade of preclinical studies led to an open-label clinical trial in Lund, where PD patients were transplanted with human fVM tissue for the first time (Winkler *et al.*, 2005). Whilst the initial two-patient study (1987) failed to demonstrate a significant benefit (mainly attributed to no conclusive evidence of surviving cells), a later re-designed trial, excitingly improved graft survival and demonstrated a clinical improvement in motor features and ^{18}F-DOPA PET imaging (Lindvall *et al.*, 1989. 1990). Such excitement, initiated several other studies to be performed across Europe and the USA. In these cases, the results were variable, but overall showed a modest improvement (Freed *et al*., 1992, Figure 1.2).

Patients eliciting greatest functional benefit, received transplants capable of both spontaneous and drug-induced dopamine release and restoration of normal dopamine signalling in the putamen, that fundamentally permitted alleviation of anti-PD medication (Mendez *et al.*, 2002; Piccini *et al*., 1999, 2000; Wenning *et al*., 1997). At the time, this was an extremely exciting, and important discovery for cell replacement therapy, demonstrating proof-of-principle evidence that dopamine-rich fVM tissue can provide both extensive and sustained functional benefit in patients.

Unfortunately, in the following trials, consistency was not always executed. Two NIH-funded double-blind clinical studies were embarked on subsequent to the open-labelled trials (Freed *et al*., 2001; Olanow *et al*., 2003), which regrettably failed to reach primary endpoints and only a subset of patients indicated a marginal functional improvement that was not significant when compared to anti-PD therapies available at the time (Freed *et al.*, 2001; Olanow *et al.*, 2003). Integral to this poor success, in part, was the introduction of several new and untested variables in the design of the trials (see 1.1.5) that impacted negatively on patient results.

Considerably alarming, and surprising from these trials was the recognition of severe off-phase graft-induced dyskinesias (GIDs) in a proportion of transplanted patients in both of the NIH-funded trials; 15% (Freed *et al.*, 2001) and 56.5% (Olanow *et al.*, 2003) respectively, and a significant proportion in Lund that were retrospectively identified (Barker *et al.*, 2016; Brundin *et al.*, 2010; Hagell *et al.*, 2002). Interestingly, all of these patients had previously experienced L-dopa induced dyskinesia prior to transplantation (Barker *et al.*, 2016).

Despite, recognition that the NIH-funded trials were designed poorly and clear evidence that when executed correctly grafts can provide substantial and significant functional benefit (Winkler *et al.*, 2005), the general consensus at the time was that the trials were a failure, and as a result there was a significant period of dormancy that halted cell therapy for many years (Breger and Lane, 2013).

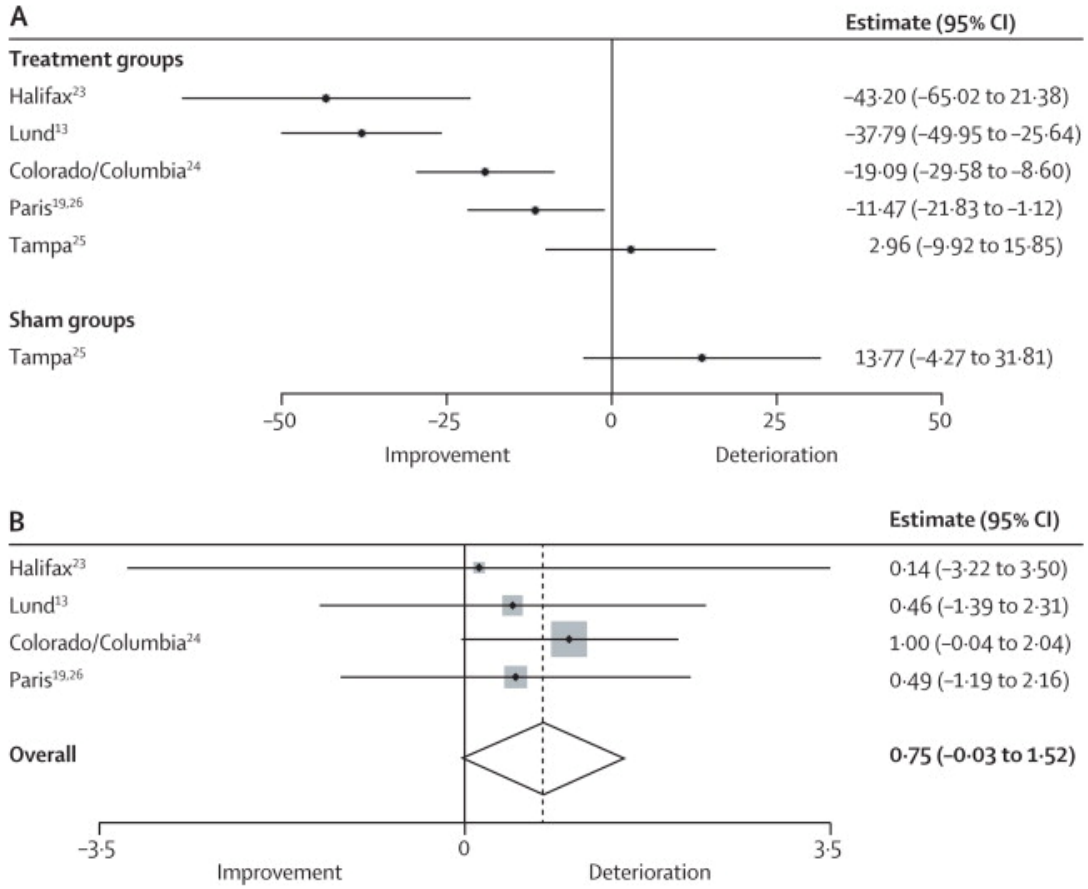

Figure 1.2 Meta-analysis of fetal dopaminergic transplantation trials and overview of clinical outcomes

(A) Mean percentage change in UPDRS for all patients in each trial. (UPDRS: unified Parkinson's disease rating scale). Shift to the left indicates a functional improvement. **(B)** Influence of age on patient outcomes. Halifax: Mendez *et al* (2002), Lund: Lindvall *et al* (1990), Colorado/Columbia: Freed *et al* (2001), Paris: Peschanski *et al* (1994) and Tampa: Olanow *et al* (2003). Figure from Barker *et al* (2013).

1.1.5 Lessons learnt from clinical trials

Whilst clearly frustrating, the NIH-funded trials did invoke greater scrutiny of the open label trials, such that retrospective assessment unveiled the optimal conditions for grafting; inclusive of delivering younger donor tissue as a dissociated cellular suspension without prior storage for a prolonged period, the need for immunosuppression (~12months), and selection of younger patients with previous responsiveness to L-dopa (Barker *et al.*, 2013; Lindvall and Bjorklund 2004; Winkler *et al.*, 2005).

Added to this, exploration into the graft-induced dyskinesia (GID) noted in a significant proportion of patients in the clinical trials, originally eluded to uneven distribution of grafted

DA neurons throughout the striatum (Ma *et al.*, 2002; Carlsson *et al.*, 2006) and/or unwarranted DA release due to excessive fibre outgrowth (Freed *et al.*, 2001). Although debated by some, it was later revealed that unintended co-grafting of neighbouring serotonergic neuroblasts were instead causative of GIDs (Mendez *et al*., 2005; Piccini *et al*., 2005). Contamination within graft preparations resulted from poor/broad tissue dissections that included hindbrain tissue (inclusive of the raphe nucleus) located caudal to the VM, an unfortunate occurrence that can be challenging to exclude entirely without compromising the yield of DA neurons (Barker *et al.*, 2013)

The ability of serotonergic (5HT) neurons to uptake L-dopa and release as DA, albeit in a dysregulated fashion, is thought to play havoc in fetal grafts. In the absence of auto-regulatory control, excessive swings in DA levels caused by false neurotransmitter release of DA from 5HT terminals, can induce dyskinesias. However, since only some transplanted patients developed GIDs despite all transplants likely containing a proportion of 5HT neurons, this suggested an additional factor was important, and it was later attributed that the relative 5HT:DA density (>2:1) in the graft was the crucial element for the development of GIDs (Carlsson *et al.*, 2009; Politis *et al.*, 2011; García *et al.*, 2016).

Further validating for the role of 5HT neurons was the marked attenuation of dyskinesia following systemic administration of the selective serotonin 1A agonist (Busipirone), that is capable of dampening neurotransmitter release (Politis, 2010). This indicated that excessive serotonergic hyperinnervation was causative, supported by other preclinical studies (Aldrin-Kirk *et al.*, 2016; Lane *et al.*, 2006; Politis *et al*., 2011). Unfortunately, the short-acting effect of busipirone means it is not a viable treatment option to resolve GIDs and pursuit of longer-acting serotonin agonists are still a remaining goal, however in the worst cases, patients received additional neurosurgical interventions, such as DBS (Politis, 2010).

Long term follow up of patients, has demonstrated that substantial and long-term functional benefit, allowing cessation of medication, can be achieved up to 18 years post-transplantation (of particular importance in light of the waning efficacy of PD therapies over time) (Kefalopoulou *et al*., 2014; Ma *et al.*, 2010). Post-mortem examination, to support this benefit, has demonstrated evidence of surviving dopamine cells with extensive synaptic integration within the striatum even after several (24) years (Kordower *et al.*, 1995, 1996; Hauser *et al.*, 1999; Piccini *et al.*, 1999, 2000) (Figure 1.3). The observation of a single

patient, losing functional benefit after 14years, despite extensive graft-derived DA innervation observed at post-mortem 24 years after receiving a transplant (Li *et al*., 2016) (Figure 1.3D-I), indicates that neurodegeneration in other areas of the brain can still impact upon clinical decline even in the presence of a graft.

Of considerable interest to the field, has been the observation of alpha-synuclein-positive inclusions in grafted dopaminergic neurons, supporting the possibility for pathological spread from host to transplanted cells (Kordower *et al*., 2008; Li *et al*., 2008, 2010, 2016). Whilst this pathological burden appears to rise over time, the mechanism is not clear, but it is thought that a 'prion-like progression' may be causative (Brundin *et al.*, 2016). This has sparked great fascination in the research and clinical transplantation community, to better understand

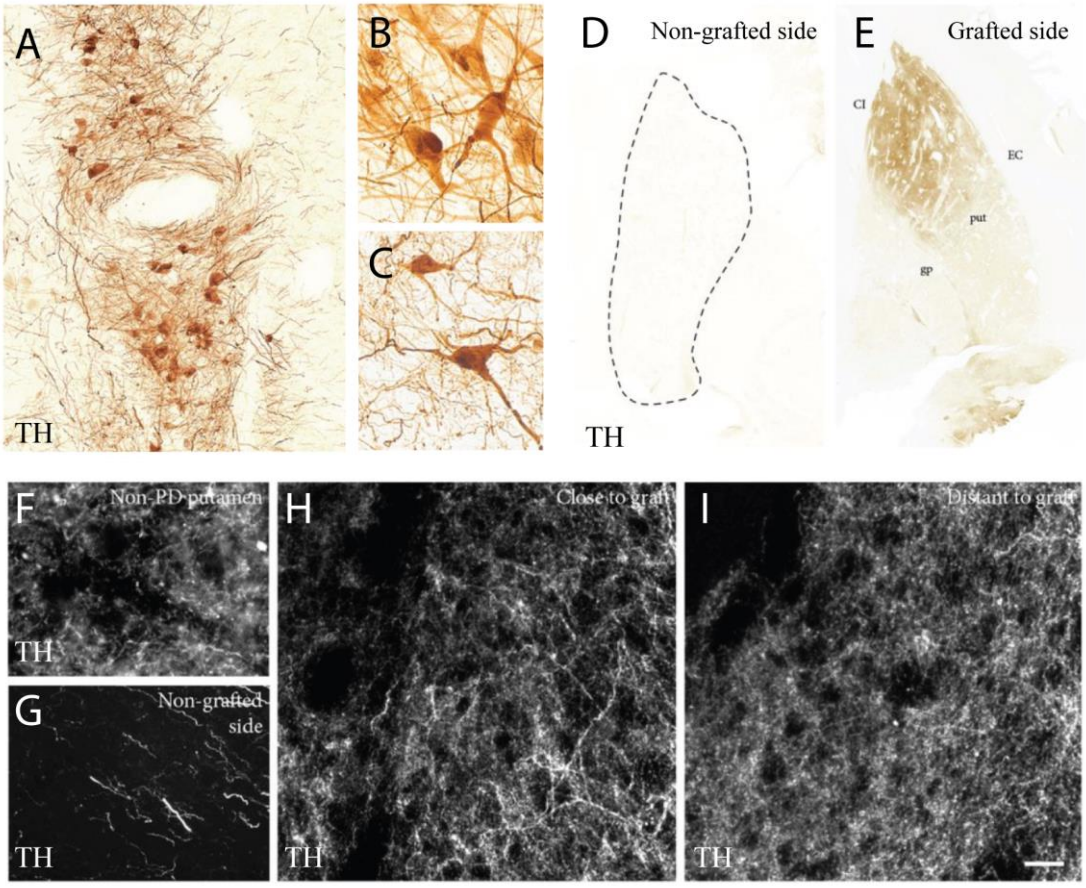

Figure 1.3 Extensive graft-derived DA reinnervation of the host putamen is retained 24 years after transplantation in a Parkinson's disease patient.
Graft-derived DA neurons in the putamen are elaborate and healthy even after 24 years **(A-C)**. Dense network of TH-positive fibres encompasses the grafted putamen **(E)**, compared to the non-grafted side that was completely devoid of TH+ fibres **(D, G)**. Extensive dopaminergic innervation was observed both close **(H)** and distant **(I)** to the graft, comparable to an age matched non-PD brain **(F)**. Figure adapted from Li *et al* (2016).

the mechanism behind disease propagation/progression. Importantly, but probably not surprising given the neurodegenerative nature of this disease, the rate of transmission seems to be significantly slow, given that only ~1-12% of DA neurons appear to be infected after 12-24years, without any obvious impact on neighbouring healthy DA neurons (Kordower *et al.*, 2008; Li *et al*., 2008, 2010, 2016). This phenomenon, at least at this point, does not appear to be a concerning limitation for CRT.

Such disparity between trial design and execution has stressed that significant attention and refinement is required to standardise and outline the design for future clinical trials. In light of this, a EU-funded open-labelled clinical trial (TRANSEURO, NCT01898390) is currently in progress with completion expected in 2021, inclusive of a 3 year follow-up (Barker, 2014). This trial will address the major issues outlined from the trials, notably 1) to optimise patient selection and immunosuppressive regimes, 2) standardise tissue preparation and composition, 3) regulate graft placement and support and 4) identify suitable clinical end-points (www.transeuro.org.uk) (Barker, 2014). Of note, the single, biggest problem encountered in the trial so far has been tissue availability and as a result only 11 out of 20 patients have received transplants (Barker *et al.*, 2019).

As such, considerable ethical and logistical barriers with the use of embryonic tissue, specifically unsustainability (requiring >3 aborted foetuses per hemisphere grafted) and difficulties to standardise, limit its use as a mainline therapy for PD (Bye *et al*., 2012; Olanow et al. 2003; Winkler *et al.*, 2005). It is hoped TRANSEURO will instead elucidate and resolve potential pitfalls to pave the way for future stem cell-derived neural transplantation.

1.2. Alternative sources of DA neurons

In acknowledgement of the limitations of fVM tissue, many alternative DA cell sources have been trialled as donor tissue for transplantation; including adrenal medullar DA cells, diencephalic DA neurons, retinal pigment epithelium cells, and carotid body cells for replacement in PD (Figure 1.5) – all with little success, since they failed to resemble authentic midbrain DA neurons, and more specifically be of A9 phenotype, capable of functionally integrating into the basal ganglia circuitry in order to restore motor function (Grealish *et al.*, 2010; Barker, 2014).

1.2.1 Embryonic development

Necessary for utilising PSCs as a donor cell source in the advancement of CRT for PD is a concrete understanding of the cascade of events that occur during development of mDA neurons. It is recognised that these neural developmental events will need recapitulating in order to generate appropriate VM-like DA progenitor donor cells. The following is a brief overview of the developmental events involved in specification of mDA neurons in the mouse and human.

During formation of the neural tube in embryonic development, two key signalling centres are created that are influential in VM development; the floor plate (FP), which distinguishes ventral identity (Placzek and Briscoe, 2005) and the isthmic organiser (IsO), that demarcates the midbrain-hindbrain boundary (Joyner *et al*., 2000; Rhinn *et al.*, 1998; Wassarman *et al*., 1997). The mutual repression of Otx2 and Gbx2 together delineate this boundary (Li & Joyner, 2001) (Figure 1.4A). These structures both secrete specific patterning molecules (namely Sonic hedgehog, Shh; Fibroblast growth factor 8, FGF8; and Wnt1) critical for sufficient induction of mDA neurogenesis (Hynes *et al.*, 1995; Hynes *et al*., 1995; Ye *et al.*, 1998, Figure 1.5A, B). Such graded signals act in concert along the rostrocaudal, dorsoventral and mediolateral axes of the neural tube dictating positional information for the early specification of ventral midbrain (vm) progenitors (Aguila *et al*., 2012). Expression of key transcription factors (LMX1b, PITX3, NURR1, EN1/2) co-ordinate the transition of vm neural progenitors into committed, post-mitotic mDA neurons (Riddle and Pollock, 2003) (Figure 1.5 C, D). LMX1b, an LIM-homedomain transcription factor (Simon *et al*., 2003), regulates the expression of PITX3 (paired-like homeodomain transcription factor 3), and promotes survival of mDA neurons. The direct regulation of tyrosine hydroxylase (TH) expression (the rate limiting enzyme in DA synthesis) by Pitx3, and induction of cell cycle arrest by Nurr1, collectively promote terminal differentiation of mDA neurons (Maxwell and Li, 2005; Prakash and Wurst, 2006). Engrailed 1 and 2 (collectively EN1/2) both play a role in early and late embryogenesis, instrumental in regionalising the developing embryo (Kornberg 1981, 1985; Wurst *et al*., 1994), as well as specification of neuronal phenotypes (Condron *et al.*, 1994; Lundell *et al*., 1996; Saueressig *et al.*, 1999; Simon *et al*., 2001).

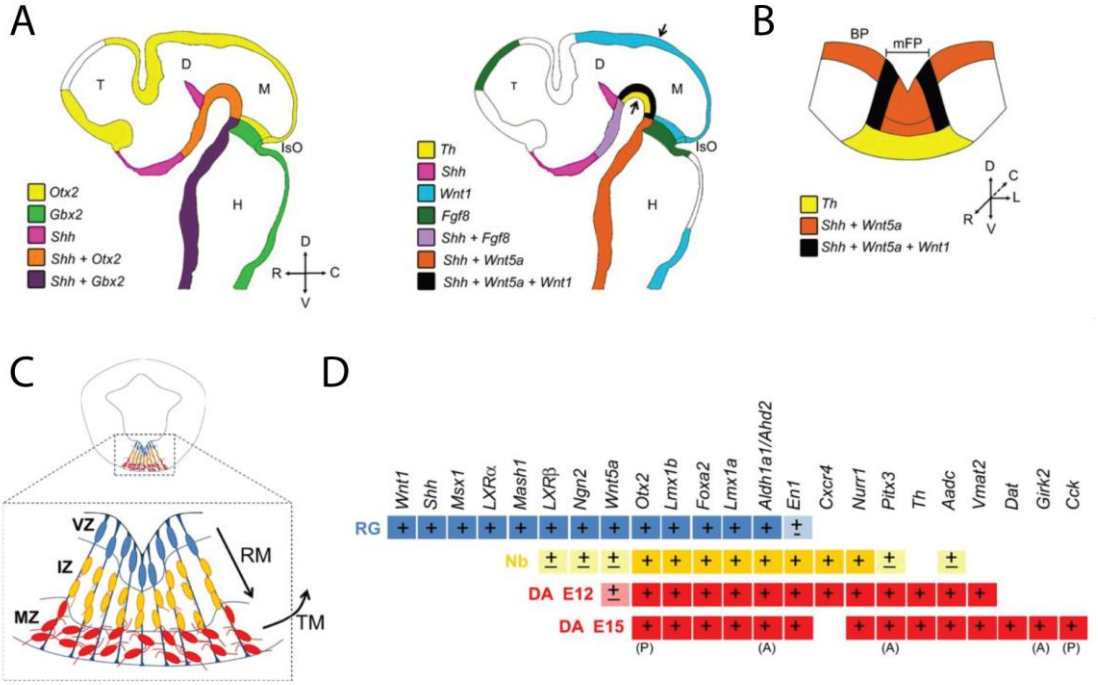

Figure 1.4 mDA development is regulated by transcription factors and morphogens
(A) Sagittal schematic of an E11.5 mouse brain. Orchestrated expression of Otx2 and Gbx2 dictates the formation of the isthmic organiser (IsO) that delineates the midbrain-hindbrain boundary. SHH, secreted by the notochord, specifies the floor plate following high SHH signalling. Collective expression of FGF8, SHH, Wnt5a and Wnt1 are key for the induction of mDA neurogenesis and define the region that gives rise to TH+ DA neurons. **(B-C)** Coronal section of the developing midbrain at E11.5 (indicated by black arrows in B). **(C)** Immature mDA progenitors (blue) divide in the ventricular zone and migrate radially across the intermediate zone (IZ) as post-mitotic neuroblasts, that become TH+ mDA neurons on reaching the marginal zone (MZ). **(D)** Panel of transcription factors and morphogens across the entire mDA lineage, of progenitors (blue), neuroblasts (yellow) and mDA neurons (red). Levels depicted as either low expression (±) or expressed (+). Figure adapted from Arenas *et al* (2015).

1.2.2 Pluripotent stem cell differentiation

The most common stem cell sources that have been pursued for DA neuron derivation are mesenchymal stem cells, induced neurons, expanded precursor cells and pluripotent stem cells (Figure 1.5) (Shen *et al.*, 2016), with the later most successful and advancing the furthest to date (Barker, 2014; Lindvall and Kokaia 2009) .

Pluripotent stem cells (PSCs), inclusive of both embryonic (ESC) and induced pluripotent (iPSCs) have emerged as a promising alternative DA source to fetal tissue for the treatment of Parkinson's disease. These cells have the various benefits of sustainability, reduced ethical issues and capacity to generate numerous highly specialised and fully functional mature cell types (Evans and Kaufman, 1981). ESCs are derived from the inner cell mass of the developing embryo, whilst adult somatic cells (e.g. fibroblasts) can be reprogrammed back

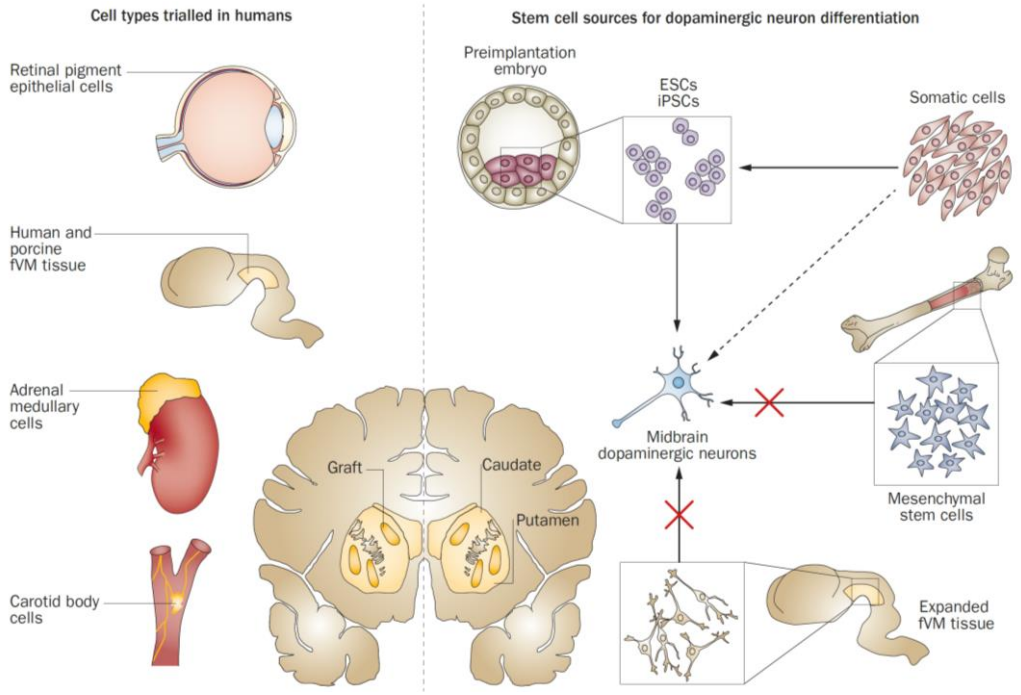

Figure 1.5. Cell-based therapies for PD – past and present.
The left hand side indicating cell types previously trialled in PD patients. Only fVM tissue has been shown to be efficacious, attributed to the ability to give rise to authentic midbrain DA neurons. The right hand shows potential cell sources that have been tested for their capacity to generate DA neurons. Pluripotent stem cells (inclusive of embryonic and induced pluripotent) have been successful, with iPSC-derived DA neurons already in clinical trial testing, efficacy has not been reported yet. Whilst other sources such as mesenchymal stem cell or expansion of fVM tissue have failed. Figure from Barker *et al* (2015).

to pluripotency by expression of transcription factors, to form iPSCs (Takahashi and Yamanaka, 2006).

Following the successful establishment of human ESCs (hESCs) (Thomson, 1998), and subsequently human iPSCs (hiPSCs) in 2007 (Takahashi and Yamanaka, 2006), there was considerable excitement to produce a differentiation protocol capable of generating stem cell-derived mDA neurons. Initial methods focused on spontaneous region-specific differentiation to a neuroectoderm origin that often adopted co-culture systems (either murine stromal cells or astrocytes) combined with SHH and FGF8 treatment. The first protocol capable of generating TH-expressing dopamine neurons was reported by Perrier *et al* (2004) , that were subsequently followed by others with similar effects but highly variable patterning efficiencies (Brederlau *et al*., 2006; Park *et al*., 2005; Perrier *et al*., 2004; Sonntag *et al*., 2007; Zeng *et al*., 2004; Roy *et al*., 2006; Cooper *et al*., 2010; Yan *et al*., 2005; Yang *et al*., 2008). Undermining this early progress was evidence of tumour formation following transplantation

that occurred in some instances (Brederlau *et al.*, 2006; Sonntag *et al.*, 2007) and more importantly the revelation that these DA neurons critically did not express the array of mDA-specific lineage markers (FOXA2/LMX1A/NURR1/EN1/PITX3/TH) that we now recognise as indicative of authentic mDA neurons (Zhao *et al.*, 2004). Such observations highlighted the need for development of advanced protocols that more closely mimicked human embryonic mDA development.

Critical in this progression was the discovery that mDA neurons are derived from the floor plate progenitors (rather than of neuroepithelial origin) (Ono *et al.*, 2007; Bonilla *et al.*, 2008). This lead to the generation of protocols focused on earlier regional patterning of hPSCs, simultaneously with neutralisation. This refined approach generated successful and highly efficient formation of authentic mDA neurons, importantly from the correct floor plate intermediate progenitor population (Kriks *et al.*, 2011), that was reported later by others (Denham *et al.*, 2012; Fasano *et al.*, 2010; Kirkeby *et al.*, 2013; Niclis *et al.*, 2017a; Xi *et al.*, 2012). With this important milestone (and rigorous validation *in vivo* that was subsequently performed), came the next step to generate good manufacturing practice (GMP)-compliant clinical grade cells. Efforts in our lab saw the development of an advanced xenogeneic-free, feeder-free, fully defined protocol, capable of both scalable expansion, and progenitor cryopreservation prior to transplantation (Niclis *et al.*, 2017a), thereby making significant headway towards the future generation of GMP-compliant clinical-grade cells.

1.2.3 Engraftment of PSC-derived DA progenitors

Work by us and others have demonstrated that following transplantation, hPSC-derived mDA neurons show robust graft survival, striatal/caudate putamen innervation and functional restoration of motor deficits in 6OHDA rodents and non-human primate models of PD (Kriks *et al.*, 2011; Denham *et al.*, 2012; Xi *et al.*, 2012; Kirkeby *et al.*, 2013; Dell'Anno *et al.*, 2014; Hallett *et al.*, 2015). These cells were also demonstrated to possess equivalent anatomical integration and efficiency to primary human fetal dopaminergic neurons (Grealish *et al.*, 2014). Added to this, grafted stem-cell derived mDA neurons displayed a remarkable capacity for target-specific and extensive circuit integration (Figure 1.6), whilst critically expressing markers of mature A9 and A10 subtypes, GIRK2 and Calbindin respectively (Grealish *et al.*, 2015; Niclis *et al.*, 2017b). Importantly, chemogenetic and optogenetic approaches, have provided conclusive evidence that amelioration of motor deficits by stem-

cell derived mDA neurons is a direct result of functional synaptic integration (Dell'Anno *et al.*, 2014; Steinbeck *et al.*, 2015; Chen *et al.*, 2016).

Despite functional success, an exhaustive comparative analysis of >30 transplant rounds of hPSC-derived vm progenitors highlighted significant variability in graft outcomes despite a consistent patterning threshold (>80% FOXA2/LMX1A) applied (Kirkeby *et al.*, 2017). Analysis of cell batches taken prior to transplantation and correlated to transplant outcome, demonstrated that grafts with a high DA neuron yield correlated positively with markers associated with the caudal VM (EN1, SPRY1, WNT1, CNPY1), but surprisingly had no correlation with many of the commonly associated early vmDA markers (FOXA2, CORIN) that are typically used as a metric for determining patterning success prior to transplantation. Such observations highlighted the need for more rigorous pre-grafting assessment (Kirkeby *et al.*, 2017). Retrospective analysis identified a higher level of rostral VM diencephalic progenitors within PSC cultures (identified by co-localisation of BARHL1+/PITX2+) that correlated with a lower DA yield following transplantation (Kirkeby *et al*., 2017).

1.2.4 Clinical translation

To improve grafting variability and adapt to full GMP standards for clinical translation, Kirkeby *et al* (2017) developed a complete GMP-compliant differentiation protocol that focused on fine tuning the rostro-caudal patterning of VM progenitors towards a more caudal mDA fate. Refinement led to an increased expression of markers indicative of a positive graft outcome, and consequentially reduced the inclusion of diencephalic progenitors. Prior to grafting, cells were profiled and selected based on low BARHL1/PITX2 and high EN1/LMX1A/FOXA2 expression levels. Whilst batch-to-batch reproducibility of differentiations could be achieved within a cell line, the recognition of extensive variability in morphogen requirements between hPSC lines has emphasised the need to optimise protocols for each cell line (Kirkeby *et al.*, 2017).

Whilst disappointing results from the fetal clinical trials significantly derailed the field for over a decade, it consequentially led to the development of TRANSEURO, a hugely valuable collaboration, that emphasised the benefits of working more closely together to push therapeutic approaches (of cell replacement therapy) forward. With stem cell based therapies closely approaching clinical trials, the stem cell field adopted a similar approach, with a global initiative (G-force PD) inclusive of the most active multidisciplinary teams. This

enabled an open discussion between global leaders on potential challenging aspects envisioned for translation to the clinic and standardisation of trial design, in the hope that comparisons can be made between trials in the future and mistakes that arose in the fetal trials can be avoided (Barker *et al*., 2015).

1.3 Strategies for improving safety and functional outcomes

Despite excitement of improved specification efficiency and graft functionality, protocols persist to contain a heterogeneous population (with ~10-13% of cells still failing to co-express the cardinal vm progenitor markers; FOXA2 together with LMX1A) prior to transplantation (Kirkeby *et al.*, 2017; Niclis *et al.,* 2017a). Surprisingly, the identity of these poorly specified cells and their potential functional impact, has been minimally investigated. This is particular concerning considering stem cell-derived DA products are already being tested in PD patients in Japan (CiRA, see press release in Nature news www.nature.com/articles/d41586-018-07407-9) as well as imminent clinical trials planned by other teams in the coming year (STEM-PD, NYTEM-PD, Summit for PD trial, Barker *et al.*, 2017).

What is clear, is that even a small fraction of these (non-vm) progenitors within transplanted material can expand extensively over time to dominate the graft, and significantly impede on the surrounding striatal tissue (Niclis *et al*., 2017b). Assessment of a number of studies to date has revealed grafts contain a significantly low proportion of DA neurons (reports ranging between 1-5%) (Doi *et al*., 2014; Kirkeby *et al*., 2012, 2017; Kriks *et al*., 2011; Niclis *et al*., 2017b; Samata *et al*., 2016). Added to this, the presence of these incorrectly patterned cells has been shown to cause significant widespread innervation of non- dopaminergic nuclei throughout the host brain that encompasses the majority of graft-derived innervation (Niclis *et al.,* 2017b) (Figure 1.6). The potential consequence of this off-target innervation on function is currently unclear.

In addition, are the concerns of potential tumour formation or tissue overgrowths by stem-cell based therapies, that may arise due to undetectable PSCs, residual highly proliferative progenitors or re-awakened quiescent stem cells. Whilst tumours have not been observed with improved differentiation protocols (unlike those observed in earlier preclinical studies using

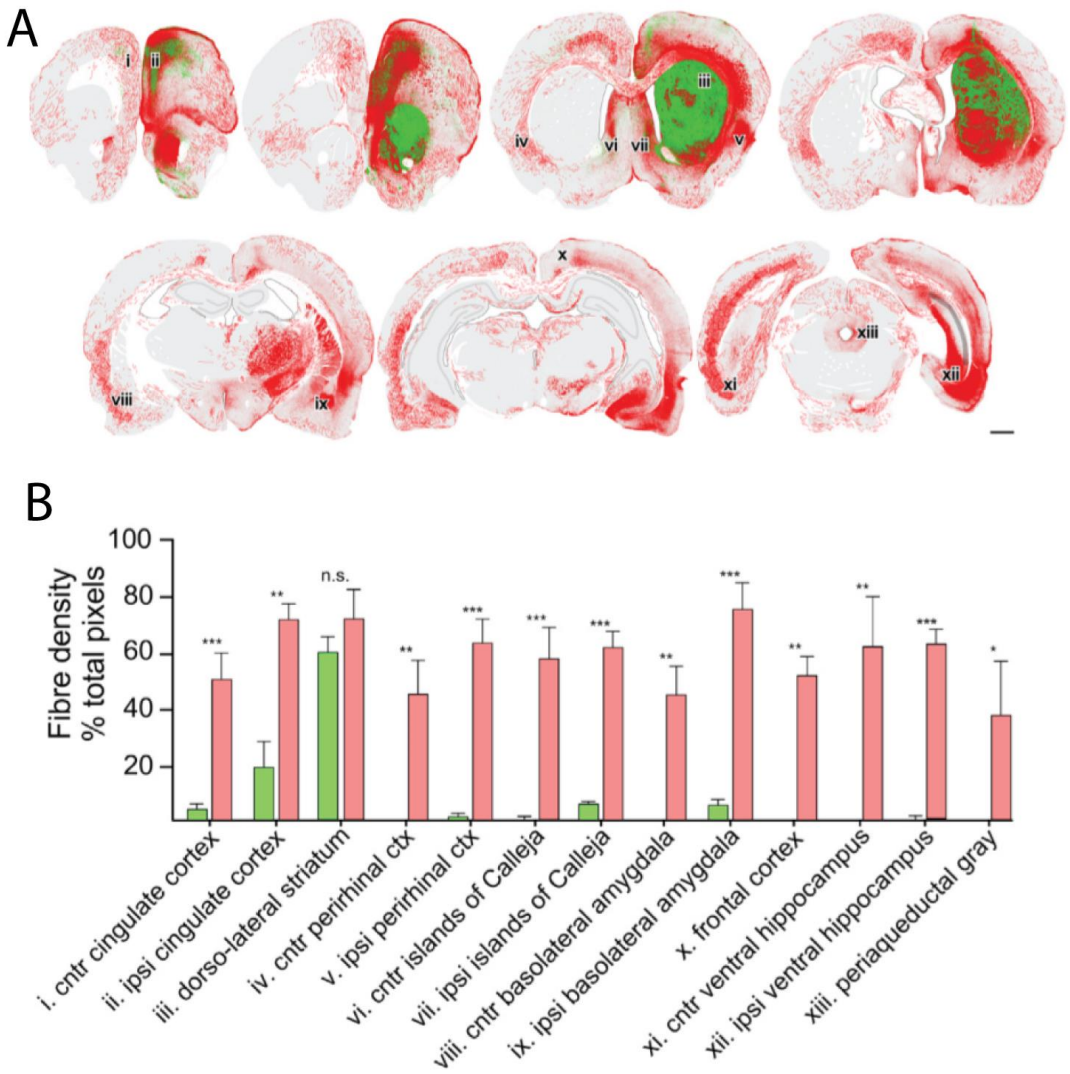

Figure 1.6 Synaptic integration of grafted cells is widespread, and mainly non-dopaminergic
(A) Coronal sections of the rodent brain indicating dopaminergic (green) and non-dopaminergic (red) innervation. **(B)** Assessment of fibre density demonstrates mDA neurons (green) innervate selectively and appropriately to developmentally appropriate targets, whilst non-mDA NCAM+ neurons (red) shows significant and wide-spread targeting across the rostral-caudal axis. Figure from Niclis *et al* (2017b).

neuroepithelial patterned cells) (Brederlau *et al.*, 2006; Sonntag *et al.*, 2007), the limited life span of animal models (<9months) has prevented a full investigation into the potential of tumorigenesis/overgrowth arising after many years, an important consideration for this long-term therapy.

Persistent heterogeneity within the differentiations and resultant low DA yields within grafts demands for refinement approaches capable of enriching for mDA neurons whilst eliminating these unwarranted, poorly specified cell types that may allow for tumorigenesis and neural

overgrowth, or alternatively may cause off-target motor effect such as those observed following the inclusion of 5HT neurons within fetal grafts. Such approaches should aim to be non-invasive and standardised whilst ensuring both safety and scalability without evident negative impact on differentiated cell types (Freed *et al*., 2001; Olanow *et al*., 2003).

1.3.1 Cellular enrichment

For this reason, efforts have been made in the field to selectively isolate correctly specified cells prior to grafting. Fluorescence-activated cell sorting (FACS) or Magnetic-activated cell sorting (MACS), targeting intracellular and extracellular proteins respectively, are capable of separating cellular populations. In the context of dopamine grafts, sorting can be utilised to select for progenitors with the appropriate mDA phenotype (Pruszak *et al*., 2007).

Initial efforts to segregate cell populations from differentiated PSC cultures were performed on rodent cultures, using fluorescent reporter lines under numerous promoters (Sox1, Sox2, DAT, NSP4) to enrich for progenitors and post-mitotic DA neurons (Chung *et al.*, 2006; Fukuda *et al*., 2006; Parmar & Li, 2007; di Porzio *et al*.,1987; Zhou *et al*, 2009). While some of these studies could avert tumour formation they commonly employed markers too broadly expressed to selectively isolate mDA progenitors/neurons (e.g. Sox1 and Sox2) or were too late in the differentiation to support isolation and survival after transplantation (e.g. DAT). Later purification studies implemented vm-specific factors, expressed on DA progenitors and young DA neuroblasts; inclusive of Hes5, Ngn2, Lmx1a, Nurr1, Pitx3. The result was improved survival and functional outcome following transplantation into the rodent brain (Ganat *et al*., 2012; Hedlund *et al*., 2008; Jönsson *et al*., 2009; Nefzger *et al*., 2012; Thompson *et al*., 2006).

Despite over a decade of efforts, isolation of VM progenitors from human PSC cultures has been met with variable success. In a number of studies, candidate markers employed for selection purposes were too broadly expressed to selectively isolate VM progenitors such as the pan-neuronal markers CD56/CD29/NCAM (Pruszak *et al.*, 2007), ventral floor plate marker (Aguila *et al*., 2014), ventral midbrain floor and basal plate markers Integrin Associated Protein and LMRT1 (Lehnen *et al.*, 2017; Samata *et al.*, 2016), as well as ventral midbrain/hindbrain marker CORIN (Doi *et al.*, 2014). Added to this, some studies conducted sorting early in the differentiation, requiring periods of extended replating prior to transplantation with the consequence of less predictive knowledge of the implanted

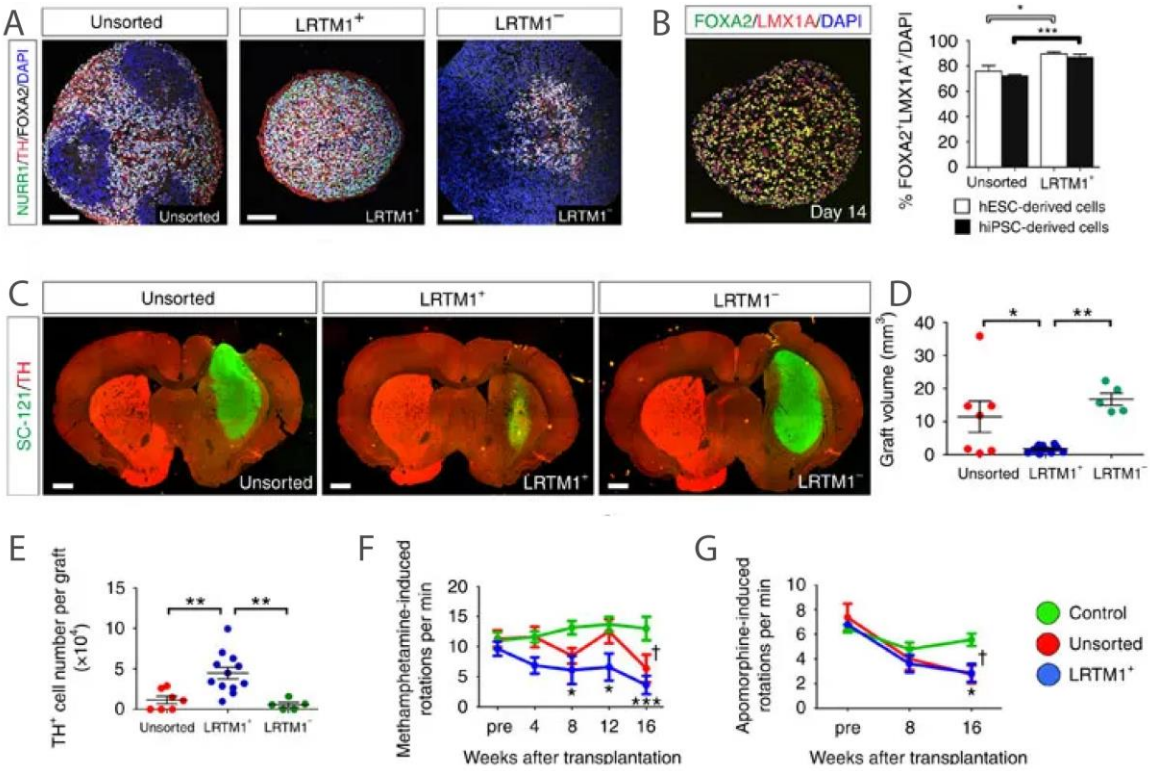

Figure 1.7 Isolated human LRTM1+ basal floor plate progenitors generate functional DA neurons with reduced overgrowth *in vivo*

(A) Unsorted and LRTM1$^-$ cells contain pockets of poorly specified progenitors (NURR1$^-$/FOXA2$^-$) that are devoid in LRTM1$^+$ cultures. **(B)** Isolation of LRTM1$^+$ cells enrich for vm progenitors (FOXA2$^+$/LMX1A$^+$) in hPSC cultures. **(C-E)** Engrafted LRTM1$^+$ progenitors generate significantly smaller grafts **(D)** with greater DA yield **(E)** compared to unsorted and LRTM1-derived transplants. **(F-G).** Grafts derived from LRTM1+ cells maintain function comparable to unsorted cells. Figure adapted from Samata *et al* (2016).

population and resultant variability across repeated grafting rounds (Samata *et al.*, 2016). Alternatively cultures that were sorted as late as day 42 of the differentiation, resulting in poor graft survival (Doi *et al.*, 2014; Lehnen *et al.*, 2017) or showed no evidence of grafting (Xia *et al.*, 2017), the later a consequence of isolation and transplantation of post-mitotic TH+ mDA neurons. Several of these approaches relied on low sorting yields impacting feasibility of large-scale production of desired progenitors required for human transplants (Doi *et al.*, 2014, Samata *et al.*, 2016*a*). Another challenge has been that rodent tissue was initially employed to identify clinically-applicable cell surface antigens on DA progenitor populations, yet translation of these approaches were unsuccessful as antibodies failed to show the same restrictive isolation or immunoreactivity in human cells (Bye *et al.*, 2015; Gennet *et al.*, 2016; Samata *et al.*, 2016) and our unpublished observations.

Most advanced in the field has been the effort to isolate leucine-rich repeats and transmembrane domains 1 (LRTM1)-expressing cells from human PSC-derived VM cultures (Samata *et al*., 2016). Transplantation of LRTM1+ cells increased the proportion of tyrosine hydroxylase (TH) expressing DA neurons within rodent grafts, with functional improvements in motor asymmetry observed as early as 8 weeks after transplantation (of note this is considerably earlier than other labs) (Figure 1.7). Repeat LRTM1+ grafting however reported 4-fold less TH+ cells within the graft, an effect likely reflecting *in vitro* variability and heterogeneity following extended periods of replating after sorting.

As a consequence of these suboptimal and/or variable outcomes, combined with the field's desire to rapidly advance to the clinic, there remains a persistent and inherent need to identify a reliable candidate marker for the enrichment of DA progenitors from human PSC-derived VM cultures.

1.3.2 Suicide gene therapy

Approaches for safety against potential tumorigenesis that can be implemented after transplantation have also been explored in preclinical studies. Whilst targeted elimination of rogue proliferative cells has been demonstrated using gamma ray irradiation (Katsukawa *et al*., 2016), this aggressive measure has a multitude of adverse side effects that can be chronic, in addition to concerns regarding its efficacy. The concept of withdrawing immunosuppression following adverse effects or overgrowth, alternatively relies on the host immune system to recognise the grafted cells as foreign (Itakura *et al.*, 2015). However, this brings its own issues of variability in immunogenicity between patients, and the consequential loss of the entire graft. Added to this, problems may arise several months after engraftment at which point these cells may evade the immune system, as indicated by the long-term (24yrs) survival of grafted cells despite only 12 months of immunosuppression (Li *et al*., 2016).

Alternatively, suicide gene therapy, has been suggested to improve the safety of stem cell transplantation. This is achieved by stable incorporation of a dormant suicide gene, encoding a protein that results in cell death only when activated by a specific compound. The most extensively studied suicide system to date is the herpes simplex virus thymidine kinase/ganciclovir (HSV/TK-GCV) system (Figure 1.8). In this enzyme based system, the

suicide gene thymidine kinase (TK) is delivered using the herpes simplex virus, rendering the cell sensitised to the prodrug ganciclovir. TK encodes for an enzyme that catalyses the phosphorylation of ganciclovir (GCV) into a highly toxic triphosphate derivative (GCV-3P), that can act as a guanosine analog, to cause termination of DNA replication, in this regard to specifically eliminate only proliferating cells expressing the TK enzyme (Morgan, 2012; Xiao *et al*., 2014).

The concept of suicide gene therapy was first introduced by Moolten and colleagues in the late 80s. They demonstrated that tumour cells, transfected with the HSV-TK gene could be sufficiently eliminated both *in vitro* and *in vivo* following administration of the pro-drug (Moolten, 1986; Moolten and Wells, 1990). While initially targeted as a tumorigenic/cancer therapy, more recently suicide gene therapy has proven to be clinically efficacious in the practice of allogeneic hematopoietic stem cell transplantation (allo-HSCT) as a therapeutic option for graft-versus-host-disease (GVHD) (Morgan, 2012). Here, TK-modified donor T cells were administered to patients, with the safe-guard that GCV can be administered to selectively mitigate active GVHD (Bonini *et al.*, 1997).

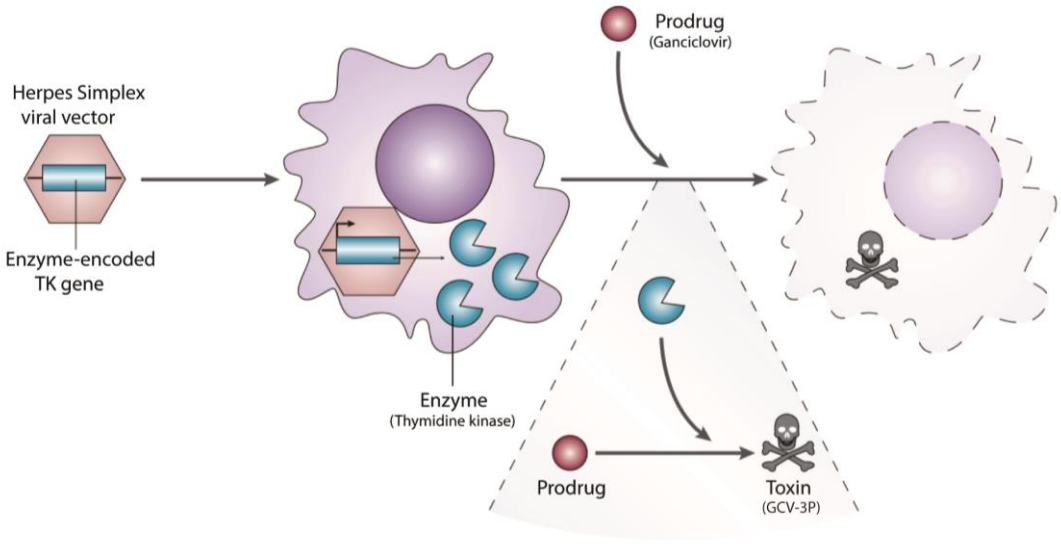

Figure 1.8 Suicide gene therapy
The prodrug-converting enzyme, thymidine kinase (TK) is delivered using the herpes simplex virus (HSV) into cell system. Administration of the prodrug, ganciclovir (GCV) is converted to a highly toxic phosphorylated metabolite by TK, that terminates DNA replication and causes apoptosis. Figure from Mccormick (2001).

More recently, others have utilised this technology to deplete the neural stem cell reservoir and directly modulate adult neurogenesis in transgenic mice models. Following GCV exposure, transgenic mice with TK expression regulated by either Nestin (Singer *et al.*, 2009; Youssef *et al.*, 2018) or doublecortin (Jin *et al*., 2010; Seo *et al*., 2015; Sun *et al*., 2012), to target neural progenitors and neuroblasts respectively, demonstrated a reduction in adult neurogenesis in the 1st and 3rd trimester, but it was only in the first trimester when cells were highly proliferative that complete elimination of dividing neural stem cells was achieved. It is thought that NSCs enter a quiescent phase during the third trimester and become less responsive to GCV (Youssef *et al.*, 2018).

Introduction of the HSV-TK suicide gene system into a pluripotent stem cell line was first reported by Schuldiner (2003). Here, they demonstrated successful ablation of teratomas following human PSC grafts in mice. This approach was utilized in further stem cell studies to a similar effect (Schuldiner, 2003; Jung *et al.*, 2007; Cheng *et al.*, 2012). To date, approaches to specifically target elimination of pluripotent stem cells have been developed under numerous pluripotent cell-specific promoters; Oct4 (Hara *et al*., 2008; Ou *et al*., 2013) and Nanog (Rong *et al*., 2012) or cell-cycle driven promoters; Ki67 (Kotini *et al*., 2016), CDK1 (Liang *et al.*, 2018). Although these have been successful in teratoma applications, their ability to remove defined populations from neural grafts remains an important goal.

Whilst exposure to GCV has been shown to completely ablate proliferating neural epithelial progenitors *in vitro* (Kotini *et al.*, 2016; Liang *et al.*, 2018), providing evidence that the HSV-TK system has the capacity to impact differentiated progeny, efforts implementing suicide gene therapy in hPSC-derived neural grafts have not been met with such success. Using this paradigm, Kotini *et al* (2016) demonstrated successful prevention of continued teratoma growth, however when hPSC-derived DA grafts were exposed to GCV for the same duration, no changes in graft volume were observed. This suggested that further work is needed to investigate if the regime employed for teratoma studies is suitable for neural grafts.

Additional concern for the employment of this technology has been the recognition of frequent GCV resistance in both iPSC-derived teratomas (Kotini *et al.*, 2016) and human T lymphocytes (Garin *et al.*, 2001). Resistance to GCV (and/or incomplete ablation) has also been identified in other suicide systems, such as the inducible caspase-9 suicide gene system (iCasp9) (Di Stasi *et al.*, 2011; Gargett and Brown, 2014; Wu *et al.*, 2014).

As the field advances towards the clinic, it will be essential for suicide approaches to implement additional fail safe features within suicide cell lines to limit emerging resistance. One such way is to protect a suicide system from inactivation. This has been most recently demonstrated by our collaborators by expressing the TK gene under the regulation of a promotor for an essential locus that is required for cell cycle progression, such as CDK1 (Liang *et al*., 2018). CDK1 is a non-redundant cyclin-depended kinase (CDK) with an essential role in mitosis (Malumbres, 2014). Thus, mutations at this locus that render the protein non-functional will stop the transition from G2 to M phase of the cell cycle and prevent cell division (Malumbres, 2014). This group further validated this safe-cell system using mathematic modelling to identify the 'safety cell level' based on the number of cells needed for a particular cellular therapy. The safe-cell level (SCL) can be defined as the number of therapeutic batches in which there is expected to be only one non-safe batch (for example an SCL of 1,000, would indicate one in a thousand batches would be unsafe) (Liang *et al.*, 2018).

1.3.3 Refining the optimal transplant age

Developmental age of harvested human and rodent fetal vm tissue for transplantation can have a significant impact on graft composition and functional outcomes, (Brundin *et al.*, 2000). Critically, there appears to be a narrow developmental window that fVM tissue can be harvested to ensure functional capacity. Several studies have determined that immature progenitors which remain proliferative, whilst being fully committed to a DA fate, and isolated prior to the peak of DA neurogenesis, leads to better graft survival, composition and striatal targeting (Kauhausen *et al.*, 2013, Bye *et al.*, 2012, Seiger and Olson, 1977., Torres *et al.*, 2007., Torres *et al.*, 2008). By comparison, cells isolated too early (prior to sufficient neural fate specification) or taken too late during development (i.e. neuroblasts susceptible to axotomy), have produced sub-optimal results, typically due to poor survival and/or low yield of DA neurons (Dunnett *et al*., 1997). Added to this, more recent studies have highlighted that A9 DA neurons precede the birth of neighbouring A10 DA neurons (Joksimovic *et al*., 2009; Blaess *et al*., 2011; Hayes *et al*., 2011; Bye *et al*., 2012), and consequently the transplantation of younger donor tissue enriches for this necessary A9 population (Bye *et al.*, 2012). In light of these results, the inherently broad, and often variable, donor ages utilised in the fetal clinical trials is thought to likely be an important contributing factor to the diverse clinical outcomes.

Despite fetal studies reporting a strong influence of vmDA fetal donor cell age on graft outcomes, there has been relatively limited comparisons of hPSC-derived vmDA grafts at varying *in vitro* developmental ages (Kirkeby *et al*., 2012; Qiu *et al*., 2017) . Further confusing the landscape has been the wide range in ages utilised for grafting (ranging from D16-42) that various groups adopt for transplantation despite several studies sharing similar differentiation protocols (Doi *et al*., 2014; Gantner *et al*., 2020; Kirkeby *et al.*, 2012; Kriks *et al.*, 2011; de Luzy *et al.*, 2019; Samata *et al.*, 2016; Wakeman *et al*., 2017). Such exploration is essential, given the imminent advancement of hPSC-derived DA progenitor grafts into the clinic and given that terminal maturation *in vitro* cannot be predictive of graft outcome.

1.4 Proposed research

As the field makes significant headway towards cell replacement therapy for Parkinson's disease it is important to recognise that other essential objectives for clinical translation remain unanswered. At the forefront, is the need to standardise hPSC-derived DA grafting outcomes to ensure patient safety and maximise graft functionality. In order to address this goal, the overarching focus of my research has encapsulated 3 aims that span two broad concepts (i) employing novel stem cell tools to eliminate unwanted graft-derived cellular populations that may evoke adverse side effects or overgrowth/tumorigenesis (Aims 1 and 2), and (ii) to understand the impact of both *in vitro* cell age at engraftment and cell line on graft outcome (Aim 3).

1.4.1 Aims of the thesis

Aim1: To investigate the potential of human ESC reporter lines to selectively isolate vmDA progenitors/precursors for transplant

Aim 2: To assess the benefits of introducing a suicide gene into the hPSC-derived donor cells to improve the safety of neural transplants targeted for Parkinson's Disease

Aim 3: To determine the optimal developmental age of hPSC-derived vm progenitors for transplantation and assess the reproducibility of grafting between and within cell lines

1.6 References

Aguila JC, Blak A, van Arensbergen J, Sousa A, Vázquez N, Aduriz A, et al. Selection Based on FOXA2 Expression Is Not Sufficient to Enrich for Dopamine Neurons From Human Pluripotent Stem Cells. Stem Cells Transl Med 2014; 3: 1032–1042.

Aguila JC, Hedlund E, Sanchez-Pernaute R. Cellular programming and reprogramming: Sculpting cell fate for the production of dopamine neurons for cell therapy. Stem Cells Int 2012; 412040.

Aldrin-Kirk P, Heuer A, Wang G, Mattsson B, Lundblad M, Parmar M, et al. DREADD Modulation of Transplanted DA Neurons Reveals a Novel Parkinsonian Dyskinesia Mechanism Mediated by the Serotonin 5-HT6 Receptor. Neuron 2016; 90: 955–968.

Arenas E, Denham M, Villaescusa JC. How to make a midbrain dopaminergic neuron. Dev 2015; 142: 1918–1936.

Barker RA. Developing stem cell therapies for Parkinson's disease: Waiting until the time is right. Cell Stem Cell 2014; 15: 539–542.

Barker RA, Barrett J, Mason SL, Björklund A. Fetal dopaminergic transplantation trials and the future of neural grafting in Parkinson's disease. Lancet Neurol 2013; 12: 84–91.

Barker RA, Drouin-Ouellet J, Parmar M. Cell-based therapies for Parkinson disease-past insights and future potential. Nat Rev Neurol 2015; 11: 492–503.

Barker RA, Farrell K, Guzman NV, He X, Lazic SE, Moore S, et al. Designing stem-cell-based dopamine cell replacement trials for Parkinson's disease. Nat Med 2019; 25

Barker RA, Parmar M, Kirkeby A, Bjorklund A, Thompson L, Brundin P. Are Stem Cell-Based Therapies for Parkinson's Disease Ready for the Clinic in 2016? J Park Dis 2016; 6: 57–63.

Barker RA, Parmar M, Studer L, Takahashi J. Human Trials of Stem Cell-Derived Dopamine Neurons for Parkinson's Disease: Dawn of a New Era. Cell Stem Cell 2017; 21: 569–573.

Barker RA, Studer L, Cattaneo E, Takahashi J. G-Force PD: a global initiative in coordinating stem cell-based dopamine treatments for Parkinson's disease. npj Park Dis 2015; 1:15017

Bjorklund A, Dunnett SB, Stenevi U, Lewis ME, Iversen SD. Reinnervation of the denervated striatum by substantia nigra transplants: functional consequences as revealed by pharmacological and sensorimotor testing. Brain Res 1980; 199: 307–333.

Bjorklund A, Stenevi U. Reconstruction of the nigrostriatal dopamine pathway by intracerebral nigral transplants. Brain Res 1979; 177: 555–560.

Bjorklund A, Stenevi U, Schmidt RH. Intracerebral grafting of neuronal cell suspensions. II. Survival and growth of nigral cell suspensions implanted in different brain sites. Acta Physiol Scand 1983; 118: 9–18.

Bonilla S, Hall AC, Pinto L, Attardo A, Götz M, Huttner WB, et al. Identification of midbrain floor plate radial glia-like cells as dopaminergic progenitors. Glia 2008; 56: 809–820.

Bonini C, Ferrari G, Verzeletti S, Servida P, Zappone E, Ruggieri L, et al. HSV-TK gene transfer into donor lymphocytes for control of allogeneic graft-versus-leukemia. Science 1997; 276: 1719–1724.

Brederlau A, Correia AS, Anisimov S V., Elmi M, Paul G, Roybon L, et al. Transplantation of Human Embryonic Stem Cell-Derived Cells to a Rat Model of Parkinson's Disease: Effect of In Vitro Differentiation on Graft Survival and Teratoma Formation. Stem Cells 2006; 24: 1433–

1440.

Breger LS, Lane EL. L-DOPA and graft-induced dyskinesia: Different treatment, same story? Exp Biol Med 2013; 238: 725–732.

Brundin P, Barker RA, Parmar M. Neural grafting in Parkinson's disease. Problems and possibilities. In: Progress in Brain Research. 2010; 184: 265–294

Brundin P, Karlsson J, Emgård M, Kaminski Schierle GS, Hansson O, Petersén Å, et al. Improving the survival of grafted dopaminergic neurons: A review over current approaches. Cell Transplant 2000; 9: 179–195.

Brundin P, Ma J, Kordower JH. How strong is the evidence that Parkinson's disease is a prion disorder? Curr Opin Neurol 2016; 29(4):459-66.

Brundin P, Nilsson OG, Strecker RE, Lindvall O, Åstedt B, Björklund A. Behavioural effects of human fetal dopamine neurons grafted in a rat model of Parkinson's disease. Exp Brain Res 1986; 65: 235–240.

Brundin P, Strecker RE, Widner H, Clarke DJ, Nilsson OG, Åstedt B, et al. Human fetal dopamine neurons grafted in a rat model of Parkinson's disease: immunological aspects, spontaneous and drug-induced behaviour, and dopamine release. Exp Brain Res 1988; 70: 192–208.

Bye CR, Jönsson ME, Björklund A, Parish CL, Thompson LH. Transcriptome analysis reveals transmembrane targets on transplantable midbrain dopamine progenitors. Proc Natl Acad Sci USA 2015; 112: e1946–e1955.

Bye CR, Thompson LH, Parish CL. Birth dating of midbrain dopamine neurons identifies A9 enriched tissue for transplantation into Parkinsonian mice. Exp Neurol 2012; 236: 58–68.

Carlsson T, Carta M, Muñoz A, Mattsson B, Winkler C, Kirik D, et al. Impact of grafted serotonin and dopamine neurons on development of L-DOPA-induced dyskinesias in parkinsonian rats is determined by the extent of dopamine neuron degeneration. Brain 2009; 132: 319–335.

Carlsson T, Winkler C, Lundblad M, Cenci MA, Björklund A, Kirik D. Graft placement and uneven pattern of reinnervation in the striatum is important for development of graft-induced dyskinesia. Neurobiol Dis 2006; 21: 657–668.

Chen Y, Xiong M, Dong Y, Haberman A, Cao J, Liu H, et al. Chemical Control of Grafted Human PSC-Derived Neurons in a Mouse Model of Parkinson's Disease. Cell Stem Cell 2016; 18: 817–826.

Cheng F, Ke Q, Chen F, Cai B, Gao Y, Ye C, et al. Protecting against wayward human induced pluripotent stem cells with a suicide gene. Biomaterials 2012; 33: 3195–3204.

Chung S, Shin BS, Hedlund E, Pruszak J, Ferree A, Kang UJ, et al. Genetic selection of sox1GFP-expressing neural precursors removes residual tumorigenic pluripotent stem cells and attenuates tumor formation after transplantation. J Neurochem 2006; 97: 1467–1480.

Clarke DJ, Brundin P, Strecker RE, Nilsson OG, Björklund A, Lindvall O. Human fetal dopamine neurons grafted in a rat model of Parkinson's disease: ultrastructural evidence for synapse formation using tyrosine hydroxylase immunocytochemistry. Exp Brain Res 1988; 73: 115–126.

Condron BG, Patel NH, Zinn K. engrailed controls glial/neuronal cell fate decisions at the midline of the central nervous system. Neuron 1994; 13: 541–554.

Cooper O, Hargus G, Deleidi M, Blak A, Osborn T, Marlow E, et al. Differentiation of human ES and Parkinson's disease iPS cells into ventral midbrain dopaminergic neurons requires a high activity form of SHH, FGF8a and specific regionalization by retinoic acid. Mol Cell Neurosci 2010; 45: 258–266.

Dauer W, Przedborski S, Schulz JB, Falkenburger BH. Parkinson's disease: mechanisms and

models. Neuron 2003; 39: 889–909.

Dell'Anno MT, Caiazzo M, Leo D, Dvoretskova E, Medrihan L, Colasante G, et al. Remote control of induced dopaminergic neurons in parkinsonian rats. J Clin Invest 2014; 124: 3215–3229.

Denham M, Bye C, Leung J, Conley BJ, Thompson LH, Dottori M. Glycogen Synthase Kinase 3b and Activin/Nodal Inhibition in Human Embryonic Stem Cells Induces a Pre-Neuroepithelial State That is Required for Specification to a Floor Plate Cell Lineage. Stem Cells 2012; 30: 2400–2411.

Doi D, Samata B, Katsukawa M, Kikuchi T, Morizane A, Ono Y, et al. Isolation of human induced pluripotent stem cell-derived dopaminergic progenitors by cell sorting for successful transplantation. Stem Cell Reports 2014; 2: 337–350.

Dunn EH. Primary and secondary findings in a series of attempts to transplant cerebral cortex in the albino rat. J Comp Neurol 1917; 27: 565–582.

Dunnett SB, Kendall AL, Watts C, Torres EM. Neuronal cell transplantation for Parkinson's and Huntington's diseases. Br Med Bull 1997; 53: 757–776.

Evans MJ, Kaufman MH. Establishment in culture of pluripotential cells from mouse embryos. Nature 1981; 292: 154–156.

Fasano CA, Chambers SM, Lee G, Tomishima MJ, Studer L. Efficient Derivation of Functional Floor Plate Tissue from Human Embryonic Stem Cells. Cell Stem Cell 2010; 6: 336–347.

Freed CR, Breeze RE, Rosenberg NL, Schneck SA, Kriek E, qi JX, et al. Survival of Implanted Fetal Dopamine Cells and Neurologic Improvement 12 to 46 Months after Transplantation for Parkinson's Disease. N Engl J Med 1992; 327: 1549–1555.

Freed CR, Greene PE, Breeze RE, Tsai WY, DuMouchel W, Kao R, et al. Transplantation of embryonic dopamine neurons for severe Parkinson's disease. N Engl J Med 2001; 344: 710–719.

Fukuda H, Takahashi J, Watanabe K, Hayashi H, Morizane A, Koyanagi M, et al. Fluorescence-Activated Cell Sorting-Based Purification of Embryonic Stem Cell-Derived Neural Precursors Averts Tumor Formation after Transplantation. Stem Cells 2006; 24: 763–771.

Ganat YM, Calder EL, Kriks S, Nelander J, Tu EY, Jia F, et al. Identification of embryonic stem cell-derived midbrain dopaminergic neurons for engraftment. J Clin Invest 2012; 122: 2928–2939.

Gargett T, Brown MP. The inducible caspase-9 suicide gene system as a 'safety switch' to limit on-target, off-tumor toxicities of chimeric antigen receptor T-cells. Front Pharmacol 2014; 5: 235.

Garin MI, Garrett E, Tiberghien P, Apperley JF, Chalmers D, Melo J V., et al. Molecular mechanism for ganciclovir resistance in human T lymphocytes transduced with retroviral vectors carrying the herpes simplex virus thymidine kinase gene. Blood 2001; 97: 122–129.

Gennet N, Tamburini C, Nan X, Li M, Kriks S, Grealish S, et al. FolR1: a novel cell surface marker for isolating midbrain dopamine neural progenitors and nascent dopamine neurons. Sci Rep 2016; 6: 32488.

German DC, Manaye KF. Midbrain dopaminergic neurons (nuclei A8, A9, and A10): Three-dimensional reconstruction in the rat. J Comp Neurol 1993; 331: 297–309.

Grealish S, Diguet E, Kirkeby A, Mattsson B, Heuer A, Bramoulle Y, et al. Human ESC-derived dopamine neurons show similar preclinical efficacy and potency to fetal neurons when grafted in a rat model of Parkinson's disease. Cell Stem Cell 2014; 15: 653–665.

Grealish S, Heuer A, Cardoso T, Kirkeby A, Jönsson M, Johansson J, et al. Stem Cell Reports Monosynaptic Tracing using Modified Rabies Virus Reveals Early and Extensive Circuit

Integration of Human Embryonic Stem Cell-Derived Neurons. Stem Cell Reports 2015; 4: 975–983.

Grealish S, Jönsson ME, Li M, Kirik D, Björklund A, Thompson LH. The A9 dopamine neuron component in grafts of ventral mesencephalon is an important determinant for recovery of motor function in a rat model of Parkinson's disease. Brain 2010; 133: 482–495.

Hagell P, Piccini P, Bjorklund A, Brundin P, Rehncrona S, Widner H, et al. Dyskinesias following neural transplantation in Parkinson's disease. Nat Neurosci 2002; 5: 627–628.

Hallett PJ, Deleidi M, Astradsson A, Smith GA, Cooper O, Osborn TM, et al. Successful function of autologous iPSC-derived dopamine neurons following transplantation in a non-human primate model of Parkinson's disease. Cell Stem Cell 2015; 16(3): 269-74.

Hara A, Aoki H, Taguchi A, Niwa M, Yamada Y, Kunisada T, et al. Neuron-like differentiation and selective ablation of undifferentiated embryonic stem cells containing suicide gene with Oct-4 promoter. Stem Cells Dev 2008; 17: 619–627.

Hartmann CJ, Fliegen S, Groiss SJ, Wojtecki L, Schnitzler A. An update on best practice of deep brain stimulation in Parkinson's disease. Ther Adv Neurol Disord 2019; 12.

Hauser RA, Freeman TB, Snow BJ, Nauert M, Gauger L, Kordower JH, et al. Long-term evaluation of bilateral fetal nigral transplantation in Parkinson disease. Arch Neurol 1999; 56: 179–187.

Hedlund E, Pruszak J, Lardaro T, Ludwig W, Vinuela A, Kim KS, et al. Embryonic stem cell-derived Pitx3-enhanced green fluorescent protein midbrain dopamine neurons survive enrichment by fluorescence-activated cell sorting and function in an animal model of Parkinson's disease. Stem Cells 2008; 26: 1526–1536.

Hegarty SV, Sullivan AM and O'Keefe GW. Midbrain dopaminergic neurons: A review of the molecular circuitry that regulates their devlopment. Developmental Biology. 2013; 379(2): 123-138.

Hynes M, Hynes M, Porter JA, Porter JA, Chiang C, Chiang C, et al. Induction of midbrain dopaminergic neurons by Sonic hedgehog. Neuron 1995; 15: 35–44.

Hynes M, Poulsen K, Tessier-Lavigne M, Rosenthal A. Control of neuronal diversity by the floor plate: Contact-mediated induction of midbrain dopaminergic neurons. Cell 1995; 80: 95–101.

Itakura G, Kobayashi Y, Nishimura S, Iwai H, Takano M, Iwanami A, et al. Controlling immune rejection is a fail-safe system against potential tumorigenicity after human iPSC-derived neural stem cell transplantation. PLoS One 2015; 10: 1–17.

Jenner P. What process causes nigral cell death in Parkinson's disease? Neurol Clin 1992; 10: 387–403.

Jin K, Wang X, Xie L, Mao XO, Greenberg DA. Transgenic ablation of doublecortin-expressing cells suppresses adult neurogenesis and worsens stroke outcome in mice. Proc Natl Acad Sci U S A 2010; 107: 7993–7998.

Jönsson ME, Ono Y, Björklund A, Thompson LH. Identification of transplantable dopamine neuron precursors at different stages of midbrain neurogenesis. Exp Neurol 2009; 219: 341–354.

Joyner AL, Liu A, Millet S. Otx2, Gbx2 and Fgf8 interact to position and maintain a mid-hindbrain organizer. Curr Opin Cell Biol 2000; 12: 736–741.

Jung J, Hackett NR, Pergolizzi RG, Pierre-Destine L, Krause A, Crystal RG. Ablation of tumor-derived stem cells transplanted to the central nervous system by genetic modification of embryonic stem cells with a suicide gene. Hum Gene Ther 2007; 18: 1182–1192.

Kefalopoulou Z, Politis M, Piccini P, Mencacci N, Bhatia K, Jahanshahi M, et al. Long-term

Clinical Outcome of Fetal Cell Transplantation for Parkinson Disease Two Case Reports. JAMA Neurol. 2014; 71(1): 83-7.

Kirkeby A, Grealish S, Wolf DA, Nelander J, Wood J, Lundblad M, et al. Generation of Regionally Specified Neural Progenitors and Functional Neurons from Human Embryonic Stem Cells under Defined Conditions. Cell Rep 2012; 1: 703–714.

Kirkeby A, Nelander J, Parmar M, Park C-H. Generating regionalized neuronal cells from pluripotency, a step-by-step protocol. Front Cell Neurosci 2013; 3(6): 64

Kirkeby A, Nolbrant S, Tiklova K, Heuer A, Kee N, Cardoso T, et al. Predictive Markers Guide Differentiation to Improve Graft Outcome in Clinical Translation of hESC-Based Therapy for Parkinson's Disease. Cell Stem Cell 2017; 20: 135–148.

Kordower JH, Chu Y, Hauser RA, Freeman TB, Olanow CW. Lewy body-like pathology in long-term embryonic nigral transplants in Parkinson's disease. Nat Med 2008; 14: 504–506.

Kordower JH, Freeman TB, Snow BJ, Vingerhoets FJG, Mufson EJ, Sanberg PR, et al. Neuropathological evidence of graft survival and striatal reinnervation after the transplantation of fetal mesencephalic tissue in a patient with parkinson's disease. N Engl J Med 1995; 332: 1118–1124.

Kordower JH, Rosenstein JM, Collier TJ, Burke MA, Chen EY, Li JM, et al. Functional fetal nigral grafts in a patient with Parkinson's disease: Chemoanatomic, ultrastructural, and metabolic studies. J Comp Neurol 1996; 370: 203–230.

Kornberg T. Compartments in the abdomen of Drosophila and the role of the engrailed locus. Dev Biol 1981; 86: 363–372.

Kornberg T, Sidén I, O'Farrell P, Simon M. The engrailed locus of drosophila: In situ localization of transcripts reveals compartment-specific expression. Cell 1985; 40: 45–53.

Kotini AG, de Stanchina E, Themeli M, Sadelain M, Papapetrou EP. Escape Mutations, Ganciclovir Resistance, and Teratoma Formation in Human iPSCs Expressing an HSVtk Suicide Gene. Mol Ther - Nucleic Acids 2016; 5: e284.

Kriks S, Shim JW, Piao J, Ganat YM, Wakeman DR, Xie Z, et al. Dopamine neurons derived from human ES cells efficiently engraft in animal models of Parkinson's disease. Nature 2011; 480: 547–551.

Lane EL, Winkler C, Brundin P, Cenci MA. The impact of graft size on the development of dyskinesia following intrastriatal grafting of embryonic dopamine neurons in the rat. 2006; 22(2), 334-45.

Lehnen D, Barral S, Cardoso T, Grealish S, Heuer A, Smiyakin A, et al. IAP-Based Cell Sorting Results in Homogeneous Transplantable Dopaminergic Precursor Cells Derived from Human Pluripotent Stem Cells. Stem Cell Reports 2017; 9: 1207–1220.

Li JY, Englund E, Holton JL, Soulet D, Hagell P, Lees AJ, et al. Lewy bodies in grafted neurons in subjects with Parkinson's disease suggest host-to-graft disease propagation. Nat Med 2008; 14: 501–503.

Li JY, Englund E, Widner H, Rehncrona S, Björklund A, Lindvall O, et al. Characterization of Lewy body pathology in 12- and 16-year-old intrastriatal mesencephalic grafts surviving in a patient with Parkinson's disease. Mov Disord 2010; 25(8): 1091-6.

Li JYH, Joyner AL. Otx2 and Gbx2 are required for refinement and not induction of mid-hindbrain gene expression. Development 2001; 128: 4979–4991.

Li W, Englund E, Widner H, Mattsson B, Van Westen D, Lätt J, et al. Extensive graft-derived dopaminergic innervation is maintained 24 years after transplantation in the degenerating

parkinsonian brain. Proc Natl Acad Sci U S A 2016; 113: 6544–6549.

Liang Q, Monetti C, Shutova M V., Neely EJ, Hacibekiroglu S, Yang H, et al. Linking a cell-division gene and a suicide gene to define and improve cell therapy safety. Nature 2018; 563: 701–704.

Lindvall O, Bjorklund A. Cell therapy in Parkinson's disease. NeuroRx 2004; 1: 382–393.

Lindvall O, Brundin P, Widner H, Rehncrona S, Gustavii B, Frackowiak R, et al. Grafts of fetal dopamine neurons survive and improve motor function in Parkinson's disease. Science 1990; 247: 574–577.

Lindvall O, Kokaia Z. Prospects of stem cell therapy for replacing dopamine neurons in Parkinson's disease. Trends Pharmacol Sci 2009; 30: 260–267.

Lindvall O, Rehncrona S, Brundin P, Gustavii B, Åstedt B, Widner H, et al. Human fetal dopamine neurons grafted into the striatum in two patients with severe parkinson's disease: A detailed account of methodology and a 6-month follow-up. Arch Neurol 1989; 46: 615–631.

Lundell MJ, Chu-Lagraff Q, Doe CQ, Hirsh J. The engrailed and huckebein genes are essential for development of serotonin neurons in the Drosophila CNS. Mol Cell Neurosci 1996; 7: 46–61.

Ma Y, Feigin A, Dhawan V, Fukuda M, Shi Q, Greene P, et al. Dyskinesia after fetal cell transplantation for parkinsonism: A PET study. Ann Neurol 2002; 52: 628–634.

Malumbres M. Cyclin-dependent kinases. Genome Biology 2014: 1–10.

Maxwell SL, Li M. Midbrain dopaminergic development in vivo and in vitro from embryonic stem cells. J Anat 2005; 207: 209–218.

Mccormick F. Cancer gene therapy: fringe or cutting edge? Nat Rev Cancer 2001; 1: 130–141.

Mendez I, Dagher A, Hong M, Gaudet P, Weerasinghe S, McAlister V, et al. Simultaneous intrastriatal and intranigral fetal dopaminergic grafts in patients with parkinson disease: A pilot study. Report of three cases. J Neurosurg 2002; 96: 589–596.

Mendez I, Sanchez-Pernaute R, Cooper O, Vinuela A, Ferrari D, Bjorklund L, et al. Cell type analysis of functional fetal dopamine cell suspension transplants in the striatum and substantia nigra of patients with Parkinson's disease. Brain 2005; 128: 1498–1510.

Moolten FL. Tumor Chemosensitivity Conferred by Inserted Herpes Thymidine Kinase Genes: Paradigm for a Prospective Cancer Control Strategy. Cancer Res 1986; 46: 5276–5281.

Moolten FL, Wells JM. Curability of tumors bearing herpes thymidine kinase genes transfered by retroviral vectors. J Natl Cancer Inst 1990; 82: 297–300.

Morgan RA. Live and let die: A new suicide gene therapy moves to the clinic. Mol Ther 2012; 20: 11–13.

Nefzger CM, Su CT, Fabb SA, Hartley BJ, Beh SJ, Zeng WR, et al. Lmx1a allows context-specific isolation of progenitors of GABAergic or dopaminergic neurons during neural differentiation of embryonic stem cells. Stem Cells 2012; 30: 1349–1361.

Niclis JC, Gantner CW, Alsanie WF, McDougall SJ, Bye CR, Elefanty AG, et al. Efficiently Specified Ventral Midbrain Dopamine Neurons from Human Pluripotent Stem Cells Under Xeno-Free Conditions Restore Motor Deficits in Parkinsonian Rodents. Stem Cells Transl Med 2017; 6: 937–948.

Niclis JC, Gantner CW, Hunt CPJ, Kauhausen JA, Durnall JC, Haynes JM, et al. A PITX3-EGFP Reporter Line Reveals Connectivity of Dopamine and Non-dopamine Neuronal Subtypes in Grafts Generated from Human Embryonic Stem Cells. Stem cell reports 2017; 9: 868–882.

Olanow CW, Goetz CG, Kordower JH, Stoessl AJ, Sossi V, Brin MF, et al. A double-blind

controlled trial of bilateral fetal nigral transplantation in Parkinson's disease. Ann Neurol 2003; 54: 403–414.

Olson L, Seiger Å. Development and growth of immature monoamine neurons in rat and man in situ and following intraocular transplantation in the rat. Brain Res 1973; 62: 353–360.

Olson L, Seiger Å. Brain tissue transplanted to the anterior chamber of the eye: 2. Fluorescence histochemistry of immature catecholamine and 5-hydroxytryptamine neurons innervating the rat vas deferens. Cell Tissue Res 1975; 158: 141–150.

Olson L, Seiger Ake. Brain tissue transplanted to the anterior chamber of the eye. Zeitschrift fur Zellforsch und Mikroskopische Anat 1972; 135: 175–194.

Ono Y, Nakatani T, Sakamoto Y, Mizuhara E, Minaki Y, Kumai M, et al. Differences in neurogenic potential in floor plate cells along an anteroposterior location: Midbrain dopaminergic neurons originate from mesencephalic floor plate cells. Development 2007; 134: 3213–3225.

Ou W, Li P, Reiser J. Targeting of herpes simplex virus 1 thymidine kinase gene sequences into the OCT4 locus of human induced pluripotent stem cells. PLoS One 2013; 8(11).

Park CH, Minn YK, Lee JY, Choi DH, Chang MY, Shim JW, et al. In vitro and in vivo analyses of human embryonic stem cell-derived dopamine neurons. J Neurochem 2005; 92: 1265–1276.

Parmar M, Li M. Early specification of dopaminergic phenotype during ES cell differentiation. BMC Dev Biol 2007; 7(86).

Perlow MJ, Freed WJ, Hoffer BJ, Seiger A, Olson L, Wyatt RJ. Brain grafts reduce motor abnormalities produced by destruction of nigrostriatal dopamine system. Science 1979; 204: 643–647.

Perrier AL, Tabar V, Barberi T, Rubio ME, Bruses J, Topf N, et al. Derivation of midbrain dopamine neurons from human embryonic stem cells. Proc Natl Acad Sci USA 2004; 101: 12543–12548.

Piccini P, Brooks DJ, Björklund A, Gunn RN, Grasby PM, Rimoldi O, et al. Dopamine release from nigral transplants visualized in vivo in a Parkinson's patient. Nat Neurosci 1999; 2: 1137–1140.

Piccini P, Lindvall O, Björklund A, Brundin P, Hagell P, Ceravolo R, et al. Delayed recovery of movement-related cortical function in Parkinson's disease after striatal dopaminergic grafts. Ann Neurol 2000; 48: 689–695.

Piccini P, Pavese N, Hagell P, Reimer J, Björklund A, Oertel WH, et al. Factors affecting the clinical outcome after neural transplantation in Parkinson's disease. Brain 2005; 128: 2977–2986.

Placzek M, Briscoe J. The floor plate: Multiple cells, multiple signals. Nat Rev Neurosci 2005; 6: 230–240.

Politis M. Dyskinesias after neural transplantation in Parkinson's disease: What do we know and what is next? BMC Med 2010; 8: 80.

Politis M, Oertel WH, Wu K, Quinn NP, Pogarell O, Brooks DJ, et al. Graft-induced dyskinesias in Parkinson's disease: High striatal serotonin/dopamine transporter ratio. Mov Disord 2011; 26: 1997–2003.

di Porzio U, Rougon G, Novotny EA, Barker JL. Dopaminergic neurons from embryonic mouse mesencephalon are enriched in culture through immunoreaction with monoclonal antibody to neural specific protein 4 and flow cytometry. Proc Natl Acad Sci USA 1987; 84: 7334–7338.

Prakash N, Wurst W. Development of dopaminergic neurons in the mammalian brain. Cell Mol Life Sci 2006; 63: 187–206.

Pruszak J, Sonntag K-C, Aung MH, Sanchez-Pernaute R, Isacson O. Markers and Methods for Cell Sorting of Human Embryonic Stem Cell-Derived Neural Cell Populations. Stem Cells 2007; 25: 2257–2268.

Rhinn M, Dierich A, Shawlot W, Behringer RR, Meur M Le, Ang SL. Sequential roles for Otx2 in visceral endoderm and neuroectoderm for forebrain and midbrain induction and specification. Development 1998; 125: 845–856.

Riddle R, Pollock JD. Making connections: The development of mesencephalic dopaminergic neurons. Dev Brain Res 2003; 147: 3–21.

Rong Z, Fu X, Wang M, Xu Y. A scalable approach to prevent teratoma formation of human embryonic stem cells. J Biol Chem 2012; 287: 32338–32345.

Roy NS, Cleren C, Singh SK, Yang L, Beal MF, Goldman SA. Functional engraftment of human ES cell-derived dopaminergic neurons enriched by coculture with telomerase-immortalized midbrain astrocytes. Nat Med 2006; 12: 1259–1268.

Samata B, Doi D, Nishimura K, Kikuchi T, Watanabe A, Sakamoto Y, et al. Purification of functional human ES and iPSC-derived midbrain dopaminergic progenitors using LRTM1. Nat Commun 2016; 7: 13097.

Saueressig H, Burrill J, Goulding M. Engrailed-1 and Netrin-1 regulate axon pathfinding by association interneurons that project to motor neurons. Development 1999; 126: 4201–4212.

Schuldiner M. Selective Ablation of Human Embryonic Stem Cells Expressing a 'Suicide' Gene. Stem Cells 2003; 21: 257–265.

Seo DO, Carillo MA, Lim SCH, Tanaka KF, Drew MR. Adult hippocampal neurogenesis modulates fear learning through associative and nonassociative mechanisms. J Neurosci 2015; 35: 11330–11345.

Shen Y, Huang J, Liu L, Xu X, Han C, Zhang G, et al. A compendium of preparation and application of stem cells in Parkinson's disease: Current status and future prospects. Front Aging Neurosci 2016; 8: 117.

Simon HH, Bhatt L, Gherbassi D, Sgadó P, Alberí L. Midbrain dopaminergic neurons: determination of their developmental fate by transcription factors. Ann N Y Acad Sci 2003; 991: 36–47.

Simon HH, Saueressig H, Wurst W, Goulding MD, O'Leary DDM. Fate of midbrain dopaminergic neurons controlled by the engrailed genes. J Neurosci 2001; 21: 3126–3134.

Singer BH, Jutkiewicz EM, Fuller CL, Lichtenwalner RJ, Zhang H, Velander AJ, et al. Conditional ablation and recovery of forebrain neurogenesis in the mouse. J Comp Neurol 2009; 514: 567–582.

Sonntag K-C, Pruszak J, Yoshizaki T, van Arensbergen J, Sanchez-Pernaute R, Isacson O. Enhanced Yield of Neuroepithelial Precursors and Midbrain-Like Dopaminergic Neurons from Human Embryonic Stem Cells Using the Bone Morphogenic Protein Antagonist Noggin. Stem Cells 2007; 25: 411–418.

Di Stasi A, Tey SK, Dotti G, Fujita Y, Kennedy-Nasser A, Martinez C, et al. Inducible apoptosis as a safety switch for adoptive cell therapy. N Engl J Med 2011; 365: 1673–1683.

Steinbeck JA, Choi SJ, Mrejeru A, Ganat Y, Deisseroth K, Sulzer D, et al. Optogenetics enables functional analysis of human embryonic stem cell-derived grafts in a Parkinson's disease model. Nat Biotechnol 2015; 33: 204–209.

Stoker TB, Torsney KM, Barker RA. Emerging treatment approaches for Parkinson's disease. Front Neurosci 2018; 12: 1–10.

Sun F, Wang X, Mao XO, Xie L, Jin K. Ablation of Neurogenesis Attenuates Recovery of Motor Function after Focal Cerebral Ischemia in Middle-Aged Mice. PLoS One 2012; 7(10): e46326.

Takahashi K, Yamanaka S. Induction of Pluripotent Stem Cells from Mouse Embryonic and Adult Fibroblast Cultures by Defined Factors. Cell 2006; 126: 663–676.

Thompson LH, Andersson E, Jensen JB, Barraud P, Guillemot F, Parmar M, et al. Neurogenin2 identifies a transplantable dopamine neuron precursor in the developing ventral mesencephalon. Exp Neurol 2006; 198: 183–198.

Thomson JA. Embryonic stem cell lines derived from human blastocysts. Science 1998; 282: 1145–1147.

Turrero García M, Chang Y, Arai Y, Huttner WB. S-phase duration is the main target of cell cycle regulation in neural progenitors of developing ferret neocortex. J Comp Neurol 2016; 524: 456–470.

Ungerstedt U. 6-hydroxy-dopamine induced degeneration of central monoamine neurons. Eur J Pharmacol 1968; 5: 107–110.

Ungerstedt U, Arbuthnott GW. Quantitative recording of rotational behavior in rats after 6-hydroxy-dopamine lesions of the nigrostriatal dopamine system. Brain Res 1970; 24: 485–493.

Ungerstedt U, Ljungberg T, Steg G. Behavioral, physiological, and neurochemical changes after 6-hydroxydopamine-induced degeneration of the nigro-striatal dopamine neurons. Adv Neurol 1974; 5: 421–426.

Wassarman KM, Lewandoski M, Campbell K, Joyner AL, Rubenstein JLR, Martinez S, et al. Specification of the anterior hindbrain and establishment of a normal mid/hindbrain organizer is dependent on Gbx2 gene function. Development 1997; 124: 2923–2934.

Wenning GK, Odin P, Morrish P, Rehncrona S, Widner H, Brundin P, et al. Short- and long-term survival and function of unilateral intrastriatal dopaminergic grafts in Parkinson's disease. Ann Neurol 1997; 42: 95–107.

Winkler C, Kirik D, Björklund A, Björklund A, Herman JP, Abrous ND, et al. Cell transplantation in Parkinson's disease: how can we make it work? Trends Neurosci 2005; 28: 86–92.

Wu C, Hong SG, Winkler T, Spencer DM, Jares A, Ichwan B, et al. Development of an inducible caspase-9 safety switch for pluripotent stem cell–based therapies. Mol Ther - Methods Clin Dev 2014; 1: 14053.

Wurst W, Auerbach AB, Joyner AL. Multiple developmental defects in Engrailed-1 mutant mice: An early mid-hindbrain deletion and patterning defects in forelimbs and sternum. Development 1994; 120: 2065–2075.

Xi J, Liu Y, Liu H, Chen H, Emborg ME, Zhang S-C. Specification Of Midbrain Dopamine Neurons From Primate Pluripotent Stem Cells. Stem Cells 2012; 30: 1655–1663.

Xia N, Fang F, Zhang P, Cui J, Tep-Cullison C, Hamerley T, et al. A Knockin Reporter Allows Purification and Characterization of mDA Neurons from Heterogeneous Populations. Cell Rep 2017; 18: 2533–2546.

Xiao X, Jin R, Li J, Bei Y, Wei T. The antitumor effect of suicide gene therapy using Bifidobacterium infantis-mediated herpes simplex virus thymidine kinase/ganciclovir in a nude mice model of renal cell carcinoma. Urology 2014; 84: 982(e15-e20).

Yan Y, Yang D, Zarnowska E.D, Du Z, Werbel B, Valliere C, et al. Directed differentiation of dopaminergic neuronal subtypes from human embryonic stem cells. Stem Cells 2005; 23: 781–790.

Yang D, Zhang Z-J, Oldenburg M, Ayala M, Zhang S-C. Human Embryonic Stem Cell-Derived

Dopaminergic Neurons Reverse Functional Deficit in Parkinsonian Rats. Stem Cells 2008; 26: 55–63.

Ye W, Shimamura K, Rubenstein JLR, Hynes MA, Rosenthal A. FGF and Shh signals control dopaminergic and serotonergic cell fate in the anterior neural plate. Cell 1998; 93: 755–766.

Yilong M, Tang C, Chaly T, Greene P, Breeze R, Fahn S, et al. Dopamine cell implantation in Parkinson's disease: Long-term clinical and 18 F-DOPA PET outcomes. J Nucl Med 2010; 51: 7–15.

Youssef M, Krish VS, Kirshenbaum GS, Atsak P, Lass TJ, Lieberman SR, et al. Ablation of proliferating neural stem cells during early life is sufficient to reduce adult hippocampal neurogenesis. Hippocampus 2018; 28: 586–601.

Zeng X, Cai J, Chen J, Luo Y, You Z-B, Fotter E, et al. Dopaminergic differentiation of human embryonic stem cells. Stem Cells 2008; 22(6): 925-40.

Zhao S, Maxwell S, Jimenez-Beristain A, Vives J, Kuehner E, Zhao J, et al. Generation of embryonic stem cells and transgenic mice expressing green fluorescence protein in midbrain dopaminergic neurons. Eur J Neurosci 2004; 19: 1133–1140.

Zhou W, Lee YM, Guy VC, Freed CR. Embryonic stem cells with GFP knocked into the dopamine transporter yield purified dopamine neurons in vitro and from knock-in mice. Stem Cells 2009; 27: 2952–2961.

Chapter 2.

Materials and Methods

2.1 Human pluripotent stem cell culture

hESC lines H1 (WA-01, WiCell, XY) and H9 (WA09, WiCell, XX) (Thomson *et al.*, 1998) and iPSC line RM3.5 (MCRI, XY) (Kao *et al.*, 2016) were maintained on Laminin-521 (5µg/ml, Biolamina) coated T25 flasks, that were pre-coated either at 37^{o}C for 2hrs or overnight at 4^{o}C. Media (mTeSR1, StemCell Technologies), supplemented with 0.5% penicillin-streptomycin (Life Technologies), was changed daily. The RM3.5 iPSC line was also cultured in 5% Knockout Serum Replacement (KSR, Life Technologies). Every 4-5 days cultures were passaged (at 70-80% confluence) with ReLeSR (StemCell Technologies) to small clusters of 5-50 cells at 1:10-1:20. All lines were frequently tested for mycoplasma (MycoAlert detection kit, Lonza), with all results negative. For long-term storage, hPSC were dissociated into small cell clumps using ReLeSR and resuspended in cryopreservation media consisting of 60% mTeSR1, 30% KSR and 10% dimethyl sulfoxide (DMSO, Life Technologies). Cell suspensions were transferred into a freezing container (Mr. Frosty^{TM}, ThermoFisher) stored at -80^{o}C and relocated to LN_2 for long storage once frozen. For resuspension into culture, frozen vials were rapidly thawed by a water bath and diluted in warmed mTeSR1 with the addition of Rock Inhibitor Y-27632 (ROCKi, Tocris Biosciences) before replating onto pre-coated T25 flasks. Thawed cells were passaged at least twice before experimental testing.

LMX1A- and PITX3-GFP hESC lines (H9 background), and CDK1-TK (H1 background) were generated as previously described (Watmuff *et al.*, 2015; Niclis *et al.*, 2017; Liang *et al.*, 2018), while the PITX3-GFP hiPSC line was a new cell line generated for experimental use in Chapter 5 and is described in greater detail below. Reporter lines were employed for the purification of LMX1A+ mDA progenitors and PITX3+ mDA precursors (Chapter 3), or to visualise and track transplanted PITX3+ mDA neurons (Chapter 5). The suicide line, CDK1-TK, was implemented to eliminate dividing cells from grafts (Chapter 4).

2.2 Generation of PITX3-eGFP hiPSC reporter line

Neon® electroporation of Donor and ZFN plasmids

To generate the new PITX3-GFP hiPSC line, confluent (70-90%) RM3.5 hiPSCs were harvested as a single-cell suspension using Accutase (SingleCell Technologies) and resuspended at a concentration of 1.0 x 10^7 cells/ml in Resuspension Buffer 'R' from the Neon® 100 µl kit (Invitrogen). Subsequent to a brief (5 min) incubation of 1 µg/1.0 x 10^6 cells of the *PITX3-eGFP-PGK-PURO* donor plasmid (originally a gift from Rudolf Jaenisch, Addgene deposit #31942; http://n2t.net/addgene:31942; RRID:Addgene_3194) from the *PITX3* CompoZr® Targeted integration kit (Sigma) on ice, equimolar ratios of supplied *PITX3* zinc-finger nuclease plasmids (*ZFN1* & *ZFN2*) were added and the sample transferred to a Neon® (Invitrogen) pipette using the Neon® tip, as per manufacturer's instructions. The cell suspension underwent electroporation under the following conditions optimized for PSCs; 1650V with 10ms pulse width and a pulse number of 3.

Expansion and screening of clones

Following electroporation, the cell suspension was diluted 1:3, 1:6 and 1:9 in mTeSR-1 supplemented with 5% KSR (ThermoFisher) and plated into 6-well plates pre-coated with Laminin-521. Media was changed after 24hrs with the addition of 0.5-1.0 µg of Puromycin to select for positive donor plasmid integration. Daily media changes of puromycin continued for a total of 13days, with large-scale cell death observed in all wells after 24 hours of exposure. Following 'puromycin selection', very small colonies began to form that expanded into large flat colonies in all wells after 3 days. Colonies (from the 1:9 dilution) were manually subcultured under a dissection microscope using a 23 needle and pipette, and replated in mTeSR1 supplemented with Y-27632 into duplicate wells of either 24- or 96-well plates

Expanded clones (for 6 days) were isolated using Accutase and genomic DNA (gDNA) was extracted using the ISOLATE II genomic isolation kit (Bioline). Following extraction according to manufacturer's specifications PCR was performed using the Phusion™ high fidelity RT-PCR kit (ThermoFisher) to confirm insertion at *PITX3* locus. Briefly, 20 ng gDNA (1 ng for vector control), 3% DMSO and all remaining kit reagents were combined with in-house designed primers amplifying through left homology arm of the donor plasmid. PCR of these samples was performed using a two-step amplification protocol with the Veriti™ thermal cycler (ThermoFisher) was programmed for 30 seconds at 98°C for initial

denaturation, 35 cycles of 10 seconds at 95°C for denaturation, 90 seconds at 72 °C for extension, and a final extension at 72°C for 10 min.

Following PCR, samples were mixed with 6x TriTrack loading dye (ThermoFisher) and separated by electrophoresis at 90 V for 45 minutes on a 1% (w/v) agarose gel in 1 x TAE buffer alongside HyperLadder™1 kb ladder (Bioline) & relevant controls. Gel was visualized at 340 nm using the UV imaging system (BioDoc-It), clones with successful integrates displayed bands at 984 bp. In addition, vector-only or human gDNA controls gave rise to bands at 1350 and 970 bp, respectively.

2.3 Neural differentiation

To initiate differentiation, confluent hPSCs (70-90%) were washed with $PBS^{Mg-/Ca-}$, dissociated into a single-cell suspension with accutase, and resuspended in mTeSR1 supplemented with ROCK inhibitor Y-27632 (10µM). Dissociated cells were seeded at an optimized density (0.225-0.375 x $10^6/cm^2$), determined for each individual cell line, to ensure 100% confluence by the next day. Prior to differentiation, cultures were washed twice with $PBS^{Mg-/Ca-}$ to eliminate remaining mTeSR1 media and differentiation started approximately 24hrs after seeding. For both protocols (Figure 2.1), dual SMAD inhibition (SB, 10mM; LDN, 200nM) was utilized from day 0-11 (D0-D11) to induct cells towards a neuroectodermal origin. For the DA protocol, a serum replacement media (SRM: DMEM/F12 + GlutaMax, 15% knockout serum replacement, 1% NEAA, 0.2% β-mercaptoethanol, 0.5% penicillin-streptomycin) that transitioned into a N2 media (DMEM/F12, 1% N2, 1% ITS-A, 1% NEAA, 0.5% penicillin-streptomycin) from D5 was utilised. For forebrain differentiation, cells were cultured in media consisting of (1:1) DMEM/F12: Neurobasal, 0.5% B27+vitA, 0.5% N2, 0.5% ITS-A, 1% GMAX, 0.5% penicillin streptomycin and 0.1% β-mercaptoethanol.

To direct cells towards a mDA progenitor phenotype, sonic hedgehog signaling was activated from D1-D7 (100ng/ml SHH C2II and 2µM purmorphamine, PM) in addition to the canonical Wnt agonist CHIR99021 from D3-13 (3µM) to promote caudalisation. Media was changed every 24 hours for the first 7days of the differentiation, to counteract small changes in morphogen concentration that may impact on patterning efficiencies, and every second day thereafter. At D11, vm progenitors were cultured in 1:1 DMEM/F12:NBM, 2% B27+vitA, 1% ITS-A, 0.5% GlutaMAX, 0.5% penicillin-streptomycin supplemented with recombinant

human glial cell-line derived factor (20ng/ml; R&D systems), recombinant brain-derived neurotrophic factor (20ng/ml, R&D system), transforming growth factor β3 (1 ng/ml; PeproTech), DAPT (10 µM, Sigma-Aldrich), ascorbic acid (200nM; Sigma-Aldrich) and dibutyryl cAMP (0.05mM; Tocris Bioscience), subsequently referred to as 'maturation media'. hPSCs specified towards a pan-forebrain progenitor fate were supplemented with FGF2 (20ng/ml) from D11-17. Forebrain neural progenitors were passaged very 5-6 days from D11 until the day of transplantation. Pan-forebrain progenitors were generated to form a proliferative neural progenitor pool to spike into VM progenitors at the time of transplantation – to assess the efficacy of the suicide gene to ablate dividing cells (Chapter 4). To assess the efficiency of the differentiations, *in vitro* cultures were fixed at defined endpoints with 4% paraformaldehyde (PFA) in 0.4M Sorensen's buffer, pH 7.3 for 10minutes. Cultures were subsequently washed with PBS $^{Mg-/Ca-}$ and kept in PBS with Sodium Azide (PBS Azide, 0.02%) at 4^{o}C for long-term storage.

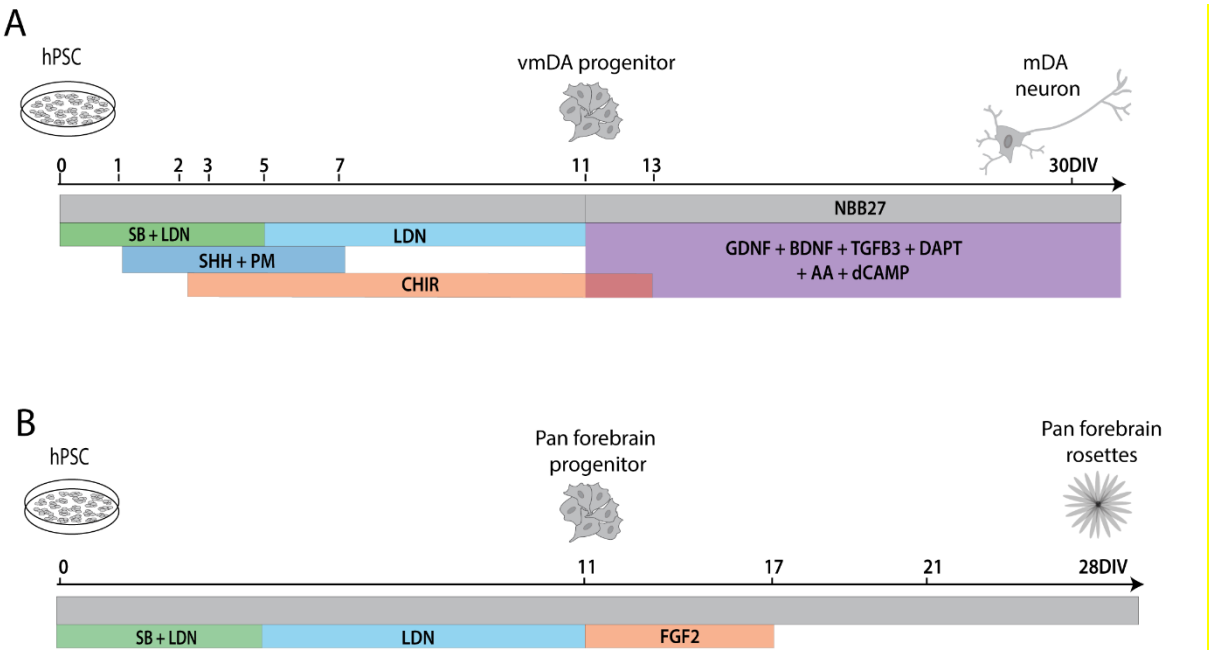

Figure 2.1 Schematic of midbrain DA and pan-forebrain neural differentiation protocols.
(A) mDA neuron differentiation. Dual-SMAD inhibition (SB, LDN) of hPSCs initiated neuroectodermal progenitor formation. Generation of floor-plate midbrain progenitors was subsequently achieved by SHH and PM to ventralise, in combination with caudalisation by the Wnt agonist, CHIR. Progenitors transitioned into a maturation media (purple) for differentiation into mature DA neurons. **(B)** Pan-forebrain progenitor specification. hPSCs exposed to dual smad inhibition formed pan-forebrain progenitors, that were expanded and matured into rosettes with the addition of FGF2. Abbreviations: Dual smad inhibitors - SB43152 (SB) and LDN193189 (LDN); Ventralising compounds - Sonic Hedgehog (SHH), purmorphamine (PM); Caudalising factors - CHIR99021 (CHIR); Dorsalisation factor - fibroblast growth factor (FGF2); Culture maturation - Glial-cell line derived neurotrophic factor (GDNF), brain-derived neurotrophic factor (BDNF), transforming growth factor β3 (TGFβ3), N-[N-(3,5-Difluorophenacetyl)-L-alanyl]-S-phenylglycine t-butyl ester (DAPT), ascorbic acid (AA), dibutyryl cAMP (dCAMP).

2.4 Fluorescent-activated cellular sorting

For FACS isolation of select populations (Chapter 3), differentiating vm cells were dissociated to single cells using Accutase (10-20minutes). Collected cell were resuspended in sorting buffer containing 90% maturation media, 10% KSR, Y-27632 (10µM) and 4'-6-Diamidino-2-Phenylindole (DAPI, 1µg/ml) at a density of 5-8x10^6 cells/ml. Cells were filtered through cell strainer cap (35µM mesh, Falcon) to remove the presence of cell doublets and/or clusters. Sorting was performed on a MoFlo XDP cell sorter (Beckman Coulter, MoFlo) at the Murdoch Children's Research Institute core facility or a FACS Aria III (BD) using a 100µM nozzle and a sheath pressure between 17-22 psi. A highly restrictive gating strategy, to exclude doublets and debris based on forward and side-scatter parameters as well as dead cells using the viability marker DAPI. Background auto-fluorescence was compensated for by an empty auto fluorescence channel (FL2-580/30), and a parental H9 (non $GFP^{cell\ line}$) sample time-matched in the vm differentiation was employed as a control to quantify and/or select GFP^+ and GFP^- cells. Single stain, secondary only or unstained controls were implemented were appropriate. FACS-isolated cell fractions were either (i) replated at 300,000 cells/cm^2 in 96-well plates and fixed after 6 hours, or passed back through the FACS machine - both targeted at confirming efficacy of the FACS isolation, or (ii) were resuspended in maturation media containing Y27632 (10µM) in preparation for transplantation. Flow cytometric analysis was conducted using FlowJo software.

2.5 Drug-induced ablation of cellular proliferation

Ganciclovir (GCV, Roche) was utilized to ablate dividing cells in culture and/or following transplantation (Chapter 4), given its ability to bind to DNA as a guanosine analog to cause cell cycle arrest. GCV was dissolved in sterile phosphate buffered saline (PBS, Life Technologies) to a final concentration of 10mg/ml. GCV was stored for up to 5 days at 4oC, or at -20oC for long-term storage. For ablation of either hPSCs or differentiated VM progenitors *in vitro*, cultures were changed daily with fresh media containing GCV at defined doses (1-50µM). Cells were exposed for a duration of 2-10 days. Following cell transplantation, intraperitoneal injections of GCV (50-100mg/kg) were administered (once or twice daily) to 6-hydroxydopamine (6-OHDA) lesioned rats. Animals were injected for a total of 8 weeks at predetermined intervals after transplantation.

2.6 Animal and Ethics approval

All animal procedures were conducted in agreement with the Australian National Health and Medical Research Council's published Code of Practice for the Use of Animals in Research, and experiments approved by The Florey Institute of Neuroscience and Mental Health Animal Ethics committee. Athymic nude mice (BALB/c-*Foxn1*^{nu}/Arc) and rats (CBH^{rnu}) were provided by the Animal Resource Centre (Canning Vale, Western Australia). Nude rodents have a severely under-developed adaptive immune system (due to a mutation in the Foxn1 gene and consequential T-lymphocyte deficiency) which avoided the need for long-term administration of immunosuppressive drugs in xeno-grafting studies. Both male and female adult rodents (>8 weeks of age) were used without preference. Animals were group housed (3-5 per cage) in individually ventilated cages on a 12:12-hour light/dark cycle with *ad libitum* access to food and water. All animal procedures were conducted in specific pathogen-free rooms.

2.7 Stereotaxic surgery

Employing a stereotaxic approach ensured precise and targeted delivery of both toxins and cells into the rodent brain (see Thompson and Parish, 2013). Under inhalant anaesthetic (2-5% isoflurane), rodents were placed in a stereotaxic frame to maintain a fixed skull position, with a nose cone attachment to provide persistent isoflurane administration (1.5-2%) throughout surgery. Rodents were administered analgesia (3mg/kg, meloxicam) to reduce post-operative pain, before a single incision was made along the midline of the scalp to expose the surface of the skull and bregma (an imperative landmark located at the junction between the occipital and parietal bones). All stereotaxic coordinates were taken relative to the location of bregma (see Table 2.1, Paxino and Franklin, 2004; Paxino and Watson, 2004). Delivery of either cells or toxin were administered by a cannula. The injection cannula consisted of a fine, pulled glass cannula (Harvard Instruments) tightly fitted to a micro-volume syringe (Hamilton) by a heated sleeve. A small burr hole was drilled in the skull and the cannula slowly lowered beneath the dura to the desired location (refer to Table 2.1).

A flow rate of 1µL/min was used and the cannula left in place for a few minutes to allow for complete diffusion and prevent backflow, before slowly withdrawing. The skin surrounding the midline of the scalp was sutured and antiseptic (Iodine solution, Betadine) applied to the wound site. Animals were checked daily for one week after surgery to monitor recovery.

Use	Deposit	Target site	AP	ML	DV	Animal	Chapter
6-OHDA lesion	Single	Substantia nigra	+3.0	±1.2	-4.2	Mouse	3,5
Cell transplant	Single	Striatum	+1.0	±2.3	-3.2	Mouse	3,5
6-OHDA lesion	Single	Medial forebrain bundle	-4.4,	±1.2	-7.8	Rats	3,4
Cell transplant	Single	Striatum	+0.5	±2.5	-4	Rats	3,4
Cell transplant	Multiple	Striatum	+0.5 +0.5 -0.5 -0.5	-3.0 -3.0 -3.0 -3.0	-3.5 -5.0 -3.5 -5.0	Rats	4

Table 2.1: Rodent stereotaxic coordinates. Anterior-posterior (AP) and medio-lateral (ML) coordinates relative to bregma. Dorso-lateral (DV) coordinates relative to the dura surface.

2.7.1 6-hydroxydopamine lesioning

To selectively ablate the host midbrain dopaminergic circuitry on one hemisphere of the brain, as a model of the dopamine depletion in PD, the catecholamine-selective neurotoxin, 6-hydroxydopamine (6-OHDA, Sigma-Aldrich) was dissolved in sterile saline containing 0.02% ascorbic acid (Sigma), with the solution stored in the dark and on ice for the duration of the surgery to prevent oxidation. A unilateral stereotaxic injection of 6-OHDA was made into the right medial forebrain bundle (MFB) for rats (3.5µl, 3.2µg/µl), or directly into the right substantia nigra for mice (1.5µl, 1.6µg/µl). 6-OHDA induced loss of DA neurons within the midbrain and consequential denervation of the striatum, as confirmed by TH immunoreactivity (Figure 2.2). This dopamine depletion induced motor deficits (described in section 2.8).

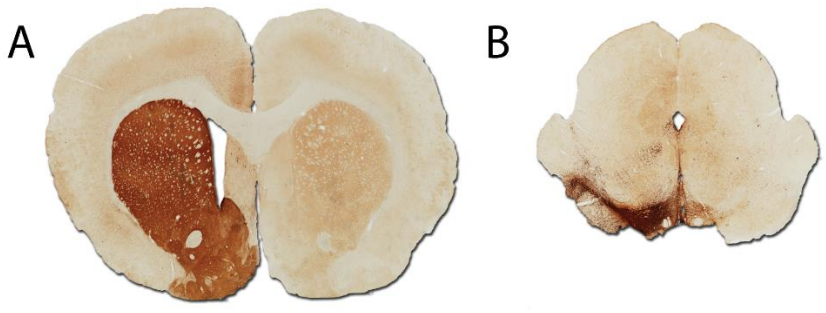

Figure 2.2 Unilateral 6-OHDA ablation of midbrain dopaminergic circuitry
Stereotaxic injection of 6-OHDA into the median forebrain bundle leads to irreversible loss of DA neuron cell bodies in the substantia nigra **(B)** and subsequent DA fibres and terminals in the striatum **(A).**

2.7.2 Cell transplantation

VM progenitors were transplanted into the striatum of rodents at different stages of differentiation (13, 19, 21, 22, 25, 30 DIV) – dependent on the study. Animals received a unilateral injection (1µL or 1.5 µL) of cells into the denervated striatum, eight weeks after lesioning according to the coordinates and details listed in Table 2.2.

Cell type	Differentiation age	Pre-treatment	Transplant	Chapter
mDA progenitors/ precursors	21DIV (mDA)	FACS	100K	3
Co-transplant: VM/pan forebrain progenitors	20DIV (mDA) 25DIV (FB)	GCV GCV	135K 15K	4
mDA progenitors/ precursors/neurons	13, 19, 22, 25, 30DIV (mDA)	-	100K	5

Table 2.2: Details of the cellular age, identity, pre-treatment and number transplanted into 6-OHDA rodents

2.8 Behavioural assessment of amphetamine rotations

Functional impact of unilateral lesioning of the nigrostriatal pathway, and motor rescue by transplanted mDA neurons can be measured by turning behavior in response to pharmacological DA stimulation. This amphetamine-based rotation test was assessed in Chapters 3 and 4. Nude rats received a single intraperitoneal injection of D-amphetamine sulphate (5mg/kg, Tocris Bioscience) and were habituated for 10 minutes before being placed in a harness within the rotometer (Accuscan Instruments) - a clear, circular chamber, employed to facilitate assessment of the number of full (360^{o}) body rotations taken in either direction. The number of rotations was recorded over a 60-minute. Unilateral lesioning of the nigrostriatal pathway leads to a deficit on the ipsilateral side (causing preferential turning behavior towards the side of the lesion). Animals that achieved >5 rotations per min across two separate testing rounds were included in the study. For any given study, animals ranked according to their total rotations and evenly stratified across treatment groups. All behavioural testing of rats was conducted with the experimenter blinded to the treatment conditions.

2.9 Transcardial perfusion and tissue processing

At desired study endpoints, animals received a lethal intraperitoneal injection of sodium pentobarbitone (100mg/kg). To ensure rapid and uniform preservation of the brain tissue,

animals were transcardially perfused with pre-warmed tyrode solution (37°C) followed by 4% paraformaldehyde (PFA). Subsequently, the brain was removed and post-fixed in PFA (2 hours) before being stored in a 20% (w/v) sucrose solution (made up in 0.1M phosphate buffer) at 4^{o}C. Cryosections of the fixed brains were generated on a freezing microtome (Leica) on a coronal plane at a thickness of 40µM in a 12 series (1:12). Sections were stored in a cryoprotectant solution (15% sucrose solution, 30% ethylene glycol, 25% 0.1M PBS and 25% distilled water) in multi-well plates at -20^{o}C.

2.10 Immunohistochemistry

Immunohistochemical analysis was performed on fixed cultures or free-floating coronal sections for volumetric analysis, cellular characterization or fiber measurements.

2.10.1 Chromagenic immunohistochemistry

Free-floating sections were washed (3x) in $PBS^{Mg-/Ca-}$ to ensure removal of residual cryoprotectant. For chromogenic labelling, the tissue was incubated in PBS containing 3% H_2O_2 and 10% Methanol for 20 minutes to quench endogenous peroxidase activity. Subsequent to 3x $PBS^{Mg-/Ca-}$ washes, sections were incubated overnight at room temperature with $PBS^{Mg-/Ca}$ Azide containing 5% donkey serum and 0.3% Triton-X (PADT) and primary antibody (according to Table 2.3). Tissue sections were agitated by a rocker to ensure consistent immersion of the sample. After overnight incubation, samples were washed 3x in $PBS^{Mg-/Ca-}$ and incubated in blocking solution containing 5% donkey serum for one hour to reduce non-specific protein binding, before a biotinylated secondary antibody (see Table 2.4) was applied for two hours. After washing, samples were incubated with avidin biotin peroxidase complex (ABC; Vectastain, Vector Laboratories) for 90 minutes to amplify the signal. Tissue was washed and then briefly exposed to 3'-3'di-amino-benzidine (0.5mg/ml, Sigma) for 2-4 minutes, followed by 1% H_2O_2 for up to 2mins to catalyse the production of a brown product and enable visualization of the graft. The tissue was again washed before mounting on gel slides and left to dry overnight. The slides containing the tissue sections were dehydrated in graded alcohol washes, cleared using xylene (OilChem) and coverslipped with DePeX mounting media (BDH Chemicals).

2.10.2 Fluorescent immunohistochemistry

For fluorescent labelling, both fixed cultures and free-floating sections were washed (3x) in $PBS^{Mg-/Ca-}$ and incubated overnight in PADT containing primary antibodies (Table 2.3).

Antibody	Species	Dilution	Supplier	Catalogue #	Target
5HT	Rabbit	1:1000	Immunostar	20080	Serotonergic neurons
Adenomatous polyposis coli, clone CC1 (APC/CC1)	Mouse	1:200 + strep	Abcam	ab16794	Oligodendrocytes
BARHL1	Rabbit	1:200	Novus Biologicus	NBP1-86513	Ventral diencephalon/midbrain
CALBINDIN-C28K	Mouse	1:1000	Swant	CB300	DA neuron subtype
ChAT	Goat	1:100	Millipore	AB144P	Cholinergic neurons
CLAUDIN V	Rabbit	1:100	Abcam	AB53765	Blood vessel tight junctions
DAPI	-	1:5000	Sigma Aldrich	D8417	DNA
DBH	Mouse	1:5000	Millipore	MAB308	Dopamine
DOUBLECORTIN	Goat	1:1000	Santa Cruz	sc-8066	Dividing neuroblast
FOXA2	Goat	1:200	Santa Cruz	sc-6554	DA progenitor
GFAP	Rabbit	1:1000	DAKO	ZO334	Astrocytes
GFP	Chicken	1:1000	Abcam	AB13970	
GFP	Rabbit	1:20000	Abcam	AB290	
GIRK2	Rabbit	1:500 + strep	Alomone Labs	APC-OO6	DA neuron subtype
HNA	Mouse	1:300	Millipore	MAB1281	Human nuclei
KI67	Rabbit	1:1000	ThermoFisher	LBVRM-9106-S1	Proliferative cells
MAP2	Rabbit	1:1000	Millipore	AB5622	Mature neuron
NCAM	Mouse		Santa Cruz	sc-106	Neural cells
NESTIN	Mouse	1:1000	Millipore	MAB1259	Neural progenitors
NEUN	Rabbit	1:1500	R&D Systems	AB104225	Neurons
NURR1	Rabbit	1:200	Santa Cruz	sc-990	DA progenitors
OCT4	Mouse	1:100	Santa Cruz	sc-5279	Stem cells
OTX2	Goat	1:500	R&D Systems	RDSAF1979	DA progenitors
PAX6	Mouse	1:50	DSHB	PAX6-s	Dorsal telencephalon
PH3	Rat	1:1000	Abcam,	AB10543	Mitosis
PITX2	Sheep	1:200	R&D Systems	AF7388	Ventral diencephalon/midbrain
RECA	Mouse	1:5000	Abd Serotec	MCA970R	Blood vessels
RFP	Rabbit	1:1000	Rockland Labs	600-901-379	
SOX2	Goat	1:300	R&D Systems	AF2018	Neural progenitors
TH	Rabbit	1:1000	Pelfreeze	P40101-0	DA neurons
TH	Sheep	1:800	Pelfreeze	P60101-0	DA neurons
TUJ1	Mouse	1:1000	Promega	G712A	Neurons

Table 2.3. Primary antibodies – details of concentration, specificity and supplier

Antibody	Species	Concentration	Source
AlexaFluor-488	Rabbit, mouse, goat, sheep, chicken	1:200	Jackson ImmunoResearch
DyLight-555	Rabbit, mouse, goat, sheep, chicken	1:200	ThermoFisher
AlexaFluor-647	Rabbit, mouse, goat, sheep, chicken	1:200	Jackson ImmunoResearch
Biotin	Rabbit, mouse	1:500	Jackson ImmunoResearch
Streptavidin conjugated	Rabbit	1:500	Jackson ImmunoResearch

Table 2.4. Secondary antibodies - details of species, concentration and source.

Following washes, tissue was blocked for one hour in PADT, and then incubated with secondary antibodies (all raised in donkey, see Table 2.4) in the dark for two hours. A final incubation of 4'-6'-diamidino-2-phenylindole (DAPI) for 15 minutes was applied, before fluorescence stained sections were mounted onto gel slides and coverslipped with fluorescent mounting media (DAKO).

2.11 Microscopy and Quantification

Brightfield images of chromogenic staining were obtained using a Leica DM6000 upright microscope. Manual live counting was performed on a Zeiss Axiovert 200 upright microscope. Fluorescence images were acquired on a Carl Zeiss Axio Observer Z.1 upright, epifluorescence or a Carl Zeiss LSM 780 confocal microscope. Light intensity, camera and imaging settings were maintained consistent across all groups for each given analysis. All quantifications were performed with the experimenter blinded to the treatment conditions (i.e. the butt of the slides covered). Scale bars have been included in figures as appropriate.

2.11.1 Phenotype characterisation: High power (20x) z-stacked sampled images were captured to quantify total number of cells either in culture or within the graft. For *in vitro* analysis, images were acquired from three technical replicates (each taken from individual wells) and repeated across three independent culture experiments. For *in vivo* analysis, field of view (FOV) images were taken from 2-3 graft sections for each individual animal. DAPI *(in vitro*) or human nucleic acid (*in vivo*) antibodies were used to quantify total cell number, and proteins of interest were assessed subsequently to determine a relative proportion. Manual counting was performed with Zen 2 Blue edition (Carl Zeiss) and Photoshop (Adobe) software. The average density of immunoreactive pixels for each FOV image taken for individual biological replicate, in addition to technical replicates was averaged to generate a single value for each assessment e.g. for assessment of TH density of innervation.

2.11.2 Volumetric analysis: The human-specific antibody, NCAM, that specifically reacts with human graft-derived cells, delineated the boundaries of the graft to enable volumetric assessment. Brightfield images were captured across the rostral-caudal axis to include all chromogenic sections (1:12 series) containing human cells. Assessment of the graft area for each individual image was quantified using Leica application suite software. The sum of these

values were then corrected to consider series sectioning, and graft volume was estimated based on Cavalieri's principle (Rosen and Harry, 1990).

2.11.3 Total GFP and TH quantification: Manual counting of LMX1A-GFP$^+$, PITX3-GFP$^+$ and TH+ cell bodies were conducted from live brightfield images at 20x magnification on an upright Axiovert (Zeiss) microscope. Cells were marked and quantified on Cell^D (Olympus) software. Total cells were adjusted based on serial sectioning (1:12).

2.11.4 DA subtype specification: To quantify A9- or A10- subtype specification, dopamine (DA) neurons were first identified by either GFP or TH immunoreactivity and assessed for co-localisation with GIRK2 (G-protein-gated inwardly rectifying K+ channel (subunit 2)) and/or Calbindin. Confocal images of grafts at 1:12 series were captured on a Zeiss LSM780. GIRK2 was employed as a marker of A9 dopaminergic neurons, located primarily in the substantia nigra pars compacta (SNpc), whereas Calbindin is expressed on A10 DA neurons that reside in the ventral tegmental area (VTA). mDA neurons were grouped as either GIRK2$^+$(A9-like), Calbindin$^+$(A10-like) or GIRK2$^+$/Calbindin$^+$ - a population also reflective of SN DA neurons within the human brain (Reyes *et al.*, 2012). Quantified data was represented as a percentage of total DA neurons.

2.11.5 TH and GFP optical fibre density measurements: 40x brightfield (10) z-stacked images were captured and compressed by a Leica DM600 in triplicate. Assessment of fiber density was sampled at specific regions of interest (dorsolateral striatum, motor cortex, pre-frontal cortex and perirhinal cortex for dopaminergic targets, as well as the non-dopaminergic targets - periventricular nucleus and the hippocampi contralateral to the graft). Colour inverted images were obtained using the 'colour range' tool on Photoshop (Adobe) to quantify the total number of reactive/unreactive pixels. Total fibre innervation was expressed as a percentage of GFP- or TH-immunoreactive pixels, taken as an average from three representative images for each brain.

2.12 Statistical analysis

All data was collected in an Excel (Microsoft Office) spreadsheet and are presented as mean $\pm$ SEM. Statistical tests employed were inclusive of one-way ANOVA with Tukey's multiple comparisons, student t-tests, two-way ANOVA with Bonferroni correction or Pearson's correlation coefficient test. The number of animals/groups are stated in the figure legends

appropriately. Corrections for multiple comparisons were implemented as appropriate. Alpha levels of $p<0.05$ were considered statistically significant with all statistical analysis performed using GraphPad Prism 8. *$p < 0.05$, **$p < 0.01$, ***$p < 0.001$ and ****$p < 0.0001$.

2.13 References

Kao T, Labonne T, Niclis JC, Chaurasia R, Lokmic Z, Qian E, et al. GAPTrap: A Simple Expression System for Pluripotent Stem Cells and Their Derivatives. Stem Cell Reports 2016; 7: 518–526.

Liang Q, Monetti C, Shutova M V., Neely EJ, Hacibekiroglu S, Yang H, et al. Linking a cell-division gene and a suicide gene to define and improve cell therapy safety. Nature 2018; 563: 701–704.

Niclis JC, Gantner CW, Alsanie WF, McDougall SJ, Bye CR, Elefanty AG, et al. Efficiently Specified Ventral Midbrain Dopamine Neurons from Human Pluripotent Stem Cells Under Xeno-Free Conditions Restore Motor Deficits in Parkinsonian Rodents. Stem Cells Transl Med 2017; 6: 937–948.

Paxino G and Franklin K. The mouse brain in stereotaxic coordinates (London:Academic). 2004.

Paxino G and Watson C. The rat brain in stereotaxic coordinates (London: Elsevier Academic). 2004.

Reyes S, Fu Y, Double K, Thompson L, Kirik D, Paxinos G, et al. GIRK2 expression in dopamine neurons of the substantia nigra and ventral tegmental area. J Comp Neurol 2012; 520: 2591–2607.

Rosen GD, Harry JD. Brain volume estimation from serial section measurements: a comparison of methodologies. J Neurosci Methods 1990; 35: 115–124.

Thompson LH, Parish CL. Transplantation of Fetal Midbrain Dopamine Progenitors into a Rodent Model of Parkinson's Disease. Methods Mol Biology. 2013; 1059: 169-80.

Thomson JA, Itskovitz-Eldor, J. Shapiro SS, Waknitz MA, Swiergiel JJ, Marshall VS, Jones JM. Embryonic stem cell lines derived from human blastocysts. Science. 1998; 282: 1145–1147.

Watmuff B, Hartley BJ, Hunt CPJ, Fabb SA, Pouton CW, Haynes JM. Human pluripotent stem cell derived midbrain PITX3$^{eGFP/w}$ neurons: A versatile tool for pharmacological screening and neurodegenerative modeling. Front Cell Neurosci 2015; 9: 104.

de Luzy, I.R., Niclis, J.C., Gantner, C.W., Kauhausen, J.A., Hunt, C.P.J., Ermine, C., Pouton, C.W., Thompson, L.H., and Parish, C.L. (2019). Isolation of LMX1a Ventral Midbrain Progenitors Improves the Safety and Predictability of Human Pluripotent Stem Cell-Derived Neural Transplants in Parkinsonian Disease. Journal of Neuroscience *39(48)*, 9521-9531. Impact factor: 6.07

Chapter 3.

Isolation of LMX1a ventral midbrain progenitors improves the safety and predictability of human pluripotent stem cell-derived neural transplants in Parkinsonian Disease

Isabelle R. de Luzy[1], Jonathan C. Niclis[1], Carlos W. Gantner[1], Jessica A. Kauhausen[1], Cameron P.J. Hunt[1,2], Charlotte Ermine[1], Colin W Pouton[2], Lachlan H. Thompson[1] and Clare L. Parish[1]

[1] The Florey Institute of Neuroscience and Mental Health, Parkville, Victoria, Australia.

[2] Monash Institute of Pharmaceutical Sciences, Monash University, Parkville, Victoria, Australia.

3.1 Abstract

Human pluripotent stem cells (hPSC) are a promising resource for the replacement of degenerated ventral midbrain dopaminergic (vmDA) neurons in Parkinson's disease. Despite recent advances in protocols for the *in vitro* generation of vmDA neurons, the asynchronous and heterogeneous nature of the differentiations results in transplants of surprisingly low vmDA neuron purity. As the field advances towards the clinic it will be optimal, if not essential, to remove poorly specified and potentially proliferative cells from donor preparations to ensure safety and predictable efficacy. Here, we utilize two novel hPSC knock-in reporter lines expressing GFP under the LMX1A and PITX3 promoters, to selectively isolate vm progenitors and DA precursors, respectively. For each cell line, Unsorted, GFP+ and GFP- cells were transplanted into male or female Parkinsonian rodents. Only rats receiving Unsorted cells, LMX1A-eGFP+ or PITX3-eGFP- cell grafts showed improved motor function over 6 months. Post-mortem analysis revealed small grafts from PITX3-eGFP+ cells, suggesting these DA precursors were not compatible with cell survival and integration. In contrast, LMX1A-eGFP+ grafts were highly enriched for vmDA neurons, and importantly excluded expansive proliferative populations and serotonergic neurons. These LMX1A-eGFP+ progenitor grafts accelerated behavioural recovery and innervated

developmentally appropriate forebrain targets whilst LMX1A-eGFP- cell grafts failed to restore motor deficits, supported by increased fibre growth into non-dopaminergic target nuclei. This is the first study to employ a hPSC-derived reporter line to purify vm progenitors, resulting in improved safety, predictability of the graft composition, and enhanced motor function.

3.2 Significance statement

Clinical trials have shown functional integration of transplanted fetal-derived dopamine progenitors in Parkinson's disease. Human pluripotent stem cell (hPSC)-derived midbrain progenitors are now being tested as an alternative cell source, however, despite current differentiation protocols generating >80% correctly specified cells for implantation, resultant grafts contain a small fraction of dopamine neurons. Cell sorting approaches, to select for correctly patterned cells prior to implantation, are being explored – yet has been suboptimal to date. This study provides the first evidence of using 2 hPSC reporter lines (LMX1A-GFP and PITX3-GFP) to isolate correctly specified cells for transplantation. We show LMX1A-GFP+, but not PITX3-GFP+, cell grafts are more predictable - with smaller grafts, enriched in dopamine neurons, showing appropriate integration and accelerated functional recovery in Parkinsonian rats.

3.3 Introduction

Clinical studies, employing human fetal tissue enriched with dopaminergic (DA) progenitors, have provided the necessary evidence that new DA neurons transplanted into the brains of Parkinson's disease (PD) patients can functionally integrate and alleviate motor symptoms for decades (Barker *et al.,* 2013). Poor standardisation procedures, limited tissue availability and ethical consideration associated with the use of fetal tissue has resulted in a shift towards the use of human pluripotent stem cells (PSC) to generate donor cells. Despite significant advancements in ventral mesencephalic differentiation protocols in recent years (Denham *et al*., 2012; Kirkeby *et al.,* 2012; Kriks *et al*., 2011; Niclis *et al.,* 2017), cultures remain asynchronous and heterogeneous, with even the most advanced current protocols reporting ~10-15% of cells fail to adopt a vm progenitor fate at times amenable to transplantation (Kirkeby *et al.,* 2017; Niclis *et al.,* 2017). While this appears to represent a relatively high specification efficiency, upon transplantation studies report low yields of tyrosine hydroxylase-expressing DA neurons within the grafts (Doi *et al*, 2014, Kirkeby *et al*, 2017,

2017, Kriks *et al*, 2011, Niclis *et al*, 2017b, Samata *et al*, 2016). These observations indicate significant expansion of other vm progenitors not destined to become DA neurons as well as proliferation of incorrectly specified non-dopaminergic progenitors *in vivo* that may also pose a risk of neural overgrowths/tumours. One also recognises the risk of incorrectly specified neuronal populations, such as serotonergic neurons within grafts, that may induce dyskinetic behaviours (Carlsson *et al.*, 2007; Politis *et al.*, 2011).

A key strategy to overcome such conundrums and ensure the reproducible generation of safe and predictable cell products for clinical translation is to selectively enrich for appropriately specified vm progenitors prior to transplantation. While a number of rodent studies have successfully isolated vm progenitors, using reporter mice/cell lines and antibodies targeted against extracellular proteins - employing both fluorescent activated cell sorting (FACS) as well as magnetic beads (MACS) (Fukuda *et al.*, 2006; Thompson *et al.*, 2006; Hedlund *et al.*, 2008; Jönsson *et al.*, 2009; Ganat *et al.*, 2012; Nefzger *et al.*, 2012; Bye *et al.*, 2015), isolation from human PSC cultures has been met with variable success. In part, this has been due to breadth of expression of the transgene/protein, timing of expression of the gene/protein and hence progenitor isolation occurring weeks prior to transplantation, and/or suboptimal specificity (or availability) of antibodies for human cells (Aguila *et al.*, 2014; Doi *et al.*, 2014; Samata *et al.*, 2016; Lehnen *et al.*, 2017).

With the field rapidly advancing to the clinic (Barker *et al.*, 2017), there is a persistent and inherent need to identify a reliable candidate marker for the enrichment of DA progenitors from human PSC-derived vm cultures. Here we assessed the capacity to isolate vm progenitors and DA precursors based upon two cardinal genes involved in vmDA development – LMX1A, an early vm determinant (Yan *et al.*, 2005; Andersson *et al.*, 2006) and PITX3, a gene required for the post mitotic maturation of DA (Smidt *et al.*, 2004). Both genes have been used to isolate vm progenitors/precursors from mouse ESC cultures (Hedlund *et al.*, 2008; Nefzger *et al.*, 2012). We demonstrate that following FACS isolation and transplantation LMX1A-eGFP+ progenitors, but not PITX3-eGFP+ DA precursor cells, resulted in a higher density of TH+ DA neurons within grafts, appropriate target innervation and consequential improved motor function, whilst critically eliminating proliferative and serotonergic populations from the grafts.

3.4 Materials and Methods

3.4.1 Human ESC culture and differentiation

Human ESC H9 reporter lines, LMX1A-eGFP and PITX3-eGFP, were cultured and differentiated under xeno-free conditions as previously described (Niclis *et al.*, 2017a). In brief, cells were cultured on Laminin-521 (10µg/ml; BioLamina) and exposed to dual SMAD inhibition (SB431542, 10µM, 0-5 days in vitro, DIV, R&D systems; and LDN193189, 200nM, 0-11DIV, Stemgent) to promote neuralisation. Regionalisation to a ventral midbrain floor plate identity was achieved by exposure to Sonic hedgehog C25II (100ng/ml; R&D systems) and Purmorphamine (2µM; Stemgent) from day 1-7DIV, in addition to Wnt agonist, CHIR 99021 (3µM; Stemgent, 3-13DIV). From 11DIV, cells were cultured in a 'maturation media' consisting of NBB27 supplemented with GDNF (20ng/ml; R&D systems), BDNF (20ng/ml, R&D system), TGFβ3 (1 ng/ml; PeproTech), DAPT (10 µM, Sigma-Aldrich), ascorbic acid (200nM; Sigma-Aldrich) and dibutyryl cAMP (0.05mM; Tocris Bioscience).

3.4.2 Fluorescence-activated cell sorting

At 21 DIV, cultures rich in vm progenitor/precursors were dissociated in Accutase (Innovative Cell Technologies) to a single-cell suspension and resuspended into a sorting buffer containing 90% maturation media, 10% knockout serum replacement, and ROCK inhibitor Y-27632 (10µM, Tocris Bioscience) to a final density of 5-8x10^6 cells/ml. Cells were filtered through cell strainer caps (35µM mesh, Falcon) to remove the presence of cell doublets and clusters. Sorting was performed on a MoFlo cell sorter (Beckman Coulter, MoFlo) or FACS Aria III using a 100-µM nozzle, sheath pressure of 17-22 psi. A fraction of cells were passed through the cell sorter, without selection, forming the Unsorted group, whilst eGFP+ and eGFP- cells were isolated using a highly restrictive gating strategy to exclude doublets and debris based on forward and side-scatter parameters, as well as dead cells using the viability marker 4'-6-Diamidino-2-Phenylindole (DAPI). Background auto-fluorescence was compensated for by an empty auto fluorescence channel (FL2-580/30), and a H9 parental cell line at the same stage of differentiation was used as a GFP- control (data not shown). FACS-isolated cell fractions were either (i) replated at 300,000 cells/cm2 in 96-well plates, (ii) passed back through the FACS machine, (both targeted at confirming efficacy of the FACS isolation), or (iii) resuspended in maturation media containing ROCK inhibitor (Y27632, 10µM, Sigma) at 100,000 cells/µL and stored on ice until the time of transplantation. Flow cytometric analysis was conducted using FlowJo software.

3.4.3 6-hydroxydopamine lesioning and cell transplantation

All animal procedures were conducted in agreement with the Australian National Health and Medical Research Council's published Code of Practice for the Use of Animals in Research, and experiments approved by The Florey Institute of Neuroscience and Mental Health Animal Ethics committee. Animals (of either sex) were group housed on a 12:12-hour light/dark cycle with ad libitum access to food and water. Surgeries were performed on athymic nude rats and nude mice under 2% isoflurane anaesthesia. Unilateral 6-hydroxydopamine (6-OHDA) lesions of the rat medial forebrain bundle (3.5µl, 3.2µg/µl) or mouse substantia nigra pars compacta (1.5µl, 1.6 µg/µl) were performed to ablate the host midbrain dopamine pathways, as previously described (Kauhausen *et al.*, 2013, Niclis *et al.*, 2017*a*).

Six weeks after lesioning, animals received a unilateral injection of either human PSC-derived LMX1a-eGFP vm progenitors or PITX3-eGFP DA precursors into the denervated striatum. For each cell line, grafts were of Unsorted, GFP+, or GFP- progenitors (1µl; 100,000 cells/µl). Stereotaxic co-ordinates were as follows in rats: 0.5mm anterior, 2.5mm lateral to Bregma and 4.0mm below the dura surface, and in mice: 0.5mm anterior, 2.5mm lateral, 4.0mm ventral), as previously described (Kauhausen *et al.*, 2013, Niclis *et al.*, 2017*b*). See Figure 3.1 for study design overview.

3.4.4 Behavioural testing

Rotational asymmetry, following intraperitoneal administration of D-amphetamine sulphate (3.5mg/kg, Tocris Bioscience), was assessed 4 weeks after 6OHDA lesioning. Only animals capable of >300 rotations in 60 minutes, confirmed on 2 independent tests/rat, were included in the study. Behavioural testing was repeated at 16, 20 and 24 weeks after cell grafting to assess the functional integration of the transplants.

3.4.5 Immunocytochemistry

In vitro cultures were fixed with 4% paraformaldehyde at day 21, or at 6 hours after FACS and *in vitro* re-plating. Rats and mice were killed by an overdose of sodium pentobarbitone (100mg/kg), and transcardially perfused with Tyrode solution followed by 4% paraformaldehyde. Brains were coronally sectioned (40µm; 12 series) on a freezing

microtome (Leica). Immunohistochemistry was performed in accordance to previously described methods (Somaa *et al.,* 2017). Primary antibodies and dilutions were as follows: 4',6-diamidino-2-phenylindole (DAPI, 1:5000; Sigma Aldrich), rabbit anti-OTX2 (1:4000; Millipore), goat anti-FOXA2 (1:200; Santa Cruz), chicken anti-GFP (1:1,000; Abcam), rabbit anti-GFP (1:20,000; Abcam), sheep anti-tyrosine hydroxylase (TH, 1:800, Pelfreeze), rabbit anti-TH (1:1,000; Pelfreeze), rabbit anti-BARHL1 (1:300, Novus Biologicus), sheep anti-PITX2 (1:500, R&D Systems), mouse anti-neural cell adhesion molecule (NCAM, 1:500; Santa Cruz), rabbit anti-NeuN (1:100; R&D Systems), mouse anti-GAD67 (1:100, Millipore), goat anti-choline acetyltransferase (ChAT, 1:100, Millipore), mouse anti-dopamine-b-hydroxylase (DBH, 1:5000, Millipore, MAB308), rabbit anti-glial fibrillary acidic protein (GFAP, 1:500, DAKO), mouse anti-adenomatous polyposis coli, clone CC1 (APC, 1:100, Abcam), mouse anti-rat endothelial cell antigen-1 (RECA1, 1:500, Serotec), rabbit anti-Claudin V (1:200, Abcam) rabbit anti-GIRK2 (1:500; Alomone Labs), mouse anti-calbindin (1:1,000; Swant Biotech), rabbit anti-KI67 (1:1,000; ThermoFisher), goat anti-doublecortin (DCX, 1:1,000; Santa Cruz), mouse anti-human nuclear antigen (HNA, 1:300; Millipore) and rabbit anti-5HT (1:1000; Immunostar). Secondary antibodies for direct detection were used at a dilution of 1:200—DyLight 488, 549 or 649 conjugated donkey anti-mouse, anti-chicken, anti-rabbit, anti-goat or anti-sheep (Jackson ImmunoResearch).

3.4.6 Microscopy and Quantification

Fluorescence images were captured using a Zeiss Axio Observer Z.1 epifluorescence or Zeiss LSM 780 Confocal Microscope, while bright and dark field images were obtained using a Leica DM6000 microscope. Grafts were delineated based upon PSA-NCAM expression and volume estimated using the Cavalieri's principle. Total number of human nuclear antigen (HNA+), green fluorescent protein (GFP+), tyrosine hydroxylase (TH+), serotonergic (5HT+) and proliferative (KI67+) cells were counted from images captured at 20X magnification. To quantify GIRK2+ and CALBINDIN+ cells within the grafts, dopamine neurons were first identified based upon TH immunoreactivity from acquired confocal images. The density of TH and NCAM labelled fibres were assessed at predetermined sites within known dopaminergic (dorsolateral striatum and cortex) and non-dopaminergic (periventricular thalamic nucleus and fimbria of the contralateral hippocampus) target nuclei, from compressed z-stacked images. Images were analysed using ImageJ software.

3.4.7 Experimental Design and Statistical Analysis

All behaviour testing and histological assessments were performed with the researcher blinded to the experimental group. A total of 48 female athymic nude rats (CBHrnu) and 13 nude mice (BALB/c-*Foxn1*^{nu}/Arc) were transplanted from two independent differentiations into rats and subsequently mice, with n=3-8 animals per group. All data are presented as mean + SEM. Statistical tests employed (inclusive of one-way ANOVA, two-way ANOVA and student t-tests), as well as number of animals/group for each analysis are stated in figure legends. Alpha levels of $p<0.05$ were considered significant with all statistical analysis performed using GraphPad Prism. *$p < 0.05$, **$p < 0.01$, ***$p < 0.001$ and ****$p < 0.0001$.

3.5 Results

3.5.1 Isolation of vm progenitor/precursors from LMX1A-eGFP and PITX3-eGFP human ESC-lines

Enhanced GFP reporter human ESC lines for the early vm progenitor gene LMX1A and later DA precursor gene PITX3 (Figure 3.1A-C), were differentiated according to the recently developed, and clinically relevant, xenogeneic-free protocol (Niclis *et al.*, 2017*a*). At the time corresponding to the FACS isolation of progenitors for transplantation, 21 days in vitro (DIV), the efficiency of the differentiating cultures could be confirmed in both stem cell lines by the co-expression of the forebrain-midbrain marker OTX2 and basal plate marker, FOXA2 (Figure 3.1D, E, J, K), accounting for >85% of all cells. At this time, the LMX1A-eGFP reporter line revealed that a significant proportion of the cultures also co-expressed LMX1A (i.e. GFP+, >70%), as previously described (Niclis *et al.*, 2017*a*), with few maturing TH+ cells emerging (Figure 3.1F-I). In contrast, PITX3 expression, visible by GFP immunocytochemistry in the differentiated PITX3-e ESC cultures, showed sparse expression (<2%) that tightly overlapped with TH (Figure 3.1L-O). Importantly, we showed low proportions of BARHL1 and PITX2 immunoreactive cells, indicative of off-target, developmentally adjacent subthalamic progenitors (Kee *et al.*, 2017), within differentiating LMX1A-GFP (Figure 3.1P) and PITX3-GFP (data not shown) cell lines.

FACS analysis of the LMX1A-GFP and PITX3-GFP cells from differentiating cultures revealed 70.2% and 1.2% of cells, respectively, expressed GFP (Figure 3.1R, V). Efficiency

of the sorting was confirmed by re-analysis of the isolated fractions by flow cytometry, as well as re-plating of the sorted fractions, and cytochemistry at 6 hours after seeding (Figure

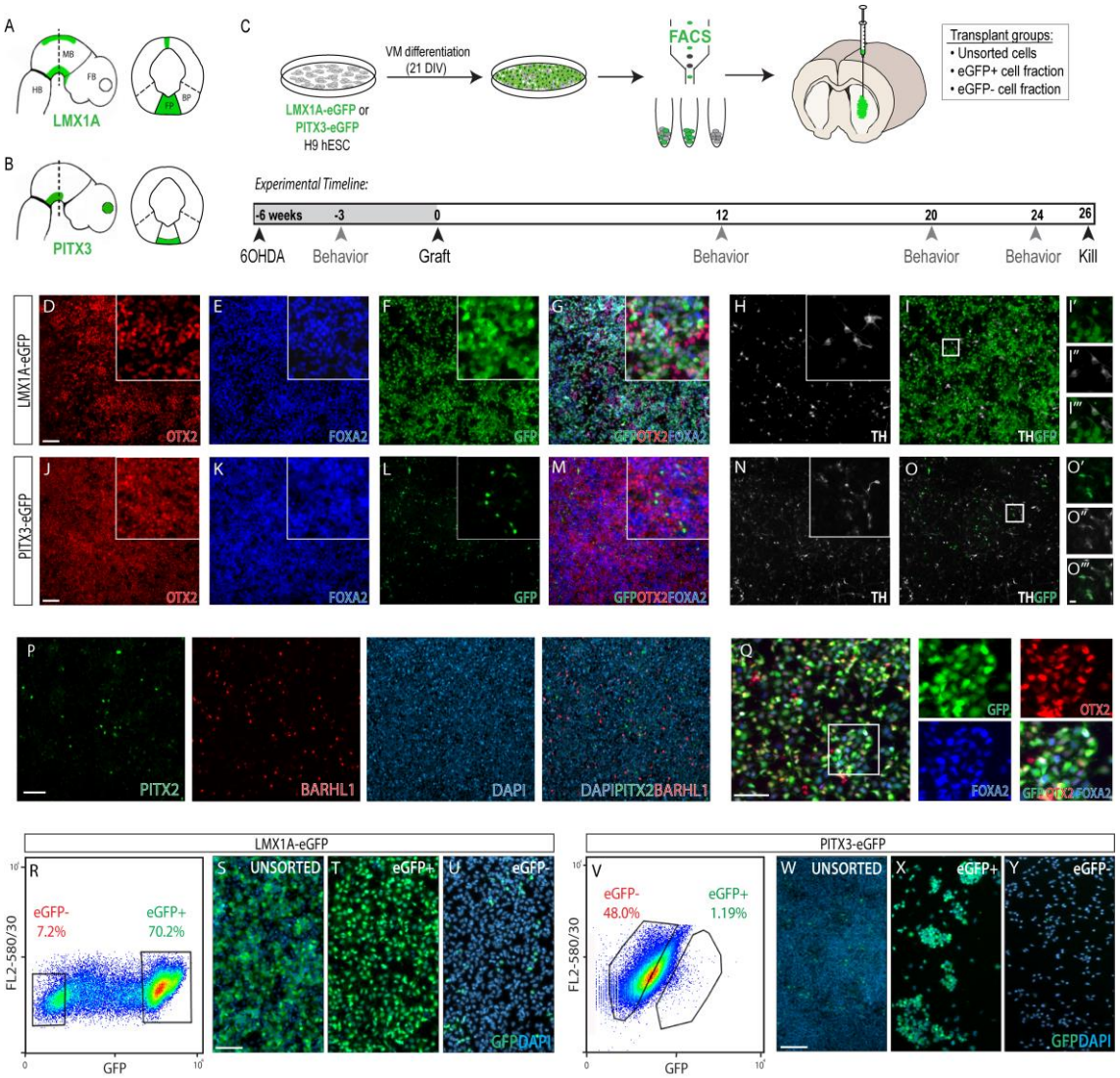

Figure 3.1. In vitro differentiation and purification of vm progenitors/precursors using LMX1A-eGFP and PITX3-eGFP human embryonic stem cell reporter lines

(A-B) Schematic coronal and sagittal views of the developing embryo depicting expression patterns of two key vmDA determinant transcription factors, **(A)** LMX1A and, **(B)** PITX3. eGFP was expressed under the promotor for these two transgenes within H9 hESC lines for the purpose of cell sorting. **(C)** Schematic detailing the differentiation, isolation and transplantation of cells derived from LMX1A-eGFP and PITX3-eGFP hESC reporter lines, and the experimental timeline for *in vivo* procedures. **(D-G, J-M)** Validation of efficient VM differentiation by co-expression of OTX2, FOXA2 and eGFP, demonstrated robust specification of vm progenitors by 21DIV. **(I, O)** Maturing dopamine neurons present within the culture at 21DIV tightly overlapped with eGFP expression**. (P)** Low proportion of PITX2+ and BARHL1+ cells confirmed cultures were not of unintended subthalamic identity. **(Q)** Immunohistochemical labelling of LMX1A-GFP+ progenitors, 6hours after sorting and replating, showing co-expression of cardinal vmDA progenitor markers OTX2, FOXA2 and LMX1A-GFP. **(R, V)** Flow cytometric plots indicating the gating for enrichment of eGFP+ and eGFP- populations within differentiating cultures at 21DIV. Successful isolation of specified populations (Unsorted, GFP+ and GFP-) from the **(S-U)** LMX1A-eGFP, and **(W-Y)** PITX3-eGFP hPSC line was confirmed by replating of cells and immunohistochemical staining for GFP and DAPI. Abbreviations: DIV, days in vitro; eGFP, enhanced green fluorescent protein; hESC, human embryonic stem cells. Scale bar: **(D-O, S-U, W-Y)**, 200uM, **(I'-I"', O'-O"'),** 20um.

3.1Q, S-U, W-Y). Within the LMX1A-eGFP positive (LMX1A-GFP+) fraction, >99.2% of cells expressed GFP, with all GFP cells confirmed to co-express cardinal vm progenitor markers OTX2 and FOXA2 (data not shown). Within the re-plated LMX1A-eGFP negative fraction (LMX1A-GFP-), 10% of cells were GFP+, a likely reflection of ongoing, asynchronous maturation of the cultures during the period of both sorting and replating (Figure 3.1U). Assessment of the sorted PITX3-eGFP cell line confirmed >95% of the replated cells from the positive fraction expressed GFP (Figure 3.1V), whilst GFP+ cells within the negative fraction were extremely rare (Figure 3.1Y).

3.5.2 Transplanted LMX1a-GFP+ progenitors, but not PITX3-GFP+ DA precursors, restore functional deficits in Parkinsonian rats

All rats included in the study showed an amphetamine-induced rotational asymmetry >5 rotations/min, prior to transplantation, that persisted over 26 weeks as a stable motor deficit in ungrafted animals (Figure 3.2A, F). As anticipated, and in alignment with human PSC-derived vm progenitor grafts by us and others (Kriks *et al.*, 2011; Kirkeby *et al.*, 2012, 2017; Doi *et al.*, 2014, Samata *et al.*, 2016, Niclis *et al.*, 2017*a, b*), transplants of unsorted cells, from both LMX1a-GFP and PITX3-GFP cell lines, resulted in near complete recovery of rotational asymmetry by 24 weeks. Grafts of LMX1A-GFP+ progenitors also showed accelerated, complete recovery, evident at 20weeks. Interestingly, PITX3-GFP- but not PITX3-GFP+ cell grafts showed improvements in motor asymmetry at 6 months.

Post-mortem analysis showed viable grafts, identified by human PSA-NCAM, in all rats 6 months after implantation, (Figure 3.2B-D, G-I). Volumetric analysis revealed that LMX1A-GFP+ grafts were significantly smaller than both Unsorted and LMX1A-GFP- cell grafts ($3.9mm^3 \pm 1.0$, $8.9mm^3 \pm 0.9$, $10.7mm^3 \pm 1.7$, respectively). Grafts of Unsorted PITX3-GFP cells were, not surprisingly, comparable to the Unsorted LMX1a-GFP cells ($9.9mm^3 \pm 1.1$), with PITX3-GFP- also of similar size ($9.3mm^3 \pm 1.5$), Figure 3.2E, J. Most evident was the reduced size of the PITX3-GFP+ cell grafts ($0.3 \pm 0.1\ mm^3$). Recognising that midbrain DA progenitors exit the cell cycle and become post-mitotic at a similar time to the onset of PITX3 expression during vm development, combined with knowledge that post-mitotic neuroblasts poorly survive transplantation, we speculated that these factors contributed to the small graft size observed. GFP labelling of these grafts confirmed low numbers of PITX3-GFP+ cells, and whilst showing a higher density of GFP+ cells (data not shown), TH+ DA neurons were

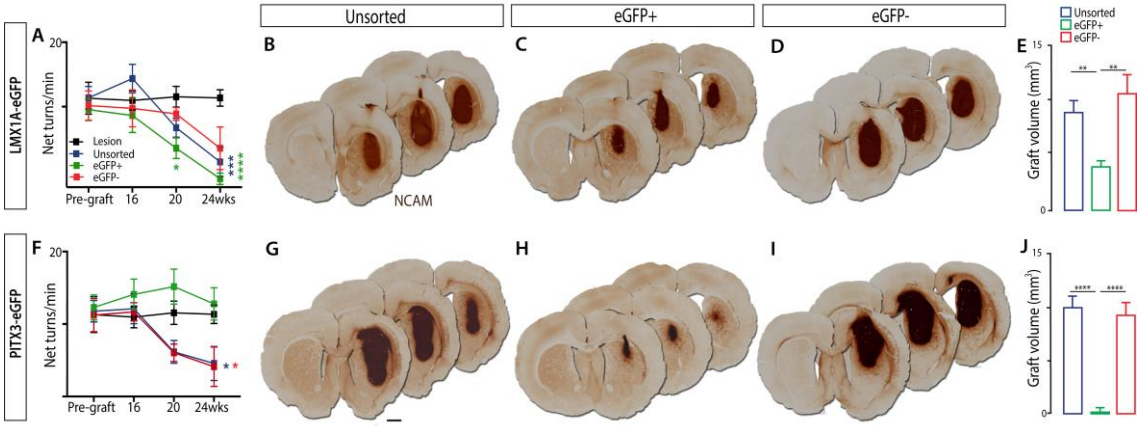

Figure 3.2. LMX1a-eGFP+ progenitors, but not PITX3-eGFP+ precursors, show engraftment and amelioration of behavioural deficits in 6-OHDA lesioned rats
(A) Transplantation of LMX1A-eGFP+ progenitors (green) resulted in an accelerated correction of rotational asymmetry in 6OHDA athymic rats, compared to grafts of Unsorted (blue) and eGFP- vm progenitors (red), Two-way ANOVA with Dunnett correction for multiple comparisons relative to 6-OHDA, Group, $F_{(3,88)} = 9.131$, $p < 0.0001$, n=6-8/group). **(B-D)** Human specific neural cell adhesion protein (NCAM) enables visualisation of the LMX1A progenitor grafts within the host striatum. **(E)** Quantitative assessment of LMX1A-eGFP progenitor grafts highlighting the smaller size of grafts derived from eGFP+ progenitors, (One-way ANOVA with Tukey's post-hoc testing, $F_{(2,14)} = 9.8$, $p = 0.0022$, n=6-8/group). **(F)** Grafting of PITX3-eGFP- and Unsorted, but not PITX3-eGFP+ cells, corrected gross motor deficits in 6OHDA rats, Two-way ANOVA, $F_{(3,120)} = 3.188$, $p = 0.0263$, n=6-8/group). **(G-I)** Coronal sections of the rat brain showing large viable grafts 6months after transplantation of Unsorted and PITX-eGFP- cells. PITX3-eGFP+ DA precursors showed poor survival and engraftment following transplantation, **(J)** confirmed by significantly reduced graft volume, (One-way ANOVA, $F_{(2,16)} = 30.61$, $p = <0.0001$, n=6-8/group). All data represents Mean ± SEM. Scale bar: **(B-D, G-I)**, 1mm.

notably sparse (591 ± 84, n=8), highlighting the lack of suitability of this reporter to isolate and enrich DA progenitor/precursors for the purpose of transplantation.

3.5.3 Transplantation of LMX1a-GFP+ vm progenitors enriches for DA neurons that are capable of innervating developmentally appropriate targets in the host brain

Reflective of the smaller size of LMX1A+ transplants (Figure 3.2E), these grafts contained significantly fewer (HNA+) cells compared to both Unsorted or LMX1A-GFP- cell grafts (Figure 3.3A). Assessment of GFP staining confirmed the efficiency of the sorting, with LMX1A-GFP+ progenitor grafts showing enrichment of GFP+ cells; both total GFP+ cells (Unsorted: 162,159 ± 14,703; LMX1A-GFP+: 225,700 ± 48,832; LMX1A-GFP-: 19,523 ± 5,937) and proportion, (Figure 3.3B, E-G). Similar to *in vitro* observations, transplants of LMX1A-GFP- progenitors resulted in grafts containing pockets of GFP+ cells (Figure 3.3G), likely reflective of the asynchronous maturation of younger progenitors adopting an LMX1a+ fate after the time of sorting and implantation.

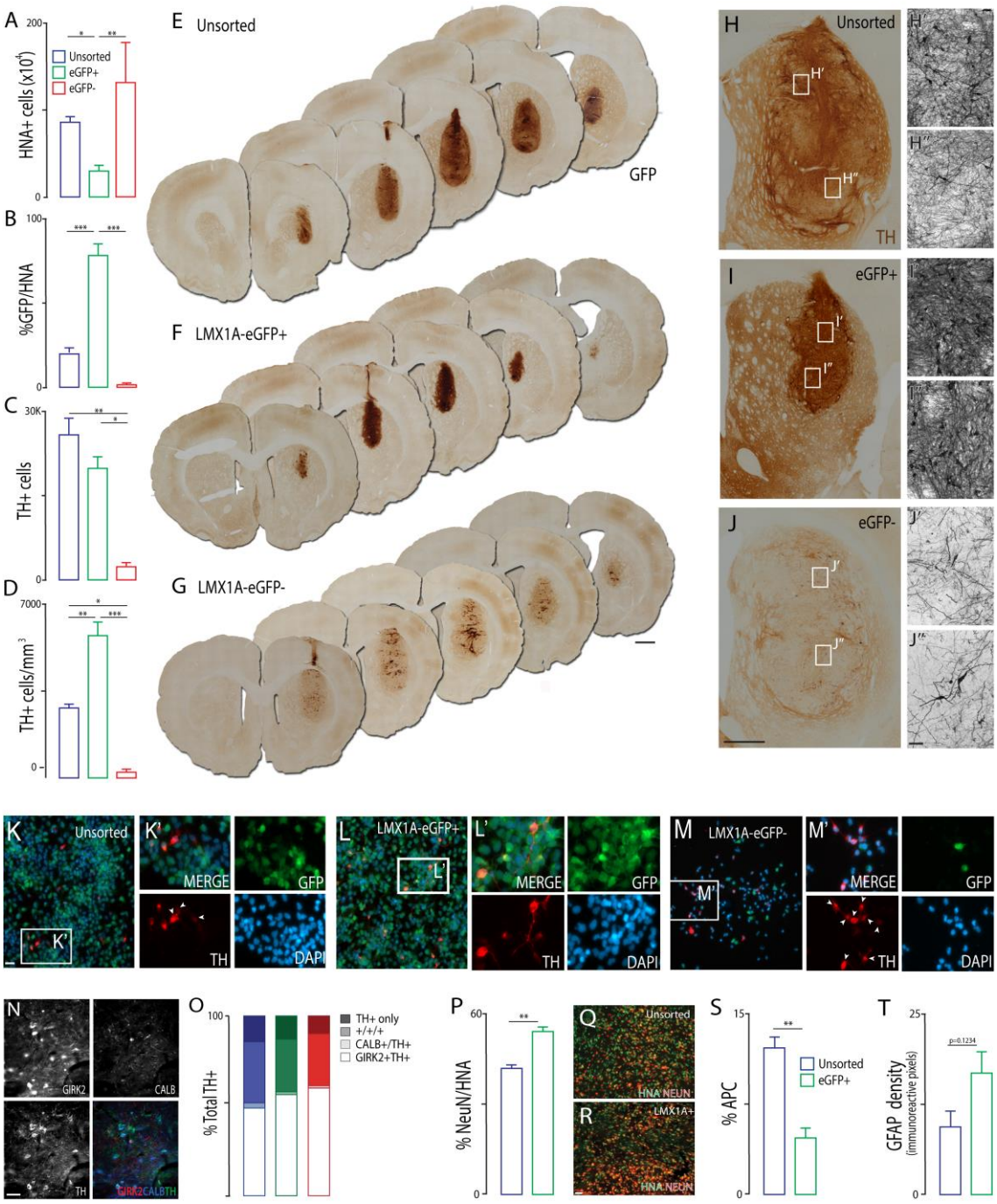

Figure 3.3. Transplants of LMX1A-eGFP+ progenitors result in discrete, homogeneous grafts with enriched density of dopaminergic neurons of maintained A9/A10 subtype specification

(A) Quantitative assessments of transplants revealed significantly fewer HNA+ cells (One-way ANOVA, $F_{(2,14)}$ = 9.445, p = 0.0025, n=6-8/group), and **(B)** enrichment of GFP expressing cells within grafts of LMX1A-GFP+ progenitors, compared to both Unsorted and LMX1A-GFP-, (One-way ANOVA, $F_{(2,13)}$ = 42.15, p = <0.0001, n=6-8/group). **(C)** While TH+ cell number did not differ from Unsorted progenitor grafts, (One-way ANOVA, $F_{(2,12)}$ = 8.445, p = 0.0051, n=6-8/group), **(D)** TH density was significantly elevated within LMX1A-GFP+ progenitor grafts, in comparison to transplants of Unsorted and LMX1A-GFP- cells, (One-way ANOVA, $F_{(2,12)}$ = 19.68, p = 0.0002, n=6-8/group). **(E)** Representative overview of Unsorted, **(F)** LMX1A-GFP+, and **(G)** LMX1A-GFP- grafts showing GFP expression. **(H-J)** Photomicrograph showing the distribution and density of TH+ cells within grafts derived from Unsorted,

LMX1A-GFP+ and LMX1A-GFP- progenitors. **(H', H")** Note the heterogeneity in TH cell density seen in Unsorted grafts, **(I', I")** by comparison to the dense homogeneous distribution observed in LMX1A-GFP+ grafts. **(J)** Transplants of LMX1A-GFP- progenitors showed few TH+ cells scattered throughout the transplant. **(K-M)** Representative images of Unsorted **(K),** LMX1A-GFP+ **(L)** and LMX1A-GFP- **(M)** progenitors 6hours after sorting and replating showing the co-expression of GFP with TH. Note that while TH+GFP+ cells numbers were low in all replated cultures, reflective of the stage of differentiation (21DIV), the LMX1A-GFP- cultures showed a high proportion of TH+GFP- cells (white arrow heads), indicative of an earlier born, non-vm, dopaminergic or adrenergic/noradrenergic cell population. **(N)** Representative images showing the co-expression of TH together with GIRK2 and/or CALBINDIN, indicative of A9- and A10-like specification. **(O)** Quantification of TH+ neurons that showed co-expression of GIRK2 and/or CALBINDIN, confirmed that transplanted LMX1A-GFP+ progenitors retained their propensity to form mature vm DA neurons of both A9- and A10-phenotype. **(P)** Isolation of LMX1A-GFP+ cells resulted in grafts significantly enriched with NeuN+ neurons, compared to unsorted VM progenitor grafts, (Unpaired t test, $t = 7.76$ $df = 4$, $p = 0.0015$, n=3-4/group). **(Q-R)** Representative photomicrographs of NeuN immunolabelled neurons within an Unsorted and GFP+ graft. **(S)** The proportion of APC+ mature oligodendrocytes were significantly reduced in LMX1A-GFP+ grafts (unpaired t test, $t = 5.32$, $df = 4$, $p = 0.006$, n=3-4/group), while the relative contribution of GFAP+ astrocytes remained unchanged (unpaired t test, n=3-4/group). All data represents Mean ± SEM, Scale bars: **(E-G, H-J)**, 1mm, **(H'-J"),** 50µm, (**N**). *p<0.05, **p<0.01, ***p<0.001.

As previously reported (Grealish *et al.*, 2014, Niclis *et al.*, 2017*b*), >85% TH+ cells in all grafts showed expression of the A9 and/or A10 proteins, GIRK2 and Calbindin, respectively, with no significant difference between any of the transplant groups (Figure 3.3K,L). In alignment with post-mortem assessment of the human midbrain (Reyes *et al.*, 2012), the majority of TH+ cells co-expressed GIRK2, alone or together with Calbindin, whilst few TH+ neurons expressed only Calbindin+.

Necessary for the functional efficiency of vm DA grafts is their capacity to send afferent projections to the host striatum. In accordance with the similar numbers of TH neurons, LMX1A+ grafts showed comparable density of innervation of the dorsal striatum and cortex to grafts of Unsorted progenitors (Figure3.4A-D). In contrast, LMX1A-GFP- progenitor grafts poorly innervated these motor-function associated nuclei (Figure 3.4A, B, E), rather showing increased connectivity with non-dopaminergic target nuclei, inclusive of the periventricular thalamic nucleus (PVN) and hippocampus (Figure 3.4F-L).

Whilst we confirmed a low proportion of STN progenitors within our cultures prior to transplantation (a rostral vm population known to express LMX1A) (Kee *et al.*, 2017), residing within the appropriately specified, more caudal, domain of the developing vm are other non-dopaminergic LMX1A-expressing progenitors. With <9% of the GFP+ cells expressing TH within GFP+ progenitor grafts (or 19%, as a proportion of total implanted cells), we sort to perform a more detailed assessment of the composition of these grafts –

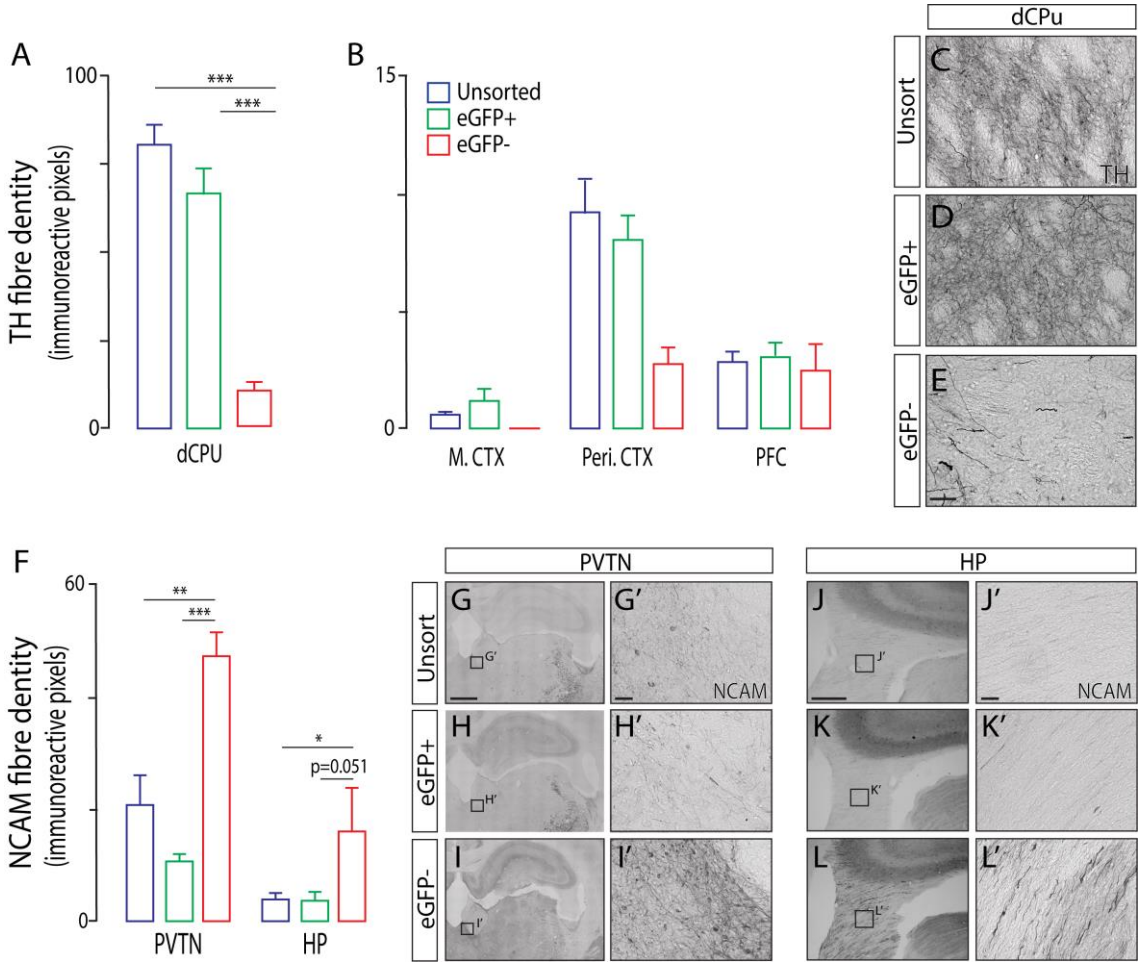

Figure 3.4. Grafts containing LMX1A- cells preferentially innervate non-dopaminergic targets.

(A) Quantitative assessment of TH+ fibre density in the dorsal caudate putamen (dCPU, One-way ANOVA, $F_{(2,10)} = 32.77$, $p = <0.0001$, n=4-6/group), **(B)** and cortex, inclusive of the motor cortex (M.CTX), perirhinal cortex (Peri.CTX) and pre-frontal cortex (PFC). **(C-E)** High power images illustrating the increased density of TH+ fibres in the striatum of Unsorted and LMX1A-GFP+ cell grafts compared to grafts derived from LMX1A-GFP- progenitors. **(F)** Quantification of human NCAM+ fiber density in the periventricular thalamic nucleus (PVTN, One-way ANOVA, $F_{(2,13)} = 16.75$, $p = 0.0003$, n=4-6/group) and fimbria of the contralateral hippocampus (HP, One-way ANOVA, $F_{(2,13)} = 4.308$, $p = 0.0367$, n=4-6/group) from grafted animals. **(G-I)** Representative photomicrographs showing increased density of NCAM+ fibers within the PVTN and, **(J-L)** HP in animals transplanted with LMX1A-GFP- progenitors, compared to grafts of Unsorted or LMX1A-GFP+ cells, demonstrative of off-target innervation. Data presented as mean ± SEM, Scale bars: **(C-E)** 50um, **(G-I, J-L)** 200uM, **(G'-I', J'-L')** 20um. **(N)** 50um.

focusing on neural specification. All neural lineages were present within the transplants with >55% of HNA+ cells co-expressing the postmitotic neuronal marker NeuN within the GFP+ progenitor grafts, significantly greater than unsorted cell grafts (Figure 3.3P-R). In contrast, sorting reduced the contribution of APC+ mature oligodendrocytes (Figure 3.3S), and no change was observed in the density of GFAP+ astrocytes (Figure 3.3T). More detailed

assessment of neuronal subpopulations revealed that DBH+, ChAT+ and GAD67+ cells were noticeably rare within the GFP+ grafts (data not shown), suggesting that the many neurons present appeared to adopt a mature neurotransmitter identity. Staining against vascular proteins targeted to the host (RECA1) verses broader/non-species specific (Claudin V), revealed that the sparse density of vessels within the grafts were of host, and not graft, origin (data not shown). Whilst quantitative assessment of GFAP+ astrocytes was not feasible (due to the dense network of staining and inability to resolve graft from host cells with certainty), there was at least some evidence of HNA+ cells failing to adopt any of the three neural lineages. Such observations reflect our incomplete knowledge of the lineage trajectories of the LMX1A+/FOXA2+/OTX2+ progenitor, and whilst recently recognised as having the capacity to give rise to mature astrocytes *in vitro* (Holmqvist *et al.*, 2015), other populations may remain to be identified.

3.5.4 Isolation of LMX1A-GFP+ progenitors reduces proliferating cell populations and eliminates serotonergic neurons from human PSC-derived vm grafts

Reflective of the general efficiency of the *in vitro* differentiation of the human PSC LMX1A-GFP cell line, and the *in vivo* maturation of the implanted progenitors, no gross neural overgrowths or tumors were observed in any grafted animals after 26 weeks. The increase in total cells, from 100,000 implanted cells to a total of 836,883 $\pm$ 54,083 cells within the implantation. Whilst the majority of cells adopted a post-mitotic fate, a small dividing population remained present at 26 weeks, identified by doublecortin and KI67 staining within Unsorted and LMX1A-GFP- progenitor grafts. Supportive of the smaller graft volumes observed, transplants of LMX1A-GFP+ progenitors contained significantly fewer dividing cells, (0.18% $\pm$ 0.01% KI67+/HNA+), (Figure 3.5A-D).

Finally, we assessed grafts for the presence of 5HT+ serotonergic neurons, a population known to contribute to the development of graft-induced dyskinesias (GID) in preclinical and clinical studies (Carlsson *et al*., 2007; Politis *et al*., 2011). Transplants of LMX1A-GFP+ progenitors eliminated serotonergic neurons, with just 2 grafts containing a single 5HT immunoreactive neuron, compared to the significantly higher numbers observed in both Unsorted (7,346 $\pm$ 1,382) and LMX1A-GFP- (2,168 $\pm$ 359) grafts, and consequently also the proportion of serotonergic to dopaminergic neurons, (DA:5HT, Figure 3.5E-I), a recognised contributing factor in the incidence of induced dyskinesias (Garcia *et al*., 2011; Politis *et al*., 2011).

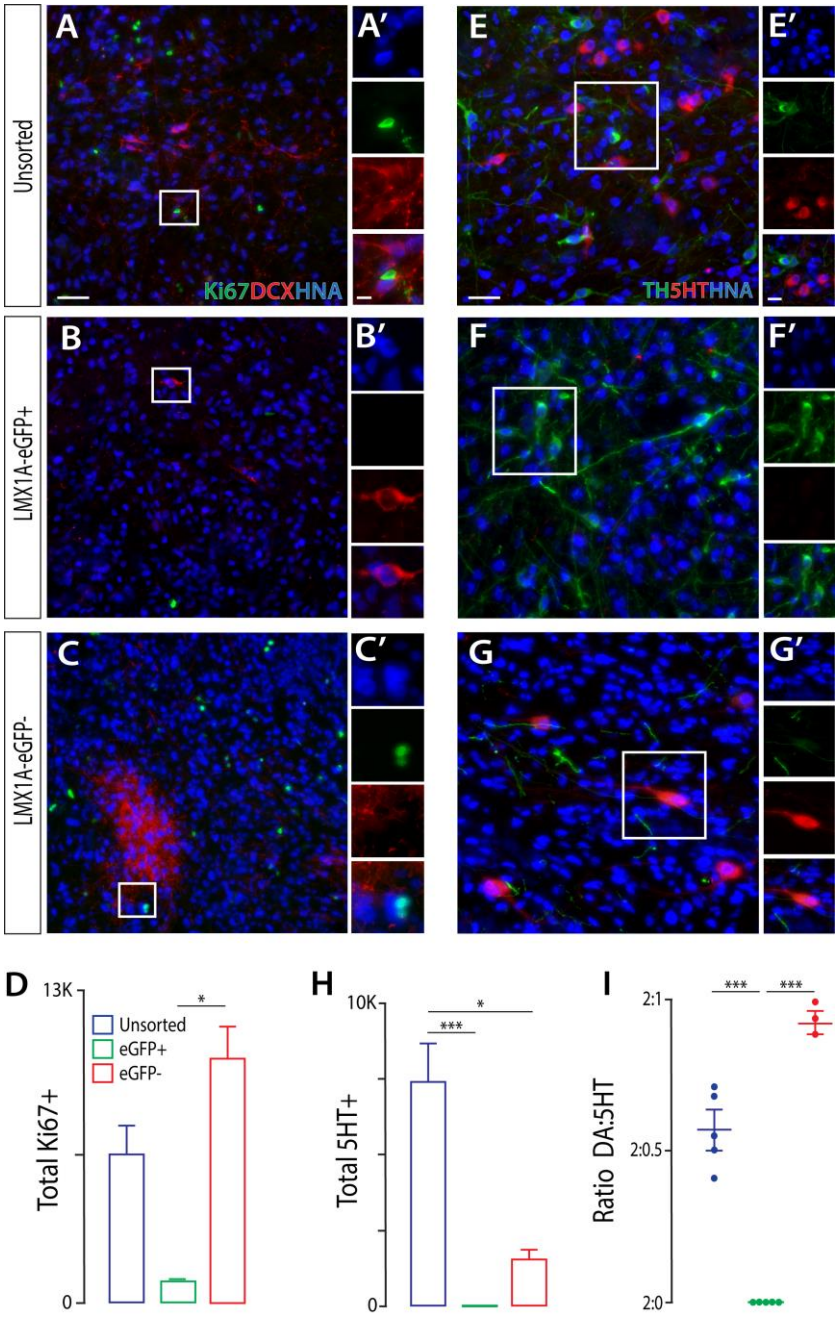

Figure 3.5. Transplantation of LMX1A-GFP+ progenitors reduces the presence of proliferating cells, and eliminates incorrectly specified serotonergic neurons within grafts

(A-C) Immunohistochemical labelling of transplants with human nuclear antigen (HNA, blue), doublecortin (DCX, red), KI67 (green) illustrating the reduction in proliferative progenitors at 6months within transplants derived from LMX1A-GFP+. **(D)** Quantification of Ki67+ cells within the LMX1A-eGFP cell grafts, One-way ANOVA, $F_{(2,6)}$ = 8.248, p = 0.019, n=4-6/group. **(E-G)** Representative photomicrographs showing dopaminergic (TH+, green), serotonergic (5HT+, red) and HNA immunolabeling within transplants of Unsorted GFP+ and GFP- progenitor grafts. **(H)** Quantification of 5HT+ cells (One-way ANOVA, $F_{(2,13)}$ = 17.26, p = 0.0003, n=4-6/group), and, **(I)** ratio of dopaminergic to serotonergic (DA:5HT) neurons within the transplants (One-way ANOVA, $F_{(2,11)}$ = 57.19, p = <0.0001, n=4-6/group), confirmed the near complete elimination of the dyskinetic-contributing cell population from grafts derived from LMX1A-GFP+ progenitors. Data represents Mean + SEM. Scale bars: **(A-C, E-G)**, 50um, **(A'-C', E'-G')**, 20um.

Demonstrating the utility and reproducibility of sorting for LMX1A-expressing progenitors, we repeated FACS isolation and transplantation into 6OHDA lesioned athymic mice. Again, we showed smaller grafts with enrichment for both GFP and TH neurons (Figure 3.6A-I). TH+ DA neuronal density within the grafts was surprisingly similar to the rats; with significant increases in density (and homogeneity) observed in the LMX1A-GFP+, compared to Unsorted and LMX1A-GFP- grafts (Figure 3.6F, I). No 5HT neurons were observed in grafts of LMX1A-GFP+ progenitors (Figure 3.6J-L).

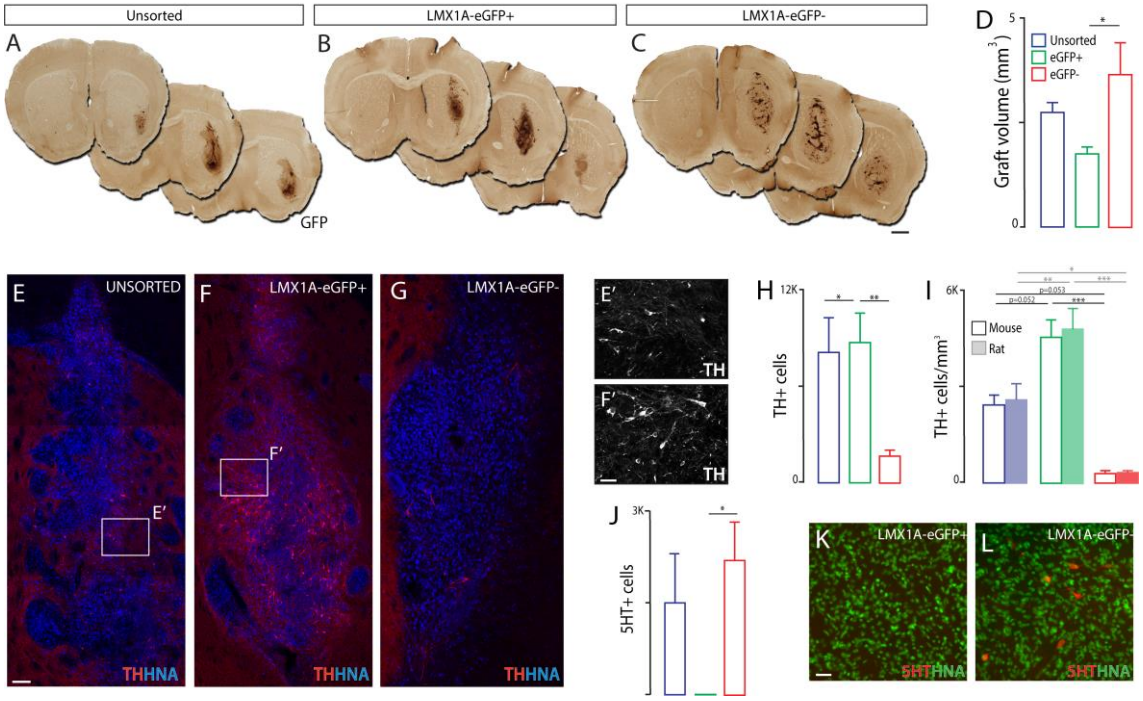

Figure 3.6. Transplantation of LMX1A-GFP+ progenitors shows high reproducibility across repeated rodent transplantation studies.
Photomicrographs showing GFP immunohistochemical labelling of representative grafts in the mouse brain following transplantation of **(A)** Unsorted, **(B)** LMX1A-GFP+ and **(C)** LMX1A-GFP- progenitors. **(D)** Volumetric assessment revealed that LMX1A-GFP+ cells form discrete grafts that were significantly smaller than LMX1A-GFP- grafts, One-way ANOVA, $F_{(2,10)} = 4.544$, $p = 0.0395$, n=4-5/group. **(E-G)** Photomontages of representative grafts in mice illustrating TH+ (red) and HNA+ (blue) labelling, and **(F')** demonstrating the enrichment of dopaminergic neurons within LMX1A-GFP+ transplants. **(H)** Quantification of total TH+ cells (Rats: One-way ANOVA, $F_{(2,12)} = 8.445$, $p = 0.0051$, n=4-6/group; Mice: One-way ANOVA, $F_{(2,15)} = 7.566$, $p = 0.0053$, n=4-5/group), and **(I)** TH cell density (Rats: One-way ANOVA, $F_{(2,12)} = 19.68$, $p = 0.0002$, n=4-6/group; Mice: One-way ANOVA, $F_{(2,9)} = 18.91$, $p = 0.0006$, n=4-5/group) within grafts derived from Unsorted, LMX1A-GFP+ and LMX1A-GFP- progenitors and transplanted into mice (open bars) and rats (closed bars). **(J)** Quantification of 5HT+ cells within LMX1A progenitor grafts in mice (One-way ANOVA, $F_{(2,9)} = 9.816$, $p = 0.0055$, n=4-5/group), showing reproducible elimination of serotonergic neurons (as seen also in transplants in rats). **(K-L)** High power images highlighting the elimination of 5HT neurons in LMX1A-GFP+ grafts. Data presented as Mean ± SEM. Scale bars **(A-C)** 1mm, **(E-G)** 500um, **(E'-F')** 20um, **(K-L)** 50um.

3.6 Discussion

Heterogeneity in graft composition following the implantation of hPSC-derived vm progenitors presents ongoing concerns for the safety and functional predictability of these cells for future clinical application in Parkinson's Disease. For these reasons, efforts to improve the homogeneity of the donor preparation, and thereby graft compositions are of significant importance. In this study we developed two GFP-expressing reporter lines, LMX1A-GFP and PITX3-GFP, to enable the selective isolation of correctly specified vm progenitors/precursors from differentiating human pluripotent stem cell cultures, at differing developmental stages. We demonstrate that transplants of LMX1A-GFP expressing progenitors result in discrete grafts with increased density of DA neurons and greater, target-appropriate innervation, resulting in accelerated functional recovery of motor symptoms, compared to Unsorted progenitor grafts. In contrast, transplants of PITX3-GFP+ cells resulted in notably small grafts with low TH+ DA neuron yields. Whilst PITX3-GFP populations have been successfully isolated from mouse ESC cultures (Hedlund *et al.*, 2008; Ganat *et al.*, 2012), the present findings are in accordance with fetal tissue grafting studies using PITX3-GFP embryos; recognising the vulnerability of this post-mitotic population to shear trauma during periods of culture detachment/dissociation, FACS and implantation (Jönsson *et al.*, 2009). Such findings highlight the need to identify a developmentally relevant differentiation stage of hPSC-derived vm progenitors that are sufficiently specified and also amenable for grafting, as has been achieved for rodent and human fetal tissue (Freeman *et al.*, 1995; Torres *et al.*, 2007; Bye *et al.*, 2012), as well as mouse PSCs (Ganat *et al.*, 2012).

In addition to the significance of enriching for DA neurons within grafts is the concomitant capacity to eliminate poorly specified and high proliferative populations that may lead to overgrowth or graft-induced dyskinesias. Whilst incorrectly specified cells are in the minority *in vitro*, due to advances in hPSC neuronal differentiation protocols (Kriks *et al.*, 2011, Niclis *et al.*, 2017*a*), these populations have a propensity for expansion following implantation and/or can impart negative effects on transplant function. On average, studies have reported a yield of 5-6% TH+ DA cells in the grafts per 100,000 cells implanted (Kriks *et al.*, 2011; Kirkeby *et al.*, 2012, 2017; Doi *et al.*, 2014, Samata *et al.*, 2016*b*, Niclis *et al.*, 2017*b*). This yield however is notably lower when expressed as a proportion of the total number of cells within the graft, given the proliferation of the vm progenitors following implantation (Samata *et al.*, 2016*a*, Niclis *et al.*, 2017*b*). The impact of the incorrectly specified cells has been most evidently demonstrated by Niclis *et al.*, where despite >85% correctly specified vm DA

progenitors present in culture (confirmed by FOXA2/OTX2/LMX1A co-expression) and maintained expression in the majority of cells observed 4weeks post-implantation, by 28 weeks graft volume increased 20-fold with no increase in TH+ cell numbers (Niclis *et al.*, 2017*a*, *b*). Also recognising this challenge, Kirkeby *et al*., describe the lack of predictability of grafting outcomes across many (>30) human PSC vm differentiations, despite consistent (>80% FOXA2/OTX2+) *in vitro* specification of the progenitors prior to transplantation (Kirkeby *et al.*, 2017). In the present study, the discrete size of LMX1A-GFP+ grafts, lack of proliferating cells, and increased proportion of TH+ DA neurons observed at 6 months, is a significant improvement and a stark contrast to grafts of the LMX1A-GFP- populations. Together these results highlight the dramatic impact of eliminating poorly specified and/or proliferating cells and underline the necessity for vm progenitor enrichment prior to grafting.

The benefit of eliminating poorly specified neural progenitors can be further appreciated in the context of recent work highlighting the level of off-target innervation made by human PSC-derived vm progenitor grafts (Niclis *et al.*, 2017*b*). While earlier studies were unable to specifically track the relative contribution of dopaminergic and non-dopaminergic innervation from the graft into the host brain, Niclis *et al*., made use of the PITX3-eGFP reporter line to demonstrate that the dopaminergic neurons within the grafts innervated developmentally appropriate host targets, inclusive of the striatum and cortex. However, the vast majority of graft-derived fibre outgrowth was non-dopaminergic, resulting in extensive axonal growth through permissive white matter tracts and significant innervation of off-target nuclei. Supporting these findings, here we demonstrate that the dopamine-enriched LMX1A-GFP+ vm progenitor grafts maintain preferential innervation of appropriate dopaminergic target nuclei with low level innervation of other nuclei. In contrast, LMX1A-GFP- grafts show enhanced innervation of target nuclei that typically have low midbrain dopaminergic innervation, such as the thalamus and hippocampus which carry unknown consequences, as well as low level dopaminergic innervation of the appropriate forebrain targets.

Elimination of serotonergic neurons, a population of cells that have been shown to contribute to graft-induced dyskinesias in both pre-clinical and clinical studies is an additional requisite in the refinement of human PSC grafting targeted for Parkinson's disease therapy (Carlsson *et al.*, 2007; Politis *et al.*, 2011). These undesirable neurons, generated in the ventral basal plate of the rostral hindbrain, reside outside the region of expression of LMX1A (see figure 3.1B, Mishima *et al.*, 2009; Kirkeby *et al.*, 2012), in contrast to other target genes, such as

FolR1 and Corin that have been employed to enrich for DA progenitors (Doi *et al.*, 2014; Gennet *et al.*, 2016). Here we demonstrate the capacity to eliminate 5HT+ serotonin cells from within LMX1A-GFP+ progenitor grafts, in both rat and mouse grafting studies. Of note, the significant reduction in 5HT+ neurons observed in grafts of LMX1A-GFP- progenitors, in comparison to the Unsorted cell grafts, reflects the stringency of the FACS gating employed within the study (Figure 3.1R), with an estimated 23% of cells excluded from both the GFP+ or GFP- pool.

The importance of cell sorting approaches for clinical applications is by no means a new concept. Most evidently demonstrated, and clinically translated, has been the purification of haematopoietic stem cells from blood for the treatment of, for example, some blood-related cancers and autoimmune diseases. Preclinical studies focused on the isolation of vm progenitors from differentiating human PSC cultures is also not novel in the context of improving the safety and predictability of transplants for PD. While a number of rodent studies successfully isolated vm progenitors, using fluorescent activated cell sorting (FACS) or magnetic beads, targeting intracellular and extracellular proteins, respectively (Fukuda *et al.*, 2006; Thompson *et al.*, 2006; Hedlund *et al.*, 2008; Jönsson *et al.*, 2009; Nefzger *et al.*, 2012; Bye *et al.*, 2015), isolation from human PSC cultures has been met with variable success.

In a number of studies, candidate markers employed for selection purposes have been recognised as too broad in their expression to selectively isolate VM progenitors - such as the pan-neuronal marker CD56/NCAM (Pruszak *et al.*, 2007), ventral floorplate marker FOXA2 (Aguila *et al.*, 2014), ventral midbrain floor and basal plate markers Integrin Associated Protein and LMRT1 (Samata *et al.*, 2016*a*; Lehnen *et al.*, 2017), as well as ventral midbrain/hindbrain marker CORIN (Doi *et al.*, 2014). Studies also conducted sorting early in the differentiation (due to timing of expression of the selectable protein) and required extended periods of replating prior to transplantation (Doi *et al.*, 2014, Samata *et al.*, 2016*b*; Lehnen *et al.*, 2017). Such replating steps undermine initial purification and may introduce downstream variability in cell composition at the time of grafting, and have been shown to result in poor TH+ survival (Doi *et al.*, 2014). Alternatively, cultures were sorted late in the vm differentiation yet were not grafted (Xia *et al.*, 2017).

.

With the rapid advancement of human PSC-derived DA progenitor grafts towards the clinic, cell sorting studies have increasingly focused on the identification of cell surface proteins, to avoid reporter cell lines. A key challenge here has been the poor translation of findings from rodent to human – with several studies employing rodent tissue to identify clinically-applicable cell surface antigens on DA progenitor populations, yet translation of these approaches showed limited success as antibodies failed to show the same restrictive isolation or immunoreactivity in human cells (Bye *et al.*, 2015; Gennet *et al.*, 2016, Samata *et al.*, 2016*b*), and our unpublished observations. The narrowing attention to cell surface markers for selection has to some degree distracted from the primary goals of demonstrating the full potential of vm DA progenitor enrichment, and the safety goals.

Focused on these tasks of safety, predictability and reproducibility, here we present the first evidence of using a fluorescent transgene to isolate and engraft hPSC-derived vm progenitors with superior outcomes to cell-surface based purification strategies. Whilst we do not claim LMX1A as the optimal target gene (recognising expression within other non-dopaminergic vm progenitors), this work provides the important impetus for sorting using a human targeted gene. Moving forward, the recent work by Kirkeby *et al*, (2017) may provide new insight into additional and/or superior sorting candidates – having recently identified genes (including ETV5, EN1, SPRY1, WNT1 and CNPY1) expressed during vm differentiation that are predictive of positive DA graft outcomes. Interestingly, several genes commonly used to monitor DA differentiation (that have been employed in sorting studies e.g. FOXA2 and CORIN), have shown poor correlates with graft outcomes (Kirkeby *et al.*, 2017). While our selected transgene, LMX1A, was shown to correlate positively with DA density in grafts (Kirkeby *et al*, 2017), the emphasis remains that additional markers are also likely needed. At this point the field is now left to ponder the risk-to-benefit ratio of taking GFP cell lines into the clinic, noting that GFP transgenes have previously been employed in tracing and targeted gene therapy clinical trials (*clinicaltrials.gov*) or the necessity of identifying a cell surface target.

In summary, improved pre-clinical sorting strategies may enable the identification of novel protein, epigenetic or transcriptomic identifiers that underpin positive DA transplantation outcomes and therefore, inform further clinically relevant interventions.

3.7 Acknowledgements

The authors thank Mong Tien for her expert technical assistance and acknowledge the support of the flow cytometry facility at the Melbourne Brain Centre. CP was supported by a Senior Medical Research Fellowship provided by the Viertel Charitable Foundation, Australia. IDL was supported by a University of Melbourne International Scholarship, Australia. CG is supported by an Australian Postgraduate Award. This work was supported by National Health and Medical Research Council Australia project grant APP1102704, and Stem Cells Australia. The Florey Institute of Neuroscience and Mental Health acknowledges the strong support from the Victorian Government and in particular the funding from the Operational Infrastructure Support Grant.

3.8 Author contributions

All experiments were performed at the Florey Institute of Neuroscience and Mental Health. Conceptualisation: IDL, JN, CLP. Investigation: IDL, JN, CG, JK, CE, CH, LT, CP. Analysis: IDL, CG, JK. Contributed unpublished reagents/analytical tools: CWP, LT, CLP. Writing – original draft: IDL, CLP. Writing – editing: IDL, CLP.

References

Aguila JC, Blak A, van Arensbergen J, Sousa A, Vázquez N, Aduriz A, et al. Selection Based on FOXA2 Expression Is Not Sufficient to Enrich for Dopamine Neurons From Human Pluripotent Stem Cells. Stem Cells Transl Med 2014; 3: 1032–1042.

Andersson E, Tryggvason U, Deng Q, Friling S, Alekseenko Z, Robert B, et al. Identification of intrinsic determinants of midbrain dopamine neurons. Cell 2006; 124: 393–405.

Barker RA, Barrett J, Mason SL, Björklund A. Fetal dopaminergic transplantation trials and the future of neural grafting in Parkinson's disease. Lancet Neurol 2013; 12: 84–91.

Barker RA, Parmar M, Studer L, Takahashi J. Human Trials of Stem Cell-Derived Dopamine Neurons for Parkinson's Disease: Dawn of a New Era. Cell Stem Cell 2017; 21: 569–573.

Bye CR, Jönsson ME, Björklund A, Parish CL, Thompson LH. Transcriptome analysis reveals transmembrane targets on transplantable midbrain dopamine progenitors. Proc Natl Acad Sci U S A 2015; 112: e1946–E1955.

Bye CR, Thompson LH, Parish CL. Birth dating of midbrain dopamine neurons identifies A9 enriched tissue for transplantation into Parkinsonian mice. Exp Neurol 2012; 236: 58–68.

Carlsson T, Carta M, Winkler C, Björklund A, Kirik D. Serotonin neuron transplants exacerbate L-DOPA-induced dyskinesias in a rat model of Parkinson's disease. J Neurosci 2007; 27: 8011–8022.

Denham M, Bye C, Leung J, Conley BJ, Thompson LH, Dottori M. Glycogen Synthase Kinase 3b and Activin/Nodal Inhibition in Human Embryonic Stem Cells Induces a Pre-Neuroepithelial State That is Required for Specification to a Floor Plate Cell Lineage. Stem Cells 2012; 30: 2400–2411.

Doi D, Samata B, Katsukawa M, Kikuchi T, Morizane A, Ono Y, et al. Isolation of human induced pluripotent stem cell-derived dopaminergic progenitors by cell sorting for successful transplantation. Stem Cell Reports 2014; 2: 337–350.

Freeman TB, Sanberg PR, Nauert GM, Boss BD, Spector D, Olanow CW, et al. The influence of donor age on the survival of solid and suspension intraparenchymal human embryonic nigral grafts. Cell Transplant 1995; 4: 141–154.

Fukuda H, Takahashi J, Watanabe K, Hayashi H, Morizane A, Koyanagi M, et al. Fluorescence-Activated Cell Sorting-Based Purification of Embryonic Stem Cell-Derived Neural Precursors Averts Tumor Formation after Transplantation. Stem Cells 2006; 24: 763–771.

Garcia J, Carlsson T, Dobrossy M, Nikkhah G, Winkler C. Impact of dopamine to serotonin cell ratio in transplants on behavioural recovery and L-dopa induced dyskinesia. Neurobiol Dis 2011; 43:576-587.

Ganat YM, Calder EL, Kriks S, Nelander J, Tu EY, Jia F, et al. Identification of embryonic stem cell-derived midbrain dopaminergic neurons for engraftment. J Clin Invest 2012; 122: 2928–2939.

Gennet N, Tamburini C, Nan X, Li M, Kriks S, Grealish S, et al. FolR1: a novel cell surface marker for isolating midbrain dopamine neural progenitors and nascent dopamine neurons. Sci Rep 2016; 6: 32488.

Grealish S, Diguet E, Kirkeby A, Mattsson B, Heuer A, Bramoulle Y, et al. Human ESC-derived dopamine neurons show similar preclinical efficacy and potency to fetal neurons when grafted in a rat model of Parkinson's disease. Cell Stem Cell 2014; 15: 653–665.

Hedlund E, Pruszak J, Lardaro T, Ludwig W, Vinuela A, Kim KS, et al. Embryonic stem cell-derived Pitx3-enhanced green fluorescent protein midbrain dopamine neurons survive enrichment by fluorescence-activated cell sorting and function in an animal model of Parkinson's disease. Stem Cells 2008; 26: 1526–1536.

Holmqvist S, Brouwer M, Djelloul M, Diaz AG, Devine MJ, Hammarberg A, et al. Generation of human pluripotent stem cell reporter lines for the isolation of and reporting on astrocytes generated from ventral midbrain and ventral spinal cord neural progenitors. Stem Cell Res 2015; 15: 203–220.

Jönsson ME, Ono Y, Björklund A, Thompson LH. Identification of transplantable dopamine neuron precursors at different stages of midbrain neurogenesis. Exp Neurol 2009; 219: 341–354.

Kauhausen J, Thompson LH, Parish CL. Cell intrinsic and extrinsic factors contribute to enhance neural circuit reconstruction following transplantation in Parkinsonian mice. J Physiol 2013; 591: 77–91.

Kee N, Volakakis N, Kirkeby A, Dahl L, Storvall H, Nolbrant S, et al. Single-Cell Analysis Reveals a Close Relationship between Differentiating Dopamine and Subthalamic Nucleus Neuronal Lineages. Cell Stem Cell 2017; 20(1): 29-40.

Kirkeby A, Grealish S, Wolf DA, Nelander J, Wood J, Lundblad M, et al. Generation of Regionally Specified Neural Progenitors and Functional Neurons from Human Embryonic Stem Cells under Defined Conditions. Cell Rep 2012; 1: 703–714.

Kirkeby A, Nolbrant S, Tiklova K, Heuer A, Kee N, Cardoso T, et al. Predictive Markers Guide Differentiation to Improve Graft Outcome in Clinical Translation of hESC-Based Therapy for Parkinson's Disease. Cell Stem Cell 2017; 20: 135–148.

Kriks S, Shim JW, Piao J, Ganat YM, Wakeman DR, Xie Z, et al. Dopamine neurons derived from human ES cells efficiently engraft in animal models of Parkinson's disease. Nature 2011; 480: 547–551.

Lehnen D, Barral S, Cardoso T, Grealish S, Heuer A, Smiyakin A, et al. IAP-Based Cell Sorting Results in Homogeneous Transplantable Dopaminergic Precursor Cells Derived from Human Pluripotent Stem Cells. Stem Cell Reports 2017; 9: 1207–1220.

Mishima Y, Lindgren AG, Chizhikov V V., Johnson RL, Millen KJ. Overlapping function of Lmx1a and Lmx1b in anterior hindbrain roof plate formation and cerebellar growth. J Neurosci 2009; 29: 11377–11384.

Nefzger CM, Su CT, Fabb SA, Hartley BJ, Beh SJ, Zeng WR, et al. Lmx1a allows context-specific isolation of progenitors of GABAergic or dopaminergic neurons during neural differentiation of embryonic stem cells. Stem Cells 2012; 30: 1349–1361.

Niclis JC, Gantner CW, Alsanie WF, McDougall SJ, Bye CR, Elefanty AG, et al. Efficiently Specified Ventral Midbrain Dopamine Neurons from Human Pluripotent Stem Cells Under Xeno-Free Conditions Restore Motor Deficits in Parkinsonian Rodents. Stem Cells Transl Med 2017; 6: 937–948.

Niclis JC, Gantner CW, Hunt CPJ, Kauhausen JA, Durnall JC, Haynes JM, et al. A PITX3-EGFP Reporter Line Reveals Connectivity of Dopamine and Non-dopamine Neuronal Subtypes in Grafts Generated from Human Embryonic Stem Cells. Stem cell reports 2017; 9: 868–882.

Politis M, Oertel WH, Wu K, Quinn NP, Pogarell O, Brooks DJ, et al. Graft-induced dyskinesias in Parkinson's disease: High striatal serotonin/dopamine transporter ratio. Mov Disord 2011; 26: 1997–2003.

Pruszak J, Sonntag K-C, Aung MH, Sanchez-Pernaute R, Isacson O. Markers and Methods for Cell Sorting of Human Embryonic Stem Cell-Derived Neural Cell Populations. Stem Cells 2007; 25: 2257–2268.

Reyes S, Fu Y, Double K, Thompson L, Kirik D, Paxinos G, et al. GIRK2 expression in dopamine neurons of the substantia nigra and ventral tegmental area. J Comp Neurol 2012; 520: 2591–2607.

Samata B, Doi D, Nishimura K, Kikuchi T, Watanabe A, Sakamoto Y, et al. Purification of functional human ES and iPSC-derived midbrain dopaminergic progenitors using LRTM1. Nat Commun 2016; 7: 13097.

Smidt MP, Smits SM, Bouwmeester H, Hamers FPT, van der Linden AJA, Hellemons AJCGM, et al. Early developmental failure of substantia nigra dopamine neurons in mice lacking the homeodomain gene Pitx3. Development 2004; 131: 1145–1155.

Somaa FA, Wang TY, Niclis JC, Bruggeman KF, Kauhausen JA, Guo H, et al. Peptide-Based Scaffolds Support Human Cortical Progenitor Graft Integration to Reduce Atrophy and Promote Functional Repair in a Model of Stroke. Cell Rep 2017; 20: 1964–1977.

Thompson LH, Andersson E, Jensen JB, Barraud P, Guillemot F, Parmar M, et al. Neurogenin2 identifies a transplantable dopamine neuron precursor in the developing ventral mesencephalon. Exp Neurol 2006; 198: 183–198.

Torres EM, Monville C, Gates MA, Bagga V, Dunnett SB. Improved survival of young donor age dopamine grafts in a rat model of Parkinson's disease. Neuroscience 2007; 146: 1606–1617.

Xia N, Fang F, Zhang P, Cui J, Tep-Cullison C, Hamerley T, et al. A Knockin Reporter Allows Purification and Characterization of mDA Neurons from Heterogeneous Populations. Cell Rep 2017; 18: 2533–2546.

Yan Y, Yang D, Zarnowska E.D, Du Z, Werbel B, Valliere C, et al. Directed differentiation of dopaminergic neuronal subtypes from human embryonic stem cells. Stem Cells 2005; 23: 781–790.

Chapter 4.

A human pluripotent stem cell line carrying a FailSafe suicide gene improves the standardization and safety of neural transplants for Parkinson's disease

Isabelle R. de Luzy[1], Kevin Law[1], Jennifer Hollands[1], Lachlan H. Thompson[1], Andras Nagy[2,3], Clare L. Parish[1].

[1] Florey Institute of Neuroscience and Mental Health, The University of Melbourne, Australia.
[2] Australian Regenerative Medicine Institute, Monash University, Melbourne, Victoria, Australia.
[3] Lunenfeld-Tanenbaum Research Institute, Mount Sinai Hospital, Toronto, Ontario, Canada.

4.1 Abstract

Human pluripotent stem cells (hPSCs) provide a valuable resource for regenerative medicine including their potential for cell transplantation. However, the presence of rogue proliferative cells within transplants presents a risk for tissue overgrowth and potential tumorigenesis. Here we utilised a hPSC line carrying a transcriptional link between the suicide gene, herpes simplex virus thymidine kinase (HSV-TK), and an essential cell division gene (CDK1), thereby presenting a suicide system targeting dividing cells yet protected against transgene inactivation, and could be employed to improve the safety of neural transplantation for Parkinson's disease. These CDK1-TK hPSCs were capable of robust ventral midbrain specification and formed healthy neural grafts upon transplantation. Early activation of the suicide gene, by ganciclovir (GCV) administration, resulted in significantly smaller grafts, without affecting the total number or subtype specification of dopamine neurons, their capacity to innervate the host striatum or ability to restore motor deficits in Parkinsonian rats. Importantly the proportion of other, non-dopaminergic neurons, of unknown functional influence, were significantly reduced. Delayed ganciclovir treatment, 5 months after grafting, had no effect on graft size or composition but significantly reduced proliferative cell number. In both paradigms, residual proliferative cells remained – a likely consequence of the suboptimal vascularisation of these neural grafts and thereby ability to deliver GCV. Combined, we present important preclinical findings for the capacity of the FailSafe suicide system to improve both the standardisation and safety of PSC-derived vm grafts for PD, as well as address safety concerns associated with PSC, thereby providing a valuable resource for clinical translation.

4.2 Introduction

Clinical trials have demonstrated the capacity of new dopamine (DA) neurons to structurally and functionally integrate into the brains of Parkinson's disease (PD) patients. More recent years have seen monumental efforts focused on using human PSCs as an ethical, sustainable and standardised alternative to fetal donor tissue for grafting. Current advanced protocols generate correctly specified ventral midbrain (VM) progenitors from hPSCs, with an estimated 90% efficiency (Kirkeby *et al.*, 2017*a*, Niclis *et al.*, 2017*a*). Surprisingly, despite this efficacy, transplantation studies using these progenitors report low yields of DA neurons within the grafts (Gantner *et al.*, 2020; Kirkeby *et al.*, 2012, 2017a; Kriks *et al.*, 2011; de Luzy *et al.*, 2019; Niclis *et al.*, 2017a; Samata *et al.*, 2016), with even the best case examples reporting just 50%. Such observations indicate that the 10% of incorrectly specified cells in culture undergo expansive proliferation following transplantation (de Luzy *et al*., 2019; Niclis *et al.*, 2017b; Samata *et al.*, 2016), with little knowledge of the impact these cells may have on graft function or potential risk of ongoing growth.

Cell sorting approaches, to eliminate unwanted and highly proliferative cell types prior to transplantation, have demonstrated varying success, yet fail to safeguard against post-transplantation adverse events such as activation of quiescent stem cells within grafts and/or tissue overgrowths that may appear with time. Post-transplantation fail-safe approaches, such as suicide gene therapies, have emerged as an alternative therapeutic option. Several approaches now exist, including inducible caspase-9 (iCas9), cytosine deaminase/5-fluorocytine and herpes simplex virus thymidine kinase (HSV-TK) (Di Stasi *et al.*, 2011), with the later system most widely studied and utilised to date. The HSV-TK system, activated by the prodrug ganciclovir (GCV), and targeted at eliminating proliferating cells, has successfully been demonstrated to prevent teratoma growth utilizing either pluripotent cell-specific promoters to drive the suicide gene, such as Oct4 *(Hara et al.*, 2008; Ou *et al.*, 2013) and Nanog (Rong *et al.*, 2012), or cell cycle-dependent driven promoters, including Ki67 (Tieng *et al.*, 2016) or CDK1 (Liang *et al.*, 2018), to target all proliferating cells. Efforts to eliminate proliferating progenitors from within lineage specified cultures and/or transplants have also been explored, with the greatest success observed clinically in the selective elimination of modified donor T lymphocytes in allogeneic hematopoietic stem cell transplants following development of graft-versus-host disease (Bonini *et al.*, 1997; Morgan, 2012). Ablation of hPSC-derived neural progenitor cells (NPC) has also been achievable *in vitro* (Tieng *et al.*, 2016; Liang *et al.*, 2018),

however efforts to eliminate NPCs and impact graft size have largely failed when employing a similar GCV regime to that employed for elimination of PSC-derived teratomas (Tieng *et al.*, 2016). A plausible explanation for these findings, and recognised shortcoming of suicide gene therapy is the risk of silencing or downregulation of the transgene and/or homologous recombination events that have been identified in PSC cultures and teratomas (Kotini *et al.*, 2016; Liang *et al.*, 2018; Tieng *et al*., 2016).

To circumvent this risk, we recently engineered a hPSC line incorporating a transcriptional link between the suicide gene and a cell division locus that is essential for cells to divide or survive. Here, HSV-TK expression was driven homozygously by the CDK1 promoter (noting the critical role for CDK1 in G2 to M phase progression during cell cycle that cannot be compensated by other CDKs) (Liang *et al.*, 2018). We sort to examine the capacity of this fail-safe system to improve the safety of neural transplants targeted for Parkinson's disease. We demonstrate that early GCV administration resulted in significantly smaller grafts at 6 months, yet maintained their full complement of DA neurons, DA innervation, and capacity to restore motor function in Parkinsonian rats, whilst importantly eliminating unwanted off-target neuronal populations. Unsurprisingly, delayed delivery of GCV failed to influence graft volume or neuronal composition, yet reduced the proportion of proliferating cells.

4.3 Materials and Methods

4.3.1 Cell culture, differentiation and ablation

The H1 human embryonic stem cell line, expressing a HSV-TK under the CDK1 promoter (and subsequently referred to as the FailSafe hPSC line), was cultured and differentiated on Laminin-521 (5ug/ml, Biolamina) under xenogeneic-free culture conditions, as previously described (Niclis *et al*., 2017). To initiate differentiation, all cells were exposed to dual-SMAD inhibition using SB431542, (10uM, R&D Systems, 0-5 days, D) and LDN193189 (100-200nM, 0-11D, Stemgent) to generate neuroectodermal progenitors. To generate ventral midbrain progenitors suitable for transplantation, cells were subsequently ventralised using Sonic hedgehog C25II (100ng/ml; R&D systems) and Purmorphamine (2uM; Stemgent) from 1-7D, in addition to caudalisation by the canonical WNT agonist CHIR 99021 (3uM; Stemgent, 3-13D). At 11D, cells were transitioned into 'maturation media' consisting of NBB27 supplemented with GDNF (20ng/ml; R&D systems), BDNF (20 ng/ml; R&D Systems), TGFβ3 (1ng/ml; PeproTech), DAPT (10μM; Sigma-Aldrich),

ascorbic acid (200 nM; Sigma-Aldrich), and dibutyryl cAMP (0.05 mM; Tocris Bioscience). In the absence of ventralising and caudalising cues, differentiating cultures generated forebrain neural progenitor cells following exposure to the dorsalising morphogen FGF2 (20ng/ml) from 11-17D, (subsequently referred to as NPCs).

For *in vitro* ablation of proliferative PSCs or VM neural progenitors, cells were exposed to ganciclovir (GCV, 1-50uM, Roche) for variable durations (2-10D). Medium (± GCV) was changed daily. For transplantation, day 20 VM and day 28 NPC cultures were dissociated in Accutase (Innovative cell technologies) and resuspended into maturation media supplemented with ROCK inhibitor (Y27632, 10uM, Sigma-Aldrich) at 150,000 cells/µl. Prior to transplantation, VM cells were spiked with pan-NPCs at a ratio of 10:1 (90% VM, 10% NPC). Dissociated cells were stored on ice until the time of implantation.

4.3.2 Surgical procedures

All animal procedures were performed in agreement with the Australian National Health and Medical Research Council's (NHMRC) published Code of Practice for the Use of Animals in Research, and approval granted by The Florey Institute of Neuroscience and Mental Health Animal Ethics committee. Animals (of either sex) were group housed on a 12:12-hour light/dark cycle with ad libitum access to food and water. Surgeries were performed on athymic (CBH^{rnu}) nude rats under 2-5% isoflurane anaesthesia. The host midbrain dopaminergic circuitry was unilaterally ablated by stereotaxic injection of 6-hydroxydopamine (6-OHDA, 3.5ul, 3.2ug/µl) into the rat medial forebrain bundle, using previously described methods (Niclis *et al.*, 2017b). At 8weeks after 6-OHDA lesioning animals received unilateral cell grafts (1.5µL, 100,000 cells/µl), at the following stereotaxic coordinates: 0.5mm anterior, 2.5mm lateral to bregma and 4.0mm below the dura surface.

Daily intraperitoneal injections (i.p.) of GCV (50mg/kg) were administered to a subset of animals from either 5-13wks ('early GCV') or from 14-21wks ('late GCV') after transplantation. In a second cohort of rats, targeted at optimising GCV delivery, animals received GCV (50-100mg/kg) either once or twice daily, from 2-10wks or from 5-13wks. Animals were injected for a total of 8 weeks in both studies.

4.3.3 Behavioural Analysis

Intraperitoneal administration of D-amphetamine sulfate (3.5mg/kg, Tocris Biosciences) was conducted 4 weeks after 6-OHDA lesioning to assess motor deficits in unilateral lesioned rats by rotational asymmetry testing. Only animals that reached a set criterion of >5rotations per minute were included in this study. To assess functional integration of transplanted cells, behavioural testing was repeated at the end of the study (24wks). Animal groups were as follows: (i) Lesion only (subsequently referred to as 'Lesion'), (ii) Lesion + GCV (referred to as 'GCV'), (ii) VM+NPC cell graft ('Cells'), (iii) Cells + GCV from 5-13 wks (Cells + early GCV), (iv) Cells + GCV from 14-21wks (Cells + late GCV). For behavioural studies, group sizes were 12-15 rats, while assessments of histology only (e.g. for assessment of grafts at earlier time points and optimisation of the GCV dosage/administration) involved group sizes of 5-6 rats.

Antibody name	Species	Concentration	Supplier	Catalogue #
BARHL1	Rabbit	1:200	Novus Biologicus	NBP1-86513
Calbindin	Mouse	1:1000	Swant	CB300
Adenomatous polyposis coli (APC)	Mouse	1:200	Abcam	ab16794
ChAT	Goat	1:100	Millipore	
DAPI	-	1:5000	Sigma Aldrich	D8417
FOXA2	Goat	1:200	Santa Cruz	sc-6554
GFAP	Rabbit	1:1000	DAKO	
GFP	Chicken	1:1000	Abcam	AB13970
GIRK2	Rabbit	1:500 + strep	Alomone Labs	APC-OO6
HNA	Mouse	1:300	Millipore	MAB1281
KI67	Rabbit	1:1000	ThermoFisher	LBVRM-9106-S1
NeuN	Rabbit	1:1500	R&D Systems	
NESTIN	Mouse	1:1000	Millipore	MAB1259
OCT4	Mouse	1:100	Santa Cruz	sc-5279
OTX2	Goat	1:500	R&D Systems	RDSAF1979
PAX6	Mouse	1:50	DSHB	NA
PH3	Rat	1:1000	Abcam,	AB10543
PITX2	Sheep	1:200	R&D Systems	AF7388
PSA-NCAM	Mouse	1:500	Santa Cruz	sc-106
RECA	Mouse	1:5000	Abd Serotec	MCA970R
RFP	Rabbit	1:1000	Rockland Labs	600-901-379
SOX2	Goat	1:300	R&D Systems	AF2018
TH	Rabbit	1:1000	Pel-freeze	P40101-0

Table. 4.1 List of primary antibodies

4.3.4 Tissue processing and Histochemistry

For confirmation of appropriate *in vitro* specification of neural progenitors, cultures were fixed using paraformaldehyde (PFA, 4%, 10mins) at varying timepoints during the differentiation (0, 8, 11, 16, 19, 25D). For assessment of graft survival, differentiation and integration, animals were killed by an overdose of sodium pentobarbitone (100mg/kg) at 5, 10 or 24wks after transplantation and transcardially perfused with 4% PFA. Brains were cryosectioned (40uM; 12 series) on a freezing microtome. Immunohistochemical analysis of fixed cultures or brain sections was performed as described previously(Somaa *et al.*, 2017). Primary antibodies and dilutions can be found in Table. 1. Secondary antibodies were used at a dilution of 1:200 (Dylight 488-, 549, or 649-conjugated donkey anti-mouse, anti-chicken, anti-rabbit, anti-goat, anti-sheep and anti-strep sourced from Jackson ImmunoResearch Laboratories).

4.3.5 Microscopy and Quantification

Brightfield imaging of chromogenic staining was performed using a Leica Microscope DM6000 microscope. Fluorescent images were obtained on a Carl Zeiss Axio Observer Z.1 epifluorescence or Carl Zeiss LSM780 confocal microscope. Images captured at 20x were used to quantify total number of DAPI+, OTX2+, FOXA2+, PITX2+, HNA+, KI67+ and RECA+ cells either in culture or within the graft. PSA-NCAM expression was used to delineate the graft boundaries and estimate graft volume according to Cavalieri's principle. Quantification of TH+ cell bodies was performed on live images. Assessment of GIRK2+ and Calbindin+ cells within the grafts were quantified based on co-localisation with TH+ dopamine neurons from acquired confocal images.

4.3.6 Statistical Analysis

All behavioural testing and histological quantification were conducted by researchers blinded to experimental groups. All data is presented as mean ± SEM. Statistical tests employed (one-way ANOVA, two-way ANOVA, Student's t tests), and number of animals/groups for each assessment are stated in the figure legends. All statistical analyses were performed using GraphPad Prism and alpha levels of $p<0.05$ were considered significant (*$p<0.05$, **$p<0.01$, ***$p<0.001$).

4.4 Results

4.4.1 Directed differentiation of FailSafe hPSCs and assessment of suicide system efficacy

Prior to transplantation we tested the capacity of the FailSafe hPSC line to generate VM progenitors suitable for transplantation and assessed the efficacy of the suicide system *in vitro*. FailSafe cells competently differentiated to vm progenitors, confirmed by the high proportion of cells co-expressing OTX2+ and FOXA2+ (81.5 ± 5.0%) at day 11 of differentiation (Figure. 4.1A, D), with minimal contamination of off-target diencephalic progenitors (Figure. 4.1B, <5%, BARHL1+ PITX2+). Whilst progenitors were isolated for transplantation at day 20 of differentiation, parallel cultures were extended to day 25 to confirm their capacity to generate tyrosine hydroxylase (TH+) expressing DA neurons (30.1 ± 0.6%, Figure. 4.1C, D) with comparable efficiency to previous studies *(Niclis et al.*, 2017a, Kriks *et al.*, 2011).

To determine the capability of the FailSafe system to ablate proliferative vm progenitors, and identify the optimal timing to initiate suicide *in vitro*, we tracked proliferation during the differentiation. As expected we observed a progressive decrease in proliferation over time (DO: 98.4 ± 1.2%, D8: 64.2 ± 3.2%, D12: 50.2 ± 2.0%, D16: 35.9 ± 3.3%, D20: 11.3 ± 1.0%, D25: 3.0 ± 0.5%, Figure. 4.2A-C,), noting >10% of cells at the time of grafting

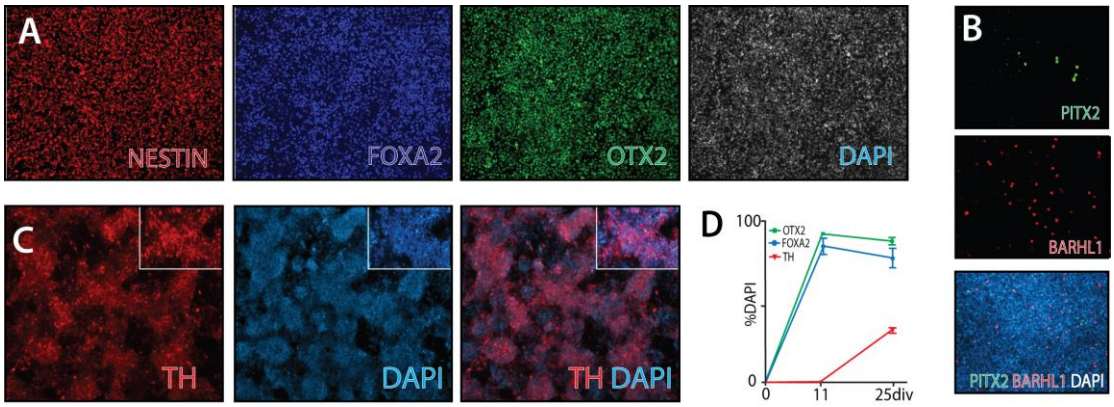

Figure 4.1. Efficient differentiation into midbrain DA neurons from a novel failsafe suicide cell line

(A-B) Competent differentiation of failsafe CDK1-TK hESC into vm progenitors was confirmed by high co-expression of OTX2, FOXA2 by 11DIV (A) and low contamination of subthalamic progenitors (PITX2+ and BARHL1+ cells). (C) Competent differentiation of vm progenitors into TH+ DA neuron at 25DIV **(C). (D)** Quantification of the co-expression of key cardinal vm markers; OTX2, FOXA2 and TH confirmed efficient vm differentiation at 11 and 25 DIV.

remained proliferative. We elected to activate the suicide gene at a time when cells were sufficiently patterned into vm progenitors, with a high proportion of dividing cells, whilst also comprising a sufficient number of post-mitotic cells to enable additional assessment of patterned into vm progenitors, with a high proportion of dividing cells, whilst also comprising a sufficient number of post-mitotic cells to enable additional assessment of potential toxicity of the prodrug. Consequently, cultures were exposed to GCV from day 9 of differentiation. Despite the fact we competently eliminated all PSCs in parallel undifferentiated cultures, only partial ablation (~50%) of proliferating vm progenitors could be achieved within the same time period, suggestive that VM progenitors may require a longer period of exposure (Figure. 4.2D). Such observation may, in part, explain why GCV regimes used to ablate teratomas failed to influence/reduce graft size following transplantation of vm progenitors by others (Tieng *et al.*, 2016).We therefore looked to prolong the duration of GCV administration. Complete elimination of all KI67+ (and PH3+) progenitors in culture could be achieved following exposure for 10 days (Fig. 4.2E-H), with the majority of remaining cells expressing TH, indicative of post-mitotic dopaminergic neurons (Figure. 4.2I-J).

4.4.2 Tracking the proliferation and maturation of vm progenitor grafts to identify the optimal age to administer ganciclovir

Previously we reported an >9-fold increase in the volume of VM progenitor grafts from 6 weeks to 24 weeks after implantation (Niclis *et al*., 2017b). Such observation suggested the presence of persistent proliferative progenitors *in vivo* and the need to better understand the growth kinetics of the grafts in order to optimally remove highly proliferative cells whilst minimally affecting the number of functioning dopamine neurons. We therefore examined graft volume and proliferation over the course of 6 months, as well as the timing at which DA progenitors became post-mitotic.

Grafts showed a significant, exponential volumetric expansion over time (5wks: 0.4 ± 0.1 mm3, 10wks: 1.1 ± 0.2 mm3, 24wks: 3.5 ± 0.4 mm3; Figure. 4.3A-C, G). Ki67 immunolabeling highlighted a large pool of proliferative cells were present at early periods after transplantation (5wks: 9306 ± 1997, 10wks: 4672 ± 629), that steadily decreased in proportion by 24weeks (1807 ± 230 KI67+/mm^3, Figure 4.3D-G). Interestingly, the total number of DA neurons remained unchanged from 5 to 24weeks (Figure, 4.3H, 5wks: 4752 ± 708, 10wks: 4635 ± 1080, 24: 5294 ± 467), resulting in a significant decrease in

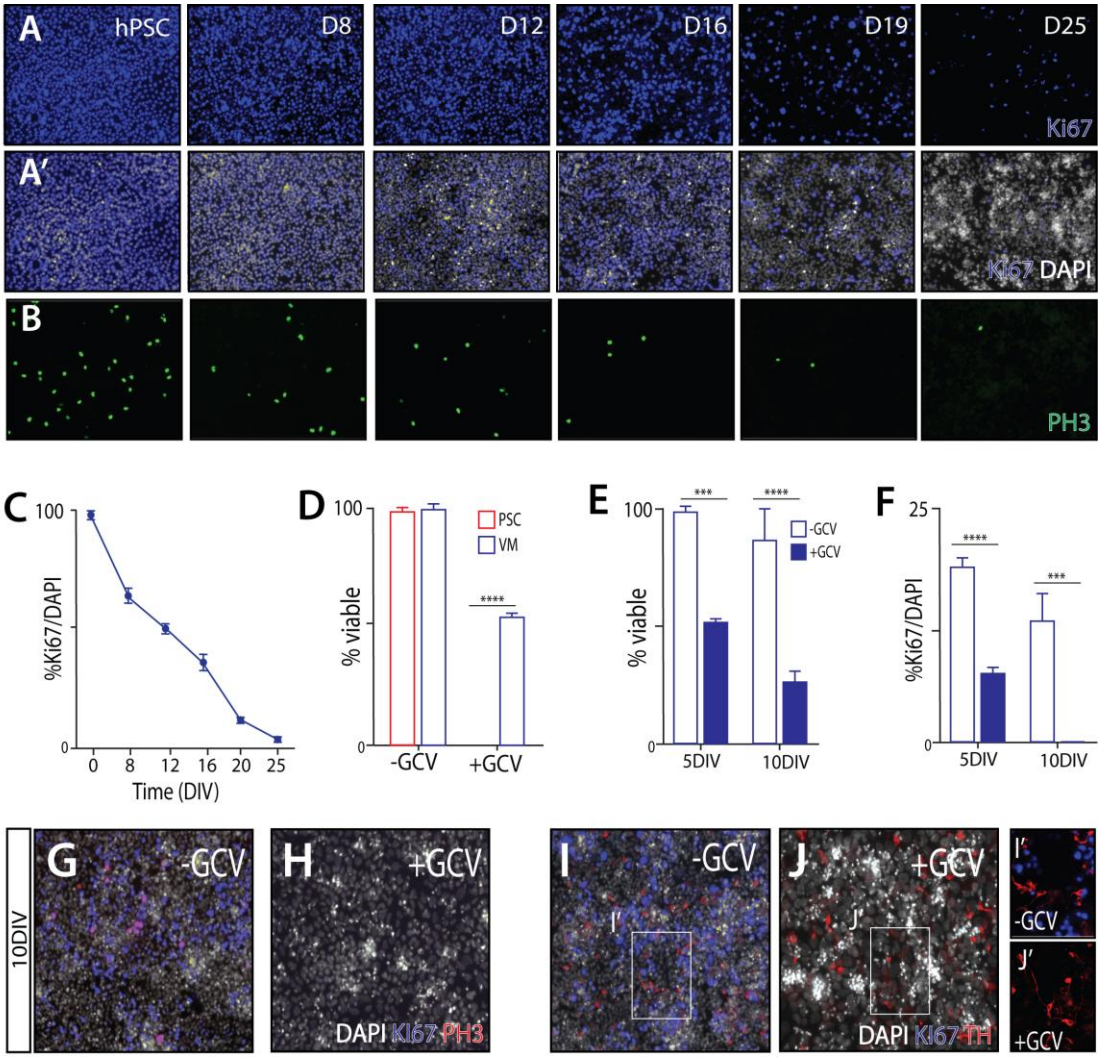

Figure 4.2. *In vitro* proliferation and elimination of stem cell-derived VM progenitors from a novel failsafe suicide cell line

(A-C) Immunohistochemical labelling of KI67 **(A)** and PH3 **(B)** tracked proliferation during the differentiation of PSC into dopamine neurons (25 DIV) and indicated a progressive decline over time **(C)**. **(D)** Addition of GCV (10uM) in culture to either PSCs (red) or PSC-derived vm progenitors (blue) suggested a prolonged exposure (>5days) is required to achieve complete elimination of all Ki67+ progenitors. **(E)** Prolonged exposure to GCV significant decrease in surviving progenitors. **(F)** Quantification of KI67+ cells following GCV exposure (closed blue bars) confirmed successful elimination of all dividing VM progenitors after 10 DIV. **(G-H)** Immunostaining of cultures for KI67 (blue) and PH3 (red) in the absence **(G)** or presence **(H)** of GCV **(I-J)** Co-labelling of KI67 and TH indicated that some cells remaining after sustained *in vitro* GCV exposure (10DIV) were post-mitotic dopaminergic neurons ($Ki67^{-}/TH^{+}$). Note the healthy morphology and fibre outgrowth of the TH neurons even in the presence of GCV **(J').** Abbreviations: PSCs; pluripotent stem cells, VM; ventral midbrain, DIV; days *in vitro*, TH; tyrosine hydroxylase, GCV; ganciclovir

dopaminergic cell density due to the continued expansion of the graft size (5wks: 15000 ± 1763 TH+/mm^3, 10wks: 4251 ± 414, 24wks: 1524 ± 83, Figure. 4.3I). As the full complement of DA neurons were present by 5wks, graft expansion observed beyond this time was a result of poorly specified progenitors not destined to become DA neurons.

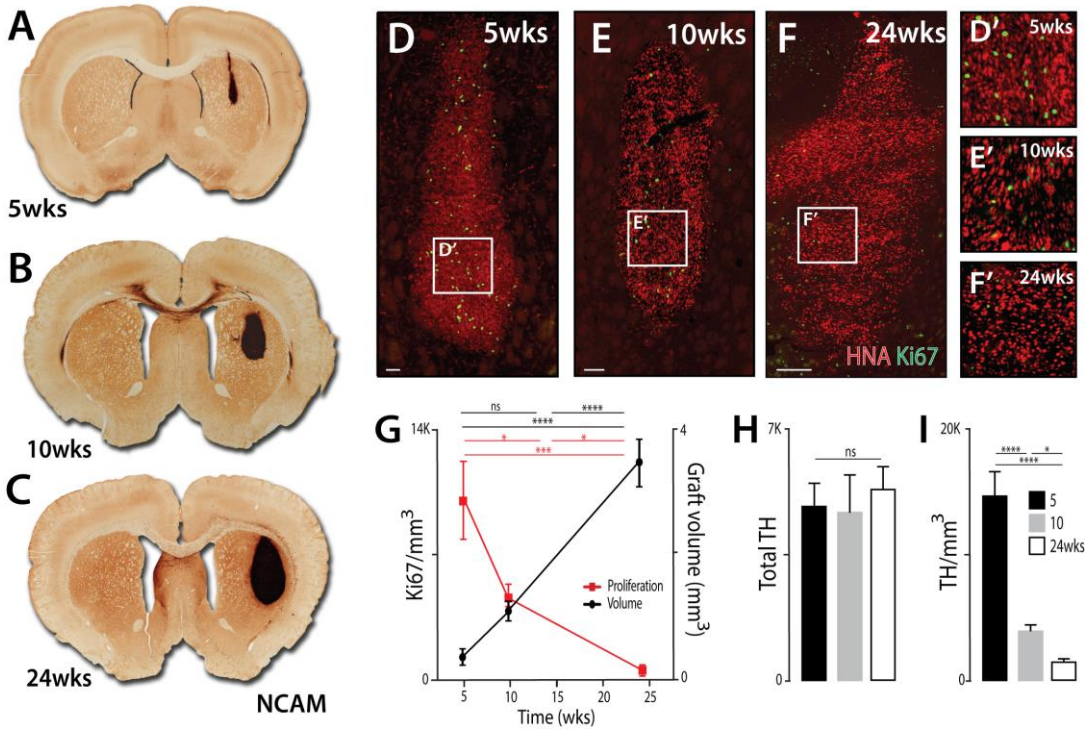

Figure 4.3. Tracking expansion of VM progenitors and birth of DA neurons after engraftment

(A-C) Coronal sections of the rat brain immunolabelled for human-specific NCAM demonstrates relative graft expansion between 5 **(A),** 10 **(B)** and 24wks **(C). (D-F)** Immunohistochemical labelling of transplants with HNA (red) and Ki67 (green). **(D'-F', G)** Quantitative assessment of all groups highlighted significant overgrowth throughout the study, but by 24wks the proportion of proliferating cells was significantly reduced. **(H-I)** Quantification of TH+ cells confirmed all dopaminergic neurons are born by 5wks **(H),** with a significant reduction in dopaminergic density over time as a result of continued graft expansion **(I).** Abbreviations: NCAM; neural cell adhesion molecule, wks; weeks, HNA; human nucleic acid

4.4.3 Early exposure to ganciclovir prevents expansion of non-DA proliferative progenitors whilst conserving DA graft composition and functionality

With knowledge of the graft kinetics, we next set out to assess the ability to suicide proliferative cells in a PSC-derived neural graft (Figure. 4.4A). Animals receiving 6-OHDA lesions were tested for amphetamine-induced motor asymmetry and only animals showing > 6 rotations/min were included in the study. With the current high efficiency of VM differentiation protocols, we purposefully spiked the donor cells with a pool of proliferative forebrain neural progenitors (PAX6+SOX2+), previously demonstrated to possess tumorigenic potential (data not shown), in order to test the capacity of the FailSafe system to eliminate dividing neural progenitors and ensure maximal safety. Such an approach was adopted as the research and clinical community continues to debate the necessity of sorting and suicide approaches for VM grafting in PD. We argue that such

suicide tools are advantageous as a safe-guarding approach, to protect against unforeseeable adverse events that may arise in patients.

The specification of the HSV-TK into a forebrain neural progenitor identity was confirmed by the co-expression of OTX2+/PAX6+/SOX2+/NESTIN+, in addition to the absence of the ventral marker FOXA2 (Supplementary 4.1A-B). At 5 weeks after grafting, the presence of both vm progenitors and forebrain NPCs was confirmed by presence or absence of cells expressing FOXA2, respectively (Supplementary 4.1C-E). To prevent elimination of vm progenitors destined to become DA neurons, ganciclovir treatment commenced after 5wks post-transplantation. In light of previous findings demonstrating no effect on graft size after 2 weeks of GCV in animals receiving HSV-TK vm progenitor grafts (Tieng *et al.*, 2016), as well as the prolonged treatment required to eliminate proliferating vm progenitors *in vitro* (Fig. 4.2D), we elected to expose animals to GCV for an extended duration (8wks) (Figure. 4.4A).

At 24 weeks after grafting, rotational testing was repeated in all animals, with a significant improvement in motor function observed only in grafted animals, irrespective of exposure to GCV (Figure 4.4B, green and blue lines), indicating that GCV had no detrimental effect on the functional DA unit of the graft. Post-mortem assessment revealed surviving grafts in all animals (visualised by the presence of human-specific PSA-NCAM staining) (Figure 4.4C-D). Grafts in the presence of GCV, however, were significantly smaller in volume (Cells: $3.5 \pm 0.4\ mm^3$; Cells+GCV: $2.5 \pm 0.2\ mm^3$), contained fewer cells (Control: 577,226 ± 70,530 HNA+, GCV: 306,451 ± 33,365 HNA+ cells), and showed a significant reduction in cell density (Figure. 4.4I-M).

Despite concerns of pro-apoptotic proteins being released and influencing neighbouring cells following suicide-induced cell death within the graft, we observed no significant difference in the number of surviving TH+ DA neurons (Cells: 5304 ± 643; Cells+GCV: 4627 ± 612, Figure. 4.4E-G), supporting the comparable improvement in functional recovery observed in untreated and GCV-treated graft animals. As a result of the significant reduction in graft volume, density of DA neurons within GCV treated grafts were significantly increased and notably more homogeneous than grafts in the absence of GCV (Cells: $5304 \pm 643/mm^3$, Cells + GCV: 4626 ±612, Figure 4.4E'-F'', H). Importantly, exposure to GCV had no impact on A9/A10 subtype specification within the graft (Figure

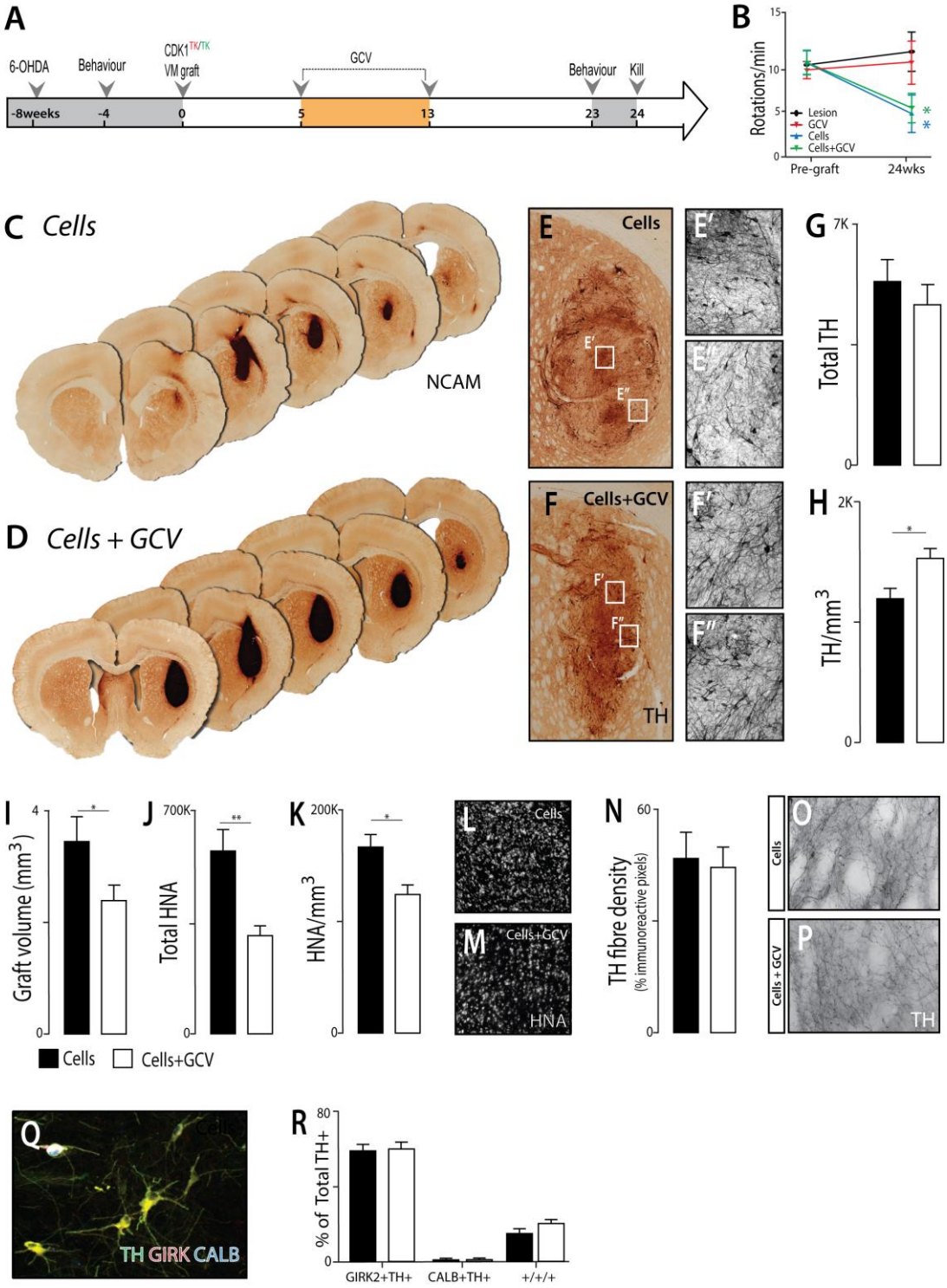

Figure 4.4. Early exposure to GCV prevents expansion of neural progenitors with no toxic effect on dopaminergic function

(A) Schematic overview of study design inclusive of behavioural testing, cell transplantation and GCV injections. **(B)** All grafted animals showed restoration of amphetamine-induced rotational asymmetry at 24wks, irrespective of GCV exposure. **(C-D)** NCAM coronal sections surviving grafts in both groups. **(E-F)** Photomicrographs showing distribution and density of TH+ cells within grafts in the presence or absence of GCV. **(G)** Exposure to GCV had no effect on TH+ cell number within the graft. **(E'-F', H)** Significant increase in dopaminergic density following GCV exposure. **(I-K)** Graphs highlighting that delayed GCV delivery generated significantly smaller grafts in volume (I), total cell number (J) with a significant decrease in density of graft-derived cells (K). **(L-M)** Representative images of HNA+ labelled cells in grafted animals (±GCV). **(N)** Quantitative assessment of TH+ fiber density in the dorsal caudate

putamen. **(O-P)** High power images illustrate maintained innervation of TH+ fibres in the striatum of animals exposed to GCV. **(Q)** Representative photomicrograph to show the co-expression of TH together with GIRK2 and/or calbindin, indicative of A9- and A10 midbrain dopaminergic subtypes. **(R)** Assessment of TH co-labelling with GIRK and/or calbindin confirmed that GCV grafts retained the capacity to form mature vm dopaminergic neurons of both A9 and A10 phenotypes.

4.4Q-R), or the ability of DA neurons to appropriately innervate striatal targets (Cells: 47.3± 6.7%, Cells + GCV: 44.7 ± 5.3%) (Figure. 4.4N-P).

Recent transcriptomic and histochemical studies of mature dopaminergic grafts have highlighted their heterogeneous composition including not only other neuronal and neural populations but also non-neural cell types, despite implanting vm progenitors of high purity (~90%) (Bye *et al.*, 2019; Tiklová *et al.*, 2019). We therefore investigated whether GCV treatment may preferentially impact a specific progenitor population and/or influence the neural specification of the grafts. We observed an overall trend of increased neuronal specification within grafts exposed to GCV (Cells: 35 ± 0.04%; Cells + GCV: 42 ± 0.04%, Figure 4.5A), indicating that the relative contribution from non-neuronal fates was reduced.

While TH cell number was unchanged across the graft groups (Figure 4.4G), we observed a significant decrease in total NeuN+ cells in GCV-treated grafts (Cells: 201422 ± 27880, Cells + GCV: 128242 ± 15300), indicating that GCV treatment could reduce the relative contribution of unwanted, non-DA neurons (Figure 4.5B-D). Further profiling, to reveal the identity of the unwanted neuronal populations eliminated by GCV, showed few and unchanged proportions of cholinergic neurons (data not shown). A reduction in both oligodendrocytes (CC1+), and density of astrocytes (GFAP+) was also observed in GCV-treated grafts (Fig. 4.5E-I). These present findings, in conjunction with prior transcriptomic analysis that highlighted an absence of other neuronal (GABAergic, glutamatergic, serotonergic) and neural populations in immature grafts (5 wks) but present at the mature stages (6 months) (Bye *et al.*, 2019), suggests the contribution from other neural and neuronal populations within the graft are born after DA neurons and therefore susceptible to GCV in the present treatment regime.

Surprisingly, the present GCV regime (‘early’ administered from 5-13 weeks post-transplantation) had no impact on the small pool of proliferative cells (~1% KI67+ cells) remaining at 24 wks (Figure 4.5J-L). Whilst this may suggest the presence of a quiescent stem cell/progenitor population that emerged after GCV treatment ceased, we were able to confirm that at least a proportion of the KI67+ cells remaining within the grafts were of host (HNA-), and not graft (HNA+) origin, and in some cases, were found in close

proximity, or localised, to host blood vessels (Figure 4.5M), as previously observed in long term neural grafts (Somaa *et al.*, 2017).

4.4.4 Late delivery of ganciclovir has no impact on graft size and composition but reduces the residual proliferative progenitor pool

Potential inclusion of undetectable tumorigenic cells within donor cells remains a realistic concern for the clinical application of hPSCs and highlights the need for strategies that can be initiated should adverse events arise to ensure patient safety. Others have demonstrated the capacity of suicide systems to protect patients from rogue grafts, by complete elimination of all grafted cells (using an alternative suicide system) (Itakura *et al.*, 2017), yet they consequentially lose all therapeutic benefit intended from the cell transplant. We therefore looked to examine the capacity of the FailSafe suicide system to be employed in this capacity - targeting elimination of quiescent, residual proliferative cells.

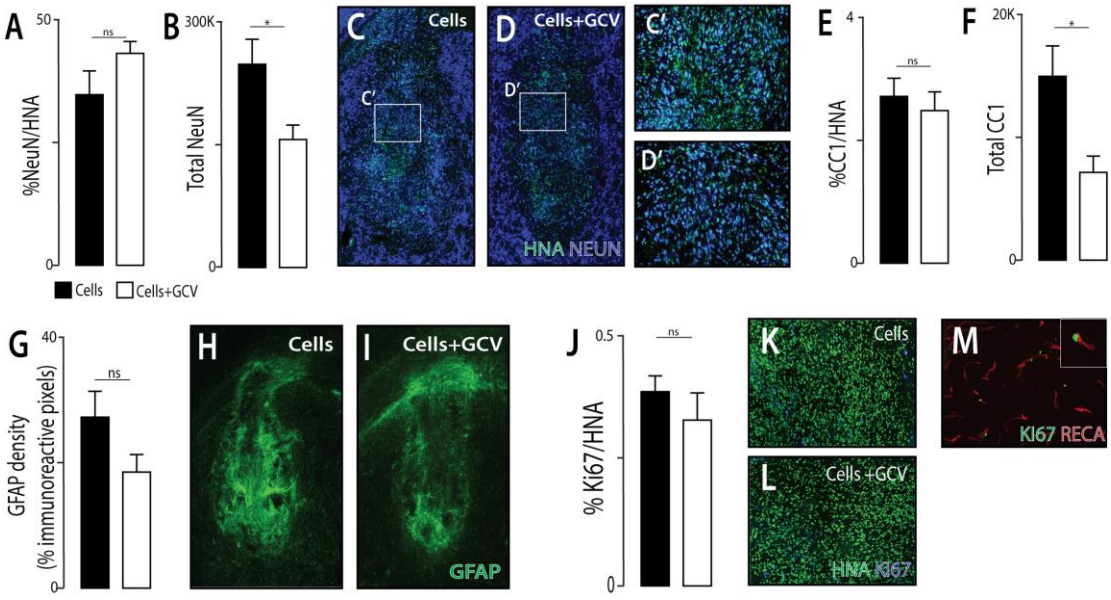

Figure 4.5. Failsafe suicide system does not preferentially eliminate specific neural populations
(A-B) Quantitative assessment of proportion and total neurons (NeuN+) in grafted animals. **(C-D, C'-D')** Photomicrographs illustrate a significant reduction in the proportion of NeuN-immunolabelled neurons (blue) only in the presence of GCV. **(E-F)** The proportion of CC1+ oligodendrocytes were unaffected by GCV, but total number was reduced. **(G)** Relative contribution of GFAP+ astrocytes remained unchanged. **(H-I)** Representative images immunolabelled with GFAP. **(J)** No change in small residual pool of proliferative cells remaining at 24wks. HNA (green), Ki67 (blue). **(K-L).** High power image showing KI67+ proliferative cells in close proximity to host (RECA+) blood vessels **(M)**.

To achieve this, in a parallel cohort of 6OHDA lesioned and grafted animals we delivered GCV from 14-22wks (Fig.4.6A). As anticipated, grafts in the presence and absence of GCV showed comparable reductions in amphetamine-induced rotational asymmetry at 24weeks (data not shown). Histological assessments again showed viable grafts in all animals and as expected, late GCV treatment had no effect on graft volume (Fig.4.6B-D), cell number (Fig. 4.6E), or density (Figure 4.6F), suggesting the majority of graft growth occurs by 14wks. Delayed exposure of the graft to GCV, however, significantly reduced the number and density of proliferative cells (Cells: 1807 ± 230 KI67/mm^3, Cells+GCV: 1211 ± 221 Ki67+/mm^3) (Figure. 4.6G-J).

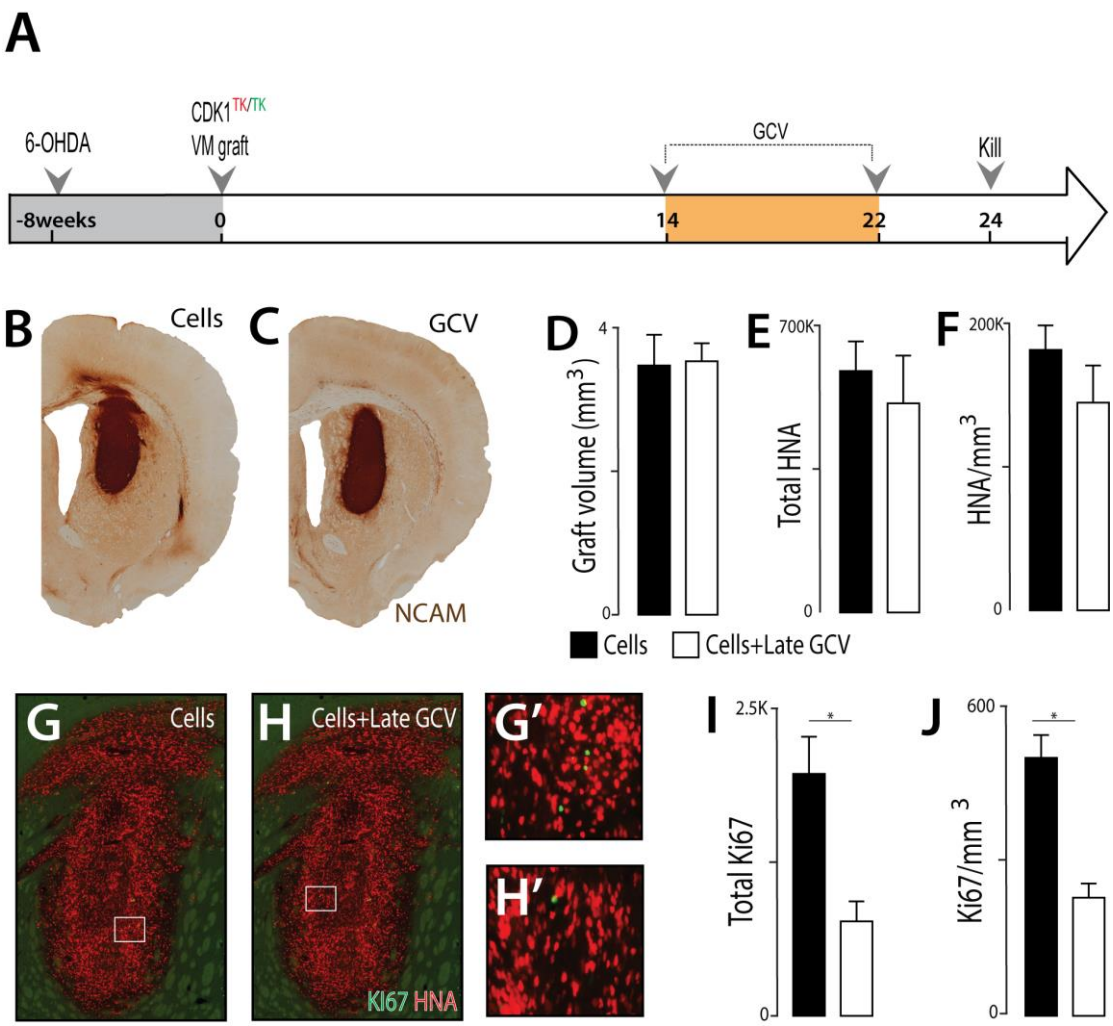

Figure 4.6. Late GCV delivery significantly reduces the number of residual proliferative cells but has no effect on graft size

(A) Schematic detailing the transplantation of cells derived from CDK1-TK suicide line and the experimental timeline for *in vivo* procedures. **(B-C)** Human specific NCAM enables visualization of grafted cells in striatum. **(D-E)** No difference in total volume or cell number were observed following late delivery of GCV. **(G-H)** Representative photomicrographs of KI67-immunolabelled proliferative cells within grafts. **(G'-H', I-J)** Grafts receiving GCV were significantly reduced in total number and density of proliferative (Ki67+) cells.

4.4.5 Modifying ganciclovir administration to target residual proliferating progenitors within neural grafts

The presence of residual graft-derived proliferative cells within grafts after prolonged GCV, initiated either early or late after transplantation, raised questions regarding the efficiency of the prodrug delivery to graft. We therefore sort to assess the impact of altering the mode of GCV treatment (by pre-treatment of cells *in vitro* 48hrs prior to grafting) or by modifying the frequency (once or twice daily) and/or dose of GCV. Pre-treatment of neural progenitors with GCV *in vitro* prior to transplantation resulted in significantly smaller grafts with a reduced number and density of KI67+ proliferative cells (Figure 4.7A-B, K-L), yet showed poor survival of TH+ DA neurons (Figure 4.7M), suggesting that many of the correctly specified progenitors, destined to become DA neurons were likely ablated. Such observations align with fetal tissue studies showing the critical importance of donor age, and the requirement of mitotic cells at the time of implantation for optimal graft survival, and high DA neuron yields (Bye *et al*., 2012; Freeman *et al*., 1995; Torres *et al*., 2007).

The observation of continued cell growth in GCV-treated cultures during the first few days of treatment in both PSCs (~2days) and NPCs (~3days) (Tieng *et al.*, 2016), suggested a potential delayed activation of the HSV-TK suicide system. We therefore tested this theory *in vivo* and treated grafts with GCV at an earlier stage, commencing 2 weeks after transplantation. Similarly, to pre-treatment *in vitro*, we found that earlier treatment also caused a negative impact on the DA population (Figure 4.7M), and failed to sufficiently ablate all residual proliferative cells (Figure 4.7L).

With observations that higher doses of GCV were required to ablate vm progenitors *in vitro* (data not shown), we sort to assess the impact of increasing the daily dose of GCV (100mg/kg) or frequency of administration (twice daily, noting the short S-phase of neural progenitors compared to PSCs). This also had minimal benefit. While graft size was reduced in both cases (Figure 4.7E-F, K), and TH cell counts remained unchanged for the high GCV dose (yet reduced for the twice daily administration), comparable to 50mg/kg GCV daily (Figure 4.3K), persistent KI67 cells still remained (Figure 4.7L).

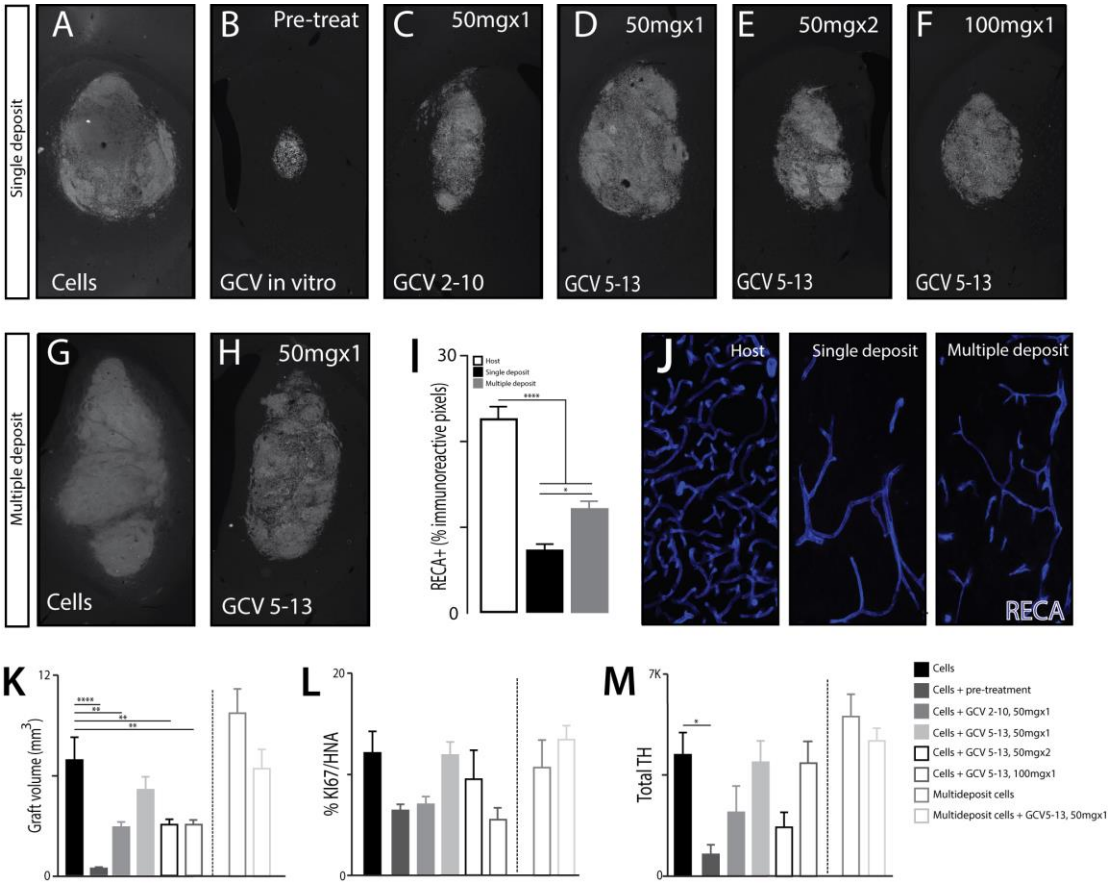

Figure 4.7. Alterations to timing, frequency and dosing of GCV failed to eliminate all proliferating cells

(A-H) Representative photomicrograph of grafted cells delivered either as single **(A-F)** or multiple deposits **(G-H)** labelled by human specific nucleic acid (HNA) demonstrates relative graft size in the presence or absence of GCV. (I) Cells delivered as multiple deposits allow for significantly greater blood vessel infiltration compared to single deposit grafts, but still remains inferior to the host vasculature. (I) Representative images depicting the relative density of RECA+ blood vessels in either single or multiple deposit grafts or host striatal tissue. **(K-M)** Graphs depicting total volume **(K)** proportion of proliferative cells **(L)** and total surviving DA neurons **(M).**

In light of failed success of altering the GCV administration, we questioned whether the problem of removing residual progenitors was due to the vascular supply of the grafts, acknowledging also the solid neural tissue generated from the progenitor grafts. We therefore examined the extent of the vascular network within the grafts. RECA1 and Claudin immunolabeling, to identify host and graft-derived vasculature, respectively, revealed minimal blood vessel formation within young grafts (5 and 10 weeks post-transplantation), that showed modest evidence of increasing in density/maturation, but remained significantly less than the host brain (5wk old graft: 3.2 ± 0.0%, 10wks: 3.03 ± 0.0%, 24wks: 6.83 ± 0.1%, host brain: 20.93 ± 0.1%, Supplementary 4.2A-E, also observed in Appendix 3). Note within the grafts, no evidence of graft-derived (Claudin+) blood vessels could be observed (data not shown). This poor vasculature supply, and thereby

influence on the capacity to deliver GCV may, in part, explain the presence of proliferative cells within neural grafts.

In assessment of the vascular supply and proliferative cells within the neural grafts, we observed a homogenous distribution of Ki67 progenitors within the graft core, yet notably fewer at the graft-host border (Figure 4.3D-F). We therefore speculated whether an increased contact with host vasculature at the graft periphery may aide in GCV delivery within these unvascularised regions. We therefore sought to assess the influence of making multiple small deposits of vm progenitors, to increase the contact between the grafted cells and the host vasculature. Multiple site grafting enhanced survival of DA neurons (as previously reported in fetal studies, Bjorklund *et al*, 1983, Figure 4.7M), and additionally promoted further infiltration of host blood vessels, yet remained notably inferior to the density of vasculature observed within the host striatal tissue (Figure 4.7I-J, Supplementary 4.2A', D) and importantly failed to provided further benefit in response to GCV over single deposit grafts (Figure 4.7K).

4.5 Discussion

In the present study we employed a suicide system to improve the safety of hPSC-derived neural transplants for PD. Utilising a transcriptional link between the suicide gene and a cell cycle essential gene, CDK1, as well as homozygous targeting, ensured the FailSafe system circumvented the risks associated with gene silencing or diploid loss of heterozygosity. We demonstrated that prolonged activation of the suicide system from (5) weeks after cell implantation had no negative impact on the functional capacity of the graft to restore motor function, yet generated significantly smaller grafts (~50% reduction in cell number), that were enriched for dopaminergic neurons and maintained targeted DA innervation capacity. In contrast, late GCV treatment from (14) weeks failed to impact on graft size yet significantly reduced the proportion of graft-derived proliferative cells. Collectively we demonstrate the benefits of the suicide-based system to improve the safety and composition of hPSC-derived neural transplants for PD.

The early activation of the suicide gene, intentionally after the identified post-mitotic birth of the DA neurons within the graft, reduced the expansion of poorly specified progenitors within the grafts. Supporting this was the maintained composite of TH+ cells within smaller grafts (resulting in increased DA density) and the overall reduction in NeuN+ neurons, indicating that the relative contribution of other, non-dopaminergic neuronal populations

was reduced. Such findings are of critical importance as the field remains largely unaware of the impact other neuronal, and non-neuronal populations, may have on graft function. Evidence does however exist for the detrimental impact of one cell type within vm progenitor grafts, with both preclinical and clinical studies providing evidence for 5HT+ serotonergic neurons contributing to graft induced dyskinesias (Carlsson *et al*., 2007; Hagell *et al*., 2002; Mendez *et al*., 2005; Politis, 2010).

Whilst smaller grafts were observed, and of maintained DA functionality, the presence of residual proliferative cells at 24 weeks after grafting raised concerns surrounding efficiency of the suicide system in the current context. With GCV administration ceased at 13 weeks, it is plausible that these cells reflect quiescent stem cells, activated after the termination of the prodrug, and suggests that periodic GCV treatment after transplantation (rather than a single prolonged period) may be required to target such populations. However, when animals were examined acutely after termination of GCV delivery (i.e. those animals receiving 'late' delivery of the prodrug from 14-22weeks), persistent proliferative cells, albeit reduced in number, remained in the grafts. In addition, unlike the early GCV treatment, these animals were not exposed to a prolonged GCV 'wash-out' period to assess whether quiescent stem cell populations may appear at more protracted stages after cessation of treatment.

Such observations lead one to questions the rigor of GCV delivery – both mode of delivery, dose and frequency. To date most stem cell-based studies employing suicide systems to ablate grafts implant PSC, providing evidence that drug activation of the systems can eliminate teratomas. Here we report the resistance of vm neural progenitors to apoptosis *in vitro*, by comparison to PSCs in culture, suggesting that ablation of teratomas may in fact be 'easier' than lineage restricted progenitors. In support of our work and others, total cell cycle length of pluripotent stem cells is significantly shorter (estimated 13-16hrs for human cells) with cells spending proportionally longer time in the DNA replication S-phase (the cell cycle phase when GCV incorporated into the DNA) (Becker *et al*., 2006; Calder *et al*., 2013; Filipczyk *et al*., 2007; Neganova *et al*., 2009), by comparison to fate restricted progenitors, whereby cycle length is longer (ranging from 25-30hours for neuronal progenitors), with proportionally less time spent in S-phase (our observations) (Calegari *et al.*, 2005; Arai *et al.*, 2011). Our present *in vitro* work highlighted that significantly longer, and higher doses, were required to ablate neural progenitors, compared to the PSCs. For the *in vivo* translation of this work, we therefore prolonged the duration of GCV to

8weeks (compared to commonly employed 1-2weeks applied in teratoma studies). We also increased the frequency of delivery, in hope of targeting the shorter S-phase within a longer cell cycle, yet with limited improvement. Additional efforts to increase the GCV concentration, noted the *in vitro* requirement for a 5-fold increased dose to ablate VM progenitors compared to PSC. Similar dose escalation *in vivo* to 100mg/kg twice daily (our unpublished observations) could not be achieved as this resulted in systemic adverse health in animals that resulted in their euthanasia. Such observations have been noted in other studies administering GCV at 100mg/kg by continuous infusion (Singer *et al.*, 2009) and at 150-300 mg/kg/day (Smee *et al.*, 1992). Whilst this is a common FDA approved drug used in the treatment of HSV and CMV without toxicity, animal studies typically utilise doses far higher than those conducted in routine treatments (5mg/kg/24hr). As a result, this approach demonstrates proof of principle *in vivo* evidence of GCV-induced cell ablation but at higher doses this may not be translatable for clinical purposes.

Despite extensive efforts focused on improved GCV penetration, all grafts still contained dividing cells. Whilst a proportion of these were determined to be of host origin, the identity of the remaining proliferative cells derived from the graft is still unknown, but previous work suggests a proportion could be associated with blood vessel formation (as seen for neural grafts, Somaa *et al*., 2017).

One is left to also question whether the ability of the drug to reach the graft contributes to the present findings and whether approaches to enhance the vascular network of these neural grafts may improve contact between proliferative cells in the grafts and GCV. Exploration into approaches designed to promote blood brain barrier permeability, such as RMP-7 or through use of redox targeting, have been shown to improve the efficacy of ablation in teratomas (Brewster *et al*., 1994; LeMay *et al*., 1998). However, the extremely short (minutes) half-life of RMP-7 raises challenges, since sustained delivery or an extended half-life will likely be required for sufficient efficacy.

Such hurdles with the HSV-TK/GCV suicide approach identified in this study, as well as potential immunogenicity of the TK transgene and adverse effects associated with long term administration of GCV (Itakura *et al.*, 2017), raises interest in alternative suicide systems that may be more appropriate for lineage restricted grafts such as the present vm progenitor grafts. For example, reduced immunogenicity and considerably shorter time requirement to eliminate PSCs (up to 24hrs) in the iCas9 system are both valuable and

attractive features for *in vivo* studies (Yagyu *et al*., 2015). This approach offers the possibility for a more targeted approach, in this regard to protect a specific population within the graft, whilst eliminating all remaining cells. Additionally, since we observe significant overgrowth by grafted cells even at initial stages, such engineering to protect specific populations, would allow even earlier commencement of GCV (<5wks) that may lead to more effective prevention of graft expansion, without impacting the dopaminergic population, that could not be prevented in this study when GCV was administered before 5wks.

With hPSC rapidly advancing to the clinic for PD, careful consideration for the utility and safety of hPSCs is required. As we embark on these trials, safety is of the upmost importance not only for a given patient but for the breadth of application of these cells in other trials and for other diseases. Poor regulation and assessment of fetal tissue trials in PD through the 1980s and 1990s created highly variable outcomes and degrees of catastrophe for both the research and clinical community. Local regulatory bodies, such as the FDA, are demanding vast numbers of animals to be grafted with a given cell batch prior to its clinical use, as well as extensive QC focused on cell proliferation, indicating that the concern for tissue overgrowth-associated risks remain evident (Kirkeby *et al*., 2017b; Studer, 2017). It is therefore of upmost importance that caution is taken when moving this alternative donor cell forward for CRT in PD.

4.6 Acknowledgements

The authors thank Mong Tien and Brianna Xuereb for their expert technical assistance. We would also like to thank Natalie Payne and Katherine Davidson for their invaluable guidance. IDL was supported by The University of Melbourne International Scholarships, Australia. CG was supported by an Australian Postgraduate Award. CP was supported by a Senior Research Fellowship provided by the National Health and Medical Research Council Australia. This research was funded by Stem Cells Australia. The Florey Institute of Neuroscience and Mental Health acknowledges the strong support from the Victorian Government and in particular the funding from the Operational Infrastructure Support Grant.

4.7 Author contributions

All experiments were performed at the Florey Institute of Neuroscience and Mental Health. Conceptualisation: IDL, CP. Investigation: IDL, KL, JH. Analysis: IDL, KL. Contributed unpublished reagents: AN, LT, CP. Writing – original draft – IDL, CP. Writing – editing: IDL, CP.

4.8 References

Arai Y, Pulvers JN, Haffner C, Schilling B, Nüsslein I, Calegari F, et al. Neural stem and progenitor cells shorten S-phase on commitment to neuron production. Nat Commun 2011; 2: 154.

Becker KA, Ghule PN, Therrien JA, Lian JB, Stein JL, Van Wijnen AJ, et al. Self-renewal of human embryonic stem cells is supported by a shortened G1 cell cycle phase. J Cell Physiol 2006: 209(3):883-93.

Bjorklund A, Stenevi U, Schmidt RH. Intracerebral grafting of neuronal cell suspensions. II. Survival and growth of nigral cell suspensions implanted in different brain sites. Acta Physiol Scand 1983; 118: 9–18.

Bonini C, Ferrari G, Verzeletti S, Servida P, Zappone E, Ruggieri L, et al. HSV-TK gene transfer into donor lymphocytes for control of allogeneic graft-versus-leukemia. Science 1997; 276: 1719–1724.

Brewster ME, Raghavan K, Pop E, Bodor N. Enhanced delivery of ganciclovir to the brain through the use of redox targeting. Antimicrob Agents Chemother 1994; 38: 817–823.

Bye CR, Penna V, de Luzy IR, Gantner CW, Hunt CPJ, Thompson LH, et al. Transcriptional Profiling of Xenogeneic Transplants: Examining Human Pluripotent Stem Cell-Derived Grafts in the Rodent Brain. Stem Cell Reports 2019; 13: 877–890.

Bye CR, Thompson LH, Parish CL. Birth dating of midbrain dopamine neurons identifies A9 enriched tissue for transplantation into Parkinsonian mice. Exp Neurol 2012; 236: 58–68.

Calder A, Roth-Albin I, Bhatia S, Pilquil C, Lee JH, Bhatia M, et al. Lengthened G1 phase indicates differentiation status in human embryonic stem cells. Stem Cells Dev 2013; 22(2): 279-95.

Calegari F, Haubensak W, Haffher C, Huttner WB. Selective lengthening of the cell cycle in the neurogenic subpopulation of neural progenitor cells during mouse brain development. J Neurosci 2005; 25: 6533–6538.

Carlsson T, Carta M, Winkler C, Björklund A, Kirik D. Serotonin neuron transplants exacerbate L-DOPA-induced dyskinesias in a rat model of Parkinson's disease. J Neurosci 2007; 27: 8011–8022.

Filipczyk AA, Laslett AL, Mummery C, Pera MF. Differentiation is coupled to changes in the cell cycle regulatory apparatus of human embryonic stem cells. Stem Cell Res 2007; 1: 45–60.

Freeman TB, Sanberg PR, Nauert GM, Boss BD, Spector D, Olanow CW, et al. The influence of donor age on the survival of solid and suspension intraparenchymal human embryonic nigral grafts. Cell Transplant 1995; 4: 141–154.

Gantner C, de Luzy IR, Kauhausen, JA, Moriarty N, Niclis JC, Bye CR, Penna V, Hunt CPJ, Ermine CM, Pouton CW, Kirik D, Thompson LH and Parish, CL. Viral Delivery Of Gdnf Promotes Functional Integration Of Human Stem Cell Grafts In Parkinsons Disease. Cell Stem Cell 2020; 26(4): 511-526.

Hagell P, Piccini P, Bjorklund A, Brundin P, Rehncrona S, Widner H, et al. Dyskinesias

following neural transplantation in Parkinson's disease. Nat Neurosci 2002; 5: 627–628.

Hara A, Aoki H, Taguchi A, Niwa M, Yamada Y, Kunisada T, et al. Neuron-like differentiation and selective ablation of undifferentiated embryonic stem cells containing suicide gene with Oct-4 promoter. Stem Cells Dev 2008; 17: 619–627.

Itakura G, Kawabata S, Ando M, Nishiyama Y, Sugai K, Ozaki M, et al. Fail-Safe System against Potential Tumorigenicity after Transplantation of iPSC Derivatives. Stem Cell Reports 2017; 8: 673–684.

Kirkeby A, Grealish S, Wolf DA, Nelander J, Wood J, Lundblad M, et al. Generation of Regionally Specified Neural Progenitors and Functional Neurons from Human Embryonic Stem Cells under Defined Conditions. Cell Rep 2012; 1: 703–714.

Kirkeby A, Nolbrant S, Tiklova K, Heuer A, Kee N, Cardoso T, et al. Predictive Markers Guide Differentiation to Improve Graft Outcome in Clinical Translation of hESC-Based Therapy for Parkinson's Disease. Cell Stem Cell 2017; 20: 135–148.

Kirkeby A, Parmar M, Barker RA. Strategies for bringing stem cell-derived dopamine neurons to the clinic: A European approach (STEM-PD). Prog Brain Res 2017; 230: 165–190.

Kotini AG, de Stanchina E, Themeli M, Sadelain M, Papapetrou EP. Escape Mutations, Ganciclovir Resistance, and Teratoma Formation in Human iPSCs Expressing an HSVtk Suicide Gene. Mol Ther - Nucleic Acids 2016; 5: e284.

Kriks S, Shim JW, Piao J, Ganat YM, Wakeman DR, Xie Z, et al. Dopamine neurons derived from human ES cells efficiently engraft in animal models of Parkinson's disease. Nature 2011; 480: 547–551.

Liang Q, Monetti C, Shutova M V., Neely EJ, Hacibekiroglu S, Yang H, et al. Linking a cell-division gene and a suicide gene to define and improve cell therapy safety. Nature 2018; 563: 701–704.

de Luzy IR, Niclis JC, Gantner CW, Kauhausen JA, Hunt CPJ, Ermine C, et al. Isolation of LMX1a ventral midbrain progenitors improves the safety and predictability of human pluripotent stem cell-derived neural transplants in Parkinsonian Disease. J Neurosci 2019; 39(48): 9521-31.

Lemay DR, Kittaka M, Gordon EM, Gray B, Stins MF, Mccomb JG, et al. Intravenous RMP-7 increases delivery of ganciclovr into rat brain tumors and enhances the effects of herpes simplex virus thymidine kinase gene therapy. Hum Gene Ther 1998; 9(7): 989–995.

Mendez I, Sanchez-Pernaute R, Cooper O, Vinuela A, Ferrari D, Bjorklund L, et al. Cell type analysis of functional fetal dopamine cell suspension transplants in the striatum and substantia nigra of patients with Parkinson's disease. Brain 2005; 128: 1498–1510.

Morgan RA. Live and let die: A new suicide gene therapy moves to the clinic. Mol Ther 2012; 20: 11–13.

Neganova I, Zhang X, Atkinson S, Lako M. Expression and functional analysis of G1 to S regulatory components reveals an important role for CDK2 in cell cycle regulation in human embryonic stem cells. Oncogene 2009; 28: 20–30.

Niclis JC, Gantner CW, Alsanie WF, McDougall SJ, Bye CR, Elefanty AG, et al. Efficiently Specified Ventral Midbrain Dopamine Neurons from Human Pluripotent Stem Cells Under Xeno-Free Conditions Restore Motor Deficits in Parkinsonian Rodents. Stem Cells Transl Med 2017; 6(3), 937-48.

Niclis JC, Gantner CW, Hunt CPJ, Kauhausen JA, Durnall JC, Haynes JM, et al. A PITX3-EGFP Reporter Line Reveals Connectivity of Dopamine and Non-dopamine Neuronal Subtypes in Grafts Generated from Human Embryonic Stem Cells. Stem cell reports 2017; 9: 868–882.

Ou W, Li P, Reiser J. Targeting of herpes simplex virus 1 thymidine kinase gene sequences into the OCT4 locus of human induced pluripotent stem cells. PLoS One 2013; 8(11).

Politis M. Dyskinesias after neural transplantation in Parkinson's disease: What do we know and what is next? BMC Med 2010; 8: 80.

Rong Z, Fu X, Wang M, Xu Y. A scalable approach to prevent teratoma formation of human embryonic stem cells. J Biol Chem 2012; 287: 32338–32345.

Samata B, Doi D, Nishimura K, Kikuchi T, Watanabe A, Sakamoto Y, et al. Purification of functional human ES and iPSC-derived midbrain dopaminergic progenitors using LRTM1. Nat Commun 2016; 7: 1–11.

Singer BH, Jutkiewicz EM, Fuller CL, Lichtenwalner RJ, Zhang H, Velander AJ, et al. Conditional ablation and recovery of forebrain neurogenesis in the mouse. J Comp Neurol 2009; 514: 567–582.

Smee DF, Morris JLB, Leonhardt JA, Mead JR, Holy A, Sidwell RW. Treatment of murine cytomegalovirus infections in severe combined immunodeficient mice with ganciclovir, (S)-1-[3-hydroxy-2- (phosphonylmethoxy)propyl]cytosine, interferon, and bropirimine. Antimicrob Agents Chemother 1992; 36: 1837–1842.

Somaa FA, Wang TY, Niclis JC, Bruggeman KF, Kauhausen JA, Guo H, et al. Peptide-Based Scaffolds Support Human Cortical Progenitor Graft Integration to Reduce Atrophy and Promote Functional Repair in a Model of Stroke. Cell Rep 2017; 20: 1964–1977.

Di Stasi A, Tey SK, Dotti G, Fujita Y, Kennedy-Nasser A, Martinez C, et al. Inducible apoptosis as a safety switch for adoptive cell therapy. N Engl J Med 2011; 365: 1673–1683.

Studer L. Strategies for bringing stem cell-derived dopamine neurons to the clinic—The NYSTEM trial.1st ed. Elsevier B.V. 2017; 230: 191-212.

Tieng V, Cherpin O, Gutzwiller E, Zambon AC, Delgado C, Salmon P, et al. Elimination of proliferating cells from CNS grafts using a Ki67 promoter-driven thymidine kinase. Mol Ther - Methods Clin Dev 2016; 3: 16069.

Tiklová K, Nolbrant S, Fiorenzano A, Björklund ÅK, Sharma Y, Heuer A, et al. Single Cell Transcriptomics Identified Stem Cell-Derived Graft Composition In A Model of Parkinson's Disease. Nat Comms 2020; 11: 2434.

Torres EM, Monville C, Gates MA, Bagga V, Dunnett SB. Improved survival of young donor age dopamine grafts in a rat model of Parkinson's disease. Neuroscience 2007; 146: 1606–1617.

Yagyu S, Hoyos V, Del Bufalo F, Brenner MK. An Inducible Caspase-9 Suicide Gene to Improve the Safety of Therapy Using Human Induced Pluripotent Stem Cells. Mol Ther 2015; 23: 1475–1485.

Supplementary Figures

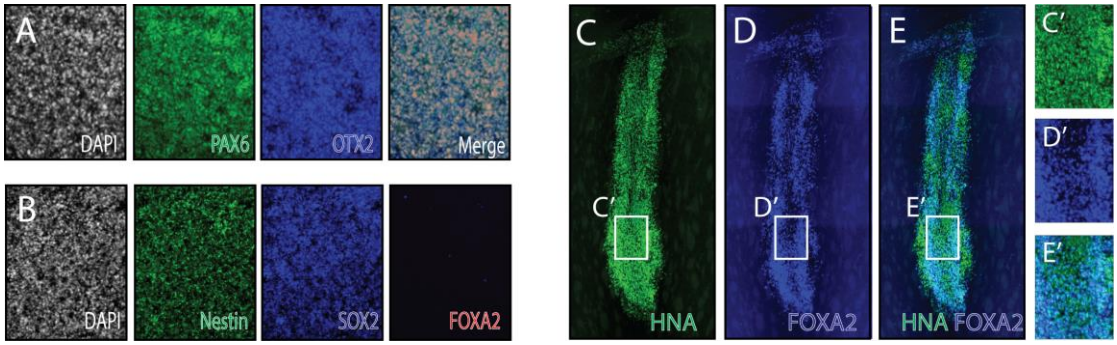

Supplementary 4.1. Characterisation of pan forebrain progenitors and relative contribution to graft composition

(A) Differentiation of CDK1-TK hPSCs patterned towards a forebrain identity was confirmed by co-expression of PAX6, OTX2 and SOX2, with absence of FOXA2. **(C)** Assessment of 5wk grafts confirmed presence of pan forebrain (FOXA2-) and vm (FOXA2+) progenitors.

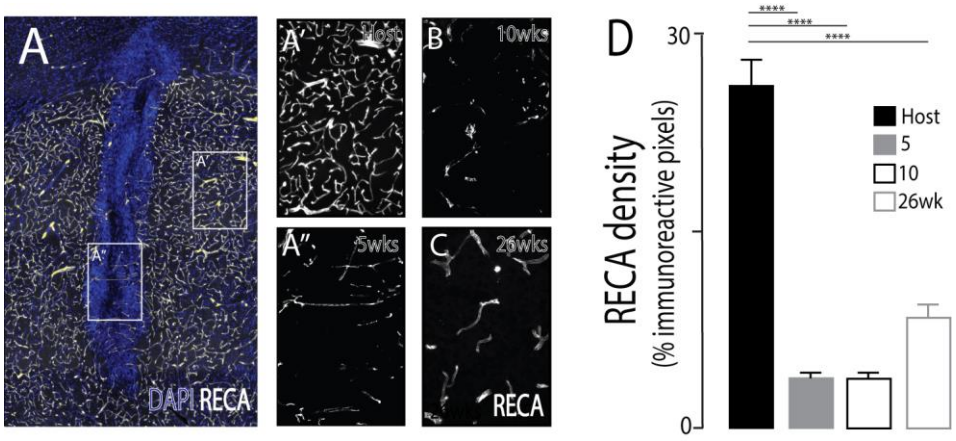

Supplementary 4.2. Poor graft vascularization may partially explain limitations of HSV-TK failsafe suicide system

(A-C) Representative images immunolabelled for DAPI (blue) and RECA (white), to illustrate host-derived RECA+ blood vessels. **(F)** A dramatic reduction in the density of blood vessels (RECA+) was observed in the graft compared to the host striatal tissue.

Chapter 5.

Identifying the optimal age of human pluripotent stem cell-derived dopaminergic progenitors for transplantation in a rodent model of Parkinson's disease

Isabelle R. de Luzy[1], Cameron P. Hunt[1], Carlos W. Gantner[1], N Moriarty[1], Jonathan C. Niclis[1], Lachlan H. Thompson[1] and Clare L Parish[1].

[1] The Florey Institute of Neuroscience and Mental Health, Parkville, Victoria, Australia.

[2] Monash Institute of Pharmaceutical Sciences, Monash University, Parkville, Victoria, Australia.

5.1 Abstract

Developmental age of donor fetal tissue has a significant impact on neural transplantation outcomes, yet has been minimally explored in relation to human pluripotent stem cells (hPSC)-derived neural transplants. Given the more recent emergence of human pluripotent stem cell (hPSC)-derived ventral midbrain dopaminergic (vmDA) progenitors into clinical application for Parkinson's Disease, we sought to shed light on the influence of neural progenitor age on graft survival, composition and integration. To address this, we examined the impact of transplanting hPSC-derived vmDA progenitors at varying days of *in vitro* differentiation (between day 13-30) into a mouse model of the disease, comparing two cell lines across multiple differentiations. Both cell lines were constructed to contain an eGFP reporter under the control of the endogenous promoter PITX3 (with one being an induced pluripotent stem cell and the other an embryonic stem cell line), to enable inter- and intra-line comparisons and specific tracking of crucial graft-derived vmDA neurons *in vitro* and *in vivo*. Post-mortem analysis at 6 months revealed small grafts from both lines transplanted with D13 and D30 progenitors, while grafts derived from D19, D22 and D25 cells were larger yet contained a higher number and proportion of non-dopaminergic cells. Grafts of D13 progenitors not only contained the highest proportion of vmDA neurons, that displayed enhanced vmDA subtype specification, but also the greatest fraction of GIRK2-expressing A9-like neurons, the vmDA subpopulation critical for motor function. Furthermore, these young progenitor grafts innervated developmentally relevant vmDA targets. Interestingly, despite highly reproducible differentiations and grafting outcome at an intra-line level, grafts of hiPSC-derived D13 progenitors showed a 6-fold greater density of vmDA neurons compared to hESC-derived grafts of the same progenitor age. These findings show that the age of hPSC-derived vmDA progenitors at the time of implantation

has a direct impact on graft survival, vmDA composition and maturation, and that careful consideration of inter-line variation is valuable prior to clinical translation into human patients.

5.2 Introduction

Dopamine (DA) pharmacotherapy remains the mainstay treatment for Parkinson's disease (PD) patients, yet adverse effects and waning efficacy, in part related to systemic drug delivery and ongoing disease progression, highlight the need for alternative therapeutic approaches. Clinical trials have demonstrated that targeted transplantation of replacement DA neurons, isolated from fetal tissue, are capable of functional integration and prolonged relief of motor symptoms in PD patients (Barker *et al.*, 2013). Despite this proof of principle, issues associated with the use of fetal tissue, including poor standardisation, limited availability and ethical concerns hinder the broader applicability of this approach.

More recently, human pluripotent stem cells (hPSC), inclusive of both embryonic (ESC) and induced pluripotent stem cells (iPSC), have been recognised as an alternative donor source – with refined protocols now capable of appropriately fate restricting these cells into ventral midbrain (VM) dopamine progenitors/neurons (Kriks *et al.*, 2011; Kirkeby *et al.*, 2012; Xi *et al.*, 2012, Niclis *et al.*, 2017*a*). Despite efficient *in vitro* specification, with >80% of cells appropriately fate restricted at the time of implantation, the overall proportion of DA neurons within the graft remains low. Likely underpinning this is the poor survival of DA progenitors during cell preparation and immediately after implantation, as has been reported for fetal tissue (Castilho *et al*, 2000; Olanow *et al*, 1996), as well as the inclusion of a seemingly low proportion of highly expansive non-mDA progenitors within the donor cells (de Luzy *et al.*, 2019).

Interestingly, several studies using fetal tissue have demonstrated that maturity of donor cells at the time of grafting can have a significant impact on graft composition and functional outcomes. More specifically, it has been recognised that donor tissue isolated prior to, rather than at the peak phase of DA neurogenesis produces larger grafts with more DA neurons as a result of increased survival and proliferation of DA neuroblasts at the time of implantation (Bye *et al*., 2012; Freeman *et al*., 1995; Gates *et al.*, 2006; Torres, *et al.*, 2007).

Added to this, more recent studies have highlighted that the A9 DA neurons (a subpopulation of VM DA neurons critical for motor function) precede the birth of

neighbouring A10 DA neurons (Blaess *et al.*, 2006; Bye *et al.*, 2012; Joksimovic *et al.*, 2009), and consequently the transplantation of younger donor tissue enriches for this necessary A9 population (Bye *et al.*, 2012; Kauhausen *et al*., 2013).

Surprisingly, there has been relatively limited comparison of PSC-derived DA progenitor age and graft outcomes, despite reports of vm donor cells ranging from day 16 to day 42 of differentiations across studies (Doi *et al*., 2014; Gantner *et al.*, 2020; Kirkeby *et al.*, 2012; Kriks *et al.*, 2011; de Luzy *et al.*, 2019; Samata *et al.*, 2016; Wakeman *et al.*, 2017). Unlike fetal tissue, the heightened risk of tumorigenesis and overgrowth associated with engraftment of younger progenitors that may be incompletely patterned or retain pluripotency needs to be considered. As such, direct hPSC-derived vm progenitor age comparisons are required to determine if differences in age of tissue employed by different groups is restricted by development and/or due to inter-line (and/or inter-differentiation) variability.

In order to address these questions, we engineered a hiPSC expressing enhanced green fluorescent protein (GFP) under the PITX3 promotor (hiPSC PITX3-eGFP), in combination with our previously reported hESC PITX3-eGFP reporter (Niclis *et al*, 2017a, 2017b, Gantner *et al*, 2020), to specifically track the DA compliment of grafts and assess the impact of vm progenitor age on graft outcomes, across cell lines and repeated differentiations. Using this approach, we demonstrate that both donor age and cell line had a significant impact on graft survival, plasticity and composition. We showed that younger donor cells generated smaller grafts that were significantly enriched for DA neurons, with the smallest inclusion of non-DA cells, that was consistent over multiple differentiations and grafting rounds.

5.3 Materials and Methods

5.3.1 Maintenance of human PSC culture

Human ESC lines H9 with PITX3-eGFP knockin (hESC PITX3-eGFP (Watmuff *et al.*, 2015), and our newly generated integration-free human induced pluripotent stem cells (hiPSC) line RM3.5 PITX-eGFP knockin (hiPSC PITX3-eGFP, described below), were cultured in xenogeneic free conditions. Both lines were confirmed to be karotypically normal and frequently tested for absence of mycoplasma (MycoAlert detection kit, Lonza). hPSCs were cultured on Laminin-521 (5µg/ml, BioLamina), in mTeSR-1 (StemCell

Technologies) supplemented with 0.5% Penicillin-Streptomycin. hiPSCs were maintained with an additional 5% KSR (ThermoFisher). Media was changed daily and ReLeSR (StemCell Technologies) used to passage every 4-6 days. Cultures were maintained at 37°C with 5% CO_2.

5.3.2 Generation of hiPSC PITX3-eGFP reporter line

Neon® electroporation of Donor and ZFN plasmids

Single cells were isolated by Accutase (Innovative Cell Technologies) at ~80% confluency and resuspended at a concentration of 1.0 x 10^7 cells/ml in resuspension buffer (Neon® 100 µl kit, Invitrogen). Addition of 1 µg/1.0 x 10^6 cells of *PITX3-eGFP-PGK-PURO* donor plasmid (originally a gift from Rudolf Jaenisch, Addgene deposit #31942; http://n2t.net/addgene:31942; RRID:Addgene_3194, Supplementary Figure 5.1A) from the PITX3 CompoZr® Targeted integration kit (Sigma) was incubated for a short (5min) period. Following incubation, equimolar ratios of PITX3 zinc-finger nuclease plasmids (ZFN1 & ZFN2) were added (Supplementary Figure 5.1A) and the sample transferred to the Neon® (Invitrogen) pipette using the Neon® tip. Cells were electroporated under optimised conditions (1650 V with 10 ms pulse width and a pulse number of 3) and replated in hPSC media (at 1:3, 1:6, 1:9 dilutions).

Expansion and screening of clones

Puromycin (0.5-1.0ug) was added for ~11days to select for successful donor plasmid integration. Treated colonies (from 1:9 dilution) were manually dissected and expanded for 6 days. Following expansion, cells were isolated and genomic DNA (gDNA) was extracted using the ISOLATE II genomic isolation kit (Bioline). Insertion of construct at PITX3 locus was confirmed by Phusion™ high fidelity RT-PCR kit (ThermoFisher). In brief, 20 ng gDNA (1 ng for vector control), 3% DMSO and all remaining kit reagents were combined with in-house designed primers (Supplementary Figure 5.1A) amplifying through the left homology arm of the donor plasmid. cDNA samples were run on a two-step amplification protocol with the Veriti™ thermal cycler (ThermoFisher) programmed for 30 seconds at 98°C for initial denaturation, 35 cycles of 10 seconds at 95°C for denaturation, 90 seconds at 72 °C for extension, and a final extension at 72°C for 10 min. PCR samples were mixed with 6x TriTrack loading dye (ThermoFisher) and electrophoretically separated at 90 V for 45 minutes on a 1% (w/v) agarose gel in 1 x TAE buffer alongside HyperLadder™1 kb ladder (Bioline) and relevant controls. The gel was visualized at 340 nm using the UV

imaging system (BioDoc-It). Successful integrated clones displayed bands at 984 bp, whilst vector-only or human gDNA controls gave rise to bands at 1350 and 970 bp, respectively. Several clones were identified for correct targeting at the PITX3 locus (see Supplementary Figure 5.1B), with clones #22 and #23 selected (due to highest expression) for expansion and differentiation to confirm PITX3-mediated eGFP expression (Figure 5.1G).

5.3.3 hPSC differentiation

The two human PITX3-eGFP reporter cell lines (ESC and iPSC) were differentiated in xeno-free conditions as previously reported with minor modifications (Kirkeby *et al.*, 2017; Niclis *et al.*, 2017a) (Figure 5.1C) . In brief, human PSC were seeded onto Laminin-521 in neural basal N2B27 media and exposed to dual SMAD inhibition (SB431542, 10µM, 0-5 days in vitro, DIV, R&D systems; and LDN193189, 200nM, 0-11DIV, Stemgent) to initiate neural induction. To pattern cells towards a ventral midbrain phenotype, sonic hedgehog C25II (100ng/ml; R&D systems) and Purmorphamine (2µM; Stemgent) were supplemented into the media for ventralisation from day 1-7DIV, in addition to the caudalizing Wnt agonist, CHIR 99021 (2.5uM; Stemgent, 2-13DIV). From 11DIV, cells were matured in the presence of glial-derived neurotrophic factor (GDNF, 20ng/ml; R&D systems), brain-derived neurotrophic factor (BDNF, 20ng/ml, R&D systems), recombinant human transforming growth factor type β3 (TGFβ3, 1 ng/ml; PeproTech), DAPT (10 µM, Sigma-Aldrich), ascorbic acid (200nM; Sigma-Aldrich) and dibutyryl cAMP (0.05mM; Tocris) until desired endpoint. At 13, 19, 21, 25 and 30DIV, differentiating cultures were dissociated in accutase and resuspended in maturation media containing ROCK inhibitor (Y-27632, 10uM, Sigma) at a density of 100,000 cells/uL. Isolated cells were stored on ice until the time of transplantation.

5.3.4 6-hydroxydopamine lesioning and cell transplantation

All animal procedures adhered to the Australian National Health and Medical Research Council's published Code of Practice for the Use of Animals in Research, and experiments approved by The Florey Institute of Neuroscience and Mental Health Animal Ethics committee. Animals were group housed on a 12:12-hour light/dark cycle with ad libitum access to food and water. Surgeries were performed on 77 athymic nude mice (BALB/c-*Foxn1*^{nu}/Arc) under 2-5% isoflurane anaesthesia. A single unilateral stereotaxic injection of 6-hydroxydopamine (6OHDA, 1.5µl, 1.6 µg/µl) was made into the right substantia nigra (co-ordinates: 3.0mm posterior, 1.2mm lateral to bregma, and 4.2mm below the dura surface) to ablate the host midbrain dopamine pathway, as previously described(Kauhausen

et al., 2013). At 3weeks after 60HDA lesioning, animals received a unilateral injection of either PITX3-eGFP hiPSC- or hESC-derived VM cells (1uL/) into the right striatum (co-ordinates: 1.0mm anterior and 2.1mm lateral, relative to bregma, and 3.0mm below the dura surface). For each cell line, grafts were isolated from 13, 19, 22, 25, 30 DIV cultures.

5.3.5 Tissue processing and Immunohistochemistry

In vitro cultures were fixed (4% paraformaldehyde, 10mins) following each transplantation timepoint (13, 19, 21, 25, 30DIV). For histological examination of graft composition and integration, mice received an overdose of sodium pentobarbitone (100mg/kg), followed by transcardial perfusion with Tyrode solution and subsequently 4% paraformaldehyde. Brains were cryosectioned on a coronal plane (40uM; 12 series) using a freezing microtome (Leica). Immunohistochemistry was achieved following previously described methods (Somaa *et al.*, 2017), using the following primary antibodies and dilutions shown in Supplementary table 5.1.

Antibody	Species	Company	Dilution
BARHL1	Rabbit	Novus Biologicals; NBP1-86513	1:200
CALBINDIN	Mouse	Swant Biotech; CB300	1:1000
FOXA2	Goat	Santa Cruz; sc-6554	1:200
GFP	Rabbit	Abcam; AB290	1:20,000
GFP	Chicken	Abcam; AB13970	1:1000
GIRK2	Rabbit	Alomone Labs; APC-006	1:500
HNA	Mouse	Millipore; MAB1281	1:300
KI67	Rabbit	ThermoFisher; LBVRM-9106-31	1:1000
MAP2B	Rabbit	Millipore; AB5622	1:1000
NCAM	Mouse	Clone Eric-1, Santa Cruz; sc-106	1:500
NESTIN	Mouse	Millipore; MAB1259	1:1000
NURR1	Rabbit	Santa Cruz, sc-990	1:200
OCT4	Mouse	Santa Cruz; sc-5279	1:100
OTX2	Rabbit	Millipore; AB9566	1:3000
PITX2	Sheep	R&D systems, AF7388	1:200
SOX2	Goat	R&D systems;	1:300
TH	Rabbit	Pelfreeze: P40101-0	1:1000
TH	Sheep	Pelfreeze: P60101-0	1:800

Table 5.1. Primary antibodies – species, company and dilution

5.3.6 Microscopy and Quantification

Bright and dark field images were obtained using a Leica DM6000 microscope, while fluorescence images were captured using a Zeiss Observer Z.1 upright epifluorescence or Zeiss LSM 780 confocal microscope. PSA-NCAM expression was used to delineate the graft and volume was estimated using the Cavalieri's Principle. Images (20x magnification) were captured to quantify total number of human nuclear antigen (HNA+), floor plate (FOXA2+) progenitors, green fluorescent protein (GFP+), tyrosine hydroxylase (TH+), and proliferative (KI67+) cells. GIRK+ and CALBINDIN+ cells within the grafts were quantified from confocal-acquired images. For GIRK and Calbindin quantifications, dopamine neurons were first identified by GFP immunoreactivity and data represented as a percentage of total dopamine neurons.

For fibre density measurements, 10 z-stack sections were captured and compressed. All areas were captured in triplicate with conserved settings. Assessment of fiber density was sampled in the dorsolateral striatum of mice (1.0mm anterior and 2.4mm lateral from bregma, and 2.8mm below the surface of the dura, according to the mouse brain atlas (Paxinos and Watson, 2004). Colour inverted images were obtained using the 'colour range' tool on Photoshop (Adobe) to isolate GFP+ labelled fibres. Total fibre innervation is expressed as a percentage of immunoreactive pixels. All images were taken in triplicate with conserved settings.

5.3.7 Statistical Analysis

All data are presented as mean $\pm$ SEM. Statistical tests employed (inclusive of one-way ANOVA, student t-tests, and pearson's correlation coefficients) are stated in figure legends. Alpha levels of $p<0.05$ were considered significant with all statistical analysis performed using GraphPad Prism. *$p < 0.05$, **$p < 0.01$, ***$p < 0.001$ and ****$p < 0.0001$.

5. 4 Results

5.4.1 Characterisation of novel hiPSC PITX3-GFP reporter line to identify and track dopaminergic neurons

To assess and compare the composition and integration of DA neurons within hPSC-derived vm grafts we employed an existing PITX3-eGFP hESC reporter line, and engineered a new, comparable hiPSC line carrying the same PITX3-eGFP construct - noting the restrictive expression of PITX3 within midbrain DA neurons in the developing

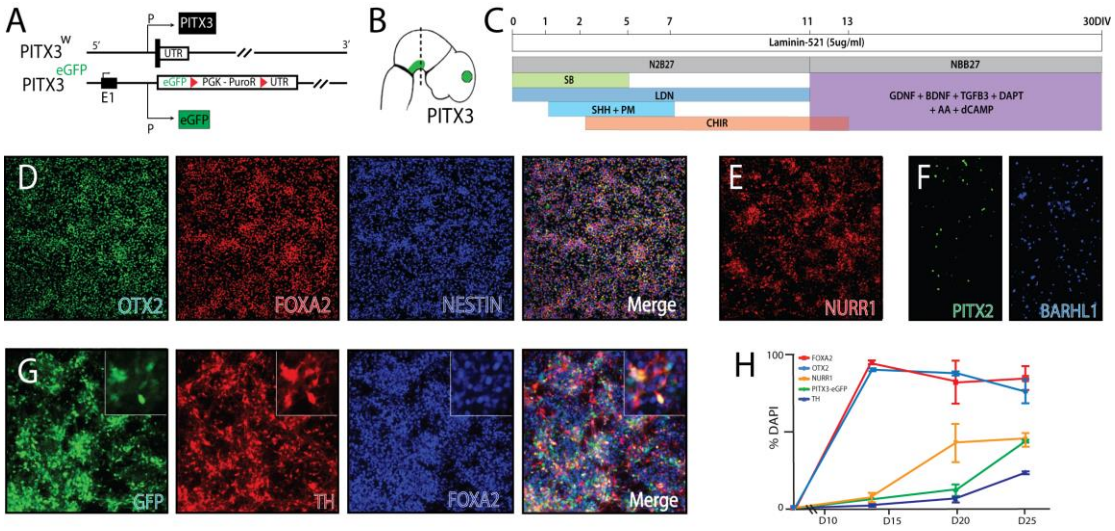

Figure 5.1. Generation and characterisation of a novel PITX3-eGFP hiPSC reporter line to enable competent identification and mapping of midbrain dopamine neurons
(A) Monoallelic insertion of eGFP at the PITX3 locus into the RM3.5 human induced pluripotent stem cell line. **(B)** Illustration depicting PITX3 expression domains in the developing embryo. **(C)** Protocol for differentiation of human PSCs into neural progenitors with ventral midbrain identity under defined, xenogeneic-free conditions. **(D-E)** Differentiated PITX3-eGFP hiPSC express high levels of markers associated with ventral floorplate/forebrain identity (OTX2, FOXA2 NURR1) with minimal contamination of off-target rostral/diencephalic progenitor populations, indicated by low numbers of PITX2+ and BARHL1+ cells at day 14. **(G)** Differentiation into mature vm dopaminergic neurons was confirmed by co-localisation of PITX3-eGFP, TH and FOXA2 at day 25 **(F'). (H)** Efficient specification and differentiation of PITX3-eGFP hiPSCs into mature dopaminergic neurons (one-way ANOVA with Tukey's post hoc test, n=3). Abbreviations: eGFP, enhanced green fluorescent protein; PSC, pluripotent stem cell; TH, tyrosine hydroxylase; hiPSC, human induced pluripotent stem cells. Data is represented as mean ± SEM.

mammalian embryo (Figure 5.1B) (Smidt *et al.*, 2004). To engineer the new line, a zinc finger nuclease pair together with a targeting vector was employed to introduce an eGFP-puromycin cassette into RM3.5 hiPSCs at exon 1 of the endogenous PITX3 locus (Figure 5.1C). Insertion of the construct at the PITX3 locus was confirmed by RT-PCR kit (Supplementary Figure 5.1B). Upon confirmation of correct targeting and integration of the transgene, the new PITX3-eGFP hiPSC line was assessed for its capacity to efficiently differentiate into vm progenitors, with comparable efficiency to PITX3-eGFP H9 hESCs.

Cells were differentiated towards a VM fate according to a clinically-relevant xeno-free differentiation protocol (Figure 5.1C) (Niclis *et al.*, 2017a). We confirmed appropriate and efficient specification by expression of key cardinal vmDA progenitor markers; FOXA2 (94.8% ± 0.9), OTX2 (91.65% ± 0.6) and NURR1 (45.25% ± 4.4), (Figure 5.1D-E, H), while importantly showing sparse expression of contaminating diencephalic progenitors (PITX2+/BARHL1+) (Figure 5.1F). These VM progenitors competently maturated into midbrain DA neurons, verified by expression of GFP and TH (GFP: 44.89% ± 2.4, TH: 23.56% ± 0.6, Figure 5.1G) at D25, which was consistent between multiple differentiations

for both the hiPSC (n=3, Figure 5.1H) and hESC (Niclis *et al*., 2017a) PITX3-eGFP reporter lines.

5.4.2 Temporal expression of key developmental markers indicates cellular maturity at the time of implantation

Prior to grafting, we tracked the progressive maturity of differentiating vm progenitors, to gain greater insight into the identity of the implanted cells. Multiple independent differentiations were performed using the two PITX3-eGFP reporter cell lines to confirm reproducibility within a cell line, and assess variability or consistency between lines. Cells were examined *in vitro* at time points in the differentiation corresponding to the intended donor ages for transplantation and spanning much of the progenitor ages employed in other studies (Figure 5.2A) (Doi *et al*., 2014; Gantner *et al.*, 2020; Kirkeby *et al.*, 2012, 2017; Kriks *et al.*, 2011; de Luzy *et al.*, 2019; Samata *et al.*, 2016). The youngest progenitor age examined was 13 days *in vitro* (D13), considered the most immature progenitor cell employed for grafting to date (Kirkeby *et al.*, 2012), and representing the end of the patterning phase of the differentiation i.e. removal of morphogens and initiation of cellular maturation. Cells were additionally examined at D19, D22 and D25 - the most routinely adopted progenitor age for grafting, and finally D30.

Introduction of factors to promote cellular maturation, caused a rapid and early elimination of OCT4+ PSCs and progressive decrease in the proportion of neural ($SOX2^{+}$) progenitors, with few remaining by D30 (Figure 5.2B-H). These progenitors differentiated into mature neurons (visualised by expression of MAP2B), that were observed in cultures from D19 (Figure 5.2C-G, Supplementary 5.2A-B). With continued differentiation, both an increase in the number and length of neurites could be detected (Figure 5.2D'-F', Supplementary Figure 5.2G'-I') that became highly arborized by D30 (Figure 5.2G', Supplementary 5.2J'). Presence of these neurite extensions, and consequential axotomy that occurs during the dissociation of cells prior to transplantation, has been demonstrated to negatively impact upon survival of implanted DA neurons, isolated from fetal tissue (Brundin *et al*., 2000), and remains a mindful consideration for these more mature progenitor transplants. Despite this, both cell lines maintained consistent progenitor specification, with a small proportion of PITX3-GFP dopaminergic neuroblasts present at D19 (Figure.2J, Supplementary 5.2B). Concomitant generation of DA neurons was observed continually over the subsequent days in culture, up to D30. (Figure 5.2K-M, Supplementary Figure 5.2C-E,

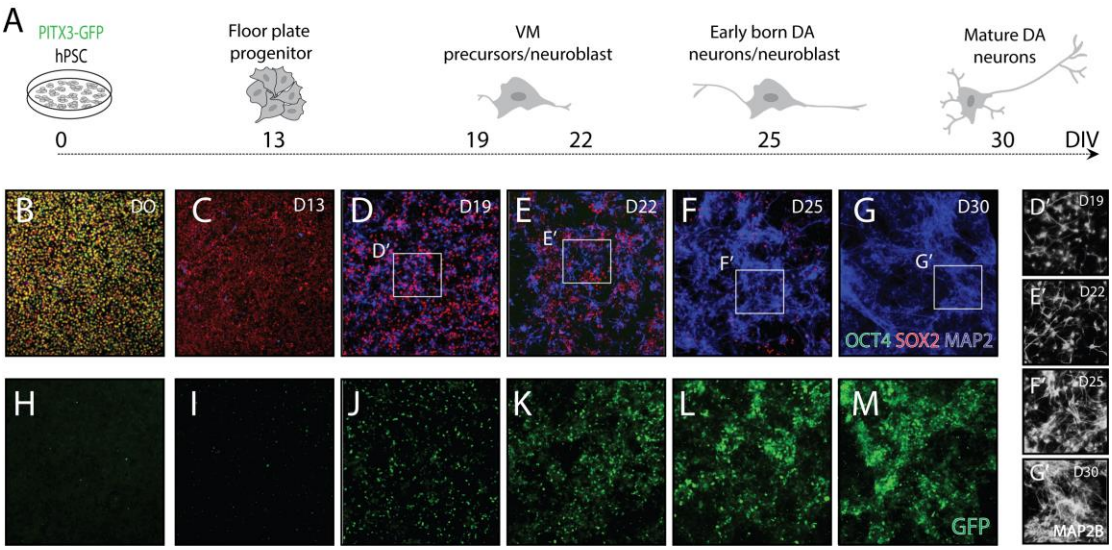

Figure 5.2. Assessment of cellular maturity prior to transplantation
(A) Schematic depicting morphology of differentiated cells at respective implantation ages **(B-M)** Photomicrographs to highlight the relative maturity of differentiated cells prior to engraftment, by expression of markers indicative of neural progenitors (SOX2+) and mature neurons (GFP+, MAP2+) (D13, D19, D22, D25 and D30). (D'-G') Note the observable increase in length of neurite extension from D19 to D30 **(D'-G')**. Abbreviations: hESC, human embryonic stem cells.

Niclis *et al.*, 2017a; Niclis *et al*., 2017b). Importantly, no OCT4+ cells were present in the cultures from any transplant stage assessed (Figure 5.2C-G).

5.4.3 Developmental age at the time of transplantation influences graft size and proportion of dopamine neurons

We next sought to examine the impact of differing progenitor age on graft composition and integration in 6OHDA mice, comparing the 2 PITX3-eGFP PSC lines. At 24 weeks post-transplantation, all animals showed viable grafts, as revealed by human-specific NCAM reactivity (Figure 5.3A-B). Volumetric assessment revealed grafts derived from the youngest (D13) and oldest (D30) progenitors were smallest in size, while intermediate age cells were significantly larger (Figure 5.3C). Commensurate with graft volume was the number of HNA+ cells within grafts for all groups (Figure 5.3D). Interestingly, whilst growth trends were similar between the 2 PSC lines (i.e. showing a binomial distribution), hESC-derived grafts were remarkably larger than hiPSC grafts for each donor progenitor age (Figure 5.3C-D). Importantly, no evidence of aberrant growth was observed at any graft age, indicating unlikely contamination of undifferentiated PSCs or insufficiently patterned progenitors, that has previously been a concern with delivery of younger differentiated cells (D13, Figure 5.3A-B).

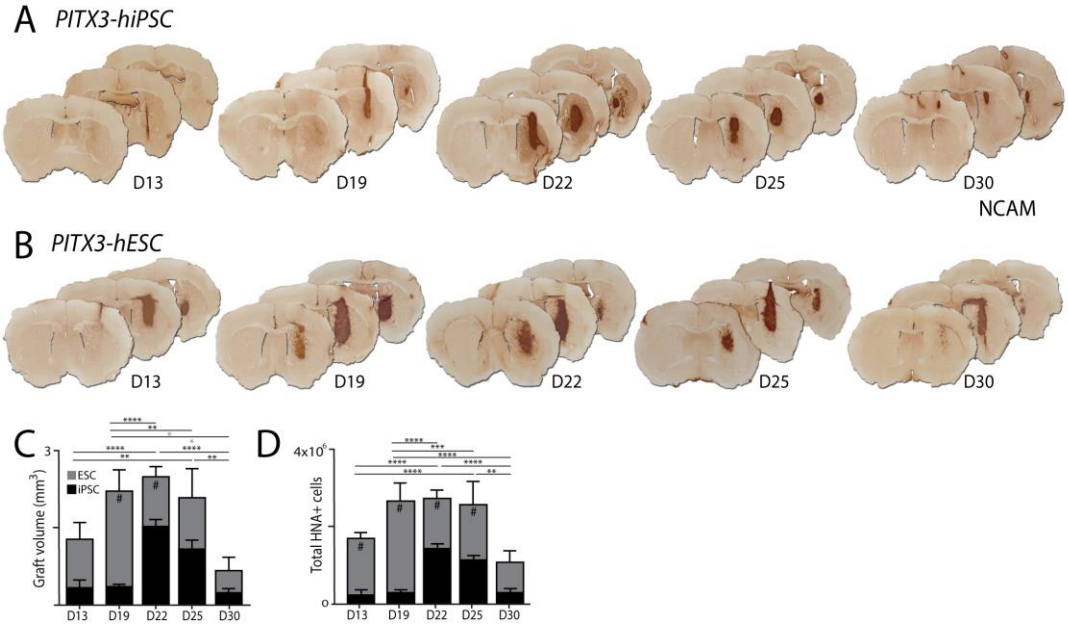

Figure 5.3. Developmental maturity at time of implantation influences graft size
(A-B) Coronal sections of the rat brain for individual representative animals for both PITX3-eGFP hiPSC **(A)** and hESC **(B)** lines at respective implantation ages. Surviving grafts can be visualised by human-specific NCAM expression. **(C-D)** Graphs highlighting that implantation age had a significant effect on graft volume **(C)** and survival of HNA+ cells **(D).** Abbreviations: NCAM, neural cell adhesion molecule; HNA, human nucleic acid. Data is represented as mean ± SEM.

Next we assessed the dopaminergic contribution of the grafts. As previously reported for the PITX3-GFP ESC line (Niclis *et al.*, 2017), the validity of PITX3-eGFP as an accurate marker of DA neurons was confirmed by co-expression with the rate-limiting enzyme in DA synthesis, TH), with ~95% of cells showing TH+ and GFP+ within grafts derived from the PITX3-GFP iPSC line (Supplementary Figure 5.3). While the largest of the hiPSC-derived grafts (D22) showed the highest number of GFP+ DA neurons (23,050 ± 3,022, Figure 5.4A, C), surprisingly of the hESC-derived transplants the relatively small D13 grafts had the most GFP+ DA neurons (11,156 ± 2,600, Figure 5.4B, E). For both cell lines, D30 progenitor grafts yielded the least DA neurons. The differences in yield of DA neurons between progenitor engraftment age, was likely reflected by the proportion of post-mitotic dopaminergic neuroblasts/neurons observed in culture prior to transplantation, which have previously been reported to survive poorly following implantation (Figure 5.2C, K-M, Figure 5.4C, E, Supplementary Figure 5.2B-E, Brundin *et al*., 2000; Jönsson *et al.*, 2009; de Luzy *et al.*, 2019; Xia *et al.*, 2017).

With the observed variability in DA yields across the cell lines and donor ages, we subsequently assessed the relative contribution of DA neurons in these grafts. Surprisingly, despite the highest number of DA neurons expressed in intermediate-stage hiPSC-derived

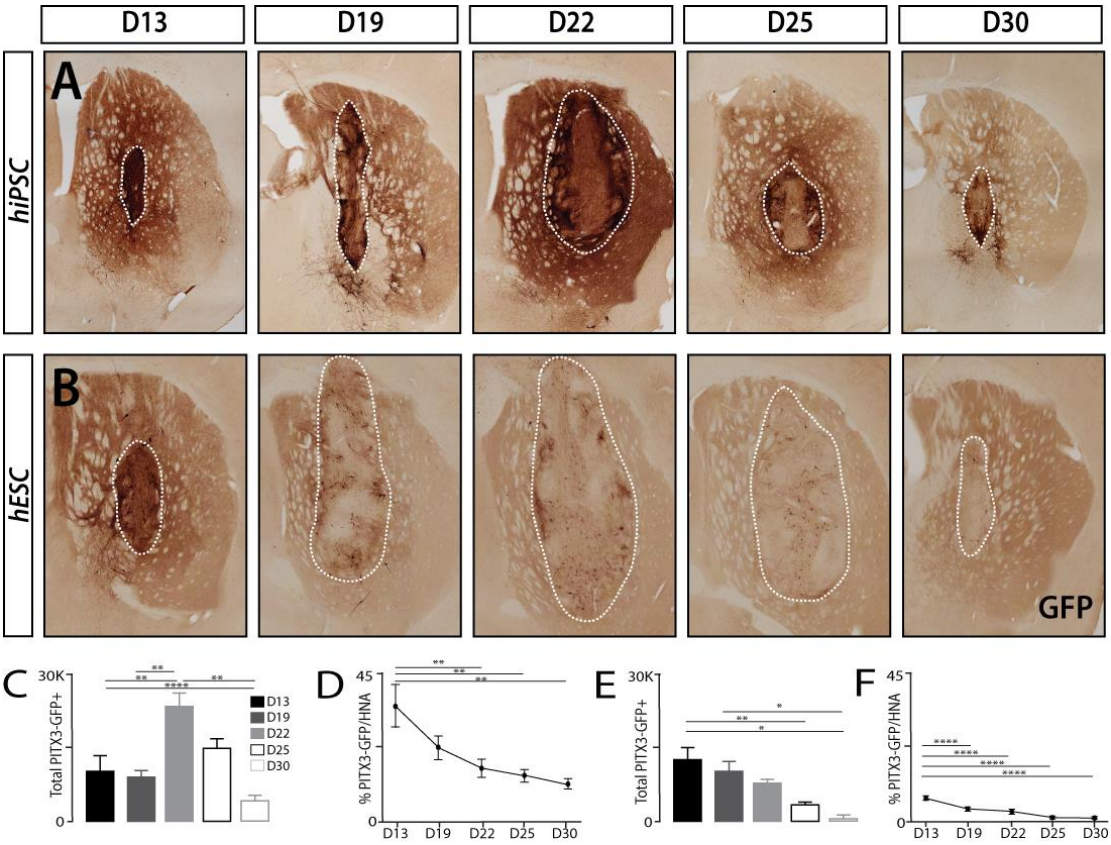

Figure 5.4. Younger progenitor grafts have the highest dopaminergic density across independent cell lines

(A-B) Photomicrographs depicting the distribution and density of GFP$^+$ dopaminergic neurons and fibre innervation within grafted animals. Note the dense homogenous network of GFP$^+$ cells present in D13 grafts, in comparison to the heterogeneous distribution (particularly within the graft core) present in later developmental aged grafts. Graphs illustrating the total yield of (PITX3-GFP$^+$) vmDA neurons within hiPSC **(C)** and hESC-derived **(E)** grafts at respective transplant ages. (D, F) Younger *in vitro* aged grafts had a significant increase in the proportion of GFP$^+$ vmDA neurons for both cell lines (D, hiPSC; F, hESC). Abbreviations: D, day. mean ± SEM. as mean ± SEM.

grafts (D22), we found that both cell lines had the greatest density of dopamine neurons within transplants generated from the youngest progenitors (D13), with a steady decrease in proportion of DA neurons within increasing donor age. Comparison of the two lines revealed a 5-fold increase in the density of GFP+ DA neurons in hiPSC-derived (hiPSC: 39.85% ± 0.06) compared to hESC-derived grafts (hESC: 6.3% ± 0.01 Figure 5.4D, F), highlighting the between line variability often noted in hPSC studies.

5.4.4 Subtype acquisition and fiber outgrowth of grafted dopaminergic neurons is influenced by donor cell age at implantation

Fetal grafting studies have demonstrated that donor age can influence the subtype specification of grafted dopaminergic neurons (Bye *et al.*, 2012). We found that grafts of all hPSC-derived donor ages had the capacity for DA neurons to adopt either an A9 or A10

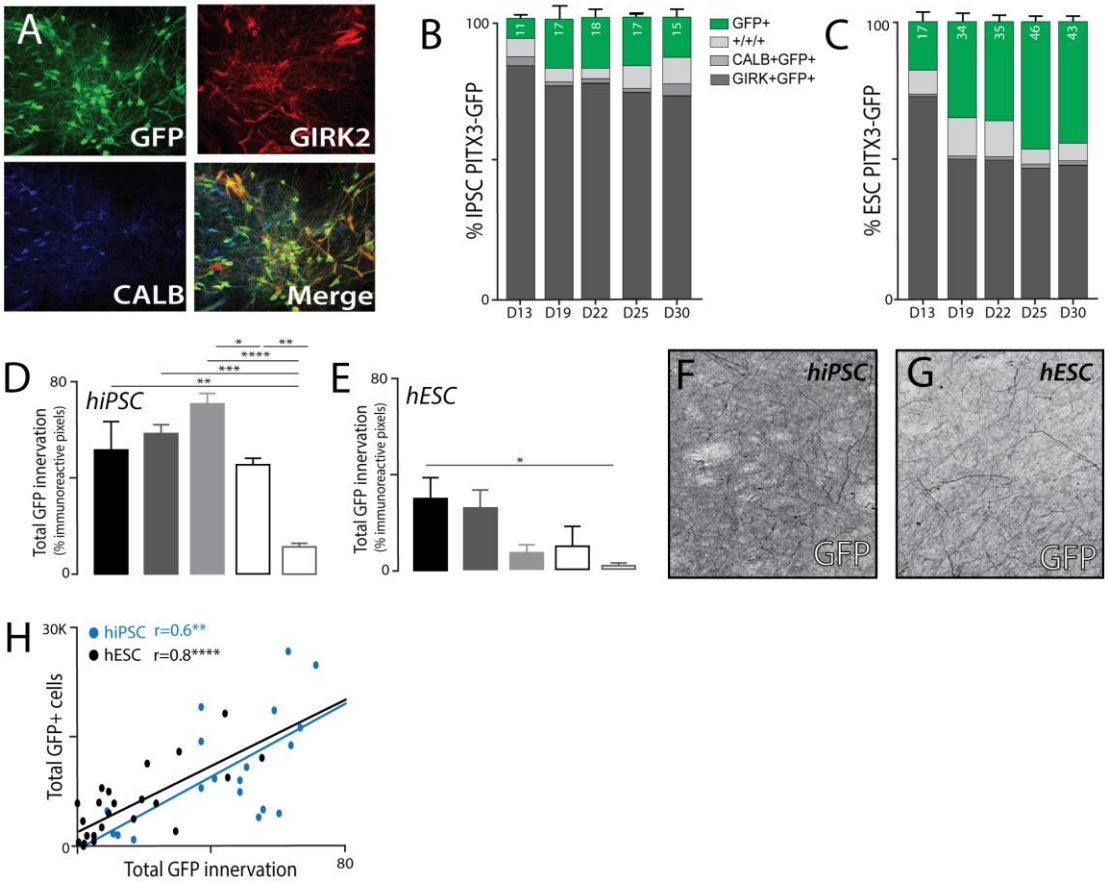

Figure 5.5. A9/A10 phenotype acquisition of grafted DA neurons and their innervation capacity is dependent on the age of the hPSC-derived progenitors at the time of implantation

(A) Representative photomicrographs showing GIRK and/or Calbindin (CALB) co-localised within GFP+ vmDA neurons in a D13 hiPSC-derived transplant. **(B-C)** Quantification of GFP+ neurons that showed co-expression of GIRK2 and/or Calbindin, confirmed both PITX3-eGFP hiPSC **(B)** and hESC **(C)** lines possessed the capacity to form mature vm DA neurons of both A9- and A10-like phenotypes (one-way ANOVA with Tukey's post hoc, n=3-4). Note the proportion of immature vmDA neurons (i.e. those failing to co-express GIRK2 and/or CALB, green bar) was reduced in younger *in vitro* age cell grafts. **(D-E)** Quantification of GFP+ fiber density within the dorsal-lateral striatum of 6-OHDA lesioned mice, transplanted with **(D)** hiPSC- or, **(E)** hESC-derived vm progenitors. **(F-G)** High power representatives illustrate a significant increase in density of GFP+ fibers in PITX3-eGFP hiPSC-derived grafts **(F)** compared to hESC-derived grafts **(G)**. **(H)** Quantitative assessment of transplants revealed a significant positive correlation between striatal innervation and total GFP+ dopaminergic neurons (Pearson's correlation coefficient, n=24-27). *r* corresponds to correlation coefficient. Abbreviations: GFP, green fluorescent protein; human induced pluripotent stem cell, hiPSC; human embryonic stem cell, hESC; ventral midbrain, vm; 60HDA, 6-hydroxydopamine. Data is represented as mean ± SEM.

phenotype, but younger donor grafts displayed the greatest DA maturation (i.e. GFP+ cells adopting GIRK and /or Calbindin co-expression) (Figure 5.5A-C). Whilst younger donor cells had a greater capacity for subtype acquisition, no bias towards either an A9 or A10 identity, unlike fetal studies that have observed an enrichment of A9 neurons in younger grafts (Bye *et al.*, 2012; Somaa *et al.*, 2015). Interestingly, not only were hiPSC-derived D13 grafts more enriched for DA neurons compared to hESC grafts, they also displayed a

higher capacity for DA maturation, with the smallest proportion of DA neurons lacking GIRK and/or Calbindin expression (hESC: 17.26 ± 0.03, hiPSC: 11.01 ± 0.02, Figure 5.5B-C).

Integration of grafted DA neurons into the host tissue was assessed using GFP innervation density within the dorsolateral striatum, the target region for the A9 DA neurons responsible for motor function. Unsurprisingly, grafts containing the highest number of DA neurons showed the highest striatal innervation (D22 hiPSC: 74.55% ± 0.02, D13 hESC:30.28% ± 0.09, percentage immunoreactive pixels within field of view), and similarly grafts containing the least DA cells (D30 for both cell lines), had the poorest innervation, (Figure 5.5D-G). Regression analysis for the two cell lines highlighted a significant positive correlation between the total number of DA neurons and relative striatal innervation (hiPSC: r^2=0.64, p=0.0039, hESC: r^2=0.76, p=<0.0001, Figure 5.5H).

5.4.5 Younger donor cells show greatest enrichment of VM dopaminergic neurons while simultaneously reducing the contribution of poorly specified cells

Recent studies are increasingly recognising the high proportion of non-DA neurons within vm progenitor grafts, cells that may present risks associated with overgrowth, unwanted side effects such as those caused by 5HT neurons, or remain of unknown influence to graft and host functions (Bye *et al.*, 2019; de Luzy *et al.*, 2019; Niclis *et al.*, 2017b). As such there is an increasing need to remain aware of the relative proportion of other cell types within grafts to ensure safety. We therefore assessed the contribution of non-DA (GFP-) cells and those showing evident off-target specification (e.g. FOXA2-) within the grafts. Consistent with previous results, grafts of younger PITX3-iPSC vm progenitors displayed the most superior results, expressing the lowest proportion of non-DA neurons (60.3 ± 5.9% GFP-), yet stable proportion of off-target cells (56.2 ± 6.9% FOXA2-), compared to older (D30) donor grafts (89.0 ± 1.5% GFP- and 57.0 ± 1.9% FOXA2-), Figure 5.6A-E, K, L. Conversely, the hESC-derived progenitor grafts showed a stable high proportion of GFP-cells (>93%), yet increasing proportion of off-target (FOXA2-) cells with increasing donor cell age, Figure 5.6F-J, O-P. For all grafts, irrespective of donor age or cell line of origin, the majority of the poorly specified (FOXA2-), undesirable cells were found within the graft core, consistent with findings in fetal studies.

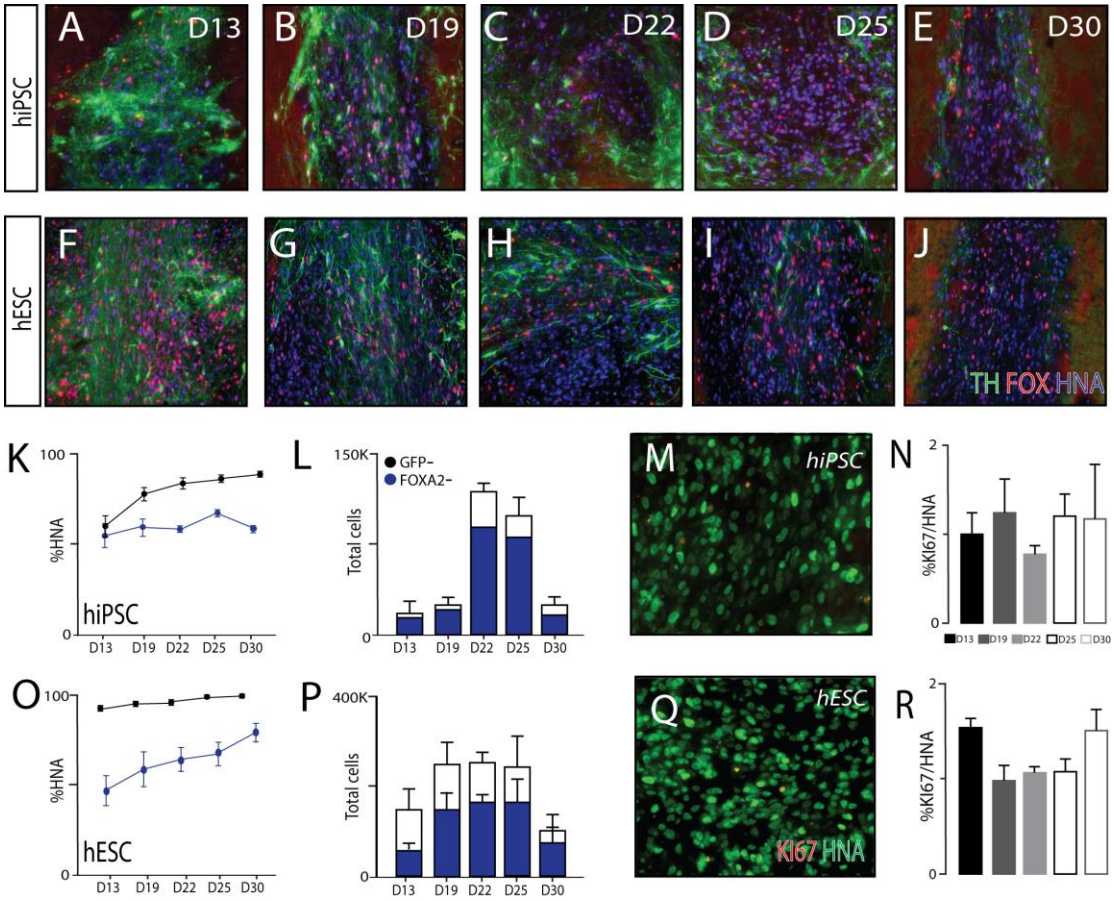

Figure 5.6. Younger *in vitro* age progenitors generate grafts with greater vm progenitor fate

(A-J) Photomontages to show relative expression of floor plate (FOXA2+) and mature dopamine (TH+) markers within grafted populations for all transplant groups. Grafts derived from D13 cells show minimal contamination of non-vm cells compared to other transplant groups, indicated by both a reduced number and proportion of GFP- and FOXA2- cells for both hiPSC **(K-L)** and hESC **(O-P)** lines. **(M, Q)** A small proportion of proliferative (HNA+Ki67+) cells remain in grafted populations. **(N, R)** Quantification of total HNA+/KI67+ cells in grafted populations for hiPSC **(N)** and hESC **(R)** lines. One-way ANOVA with Tukey's post hoc, n=4-6. Data is represented as mean ± SEM.

Within the non-DA and off-target populations, of greatest concern is the presence of rogue proliferative cells that may continue to divide long-term – this is of particular trepidation with delivery of notably early-stage progenitors (D13). Surprisingly, however, at 6 months after transplantation few dividing cells (<2%) remained present within the grafts, with no differences observed between donor cell age, or across lines (Figure 5.6M-N, Q-R).

5.4.6 Grafting outcome is reproducible across independent differentiations

In light of the present observations from hESC and hiPSC progenitor grafts, we questioned whether discrepancies were a consequence of the different cells lines used and/or variability in the in vitro differentiations prior to grating. To address this, we performed repeat grafting from 2 independent differentiations. Recognising the poor outcomes obtained from older

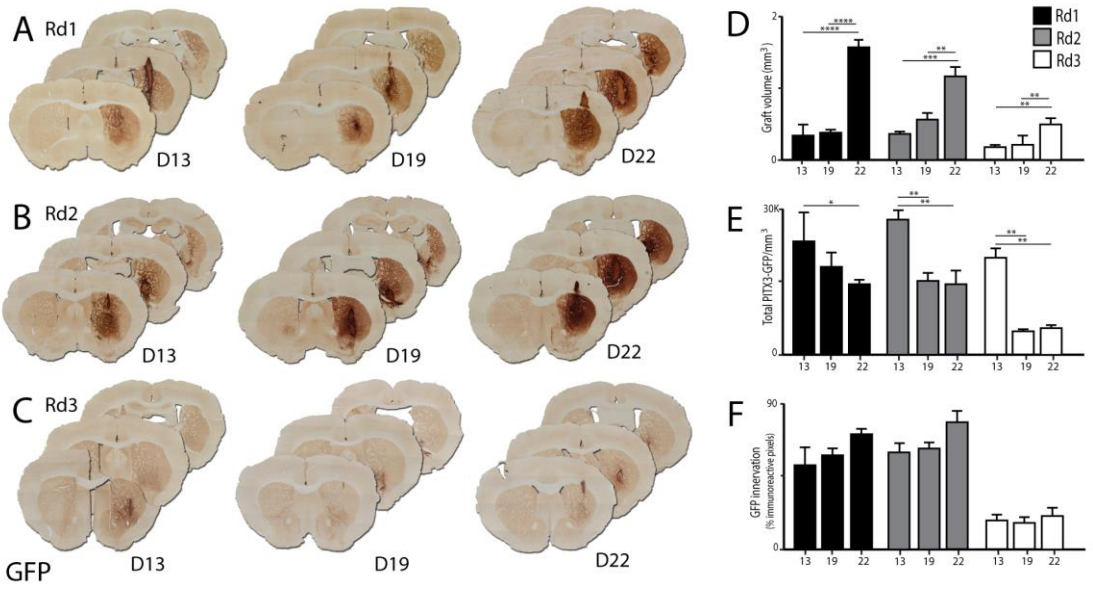

Figure 5.7. Reproducibility across repeated experiments demonstrates robustness of hiPSC PITX3-eGFP reporter line
(A-C) Schematic panel depicting representative GFP images of D13, D19 and D22 hiPSC grafts across three repeated grafting rounds. Images are inclusive of 3 sections from an individual representative animal across rostral-caudal axis. **(D)** Graphs highlighting that repeated transplants show similar trends in respect to **(D)** graft volume, **(E)** proportion of GFP+ neurons and **(F)** striatal reinnervation (one-way ANOVA with Sidak's post hoc, n=4-6). Data is represented as mean ± SEM.

grafts (for both hESC and hiPSC lines), as well as the superior grafting outcome in hiPSC grafts, we focused only on the younger donor ages (D13, 19, 22) from the hiPSC line.

Cells were again transplanted at specified donor ages into 6-OHDA mice and histologically assessed at 6 months. All animals had surviving grafts (as observed by GFP) (Figure 5.7A-C). Consistent with the previous study, we were able to reproduce comparable trends in graft outcomes between donor ages, across the repeated grafting experiments. That is, younger (D13) grafts remained the smallest (Figure 5.6D) with the greatest proportion of GFP+ neurons (Figure 5.7E), and maintained innervation (Figure 5.7F), while older (D22) donor cell grafts were largest, with the smallest fraction of GFP+ neurons. Collectively, these results confirmed that younger donor cells lead to the most optimal grafting outcome, and was consistent across differentiations and grafting rounds.

5.5 Discussion

Engraftment of hPSC-differentiated vm cells at different developmental stages had a significant impact on graft outcome. We found that cells differentiated between 13 and 30 days were all sufficiently specified and amenable to transplantation, but younger cells

generated grafts with the greatest DA neuron density. Older grafts (derived from cells cultured for more than 22days) had significantly lower numbers of DA neurons, which was likely due to the poor survival of post-mitotic neurons present in culture at the time of transplantation. These results highlight the importance of assessing cellular identity and maturity prior to transplantation, as a guide to determine the most suitable transplantation ages for each individual cell line. Surprisingly, while the same number of correctly specified progenitors (>95% OTX2/FOXA2 co-expression) were implanted into all animals, the number of unwanted off-target cells present at 6months was variable and found to be lowest in younger grafts. These observations lead one to question whether ongoing culturing, prior to implantation 'primes' poorly specified cells for in vivo expansion, while younger progenitors more rapidly adopt a post-mitotic fate.

The recognition of younger donor grafts producing the most optimal grafting outcome has also been seen for fetal studies (Torres *et al.*, 2007; Bye *et al.*, 2012; Kauhausen *et al.*, 2013). Despite similarities between the two donor cell sources, we also identified several differences. Here we describe that younger PSC-derived vm progenitors (i.e. D13) produce the smallest grafts, while fetal tissue studies report significantly larger grafts from younger donor ages (Freeman *et al.*, 1995; Gates *et al.*, 2006; Torres *et al.*, 2007; Bye *et al.*, 2012; Kauhausen *et al.*, 2013), suggesting a potential difference in survival between fetal-derived and human PSC-derived vm progenitors following implantation. This finding may also be confounded by the highly expansive non-DA progenitor pool not typically present in fetal grafts. Additionally, the preferential enrichment of A9 DA neurons (the population of cells integral for motor recovery) seen with transplantation of younger tissue derived from fetal ventral midbrain (fVM), was not observed for PSC-derived grafts. Instead, younger *in vitro* progenitor PSC-derived grafts, had an enrichment of both A9 and A10 DA neurons. As a consequence, younger *in vitro* age grafts had a smaller proportion of DA neurons that failed to acquire a A9/A10 phenotype, indicating an increased capacity for DA maturation. This effect on maturation did not appear to influence striatal reinnervation. Further studies will be required to determine whether this increase in A9/A10 fate acquisition (a measure of DA maturation) also influences the functionality of these grafts and their capacity to restore motor deficits.

To assess if differences in donor age were consistent between differentiations, we implanted cells from a further two independent differentiations and grafting rounds. Excitingly, younger donor grafts demonstrated superior outcomes across all rounds. Whilst

being significantly smaller than grafts derived from older progenitors, these grafts consistently demonstrated the highest dopaminergic enrichment. This indicated that outcomes from each cell line can be maintained confidently. Such reproducible findings regarding donor age, as well as reproducibility within a cell line, will help guide future transplant approaches, as well as aid in the selection of cell surface markers at the appropriate developmental age.

Lacking in the field has been a direct comparison between hPSC lines in their ability to form dopaminergic grafts. In this study, we compared hPSC from either an ESC or iPSC background. Both PSC lines competently differentiated (with similar in vitro efficacy) and successfully engrafted into 6-0HDA mice. Grafts displayed a similar trend between grafting ages with respect to total graft volume, DA cell density, A9/A10 DA subtype specification and striatal innervation. Interestingly, groups that contained the highest number of dopaminergic neurons were significantly different between cell lines. Furthermore, irrespective of delivering the same number of progenitors (100,000 cells) for both hPSC lines, actual cell numbers were diverse. These results highlight the importance of characterising cells *in vivo* on a line-to-line basis, but also suggests further efforts may be required to standardise differentiation protocols. Investigation into the state of pluripotency between individual lines may underpin these differences, such that some lines represent a more 'primed' state than others. If this is indeed the case, efforts to revert hPSCs to a common naïve state, prior to commencement of differentiation, may improve reproducibility across cell lines, as has been demonstrated for mouse PSCs (Alsanie *et al.*, 2017; Ghimire *et al.*, 2018).

Current consensus in the field has focused on delivering vm progenitors at an 'intermediate stage' of differentiated – corresponding to a time after completion of neuralisation and morphogen patterning yet prior to the birth of post-mitotic DA neuroblasts. The results of the present study, however, suggest younger progenitor grafts are more appropriate. Before further consideration of younger grafts, rigorous pre-clinical assessment will be required to confirm these donor cells have the capacity for DA release and restoration of motor function in a PD model comparative to conventional approaches (Kriks *et al.*, 2011; Kirkeby *et al.*, 2017; Gantner *et al*, 2020). Added to this, more extensive assessment of graft composition by employing, for example, xenograft transcriptional profiling techniques (Bye *et al*., 2019, Appendix 2) will be required, as well as an understanding of the relative contribution of both DA and non-DA graft innervation/integration, to confirm the presence/absence of unknown cells within grafts that may halt translation. With the

rapid advancement of hPSC-derived mDA late-stage progenitors into the clinic (and the first Parkinson's disease patients already receiving transplants in Japan in late 2018, see press release in Nature news www.nature.com/articles/d41586-018-07407-9), these findings are particularly relevant and raises interest to consider if we are in fact moving into the clinic with the most suitable donor age for transplantation into Parkinson's disease patients.

5.6 Acknowledgements

The authors thank Mong Tien and Brianna Xuereb for their expert technical assistance. IDL was supported by a University of Melbourne International Scholarship, Australia. CG was supported by an Australian Postgraduate Award. CP was supported by a Senior Medical Research Fellowship provided by the National Health and Medical Research Council Australia. This research was funded by Stem Cells Australia. The Florey Institute of Neuroscience and Mental Health acknowledges the strong support from the Victorian Government and in particular the funding from the Operational Infrastructure Support Grant.

5.7 Author contributions

All experiments were performed at the Florey Institute of Neuroscience and Mental Health. Conceptualisation: IDL, CP. Investigation: IDL, JN, CPH. Analysis: IDL, CG, NM. Contributed unpublished reagents: LT, CP. Writing – original draft – IDL, CP. Writing – editing: IDL, CP.

5.8 References

Alsanie WF, Niclis JC, Hunt CP, De Luzy IR, Penna V, Bye CR, et al. Specification of murine ground state pluripotent stem cells to regional neuronal populations. Sci Rep 2017; 7: 1–16.

Barker RA, Barrett J, Mason SL, Björklund A. Fetal dopaminergic transplantation trials and the future of neural grafting in Parkinson's disease. Lancet Neurol 2013; 12: 84–91.

Blaess S, Corrales JMD, Joyner AL. Sonic hedgehog regulates Gli activator and repressor functions with spatial and temporal precision in the mid/hindbrain region. Development 2006; 133: 1799–1809.

Brundin P, Bio T, Hansson O. Improving the survival of grafted dopaminergic neurons : A review over current approaches. Cell Transplant 2000; 9(2): 179-95.

Bye CR, Penna V, de Luzy IR, Gantner CW, Hunt CPJ, Thompson LH, et al. Transcriptional Profiling of Xenogeneic Transplants: Examining Human Pluripotent Stem Cell-Derived Grafts in the Rodent Brain. Stem Cell Reports 2019; 13: 877–890.

Bye CR, Thompson LH, Parish CL. Birth dating of midbrain dopamine neurons identifies A9 enriched tissue for transplantation into Parkinsonian mice. Exp Neurol 2012; 236: 58–68.

Castilho RF, Hansson O, Brundin P. Improving the survival of grafted embryonic dopamine neurons in rodent models of Parkinson's disease. Prog Brain Res 2000; 127: 203–231.

Doi D, Samata B, Katsukawa M, Kikuchi T, Morizane A, Ono Y, et al. Isolation of human induced pluripotent stem cell-derived dopaminergic progenitors by cell sorting for successful transplantation. Stem Cell Reports 2014; 2: 337–350.

Freeman TB, Sanberg PR, Nauert GM, Boss BD, Spector D, Olanow CW, et al. The influence of donor age on the survival of solid and suspension intraparenchymal human embryonic nigral grafts. Cell Transplant 1995; 4: 141–154.

Gantner C, de Luzy IR, Kauhausen, JA, Moriarty N, Niclis JC, Bye CR, Penna V, Hunt CPJ, Ermine CM, Pouton CW, Kirik D, Thompson LH and Parish, CL. Viral Delivery Of Gdnf Promotes Functional Integration Of Human Stem Cell Grafts In Parkinsons Disease. Cell Stem Cell 2020; 26(4): 511-526.

Gates MA, Torres EM, White A, Fricker-Gates RA, Dunnett SB. Re-examining the ontogeny of substantia nigra dopamine neurons. Eur J Neurosci 2006; 23: 1384–1390.

Ghimire S, Van Der Jeught M, Neupane J, Roost MS, Anckaert J, Popovic M, et al. Comparative analysis of naive, primed and ground state pluripotency in mouse embryonic stem cells originating from the same genetic background. Sci Rep 2018; 8: 1–11.

Joksimovic M, Anderegg A, Roy A, Campochiaro L, Yun B, Kittappa R, et al. Spatiotemporally separable Shh domains in the midbrain define distinct dopaminergic progenitor pools. Proc Natl Acad Sci U S A 2009; 106: 19185–19190.

Jönsson ME, Ono Y, Björklund A, Thompson LH. Identification of transplantable dopamine neuron precursors at different stages of midbrain neurogenesis. Exp Neurol 2009; 219: 341–354.

Kauhausen J, Thompson LH, Parish CL. Cell intrinsic and extrinsic factors contribute to enhance neural circuit reconstruction following transplantation in Parkinsonian mice. J Physiol 2013; 591: 77–91.

Kirkeby A, Grealish S, Wolf DA, Nelander J, Wood J, Lundblad M, et al. Generation of Regionally Specified Neural Progenitors and Functional Neurons from Human Embryonic Stem Cells under Defined Conditions. Cell Rep 2012; 1: 703–714.

Kirkeby A, Nolbrant S, Tiklova K, Heuer A, Kee N, Cardoso T, et al. Predictive Markers Guide Differentiation to Improve Graft Outcome in Clinical Translation of hESC-Based Therapy for

Parkinson's Disease. Cell Stem Cell 2017; 20: 135–148.

Kriks S, Shim JW, Piao J, Ganat YM, Wakeman DR, Xie Z, et al. Dopamine neurons derived from human ES cells efficiently engraft in animal models of Parkinson's disease. Nature 2011; 480: 547–551.

de Luzy IR, Niclis JC, Gantner CW, Kauhausen JA, Hunt CPJ, Ermine C, et al. Isolation of LMX1a ventral midbrain progenitors improves the safety and predictability of human pluripotent stem cell-derived neural transplants in Parkinsonian Disease. J Neurosci 2019; 39(48): 9521-31.

Niclis JC, Gantner CW, Alsanie WF, McDougall SJ, Bye CR, Elefanty AG, et al. Efficiently Specified Ventral Midbrain Dopamine Neurons from Human Pluripotent Stem Cells Under Xeno-Free Conditions Restore Motor Deficits in Parkinsonian Rodents. Stem Cells Transl Med 2017; 6: 937–948.

Niclis JC, Gantner CW, Hunt CPJ, Kauhausen JA, Durnall JC, Haynes JM, et al. A PITX3-EGFP Reporter Line Reveals Connectivity of Dopamine and Non-dopamine Neuronal Subtypes in Grafts Generated from Human Embryonic Stem Cells. Stem cell reports 2017; 9: 868–882.

Olanow CW, Fahn S. Fetal nigral transplantation as a therapy for Parkinson's disease. Restor Ther Park Dis 2006; 19: 93–118.

Samata B, Doi D, Nishimura K, Kikuchi T, Watanabe A, Sakamoto Y, et al. Purification of functional human ES and iPSC-derived midbrain dopaminergic progenitors using LRTM1. Nat Commun 2016; 7: 13097.

Smidt MP, Smits SM, Bouwmeester H, Hamers FPT, van der Linden AJA, Hellemons AJCGM, et al. Early developmental failure of substantia nigra dopamine neurons in mice lacking the homeodomain gene Pitx3. Development 2004; 131: 1145–1155.

Somaa FA, Bye CR, Thompson LH, Parish CL. Meningeal cells influence midbrain development and the engraftment of dopamine progenitors in parkinsonian mice. Exp Neurol 2015; 267: 30–41.

Somaa FA, Wang TY, Niclis JC, Bruggeman KF, Kauhausen JA, Guo H, et al. Peptide-Based Scaffolds Support Human Cortical Progenitor Graft Integration to Reduce Atrophy and Promote Functional Repair in a Model of Stroke. Cell Rep 2017; 20: 1964–1977.

Torres EM, Monville C, Gates MA, Bagga V, Dunnett SB. Improved survival of young donor age dopamine grafts in a rat model of Parkinson's disease. Neuroscience 2007; 146: 1606–1617.

Wakeman DR, Hiller BM, Marmion DJ, Mcmahon CW, Corbett GT, Mangan KP, et al. Stem Cell Reports. Stem Cell Reports 2017; 9: 149–161.

Watmuff B, Hartley BJ, Hunt CPJ, Fabb SA, Pouton CW, Haynes JM. Human pluripotent stem cell derived midbrain PITX3$^{eGFP/w}$ neurons: A versatile tool for pharmacological screening and neurodegenerative modeling. Front Cell Neurosci 2015; 9: 104.

Xi J, Liu Y, Liu H, Chen H, Emborg ME, Zhang S-C. Specification Of Midbrain Dopamine Neurons From Primate Pluripotent Stem Cells. Stem Cells 2012; 30: 1655–1663.

Xia N, Fang F, Zhang P, Cui J, Tep-Cullison C, Hamerley T, et al. A Knockin Reporter Allows Purification and Characterization of mDA Neurons from Heterogeneous Populations. Cell Rep 2017; 18: 2533–2546.

5.9 Supplementary Figures

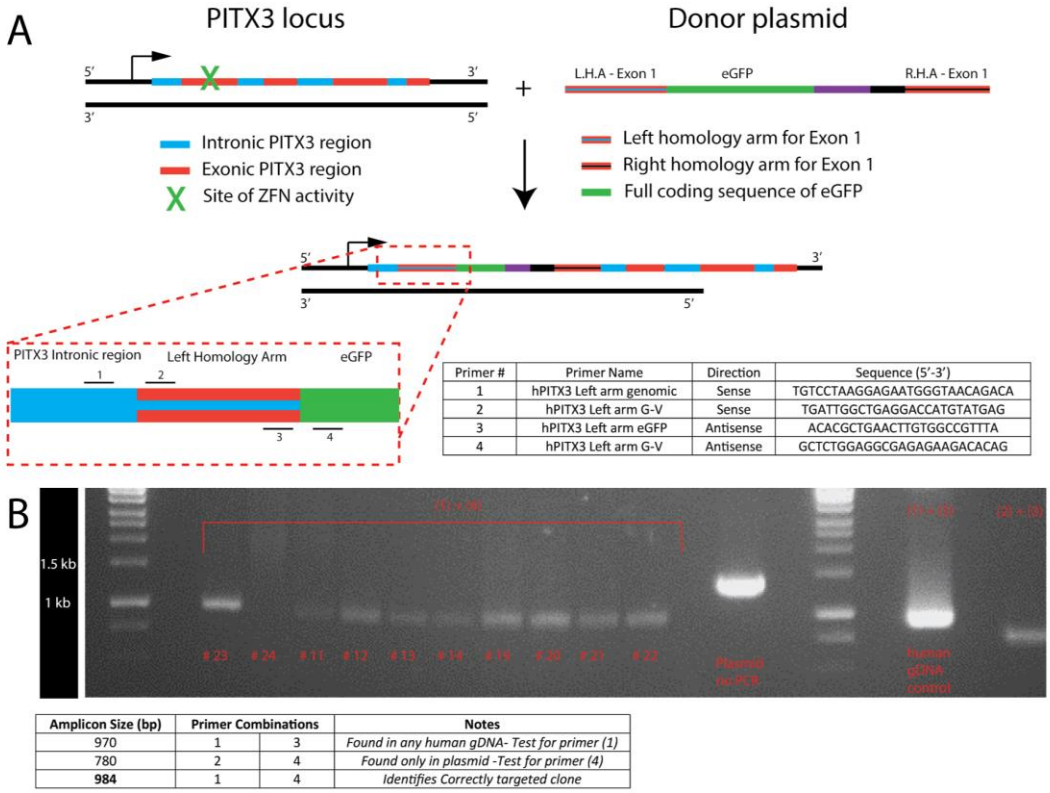

Primer #	Primer Name	Direction	Sequence (5′-3′)
1	hPITX3 Left arm genomic	Sense	TGTCCTAAGGAGAATGGGTAACAGACA
2	hPITX3 Left arm G-V	Sense	TGATTGGCTGAGGACCATGTATGAG
3	hPITX3 Left arm eGFP	Antisense	ACACGCTGAACTTGTGGCCGTTTA
4	hPITX3 Left arm G-V	Antisense	GCTCTGGAGGCGAGAGAAGACACAG

Amplicon Size (bp)	Primer Combinations		Notes
970	1	3	*Found in any human gDNA- Test for primer (1)*
780	2	4	*Found only in plasmid -Test for primer (4)*
984	1	4	*Identifies Correctly targeted clone*

Supplementary Figure 5.1. Generation of hiPSC PITX3-eGFP reporter
(A) Schematic of ZFN plasmids and PITX3 donor vector, and specifically designed primers to amplify the left homology arm of the donor plasmid. **(B)** RT-PCR bands identified clones with correct construct integration at the PITX3 locus

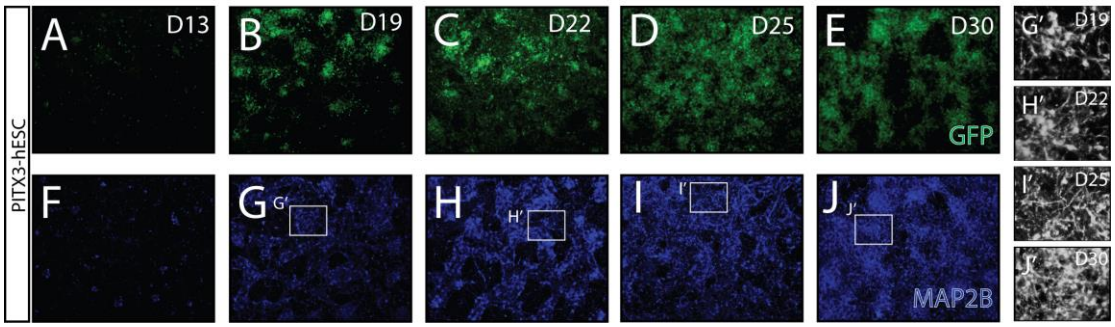

Supplementary Figure 5.2. Cellular maturity prior to engraftment in hESC-derived cultures

(A-J) Expression of GFP (green) and MAP2 (blue) during differentiation indicates relative cellular maturity and proportion of vmDA neurons at the time of implantation for the hESC reporter. Note the increased number and length of neurites at later stages of differentiation, with a significant proportion already present at D19 (G'-J').

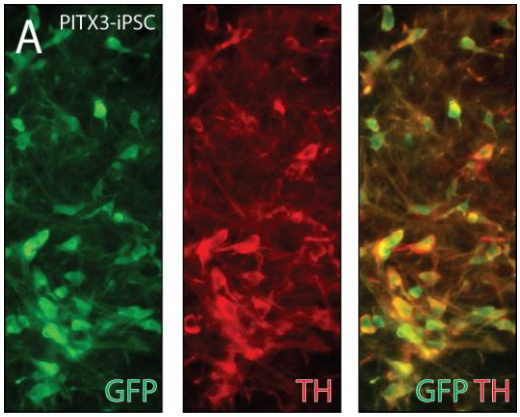

Supplementary Figure 5.3. Grafts derived from the hiPSC PITX3-eGFP reporter line show high specificity to the rate-limiting enzyme in DA synthesis
(A) Photomontages of a 6 month hiPSC-derived graft demonstrating that the PITX3-eGFP reporter tightly overlaps with TH+ dopamine neurons.

Chapter 6.

Discussion

Stem cells hold significant promise as a tool for regenerative therapy. Since the successful isolation and maintenance of PSCs (Thomson *et al.*, 1998), great efforts have been made to generate neural subtypes from PSCs with high specificity, that in the future may have the potential to restore functional deficits in a number of neurodegenerative diseases and neural traumas.

6.1 Employment of lineage-restricted reporter cell lines for aiding isolation and tracing of dopamine populations

Fluorescent reporter cell lines have made a remarkable contribution to advancing our understanding of stem cells and development. Such tools provide a means to accurately detect, isolate and track specific cellular populations.

Traditional antibody staining for the identification of midbrain floor plate progenitors within PSC-derived cultures has heavily relied on co-expression of the fore/midbrain marker OTX2, in combination with the basal/floor plate marker FOXA2, however this combination is still inclusive of basal plate progenitors present in vm cultures and transplants. Competent identification of midbrain floor plate progenitors can be achieved with the addition of LMX1A, a more restrictive floor plate marker (Kirkeby *et al.*, 2012; Kriks *et al.*, 2012), which has allowed more rigorous assessment of successful and unsuccessful *in vitro* differentiations and grafting (Niclis *et al*., 2017).

In chapter 3, we explored the capacity to utilise this gene (LMX1A) as a sorting marker to improve DA grafting. Utilising the LMX1A-GFP reporter line to isolate mDA progenitors, we demonstrated the capacity to reduce the overgrowth and proliferation of unwanted cell populations, as well as completely eliminate serotonergic neurons (a neuronal population known to underpin graft-induced dyskinesias) (Politis, 2010; Politis *et al.*, 2011). Such refinement also significantly enriched the proportion of DA neurons. These enriched grafts displayed preferential innervation of appropriate dopaminergic targets (namely the dorsolateral striatum) and importantly restored motor function. Whilst, LMX1A- cell grafts

contained few DA neurons, most evident from these grafts was their surprising preferential off-target innervation of non-DA targets (including the periventricular nucleus and contralateral hippocampi). The potential impact of such innervation at these non-DA targets for patients is currently unknown. The collective results presented in chapter 3 highlight a significant refinement and improvement upon existing transplantation approaches that have been adopted for the present clinical trial, and highlights the stability and robustness of LMX1A+ isolated mDA progenitors for transplantation.

In an additional sorting approach, we employed an alternative reporter line, targeting the PITX3 locus, to isolate DA precursors for the enrichment of dopamine grafts, given its high selectivity for authentic mDA neurons (Chapter 3). While grafts of LMX1A-GFP+ vm progenitors generated healthy grafts, FACS-isolated PITX3+ DA precursors were not amenable for transplantation, indicating along with other studies, that the developmental-age of selected marker/s for purification and engraftment should be considered (Jönsson *et al*., 2009; Xia *et al*., 2017). Another consideration is the absence of supportive cells in the PITX3+ grafts, that are typically observed in unsorted grafts and identified in the LMX1A+grafts (Chapter 3). Although these supportive cells were shown to be redundant for transplantation of rodent DA neurons (Thompson *et al.*, 2006; Jönsson *et al.*, 2009), they may be required for successful engraftment of human cells. Interestingly, this effect did not translate *in vitro*. Isolated PITX3+ precursors survived replating after sorting with no impact on survival, and were maintained in culture for up to 40 days *in vitro* (DIV), suggesting that isolated precursors appear to be most vulnerable to shear trauma during transplantation, in combination to their implantation into the adult brain – an environment devoid of appropriate morphogen and pro-survival proteins typical of the developing brain (that is achievable, to some extent, in sustained *in vitro* cultures).

Another key example highlighting the importance and utility of reporter lines in this field has stemmed from recent work examining the dopaminergic innervation of the host tissue by hPSC-derived vm progenitors. Previous efforts to assess the capacity of these progenitors to functionally integrate has focused on assessments using human specific antibodies such as the neural cell adhesion molecule (NCAM) (Kriks *et al.*, 2011; Kirkeby *et al.*, 2012; Grealish *et al.*, 2014), as the commonly employed dopamine-identifying antibody, tyrosine hydroxylase (TH) failed to discriminate between graft and host dopamine cells and fibres. However, such an approach, focused on NCAM, failed to highlight the relative contribution

and extent of non-dopaminergic innervation. Alternatively, the engineering of a PITX3-GFP hPSC reporter line has enabled highly specific assessment of the total dopamine contribution in the graft, and pattern of innervation, whilst simultaneously highlighting how extensive the non-DA contribution was (i.e. NCAM+GFP- fibres). Alarming to the field using this approach, was the identification of extremely widespread innervation throughout the rostral-caudal axis of the brain, that was mainly non-dopaminergic (Niclis *et al*., 2017b). This observation, further supports the precedent for strategies, such as cellular sorting, to minimise unwanted cell/neuronal populations.

Reporter lines are an invaluable tool for preclinical research, but their utility in a clinical setting remains questionable (Brazelton and Blau, 2005; Ansari *et al.*, 2016). Observations of GFP-induced immunogenicity and cytotoxicity in both rodent and non-human primate models have been observed, thereby raises concern of utility (Ansari *et al*., 2016; Re *et al*., 2004). However, despite this, GFP reporters employed in clinical trials have met Phase I safety requirements in the context of viral immunotherapy, resulting in advancement to Phase 2 testing (Gaudinski *et al.*, 2018, see NCT02759588 or NCT02840487 at *clinicaltrials.gov*). Other fluorescent analogs (CFP, YFP) require further exploration, particularly as early results suggest they may have reduced cytotoxicity (Taghizadeh and Sherley, 2008; Ansari *et al.*, 2016). This leaves the field to ponder on the risk of potential cytotoxicity and immune modulation using GFP reporter lines, balanced with the benefit of removing unsafe cell types. Regardless, the knowledge gained from reporter lines in preclinical studies, will fundamentally aid in the selection of cell surface antigens, for future clinical applications.

6.2 Suicide transgene activation improves stem cell graft safety

Whilst cellular sorting has significantly advanced the field forward in regards to generating more homogenous grafts, as well as minimising other cellular populations that may pose risks to patients, there remain safety issues associated with the implantation of hPSC-derived progenitors. Most evident is the risk of 'rogue' cells evading the sorting procedure (noting our work in Chapter 3 reported a 1% risk of non-GFP cells being included within the GFP+ fraction). With this in mind, alternative approaches such as suicide gene therapy that offer further protection to eliminate rogue proliferative populations that may present following transplantation have been pursued.

In Chapter 4 we demonstrate that prolonged activation of the suicide gene (by GCV administration for 8weeks, commencing 6weeks after transplantation) was sufficient to reduce graft overgrowth/proliferation (a 50% reduction in cell number), with no toxicity to DA neurons, resulting in a significant enrichment of mDA neurons and maintained efficacy for restoring motor deficits in PD rats. Within these grafts, however, remained residual proliferative cells that may or may not pose a long-term risk. Interestingly, the delayed delivery of GCV (commencing 14 weeks after grafting and sustained for 8weeks) had no impact on graft size, but was capable of significantly reducing the residual proliferative progenitor pool. However, unlike the early GCV treatment, these animals were not exposed to a prolonged GCV 'wash-out' period to assess whether quiescent stem cell populations may appear at more protracted stages after cessation of treatment.

In both instances, the persistent presence of proliferative cells after either early or late delivery of GCV, suggested grafts may not be receiving adequate exposure to the drug. To address this problem, we tested the impact of modulating GCV treatment in a second cohort of animals. Increased exposure to GCV (by modulation of concentration or frequency) had minimal additional benefit that was not significantly different to the original study. It was only when cells were treated to GCV prior to transplantation that grafts were significantly smaller, but in this case contained few dopaminergic neurons, indicative that this treatment resulted in the transplantation of a precursor population too mature for the physical trauma of implantations, previously described for fetal tissue grafts and our own observation of the developmental age of the hPSC-derived vm cells for grafting (Chapter 5)

Despite a conscientious effort to promote delivery of GCV, all grafts still contained proliferative cells, suggesting that this system is currently not a safety tool but instead can be used to refine overgrowth and improve the purity of the grafts, by elimination of a proportion of progenitors that result in enlarged grafts.

It was interesting that the effect seen in hPSC-derived teratomas (i.e. total elimination of dividing cells) was not observed in our study. However, it is crucial to recognise the intrinsic developmental differences in cell cycle between proliferative cell types. Differentiated neural progenitors have a significantly longer cell cycle, with a shortened S-phase (the phase in which GCV elicits its effect) relative to PSC (Calegari *et al.*, 2005; Lange and Calegari, 2010; Arai *et al.*, 2011; Turrero García *et al.*, 2016). Therefore, the time-period that GCV-induced

ablation is effective in neural progenitors is notably shorter and less frequent. Additionally, grafts exhibited inferior graft vascularisation in comparison to the well-vascularised host (also observed in other work from our lab, Appendix 2), and unlike self-vascularising PSC-derived teratomas (Zhang *et al.*, 2008) . Further study will be necessary to illuminate the ideal duration and dose of GCV, as well as vascular network, for competent elimination of all proliferative cells within a neural graft.

6.3 Optimal developmental age for transplantation

Many lessons learnt from preclinical and clinical fetal tissue grafting for Parkinson's disease have impacted the field of hPSC-derived transplantation. Surprisingly, however, the impact of donor age, despite being extensively explored for fetal tissue (Brundin *et al*., 2000; Bye *et al*., 2012; Freeman *et al*., 1995; Gates *et al.*, 2006; Torres *et al.*, 2007), has not translated or been documented for hPSC-derived progenitors. As a result, this has caused considerable discrepancies in age of donor cells transplanted between different laboratories. To understand the impact of donor age on stem cell grafts, we transplanted differentiated ventral midbrain cells at a series of points during the differentiation, spanning the ages currently adopted by different groups (de Luzy *et al.*, 2019; Doi *et al.*, 2014; Gantner *et al.*, 2020; Kirkeby *et al.*, 2012; Kriks *et al*., 2011; Samata *et al*., 2016; Wakeman *et al*., 2017).

While current consensus in the field heavily focuses on the transplantation of late-stage progenitors (and is the choice for the current clinical trials underway in Japan, commenced in October 2018), we surprisingly found over three separate grafting rounds that fully-specified early-stage progenitors (isolated at day 13 of the differentiation) generated the most homogeneous DA grafts. Unlike younger grafts, older progenitors generated grafts with poor DA specification, containing a considerably higher component of unwanted, off-target cells. We recommend that future studies transplanting younger VM progenitors should involve the implantation of a higher number of cells to determine the full capacity of these VM DA enriched transplants to functionally integrate and restore motor deficits in PD models. In the context of clinical application, this suggests that further assessment is needed to determine if younger grafts are in fact superior to late-stage progenitors. Key to this will be rigorous assessment of functionality, DA release, synaptic integration and graft composition. Such findings will be informative for other transplanted neural cell types such as replacement of medium spiny neurons for Huntington's Disease or cortical neurons for stroke.

Whilst we observed consistency within cell lines, different PSC lines showed considerable inter-line variability, particularly for total number of DA neurons. Similarly, recognised differences in morphogen gradient requirements for *in vitro* differentiation between PSC lines has been observed by others (Kirkeby *et al*., 2017a), and collectively these highlight the imperative need to assess each line on an individual basis.

6.4 Clinical implications and future directions

Within just 7 years of generating *bona fide* ventral midbrain dopaminergic neurons from human PSCs (Kriks *et al.*, 2011), the first Parkinson's Disease patient has been transplanted with hPSC-derived mDA progenitors (Jun Takahashi's team, Kyoto University, Oct 2018 – for press release in Nature news, see https://www.nature.com/articles/d41586-018-07407-9), with two other teams planning to commence trials in 2020 (Kirkeby *et al*., 2017b; Studer, 2017). Despite the excitement, there remains concerns within the research community that these trials may have advanced prematurely.

One recognises that significant progress has been made in recent years to translate stem-cell derived DA progenitors into the clinic, with many of the hurdles already met (Kirkeby *et al*., 2017b; Studer, 2017). Current teams embarking on clinical trials have opted to use either hESC- or hiPSC-derived cell products. The obvious advantage of hiPSCs is their ability to avoid ethical and immunogenicity issues, however the requirement to generate a single line per patient (i.e. patient-derived) brings about its own drawbacks given the need to comprehensively test multiple cell lines, the increased risk of genetic and epigenetic abnormalities and potential inclusion of disease-carrying mutations, which can be avoided with a hESC approach.

In more recent years and fundamental for translation, work by others and in our lab, have made headway towards the development of full current GMP (cGMP)-compliant protocols that can competently generate highly efficient and reproducible authentic mDA neurons (Kirkeby *et al*., 2017a; Niclis *et al*., 2017a; Studer, 2017), that are now capable of engraftment and functionality (Kirkeby *et al*., 2017b; Studer, 2017).

Added to this, of importance will be generation of large-scale cell banks of cryopreserved mDA cells. These banks will provide a means to transplant animal models to confirm safety, survival and functionality of grafted cells, as well as conduct QC assays and sterility testing, before transplanting the same cells into the patient(s). Evidence of successful cryopreservation has been observed for both mDA progenitors and neurons (Drummond *et al*., 2020; Kirkeby *et al*., 2017b; Niclis *et al*., 2017a; Studer, 2017; Wakeman *et al*., 2017), with appropriate pre-clinical scalability, sterility and efficacy testing already performed (Kirkeby *et al*., 2017b; Studer, 2017). Importantly, batch-to-batch reproducibility of differentiations could be demonstrated within an individual cell line (Kirkeby *et al*., 2017a; Studer, 2017), as well as consistency across multiple cell lines, the later however highlighted significant variability in patterning requirements between lines, that could be overcome by optimising morphogen gradients (Kirkeby *et al*., 2017a). The benefits of significant expansion during the differentiation means a low starting number of ~1 million PSCs can generate a remarkably high yield of vm progenitors (~300 million vm progenitors in 7 x T175 flasks), indicating that only minimal scalability is likely to be required (Kirkeby *et al*., 2017b). Kirkeby *et al* (2017a) state that cryopreservation of progenitors from a single differentiation, should provide sufficient cells for both Phase 1/II of the STEM-PD planned clinical trials, as well as all pre-clinical testing requirements. An important consideration to avoid potential risks associated with batch-batch variations that may arise. A final consideration prior to clinical translation, will be toxicity, biodistribution and extensive safety testing of the proposed cell product. Added to this, standardisation of an immunosuppression regime for hESC-derived cell transplants will be require to minimise graft rejection.

Although these advancements are significant, several concerns still remain, notably graft safety, but also survival and inferior innervation. The most evident remains the low proportion of functional dopamine neurons present within vm progenitor grafts. As reviewed by Niclis *et al* (2017a), across the majority of preclinical studies to date, almost 95% of the grafts remain non-dopaminergic. Lacking in the field until more recently has been a full characterisation of the grafts, to determine the composition of these undefined cells that occupy 95% of total grafted cells. In parallel work, within the Parish laboratory we developed a method to rapidly and efficiently transcriptionally profile xenogeneic transplants. This methodological approach, reliant on identifying transcript differences between graft and host species, has enabled us to examine the full composition of LMX1A+ grafts (derived according to Chapter 3). While we had previously reported these LMX1A+ grafts eliminated

5HT neurons (Chapter 3), profiling identified the presence of other neuronal populations (Gabaergic/Glutamatergic) as well as high proportions of other neural (oligodendrocyte and astrocyte) populations (Bye *et al*., 2019, Appendix 2).

Whilst this is a valuable new tool that will enable the field to understand the overall composition of graft, it fails to provide information on the relative proportions each population makes to the graft (since it assesses total RNA levels and is unable to distinguish high expression in few cells from low expression across many cells). Complimenting this technique is the recent work of Malin Parmar's group that has performed single cell profiling of both fetal and stem cell-derived vm grafts (Tiklová *et al.*, 2019). This has been highly informative yet is exceedingly laborious, costly and requires a high level of skill. Added to this, is the considerably lower neuronal content (<10%) observed in the scRNA-seq analysis (Tiklová *et al.*, 2019) compared to immunohistochemical analysis, likely reflecting a limitation of this technique that RNA may not be optimally collected from these mature cells and as a result biases towards younger progenitors. Nevertheless, these two techniques provide a very complimentary set of tools for the field to move forward to a greater understanding of graft composition.

Assessment at the single cell level allowed identification of a novel population of cells, identified as vascular leptomeningeal cells (vLMCs), and found to be unique to PSC-derived VM grafts (Tiklová *et al.*, 2019). Presence of vLMCs in stem-cell derived grafts have subsequently been observed across several PSC lines (Tiklová *et al.*, 2019). These cells were identified in close proximity to blood vessels, suggesting a potential role in graft vascularisation. Interestingly fetal studies, have elucidated that meningeal cells present within fetal donor material, known to secrete a variety of trophins, were beneficial and promoted both differentiation and synaptic integration of dopamine neurons (Somaa *et al*., 2015). Whether the vLMCs found in hPSC-derived grafts will behave in the same manner is currently unknown. Of interest, the presence of this cell type in LMX1A-enriched grafts was minimal in comparison (Bye *et al*., 2019, Appendix 2). Such disparity may be explained by differences in differentiation protocols and/or cell lines.

Whilst the Parmar group and others have recognised that fetal grafts are heterogeneous, containing a mixture of neuronal cell types (DA, 5HT, GABA, encephalin and substance P-containing neurons), and that DA neurons are a small contribution (Bolam *et al*., 1987;

Dunnett *et al*., 1988; Mahalik & Clayton, 1991; Thompson *et al*., 2008), the recognised differences between fetal and ESC grafts (particularly the obvious lack of pluripotent cells and vLMCs in fetal grafts), mean it is difficult to draw comparisons from the fetal clinical trials in regard to cellular behaviour and safety. As such, these two techniques have provided a warning to consider if these other cell types identified within the graft will elicit negative side effects for patients. Of note, in addition to the well-observed modulatory effects of serotonergic neurons (Freed *et al*., 2001; Hagell *et al*., 2002; Olanow *et al*., 2003), GABAergic precursors have been linked to behavioural recovery in the 6-OHDA model, indicating that other non-DA populations may also play a role in recovery (Martínez-cerdeño *et al.*, 2014). In summary, these new techniques highlight the vast array of other cell types present in these vm progenitor grafts, even when enrichment approaches are adopted such as isolation of LMX1a+ progenitors.

With this in mind, pursuit of more restrictive sorting candidates will be critical for optimal clinical translation. The proneural gene Neurogenin 2 (Ngn2), the orphan nuclear receptor Nurr1 and engrailed-1 (EN1), all with greater restriction within the VM and critical for DA development, represent obvious candidates. Demonstrative of plausible success, Ngn2-mDA precursors isolated from Ngn2-GFP expressing mice, have been shown to be both transplantable and give rise to a significantly greater proportion of mDA neurons, that were importantly devoid of serotonergic neurons (Bye *et al*., 2015; Thompson *et al*., 2006).The authors suggest these isolated cells resembled Nurr1-expressing precursors, which have been recognised in mouse studies to be of an optimal age and expression domain to enrich transplants (Ganat *et al.*, 2012). Future efforts will be required to determine if effects seen in fetal tissue will translate utilising Ngn2, Nurr1 and/or EN1 reporters on the more heterogeneous and asynchronous PSC-derived differentiations.

Cell surface candidate are highly attractive for clinical translation since they avoid risks of immunogenicity and cytotoxicity associated with fluorescent reporters. Despite early hopes of the cell surface marker Alcam, a marker of floor plate basal progenitors, in its ability to significantly enrich DA neurons in rodent fetal grafts (Bye *et al*., 2015), this approach failed to translate to human PSC, due to expression also at the pluripotent stage (our unpublished findings). More recently, LRTM1, indicative of floor plate basal midbrain progenitors, has shown significant promise, being the most restrictive cell surface marker identified so far, with capacity to increase DA yield within hPSC-derived vm grafts (Samata *et al*., 2016).

However, failure to reproduce results competently, likely due to the early sorting and subsequent sub-culturing required for several days prior to transplantation is of concern. Furthermore, in comparison to LMX1A which is restricted to the floor plate, LRTM1 is expressed in both floor and basal plate regions (Samata *et al*., 2016), the potential consequence of this wider expression has not been extensively investigated.

Difficulties translating results observed in fetal (Bye *et al*., 2019) and mESC studies (Gennet *et al*, 2016) to hPSC-derived transplants, suggests identification of markers at the hPSC level may be more appropriate. More recently, an exhaustive comparison of PSC-derived DA grafts across >30 different grafting rounds has identified several markers (EN1, SPRY1, WNT1, CNPY1, ETV5), indicative of a positive DA outcome (Kirkeby *et al*., 2017) that may be potential sorting candidates to consider for future studies.

Identification of novel cell surface proteins superior to current approaches still remains an important goal. Isolation of potentially more restrictive populations using reporters, such as those mentioned previously, could potentially be screened to identify new cell surface markers. Critical to the success of cellular sorting will be selection of markers that are restricted to the mDA population, as well as expressed early enough to survive transplantation. Whilst focus remains on cell surface markers for clinical translation, the risk of residual antibodies attached to the cell surface may bring about its own issue of immunogenicity.

In Chapter 4, we observed the capacity of the HSV-TK system to improve graft outcomes by reducing overall graft size without impact on the dopaminergic population and their functional capacity to restore motor deficits. However, we also observed the limitation of this system in its failure to completely ablate all proliferative cells within the grafts and thereby not providing the necessary safety. We acknowledged that vm progenitor grafts show poor vascularisation that may underpin suboptimal delivery of the suicide-activating drug GCV. To address this, one future approach may be to co-transplant additional cells and/or delivery of factors to promote vascularisation. Sustained delivery of vascular maturing proteins, such as BDNF, VEGF or EPO, may be of benefit to achieve this goal. Of interest, the neurotrophic factor BDNF, in addition to promoting graft survival, neuronal maturation and plasticity, has more recently been shown to play a role in promoting graft vascularisation for neural grafts in the stroke infarcted brain (Nisbet *et al.*, 2018). Additionally, agents that permeabilise the

blood brain barrier (BBB) may further improve penetration of the suicide-activating drug into the brain parenchyma. RMP-7 (Labradimil), a synthetic bradykinin analog, has shown benefit in PSC-derived teratoma approaches, but its applicability for neural grafts is more complex due to an extremely short half-life of the drug (Brewster *et al*., 1994; May *et al*., 1998). For efficacy, infusion would be required to prevent rapid restoration of the BBB, that can happen within 2-5minutes after cessation of RMP-7 (Emerich *et al*., 2001). With no, or very limited graft-derived vasculature present within DA grafts (Tiklová *et al*., 2019), and minimal infiltration of host blood vessels (Appendix 4), engraftment of supportive hPSC-derived endothelial cells for blood vessel formation may be essential and preferential over other strategies discussed above.

Alternatively, other suicide systems may have superior outcomes to our employed HSV-TK/GCV approach for vm grafting. The iCas9 system is already available and shown to be efficacious for tackling tumorigenesis in PSC applications (Kojima *et al*., 2019; Yagyu *et al*., 2015) . This approach offers targeted suicide of all grafted cells, however could be considered with additional engineering targeted at simultaneously protecting mDA progenitors (i.e. by excision of the iCas9 within EN1 or NURR1 expressing cells), this could be employed for refinement, as well as safety. Since the progenitor pool is protected here, and therefore no concerns of eliminating mDA neurons, there is an opportunity for earlier treatment *in vivo* or pre-treatment *in vitro* following expression of the targeted gene. Less explored suicide systems, such as the CD/5-fluorocytosine system or monoclonal antibody-mediated approaches, may also be interesting avenues to pursue for future studies (Jones *et al*., 2014).

In the final results chapter, we focused on identifying the optimal maturation stage of the differentiating hPSC-derived vm progenitors/precursors for transplantation (Chapter 5). These results highlighted the importance of characterising cells *in vivo* on a line-to-line basis, but suggests further efforts may be required to standardise differentiation protocols, as well as determine if these differences arise at the pluripotent level. Understanding of the true ‘stemness’ of individual PSC lines, and whether certain lines are more primed than others, or have different epigenetic profiles, is currently lacking. With more insight, this may indicate that all PSC lines may need to be reverted to an equivalent naïve starting point prior to differentiation, to improve and standardise pattering efficiencies, as has been shown by us and others through exposure to the inhibitor cocktails (2i) for mESCs (Alsanie *et al*., 2017,

Appendix 1; Ghimire *et al*., 2018) and (5i) for hPSCs (Lee *et al.*, 2017), that may fundamentally aid in standardising grafting outcomes.

Despite significant headway in the field of transplantation for PD, engraftment of grafted hPSC-derived DA neurons remains relatively poor and connectivity inferior to their human VM fetal counterparts (Grealish *et al.*, 2014). This is likely a result of the adult brain being a notably less permissive environment than in development with many developmental cues either downregulated or absent. Such observations suggest that efforts to restore the physical and trophic environment may be advantageous to promote survival, differentiation and axonal connectivity of grafted mDA neurons. Extensive pre-clinical and clinical studies have demonstrated that glial cell line-derived neurotrophic factor (GDNF) plays a significant role in survival, plasticity and metabolism of DA neurons, with benefits more recently observed in our lab by over-expressing GDNF in DA-rich fetal VM grafts (Kauhausen *et al*, 2013). Most recently the team has advanced on this work, now exploring the benefit of GDNF on human PSC-derived vm progenitor grafts. Due to the results observed in Chapter 3, we were able to utilise LMX1A+ purified hPSC-derived grafts as a platform to assess the effect of modulating the external environment by GDNF.

Similar to fetal studies, targeted viral delivery of GDNF not only promoted survival and functional recovery but also influenced plasticity of grafted mDA neurons in LMX1A+ grafts (according to Chapter 3) (Gantner *et al*., 2020). Intriguingly, this synaptic benefit was found to be time-dependent. Whilst early delivery of GDNF, prior to implanting the vm progenitors, promoted graft survival, it impeded on their capacity of the DA neurons to innervate the host tissue, with these cells preferentially self-innervating the graft. In contrast, when GDNF delivery was delayed, with viral delivery of AAV-GDNF administered several weeks after transplantation, there was no impact on cell survival, but rather caused extensive DA plasticity and innervation of the host, increased dopamine metabolism and consequently motor function (Gantner *et al*., 2020) These combined findings suggest that a bi-phasic approach may be more appropriate, whereby GDNF can be acutely delivered to promote survival upon engraftment, and later re-activated to modulate axonal plasticity at a time when the DA neurons have already extended axon outside of the graft core. To achieve this a more sophisticated delivery approach is required, such as an inducible system that allows for controlled time and dose-dependent GDNF release, such as that recently described by Clive Svendsen' group (Akhtar *et al.*, 2018).

Several other growth and guidance cues, such as Netrin1, Sema3F and EphrinA proteins, are known modulators of synaptic DA plasticity (Van den Heuvel & Pasterkamp., 2008). Within our team, we have additionally described the benefit of delivering SDF1, by inclusion of meninges in the donor material, as well as Wnt5a to promote DA graft plasticity, with SDF1 also reported to increase the relative proportion of A9 DA neurons within fetal grafts (Parish *et al.*, 2008; Somaa *et al.*, 2015). It remains to be determined whether these proteins also influence hPSC-derived DA progenitor grafts.

While extensive attention has been paid to understanding the plasticity of mDA neurons in development (Van den Heuvel and Pasterkamp, 2008), and to a lesser extent, fetal tissue grafts, seemingly little attention has been paid to the role the extracellular matrix (ECM) plays in the maturity and function of mDA neurons. Previously thought of as merely an anchorage for cells, more recent years have recognised that the ECM provides signalling cues to cells to also influence their proliferation, differentiation and plasticity (Theocharidis *et al*., 2014), inclusive of mDA neurons (Zhang *et al*., 2017). In light of this, we have looked to more closely recapitulate this environment for our grafted vm progenitors by engineering scaffolds to mimic the laminin signalling typical of the brains ECM. These hydrogel-based scaffold were designed not only to provide a trophic and physical support for the donor cells, but also with the added bonus of protection against shear forces during *in vivo* delivery, and subsequent integration into the host brain. These scaffolds can also be used as a vehicle to sustain and localize protein delivery over weeks to months. Utilising these scaffolds to encapsulate GDNF together with isolated LMX1A+ progenitors (according to Chapter 3), we were able to increase the survival of grafted mDA neurons and enhance both graft plasticity (by enriching the A9 DA population) and DA synapse formation (*Appendix 4*). Collectively, these led to restoration of motor function (*Appendix 4*).

This new work focused on the potential utility of bioengineered scaffolds to improve graft outcomes opens many new avenues for consideration, such as the capacity to use these hydrogels to deliver other proteins, inclusive of pro-survival cues. Factors such as rho kinase inhibitors (ROCKi), which are routinely used for expanding PSCs (Watanabe *et al*., 2007), as well as caspase inhibitors (QVD) and JNK inhibitors (SP600125) could be interesting candidates that already provided benefit in both pluripotent and fetal applications (Claassen *et al*., 2009; Emre *et al*., 2010; Hossini *et al*., 2016; Rawal *et al*., 2007).

A remaining evident consideration for human PSC-derived grafting is the issue of graft rejection. Immunogenicity of hESC-derived grafts means that patients would need to be exposed to immunosuppression transiently for at least 12 months to prevent allograft rejection, which comes with a raft of side effects and complications. In an ideal world, one would generate iPSCs from a patient for the purpose of autologous grafting, however, in reality the variability between lines would mean comprehensive optimisation, validation, safety and QC testing bringing about significant technical, regulatory and financial challenges. Regulatory issues such as increased risk of genetic and epigenetic abnormalities with generation of iPSCs, has recently led to the premature suspension of the first-in-human clinical trials utilising patient-derived RPE cells to treat macular degeneration (Garber, 2015). Added to this is the consideration of using a patient's own cells which likely carry disease-contributing genes, and thus the heightened susceptibility these cells may have to neurodegeneration. Rest assured, retrospective assessment of fetal grafting has reported that while some evidence of disease transmission can occur from the adult/aged host into grafted cells, the proportion of these cells carrying pathological hallmarks of PD remains low (Kordower *et al*., 2008; Li *et al*., 2008, 2010, 2016). Overall, the field has come to recognise that the future of human PSC grafting for PD will most likely involve allogeneic grafting (cells from one individual, ESC or IPSC of origin, implanted into another). With this comes the need to consider the immunological challenge.

Development of strategies that avert the need for immunosuppressant agents are therefore desirable. Donor-recipient matching has been suggested, whereby cell banks of hiPSC lines can be generated from donors with the most common human leukocyte antigen (HLA) profiles. Whilst HLA matching has eluded to the potential for improved engraftment in both retinal or dopaminergic transplants (the later showing benefit over the conventional immunosuppressant agent tacrolimus) (Morizane *et al.*, 2017), other attempts have not been met with such success, despite applying similar matching criteria (Badin *et al*., 2019). Added to this, the considerable number of lines still required to cover the majority of the population brings its own issues as discussed for autologous grafting, as well as failure to serve rare donors, collectively make this approach challenging.

As a result, several labs have pursued alternative means to evade the immune response whilst importantly focused on minimising the number of lines required for population coverage.

Utilising modern genetic engineering/editing techniques, cloaked hPSC lines with enhanced immunocompatibility have emerged and shown promise in evading the immune response (Deuse *et al*., 2019; Gornalusse *et al*., 2017; Han *et al*., 2019; Harding *et al*., 2019; Xu *et al*., 2019). Excitingly, and important for clinical translation, is the potential for a generic line capable of global coverage, that may be achievable with this approach. In addition to the several other benefits discussed previously, scaffold-based hydrogels may also restrict migration of host immune cells, as has been seen with fetal studies (Moriarty *et al*., 2017). Interestingly, this phenomenon was not observed when assessed at later stages in hPSC-derived grafts, but immunogenicity at earlier stages is yet to be determined (*Appendix 4*). However, these approaches collectively raise their own safety issues, given the ability of grafted cells to evade immune surveillance. This may become problematic if unwanted effects arise in the graft, and suggests an *in vivo* safe-guard such as suicide gene therapy (discussed in Chapter 4), may be required as a preventative measure.

It is currently an extremely exciting time for stem cell therapy, with the potential to make a huge impact to the lives of Parkinson's disease patients. Whilst this past decade has seen significant progress towards delivering PSC-derived vm progenitors for therapy, it is important to recognise the remaining hurdles that still require attention. This thesis has focused on shedding light on these less commonly reported limitations and explored several solutions to implement or consider for future dopamine grafting studies and clinical trials to improve grafting outcomes.

References

Akhtar AA, Gowing G, Kobritz N, Savinoff SE, Garcia L, Saxon D, et al. Inducible Expression of GDNF in Transplanted iPSC-Derived Neural Progenitor Cells. Stem Cell Reports 2018, 10(6): 1696-1704.

Alsanie WF, Niclis JC, Hunt CP, De Luzy IR, Penna V, Bye CR, et al. Specification of murine ground state pluripotent stem cells to regional neuronal populations. Sci Rep 2017; 7: 1–16.

Ansari AM, Ahmed AK, Matsangos AE, Lay F, Born LJ, Marti G, et al. Cellular GFP Toxicity and Immunogenicity : Potential Confounders in in Vivo Cell Tracking Experiments. Stem Cell Rev Reports 2016: 553–559.

Arai Y, Pulvers JN, Haffner C, Schilling B, Nüsslein I, Calegari F, et al. Neural stem and progenitor cells shorten S-phase on commitment to neuron production. Nat Commun 2011; 2: 154.

Badin R, Bugi A, Williams S, Vadori M, Michael M, Jan C, et al. MHC matching fails to prevent long-term rejection of iPSC-derived neurons in non-human primates. Nat Commun 2019; 10: 4357.

Bolam JP, Freund TF, Björklund A, Dunnett SB, Smith AD. Synaptic input and local output of dopaminergic neurons in grafts that functionally reinnervate the host neostriatum. Exp Brain Res 1987; 68(1): 131-46.

Brazelton TR, Blau HM. Optimizing Techniques for Tracking Transplanted Stem Cells In Vivo. Stem Cells 2005; 23: 1251–1265.

Brewster ME, Raghavan K, Pop E, Bodor N. Enhanced delivery of ganciclovir to the brain through the use of redox targeting. Antimicrob Agents Chemother 1994; 38: 817–823.

Brundin P, Bio T, Hansson O. Improving the survival of grafted dopaminergic neurons : A review over current approaches. Cell Transplant. 2000; 9(2): 179-95.

Bye CR, Jönsson ME, Björklund A, Parish CL, Thompson LH. Transcriptome analysis reveals transmembrane targets on transplantable midbrain dopamine progenitors. Proc Natl Acad Sci U S A 2015; 112: e1946–e1955.

Bye CR, Penna V, de Luzy IR, Gantner CW, Hunt CPJ, Thompson LH, et al. Transcriptional Profiling of Xenogeneic Transplants: Examining Human Pluripotent Stem Cell-Derived Grafts in the Rodent Brain. Stem Cell Reports 2019; 13: 877–890.

Bye CR, Thompson LH, Parish CL. Birth dating of midbrain dopamine neurons identifies A9 enriched tissue for transplantation into Parkinsonian mice. Exp Neurol 2012; 236: 58–68.

Calegari F, Haubensak W, Haffher C, Huttner WB. Selective lengthening of the cell cycle in the neurogenic subpopulation of neural progenitor cells during mouse brain development. J Neurosci 2005; 25: 6533–6538.

Claassen DA, Desler MM, Rizzino A. ROCK inhibition enhances the recovery and growth of cryopreserved human embryonic stem cells and human induced pluripotent stem cells. Mol Reprod Dev 2009; 76: 722–732.

de Luzy IR, Niclis JC, Gantner CW, Kauhausen JA, Hunt CPJ, Ermine C, et al. Isolation of LMX1a ventral midbrain progenitors improves the safety and predictability of human pluripotent stem cell-derived neural transplants in Parkinsonian Disease. J Neurosci 2019; 39(48): 9521-31.

Deuse T, Hu X, Gravina A, Wang D, Tediashvili G, De C, et al. Hypoimmunogenic derivatives of induced pluripotent stem cells evade immune rejection in fully immunocompetent allogeneic recipients. Nat Biotechnol 2019; 37: 252–258.

Doi D, Samata B, Katsukawa M, Kikuchi T, Morizane A, Ono Y, et al. Isolation of human induced pluripotent stem cell-derived dopaminergic progenitors by cell sorting for successful transplantation. Stem Cell Reports 2014; 2: 337–350.

Drummond NJ, Dolt KS, Canham MA, Kilbride P, John Morris G, Kunath T. Cryopreservation of midbrain dopaminergic neural cells differentiated from human embryonic stem cells. Bioxriv 2020: doi.org/10.1101/2020.02.11.944272.

Dunnett SB, Hernandez TD, Summerfield A, Jones GH, Arbuthnott G. Graft-derived recovery from 6-OHDA lesions: specificity of ventral mesencephalic graft tissues. Exp Brain Res 1988; 71(2): 411-24.

Emerich DF, Dean RL, Osborn C, Bartus RT. The development of the bradykinin agonist labradimil as a means to increase the permeability of the blood-brain barrier: From concept to clinical evaluation. Clin Pharmacokinet 2001; 40: 105–123.

Emre N, Vidal JG, Elia J, O'Connor ED, Paramban RI, Hefferan MP, et al. The ROCK inhibitor Y-27632 improves recovery of human embryonic stem cells after fluorescence-activated cell sorting with multiple cell surface markers. PLoS One 2010; 5: 1–10.

Freeman TB, Sanberg PR, Nauert GM, Boss BD, Spector D, Olanow CW, et al. The influence of donor age on the survival of solid and suspension intraparenchymal human embryonic nigral grafts. Cell Transplant 1995; 4: 141–154.

Ganat YM, Calder EL, Kriks S, Nelander J, Tu EY, Jia F, et al. Identification of embryonic stem cell-derived midbrain dopaminergic neurons for engraftment. J Clin Invest 2012; 122: 2928–2939.

Gantner C, de Luzy IR, Kauhausen, JA, Moriarty N, Niclis JC, Bye CR, Penna V, Hunt CPJ, Ermine CM, Pouton CW, Kirik D, Thompson LH and Parish, CL. Viral Delivery Of Gdnf Promotes Functional Integration Of Human Stem Cell Grafts In Parkinsons Disease. Cell Stem Cell 2020; 26(4): 511-526.

Garber K. RIKEN suspends first clinical trial involving induced pluripotent stem cells. Nat Biotechnol 2015; 33: 890–891.

Gates MA, Torres EM, White A, Fricker-Gates RA, Dunnett SB. Re-examining the ontogeny of substantia nigra dopamine neurons. Eur J Neurosci 2006; 23: 1384–1390.

Gaudinski MR, Houser K V., Morabito KM, Hu Z, Yamshchikov G, Rothwell RS, et al. Safety, tolerability, and immunogenicity of two Zika virus DNA vaccine candidates in healthy adults: randomised, open-label, phase 1 clinical trials. Lancet 2018; 391: 552–562.

Gennet N, Tamburini C, Nan X, Li M. FolR1: A novel cell surface marker for isolating midbrain dopamine neural progenitors and nascent dopamine neurons. Sci Rep 2016; 6: 1–10.

Ghimire S, Van Der Jeught M, Neupane J, Roost MS, Anckaert J, Popovic M, et al. Comparative analysis of naive, primed and ground state pluripotency in mouse embryonic stem cells originating from the same genetic background. Sci Rep 2018; 8: 1–11.

Grealish S, Diguet E, Kirkeby A, Mattsson B, Heuer A, Bramoulle Y, et al. Human ESC-derived dopamine neurons show similar preclinical efficacy and potency to fetal neurons when grafted in a rat model of Parkinson's disease. Cell Stem Cell 2014; 15: 653–665.

Hagell P, Piccini P, Björklund A, Brundin P, Rehncrona S, Widner H, et al. Dyskinesias following neural transplantation in parkinson's disease. Nat Neurosci 2002; 5: 627–628.

Han X, Wang M, Duan S, Franco PJ, Kenty JH, Hedrick P. Generation of hypoimmunogenic human pluripotent stem cells. PNAS 2019; 116(21): 10441-10446.

Harding J, Vintersten-Nagy K, Shutova M, Yang H, Tang JK, Massumi M, et al. Induction of

long-term allogeneic cell acceptance and formation of immune privileged tissue in immunocompetent hosts. bioRxiv 2019: 716571.

Hossini AM, Quast AS, Plötz M, Grauel K, Exner T, Küchler J, et al. PI3K/AKT signaling pathway is essential for survival of induced pluripotent stem cells. PLoS One 2016; 11: 1–27.

Jones BS, Lamb LS, Goldman F, Di Stasi A. Improving the safety of cell therapy products by suicide gene transfer. Front Pharmacol 2014; 5: 1–8.

Jönsson ME, Ono Y, Björklund A, Thompson LH. Identification of transplantable dopamine neuron precursors at different stages of midbrain neurogenesis. Exp Neurol 2009; 219: 341–354.

Kauhausen J, Thompson LH, Parish CL. Cell intrinsic and extrinsic factors contribute to enhance neural circuit reconstruction following transplantation in Parkinsonian mice. J Physiol 2013; 591: 77–91.

Kirkeby A, Grealish S, Wolf DA, Nelander J, Wood J, Lundblad M, et al. Generation of Regionally Specified Neural Progenitors and Functional Neurons from Human Embryonic Stem Cells under Defined Conditions. Cell Rep 2012; 1: 703–714.

Kirkeby A, Nolbrant S, Tiklova K, Heuer A, Kee N, Cardoso T, et al. Predictive Markers Guide Differentiation to Improve Graft Outcome in Clinical Translation of hESC-Based Therapy for Parkinson's Disease. Cell Stem Cell 2017; 20: 135–148.

Kirkeby A, Parmar M, Barker RA. Strategies for bringing stem cell-derived dopamine neurons to the clinic: A European approach (STEM-PD). Prog Brain Res 2017; 230: 165–190.

Kojima K, Miyoshi H, Nagoshi N, Kohyama J, Itakura G, Kawabata S, et al. Selective Ablation of Tumorigenic Cells Following Human Induced Pluripotent Stem Cell-Derived Neural Stem/Progenitor Cell Transplantation in Spinal Cord Injury. Stem Cells Transl Med 2019; 8: 260–270.

Kordower JH, Chu Y, Hauser RA, Freeman TB, Olanow CW. Lewy body-like pathology in long-term embryonic nigral transplants in Parkinson's disease. Nat Med 2008; 14: 504–506.

Kriks S, Shim JW, Piao J, Ganat YM, Wakeman DR, Xie Z, et al. Dopamine neurons derived from human ES cells efficiently engraft in animal models of Parkinson's disease. Nature 2011; 480: 547–551.

Lange C, Calegari F. Cdks and cyclins link G1 length and differentiation of embryonic, neural and hematopoietic stem cells. Cell Cycle 2010; 9: 1893–1900.

Lee JH, Laronde S, Collins TJ, Shapovalova Z, Tanasijevic B, McNicol JD, et al. Lineage-Specific Differentiation Is Influenced by State of Human Pluripotency. Cell Rep 2017; 19: 20–35.

Lemay DR, Kittaka M, Gordon EM, Gray B, Stins MF, Mccomb JG, et al. Intravenous RMP-7 increases delivery of ganciclovr into rat brain tumors and enhances the effects of herpes simplex virus thymidine kinase gene therapy. Hum Gene Ther 1998; 9(7): 989–995.

Li JY, Englund E, Holton JL, Soulet D, Hagell P, Lees AJ, et al. Lewy bodies in grafted neurons in subjects with Parkinson's disease suggest host-to-graft disease propagation. Nat Med 2008; 14: 501–503.

Li JY, Englund E, Widner H, Rehncrona S, Björklund A, Lindvall O, et al. Characterization of Lewy body pathology in 12- and 16-year-old intrastriatal mesencephalic grafts surviving in a patient with Parkinson's disease. Mov Disord 2010; 25(8):1091-6.

Li W, Englund E, Widner H, Mattsson B, Van Westen D, Lätt J, et al. Extensive graft-derived dopaminergic innervation is maintained 24 years after transplantation in the degenerating parkinsonian brain. Proc Natl Acad Sci U S A 2016; 113: 6544–6549.

Mahalik TJ, Clayton GH. Specific outgrowth from neurons of ventral mesencephalic grafts to the catecholamine-depleted striatum of adult hosts. Exp Neurol 1991; 113: 18–27.

Martínez-cerdeño V, Noctor SC, Espinosa A, Ariza J, Parker P, Orasji S, et al. NIH Public Access. 2014; 6: 238–250.

Moriarty N, Pandit A, Dowd E. Encapsulation of primary dopaminergic neurons in a GDNF-loaded collagen hydrogel increases their survival , re-innervation and function after intra-striatal transplantation. Sci Rep 2017: 1–14.

Morizane A, Kikuchi T, Hayashi T, Mizuma H, Takara S, Doi H, et al. MHC matching improves engraftment of iPSC-derived neurons in non-human primates. Nat Commun 2017; 8: 1–12.

Nelakanti RV, Kooreman NG, Wu JC. Teratoma formation: A tool for monitoring pluripotency in stem cell research. Curr Protoc Stem Cell Biol 2015; 32.

Niclis JC, Gantner CW, Alsanie WF, McDougall SJ, Bye CR, Elefanty AG, et al. Efficiently Specified Ventral Midbrain Dopamine Neurons from Human Pluripotent Stem Cells Under Xeno-Free Conditions Restore Motor Deficits in Parkinsonian Rodents. Stem Cells Transl Med 2017; 6: 937–948.

Niclis JC, Gantner CW, Hunt CPJ, Kauhausen JA, Durnall JC, Haynes JM, et al. A PITX3-EGFP Reporter Line Reveals Connectivity of Dopamine and Non-dopamine Neuronal Subtypes in Grafts Generated from Human Embryonic Stem Cells. Stem cell reports 2017; 9: 868–882.

Nisbet DR, Wang TY, Bruggeman KF, Niclis JC, Somaa FA, Penna V, et al. Shear Containment of BDNF within Molecular Hydrogels Promotes Human Stem Cell Engraftment and Postinfarction Remodeling in Stroke. Adv Biosyst 2018; 2: 1–13.

Olanow CW, Goetz CG, Kordower JH, Stoessl AJ, Sossi V, Brin MF, et al. A double-blind controlled trial of bilateral fetal nigral transplantation in Parkinson's disease. Ann Neurol 2003; 54: 403–414.

Parish CL, Castelo-Branco G, Rawal N, Tonnesen J, Sorensen AT, Salto C, et al. Wnt5a-treated midbrain neural stem cells improve dopamine cell replacement therapy in parkinsonian mice. J Clin Invest 2008; 118(1): 149-60.

Politis M. Dyskinesias after neural transplantation in Parkinson's disease: What do we know and what is next? BMC Med 2010; 8: 80.

Politis M, Oertel WH, Wu K, Quinn NP, Pogarell O, Brooks DJ, et al. Graft-induced dyskinesias in Parkinson's disease: High striatal serotonin/dopamine transporter ratio. Mov Disord 2011; 26: 1997–2003.

Rawal N, Parish C, Castelo-Branco G, Arenas E. Inhibition of JNK increases survival of transplanted dopamine neurons in Parkinsonian rats. Cell Death Differ 2007; 14: 381–383.

Re F, Srinivasan R, Igarashi T, Marincola F, Childs R. Green fluorescent protein expression in dendritic cells enhances their immunogenicity and elicits specific cytotoxic T-cell responses in humans. Exp Hematol 2004; 32: 210–217.

Samata B, Doi D, Nishimura K, Kikuchi T, Watanabe A, Sakamoto Y, et al. Purification of functional human ES and iPSC-derived midbrain dopaminergic progenitors using LRTM1. Nat Commun 2016; 7: 13097.

Somaa FA, Bye CR, Thompson LH, Parish CL. Meningeal cells influence midbrain development and the engraftment of dopamine progenitors in parkinsonian mice. Exp Neurol 2015; 267: 30–41.

Studer L. Strategies for bringing stem cell-derived dopamine neurons to the clinic - The NYSTEM trial. Prog Brain Res. 2017; 230: 191-212.

Taghizadeh RR, Sherley JL. CFP and YFP, but not GFP, provide stable fluorescent marking of rat hepatic adult stem cells. J Biomed Biotechnol 2008; 2008: 453590.

Theocharidis U, Long K, ffrench-Constant C, Faissner A. Regulation of the neural stem cell compartment by extracellular matrix constituents. Prog Brain Res 2014; 214: 3–28.

Thompson LH, Andersson E, Jensen JB, Barraud P, Guillemot F, Parmar M, et al. Neurogenin2 identifies a transplantable dopamine neuron precursor in the developing ventral mesencephalon. Exp Neurol 2006; 198: 183–198.

Thompson LH, Kirik D, Björklund A. Non-dopaminergic neurons in ventral mesencephalic transplants make widespread axonal connections in the host brain. Exp Neurol 2008; 213: 220–228.

Thomson JA, Itskovitz-Eldor, J. Shapiro SS, Waknitz MA, Swiergiel JJ, Marshall VS, Jones JM. Embryonic stem cell lines derived from human blastocysts. Science 1998; 282: 1145–1147.

Tiklová K, Nolbrant S, Fiorenzano A, Björklund ÅK, Sharma Y, Heuer A, et al. Single Cell Transcriptomics Identified Stem Cell-Derived Graft Composition In A Model of Parkinson's Disease. Nat Comms 2020; 11: 2434.

Torres EM, Monville C, Gates MA, Bagga V, Dunnett SB. Improved survival of young donor age dopamine grafts in a rat model of Parkinson's disease. Neuroscience 2007; 146: 1606–1617.

Turrero García M, Chang Y, Arai Y, Huttner WB. S-phase duration is the main target of cell cycle regulation in neural progenitors of developing ferret neocortex. J Comp Neurol 2016; 524: 456–470.

Van den Heuvel DM, Pasterkamp RJ. Getting connected in the dopamine system. Prog Neurobiol 2008; 85: 75–93.

Wakeman DR, Hiller BM, Marmion DJ, Mcmahon CW, Corbett GT, Mangan KP, et al. Stem Cell Reports. Stem Cell Reports 2017; 9: 149–161.

Watanabe K, Ueno M, Kamiya D, Nishiyama A, Matsumura M, Wataya T, et al. A ROCK inhibitor permits survival of dissociated human embryonic stem cells. Nat Biotechnol 2007; 25: 681–686.

Xia N, Fang F, Zhang P, Bothner B, Lee JH. A Knockin Reporter Allows Purification and Characterization of mDA Neurons from from Heterogeneous Populations. Cell Reports 2017; 18: 2533–2546.

Xu H, Wang B, Ono M, Kagita A, Fujii K, Sasakawa N, et al. Targeted Disruption of HLA Genes via CRISPR-Cas9 Generates iPSCs with Enhanced Immune Compatibility. Cell Stem Cell 2019; 24: 566-578.

Yagyu S, Hoyos V, Del Bufalo F, Brenner MK. An Inducible Caspase-9 Suicide Gene to Improve the Safety of Therapy Using Human Induced Pluripotent Stem Cells. Mol Ther 2015; 23: 1475–1485.

Zhang D, Yang S, Toledo EM, Gyllborg D, Saltó C, Villaescusa JC, et al. Niche-derived laminin-511 promotes midbrain dopaminergic neuron survival and differentiation through YAP. Sci Signal 2017; 10(493): 4165.

Appendix 1. Specification of murine ground state pluripotent stem cells to regional neuronal populations

SCIENTIFIC REPORTS

OPEN

Specification of murine ground state pluripotent stem cells to regional neuronal populations

Received: 21 June 2017
Accepted: 8 November 2017
Published online: 22 November 2017

Walaa F. Alsanie[1,4], Jonathan C. Niclis[1], Cameron P. Hunt[1,2], Isabelle R. De Luzy[1], Vanessa Penna[1], Christopher R. Bye[1], Colin W. Pouton[2], John Haynes[2], Jaber Firas[3], Lachlan H. Thompson[1] & Clare L. Parish[1]

Pluripotent stem cells (PSCs) are a valuable tool for interrogating development, disease modelling, drug discovery and transplantation. Despite the burgeoned capability to fate restrict human PSCs to specific neural lineages, comparative protocols for mouse PSCs have not similarly advanced. Mouse protocols fail to recapitulate neural development, consequently yielding highly heterogeneous populations, yet mouse PSCs remain a valuable scientific tool as differentiation is rapid, cost effective and an extensive repertoire of transgenic lines provides an invaluable resource for understanding biology. Here we developed protocols for neural fate restriction of mouse PSCs, using knowledge of embryonic development and recent progress with human equivalents. These methodologies rely upon naïve ground-state PSCs temporarily transitioning through LIF-responsive stage prior to neural induction and rapid exposure to regional morphogens. Neural subtypes generated included those of the dorsal forebrain, ventral forebrain, ventral midbrain and hindbrain. This rapid specification, without feeder layers or embryoid-body formation, resulted in high proportions of correctly specified progenitors and neurons with robust reproducibility. These generated neural progenitors/neurons will provide a valuable resource to further understand development, as well disorders affecting specific neuronal subpopulations.

Murine pluripotent stem cells (mPSCs) are a powerful research tool to study development, establish *in vitro* disease models, and facilitate advances in transplantation and drug screens, targeted at neural repair. Since their initial isolation more than three decades ago[1], mouse embryonic stem cells (mESCs) have been widely used for these aforementioned purposes, however limitations associated with variability and heterogeneity of differentiation protocols have hampered progress.

A key limitation inherrant in early protocols is the reliance on co-culture with stromal cell lines to promote neural induction[2,3]. Although co-culture protocols demonstrate moderate neuralization, variable differentiation efficiencies are unavoidable due to batch-to-batch variation in feeder secreted factors including immunogenic proteins, growth factors and extracellular matrix ligands. While feeder-free neural differentiation alternatives have been developed, they rely on the spontaneous differentiation properties of mESCs in 3-dimensional embyoid bodies (EBs) or 2D cultures, which are inherently variable[4–6]. Specifically, spontaneous differentiation results in contamination with non-neuronal derivatives and/or generates highly heterogeneous cultures. Thus, new protocols to derive specific neural populations under defined culture conditions are warranted.

Studies of fetal CNS development have identified key morphogens involved in the formation of specific brain regions, such as the ventralizing factor sonic hedgehog (SHH) and caudalizing proteins fibroblast growth factor 8 (FGF8) and Wnt1[7]. Significant advancements in the differentiation of human PSCs into restricted neural lineages has come with the early administration of these factors concurrently during neuralization[8–11], resulting in highly homogenous neural populations that accurately reflect not only CNS regions but also lineage subtypes.

A final consideration is the pluripotent state of the cells at the commencement of differentiation. Two states of mESCs have been described– (i) Serum and LIF (S/L)-dependent ESCs which reflect a more unstable pluripotent

[1]The Florey Institute of Neuroscience and Mental Health, The University of Melbourne, Melbourne, Australia. [2]Monash Institute of Pharmaceutical Sciences, Monash University, Melbourne, Australia. [3]The Australian Regenerative Medicine Institute, Monash University, Melbourne, Australia. [4]Present address: The Department of Medical Laboratories, The Faculty of Applied Medical Sciences, Taif University, Taif, Saudi Arabia. Correspondence and requests for materials should be addressed to C.L.P. (email: clare.parish@florey.edu.au)

state of the pre-implantation blastocyst's inner cell mass (and most widely employed in ESC studies), and (ii) naïve mESCs, also refered to as 'ground-state' stem cells, that represent a stable pre-implantation stage[12]. Naïve state cells are obtained by culturing mESCs in a defined medium (2i) that contains MEK and GSK3ß inhibitors to maintain this ground state and block differentiation signals[13]. These naïve mESCs have numerous advantages over S/L-responsive mESC that are cultured in batch-variable serum-based medium, including greater morphological homogeneity, enriched expression of pluripotential transcription factors and reduced levels of lineage -specific transcripts[14–17]. In this regard, naïve mESC are likely to improve the efficiency and reproducibility of differentiation.

For the first time, we successfully induced neural differentiation of naïve mESCs and compared derivatives to S/L-dependent mESC counterparts. Subsequently, we utilized naïve pluripotent stem cells (PSCs), and advances in hPSC differentiation techniques, to establish methods to derive four region-specific (dorsal forebrain, ventral forebrain, ventral midbrain and hindbrain) neural populations. Of these regions, the ventral forebrain was further divided into rostral and caudal subpopulation, inclusive of ganglionic eminence and hypothalamic-like progenitors, respectively. These (5) novel protocols importantly rely on the early patterning and specification of PSCs using targeted morphogens and small signaling molecules delivered within the first days of neural induction. Extensive cytochemical, cell sorting and transcriptional profiling of the cells confirmed regional specification of resultant progenitors and neurons.

Experimental Procedures

Maintenance of PSCs. The mouse ESC lines, E14TG2a (ATCC, USA), and our generated reporter lines (Lmx1a-eGFP and Pitx3-eGFP,[18,19], as well as the fibroblast-derived induced pluripotent stem cells (IPSCs) line, M2RttA/OKSM, were maintained undifferentiated in either: (i) a basic leukemia inhibitory factor (LIF) medium including serum, or (ii) serum-free 2i medium. Basic LIF medium consisted of Knockout DMEM, 15% fetal bovine serum (FBS, Sigma-Aldrich), 1x penicillin/streptomycin (P/S), 1x glutamax, 1x non-essential amino acids (NEAA), 0.11 mM beta-mercaptoethanol and 2000 IU/ml LIF (Millipore). 2i medium consisted of DMEM/F12, 1x N2 supplement, 1x B27–vitamin A, 1x P/S, 1x glutamax, 1x NEAA, 0.11 mM beta-mercaptoethanol, 2000 IU/ml LIF, 1 uM MEK inhibitor PD0325901 (Stemgent) and 3 uM GSK3 inhibitor CHIR9902 (Stemgent). All PSC were maintained on gelatinized 35 mm dishes under feeder-free conditions. Cells were passaged every second day using accutase (STEMCELL Technologies), for ground state PSC, and 0.025% trypsin-EDTA for S/L-dependent PSC. All reagents were purchased from GIBCO unless stated otherwise.

PSC differentiation. Naïve PSCs or S/L-dependent PSCs (subsequently refered to as S/L PSCs) were seeded on 0.1% (v/v) gelatinized 48 well plates at a density of 5.0×10^3 cells per well and incubated overnight in LIF basic medium prior to differentiation. A combination of serum replacement medium (SRM) and N2 medium, supplemented with 200 nM LDN193189 (Tocris), were used for early patterning stage under gradient conditions, (day0: 100% SRM; day1: 75%SRM:25%N2; day2: 50%SRM:50%N2; day3: 25%SRM:75%N2). SRM consisted of Knockout DMEM, 1x P/S, 1x glutamax, 1x NEAA, 0.11 mM beta-mercaptoethanol and 15% knockout serum. N2 medium components included DMEM/F12, 1x P/S, 1x glutamax, 1x NEAA, 0.11 mM beta-mercaptoethanol, 1x ITS-A supplement and 1x N2 supplement. This SRM/N2 gradient media was subsequently refered to as 'Patterning media'. For medial ganglionic eminence differentiation, cells were additionally cultured in a 'ventralizing media' from day 6–10, consisting of DMEM/F12, 1x P/S, 1x glutamax, 1x NEAA, 0.11 mM beta-mercaptoethanol, 1x ITS-A, 1x N2 supplement and 1x B27+ vitaminA supplement. Finally, N2B27 medium was utilized for the maturation stage. 'Maturation medium' consisted of 1:1 mixture of DMEM/F12 and Neurobasal medium, 1x P/S, 1x glutamax, 1x NEAA, 0.11 mM beta-mercaptoethanol, 1x ITS-A, 1x N2 supplement and 1x B27+ vitamin A supplement.

Dorsal forebrain differentiation protocol. For the duration of early patterning (day 0–7), culture media was supplemented with LDN193189 (200 nM, Tocris), with FGF2 (20 ng/ml, Peprotech) added to the media from day 2. Note media was changed daily from day 0–7. Cells were switched to 'maturation medium' consisting of: N2B27 supplemented with glial cell-derived neurotrophic factor (GDNF, 30 ng/ml, R&D), brain-derived neurotrophic factor (BDNF, 30 ng/ml, R&D), ascorbic acid (AA, 0.2 mM, Sigma-Aldrich) and the γ-secretase/Notch inhibitor DAPT (10 uM, Tocris) from day 7–14, with media replaced every 2 days, Fig. 3A.

Ventral mesodiencephalic differentiation protocol. Ventralization from the default dorsal forebrain phenotype was achieved by modulation of the Shh signaling pathway using Shh recombinant protein (C24II, 200 ng/ml) from day 1–7 of PSC patterning[20]. This supplementation of the media was employed firstly to demonstrate broad neural ventralization of the PSC (resulting in a 'ventral mesodiencephalic' population), and was compared to dorsal forbrain and hindbrain regions. Refinement of this 'ventral mesodiencephalic' protocol, through the timely delivery of factors to modulate ventralisation (Shh and Wnt) and caudalization (Wnt and FGF8), resulted in more restricted VF fates including rostral VF populations reflective of the ganglionic eminences, a more caudal VF populations inclusive of 'hypothalamic -like' neurons and finally a ventral midbrain population. These refined VF and VM protocols are detailed below.

Caudal ventral forebrain differentiation protocol. For caudal ventral forebrain (cVF) specification, inclusive of hypothalamic-like neural progenitors/neurons, the patterning medium was supplemented with LDN193189 (200 nM, Tocris), SHH (24CII) (200 ng/ml, R&D) and the smoothened receptor agonist purmorphamine (2 uM,

PM) (Stemgent) from day 1–7. From day 3–7, FGF2 (20 ng/ml) was added to the media. On day 7–14, cells were transitioned to maturation medium, Fig. 4A.

Rostral Ventral forebrain differentiation protocol. For rostral ventral forebrain (rVF) specification, including ganglionic eminence-like progenitors/neurons, patterning medium was supplemented with LDN193189 (200 nM), and early ventralisation controlled using the Wnt signaling antagonist XAV939 (2 uM, Tocris) from day 0–5. At day 6, medium was supplemented with Shh (200 ng/ml), and PM (2 uM), and changed at day 7 and 9. The medium was switched to maturation medium from day 10–14, with media changes every 2 days, Fig. 5A.

Ventral midbrain differentiation protocol. For ventral midbrain specification, SHH (200 ng/ml), PM (2 uM) and FGF8 (25 ng/ml) were added to the patterning media from day 1–7, and further supplemented with CHIR9902 (0.3 uM) from day 2–7, as well as FGF2 (20 ng/ml) on day 3–7. From day 7–14 cells were cultured in maturation medium, Fig. 6A.

Hindbrain differentiation protocol. For hindbrain specification, S/L-dependent mouse PSC were cultured in patterning media supplemented with SHH (200 ng/ml) from day 0, with PM (2 uM) and FGF8 (25 ng/ml) added from day 1. On day 2, CHIR99021 (1.5 uM) was added to the media as well as FGF2 (20 ng/ml) at day 3. Media was changed daily from day 0–5. On day 7, differentiated cells were changed into maturation medium, with medium changes every second day until day 14, Fig. 7A.

Immunocytochemistry and Quantification. Day 0 (undifferentiated PSCs) and day 7, 11 or 14 differentiated cells were fixed and immunostained, using previously described methods[21]. See Supplementary table 1 for primary antibodies. Secondary antibodies, generated in donkey and conjugated to Alexa Flour 488, 555 and 649 were used at 1:200 (Jackson Immunoresearch). 4′,6-diamidino-2-phenylindole (DAPI, SigmaAldrich) nuclear counterstain (1:2000) was used to visualize cells in culture. All the images were captured using a fluorescence microscope (Zeiss Axio Observer Z1).

Quantification of TH+/FoxA2+ and TH+/Pitx3+ (GFP) immunoreactive cells within caudal ventral forebrain and ventral midbrain cultures at day14, established from naïve mESC and iPSC, were performed to differentiate between the dopaminergic neurons generated within these two culture conditions. Using a 20x objective, ten fields of views from three technical, and performed on at least 3 biological replicates were counted. Quantification was performed using Zen Blue software (Zeiss).

Flow cytometry. Intracellular staining was performed using BD transcription factors staining kit (BD), according to the manufacturer instructions with modifications. In brief, cells (1×10^6/tube) were incubated with BD Horizon fixable viability dye450 (1:1000) diluted in PBS (4 °C, 25 min). Cells were rinsed in PBS, resuspended in fixation buffer (4 °C, 45 min), and washed with ice-cold permeabilization/washing buffer. Fixed cells were incubated with primary antibodies (see supplementary table 1), diluted in permeabilization/washing buffer, overnight at 4 °C. The following day, cells were washed in permeabilization/washing buffer and incubated in secondary antibody (anti mouse-APC,1:500, Santa Cruz), for 45 minutes. After 3x washes in permeabilization buffer, cells were resuspended in ice-cold 500ul running flow buffer consisting of 1% bovine serum albumin (BSA) (Sigma-Aldrich) and 0.5 mM EDTA (Sigma-Aldrich) diluted in PBS. Flow cytometry analysis was performed using Beckman-Coulter CyAn analyzer (Beckman-Coulter), Summit 4.3 software (Beckman-Coulter) and Flowlogic software (Inivai technologies). Single cells were gated based on forward-side scatter profiles and dead cells excluded using violet Horizon viability dye (data not shown). Undifferentiated ESCs were used as a negative control to set gates.

Quantitative real-time PCR. Total RNA was extracted at day 0, 7 and 14 using Trizol (Ambion). RNA was converted to cDNA and subsequently analyzed using quantitative real-time PCR (qPCR), using previously described methods[22], to show the expression of 7 pluripotency-related genes (*Nanog*, *Sox2*, *Oct4*, *Rex1*, *Bmp7*, *Wnt7a* and *Id1*) as well as the temporal expression of numerous regionally specified neural-related genes (*Pax6*, *Emx2*, *Nkx2.1*, *Gsx2*, *Otp*, *Nhlh2*, *TH*, *En1*, *Nurr1*, *Lmx1a*, *Zic1* and *Hoxa1*). More detailed analysis, to further confirm GE differentiaton, was performed at days 0, 10 and 14, and included the following genes: *Nkx2.1*, *Gsx2*, *Lhx2*, *Olig2*, *Dlx2* and *Gad67*. See Supplementary Table 2 for primer sequences.

Student t-tests and One-way *ANOVA*s were performed where appropriate to identify differences within the data, with significance set at $p < 0.05$.

Results

Improved neural differentiation from naïve mESCs. S/L-dependent mESCs (cultured in serum and LIF medium[1]) and naïve mESCs (cultured in 2i medium[13]), were first examined by immunocytochemistry to confirm robust expression of cardinal pluripotent transcription factors, Oct4 and Sox2 (Fig. 1A,B). Consistent with this observation, quantitative PCR revealed similar high levels of expression for the pluripotency genes *Oct4*, *Sox2*, *Nanog* and *Rex1* in both S/L-dependent and naïve mESC cultures (Fig. 1C). Further, flow cytometry quantification could not statistically distinguish the two mESC populations, with ≥98% of cells immunoreactive for Oct4 (Fig. 1G,G'). While naïve ground state and S/L-dependent PSC displayed similarities in their expression of pluripotent genes, recent studies have recognized transcriptional differences between these two pluripotent staged cell populations[15]. In concerrence, we show significantly elevated expression of *Wnt7a* and *Id1*, as well as a down regulation of Bmp7, in our S/L-dependent mESCs compared to naïve mESCs, Fig. 1D.

S/L-dependent and naïve mESCs were directed towards a neural fate by antagonism of Smad signaling, similar to that widely employed for monolayer-based differentiation cultures of human PSC, Figure 1E,E'[23]. This

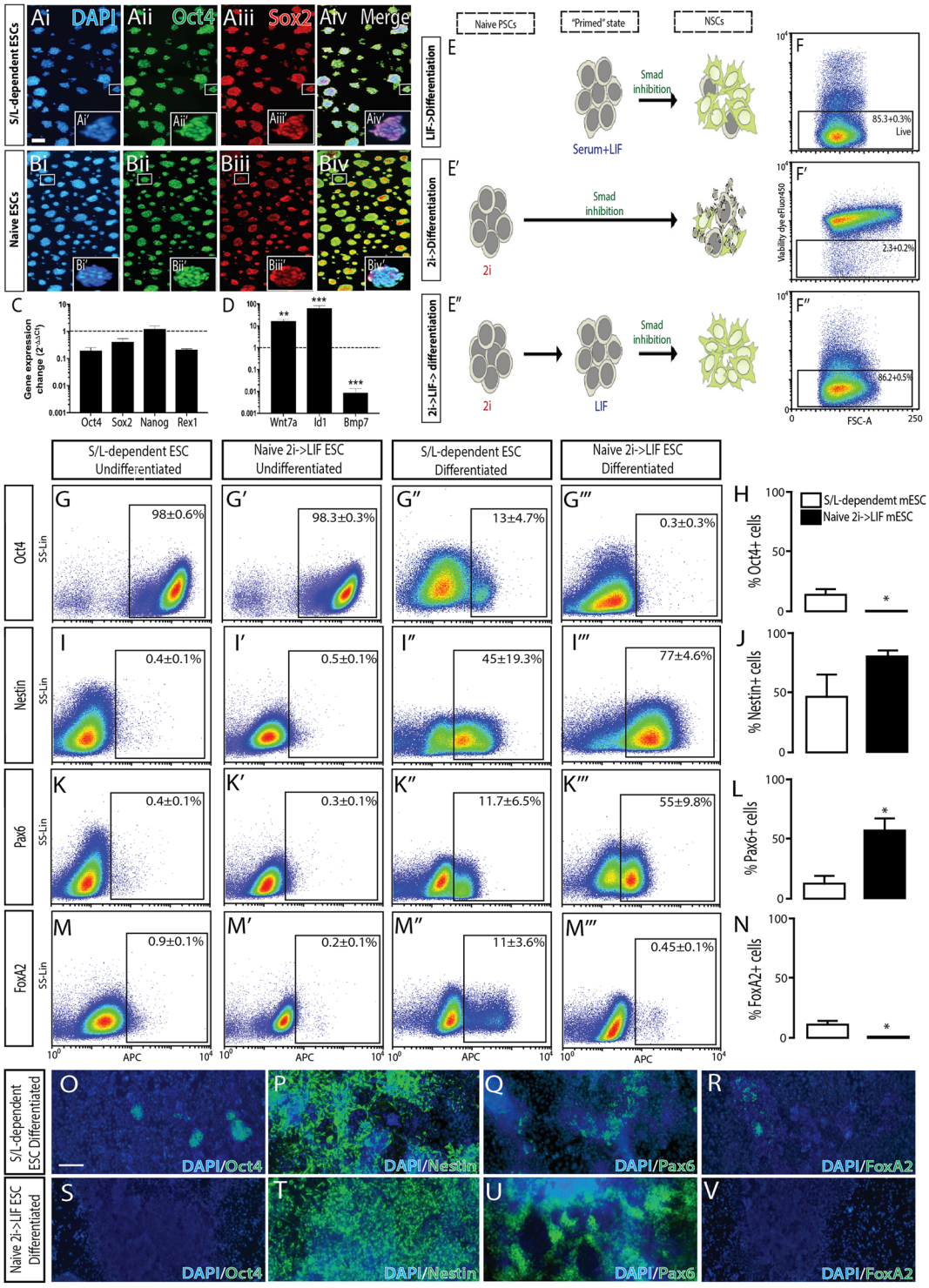

Figure 1. Ground state naïve mESC, compared to serum/LIF-dependent mESC, improve neural specification. S/L-dependent and naïve mESC, labeled with (Ai,Bi) DAPI, show indistinguishable and high expression of pluripotency transcription factors (Aii,Bii) Oct4 and, (Aiii,Biii) Sox2 prior to differentiation. (Aiv,Biv) Merge images. (**C**) Transcriptional profiling confirmed expression of pluripotency genes in undifferentiated naïve and S/L-dependent mESCs. Data represents change in gene expression levels in S/L-dependent mESC (bars), compared to naïve cultures (normalized to 1, dotted line). (**D**) Reflective of differences in pluripotency states, S/L-dependent mESCs showed elevated *Wnt7a* and *Id1*, as well as downregulation of *Bmp7* expression, compared to naïve mESC. (**E**) Schematic depicting the effect of LIF and/or 2i initiated neural differentiation from S/L-dependent verses naïve mESC. (E") Transient exposure of naïve PSC to LIF resulted in improved neural specification, and elimination of PSC upon differentiation. (**F**) Flow cytometry plots show high viability of differentiated S/L-dependent mESC at day7, (Fi) yet poor survival of naïve mESC differentiation from 2i media, (Eii) an effect that could be circumvented by transient culturing in LIF media. Flow cytometry plots for

(**G**) Oct4, (**I**) Nestin, (**K**) Pax6 and (**M**) FoxA2 in undifferentiated and day 7 differentiated cultures. Comparative quantitative analysis of FACS plots for S/L-dependent mESC and naïve mESCs at day7 after differentiation for (H) Oct4, (**J**) Nestin, (**L**) Pax6 and (**N**) FoxA2. Upon differentiation, naïve ESC cultures showed reduced proportions of contaminating Oct4+ PSC, elevated neuralization (Nestin+) and appropriate default dorsal forebrain specification, as indicated by reduced FoxA2+ and elevated Pax6+ cells in culture. Representative images of (**O**,**S**) Oct4, (**P**,**T**) Nestin, (**Q**,**U**) Pax6 and (**R**,**V**) FoxA2 immunostaining from primed and naïve mESCs differentiated under neural conditions for 7days. Note the absence of both Oct4+ PSCs and FoxA2 off-target ventral neural progenitors, as well as expansive Nestin+ and Pax6+ NPC in cultures derived from naïve mESC, compared to S/L-dependent mESC. Data (n = 4) represents mean ± SEM, Students t-test. Scale bars: A-B = 100 um, O-V = 50um. *$p < 0.05$, **$p < 0.01$, ***$p < 0.001$. mESC: mouse embryonic stem cell; NPC: Neural pluripotent stem cells; PSC: pluripotent stem cells; S/L: Serum and LIF.

minimalist default differentiation system produced a heterogeneous population of cell types from S/L-dependent mESCs following 7 days of differentiation, including Nestin immunoreactive cells indicative of NPCs (45 ± 19.3%, Fig. 1I",J,P), some of which possessed a dorsal forebrain identity as shown by expression of the dorsal marker Pax6 (11.7 ± 6.5%, Fig. 1K",L,Q), or a ventral identity determined by expression of the floor-plate marker FoxA2 (11 ± 3.6%, Fig. 1M",N,R).

Differentiation of naïve mESCs under the same conditions was significantly compromised by excessive cell death and limited NPC fate acquisition (Fig. 1E',F'). We speculated these complications arose from directing naïve pluripotent cells into a neural fate immediately. To circumvent this, 2i cultured naïve mESCs were subjected to a 24-hour incubation in LIF-primed media prior to Smad inhibitor exposure (Fig. 1E") to mimic the graduated transition that occurs during embryonic development from the pre-implantation (naïve pluripotency) to post-implantation stage, and then to germ layer restriction.

Indeed, differentiated naïve mESCs that incorporated a LIF-primed transition showed high viability (>86%, Fig. 1F"), efficiently neuralized (77 ± 4.6% Nestin expression, Fig. 1I",J) and generated a homogenous population of NPCs (Fig. 1T). Although the increase in Nestin expression in naïve-LIF-differentiated cultures was not significant compared to differentiation of S/L-dependent cultures (Fig. 1J), patterning from a naïve state was drastically less variable (Fig. 1P,T), and contained extremely few OCT4-positive cells (0.3 ± 0.3% vs 13 ± 4.7% Oct4+, Fig. 1G",G",H,O,S). Furthermore, naïve-LIF-differentiated cultures acquired a more reproducible and restricted phenotype, with Pax6 expressed in 55 ± 9.8% of day 7 cultures (Fig. 1K",L,U), and the absence of off-target floor-plate progenitors marked by FoxA2 (Fig. 1M",N,V). These results demonstrate for the first time a feeder-free monolayer directed differentiation platform for the robust production of NPCs from naïve mESCs.

It is important to note that neuralization via Smad inhibition was achieved by blocking only one of two major Smad families. Specifically, the BMP inhibitor LDN193189 was used to block Smads 1/5/8 while the TGF-β pathway, that regulates Smad 2/3 signaling and is typically co-inhibited in human neural differentiations, was not modulated. This was due to our observation that Smad 2/3 inhibition (using SB431542) prevented naïve mESC exiting from their pluripotent state, with cells showing maintained Oct4 expression (data not shown) – a finding that supports previous studies describing the necessity for Smad 2/3 suppression in the maintenance of ground state identity[24].

Bi-directional regional neural specification. In light of the improved reproducibility and homogenicity of neural induction from naïve, compared to S/L-dependent, mESC cutlures we next assessed the capacity for ground state cells to be redirected along developmental dorso-ventral and rostro-caudal axes using a range of small molecules and morphogens to mimic *in vivo* embryonic signals and obtain dorsal forebrain, ventral mesodiencephalic and hindbrain cultures (Fig. 2). Naïve mESCs differentiated in basal Smad inhibition conditions (LDN193189 from day 0–7) resulted in the 'default' acquisition a dorsal forebrain identity with progenitors expressing the forebrain-midbrain marker Otx2, dorsal transcription factor Pax6, as well as absence of the ventral marker, FoxA2, and hindbrain marker, Zic1 (Fig. 2D–K). Ventralization from this dorsal phenotype was achieved with the addition of Shh (day 1–7), causing a predicted loss of Pax6 expression, upregulation of FoxA2, and maintenance of Otx2 identity (Fig. 2L–O). In the absence of caudalising cues, the resultant population was a heterogeneous pool of both ventral diencephalic and ventral mesencephalic progenitors, here termed 'ventral mesodiencephalic', Fig. 2L–O.

The addition of high concentrations of the GSK3ß inhibitor and potent caudalizing small molecule CHIR9902 (day 2–7), as well as FGF8, was sufficient to push culture identity beyond the isthmic organizer, resulting in the generation of hindbrain NPCs, as determined by upregulation of Zic1 and surpression of Otx2 expression (Fig. 2P–S). Each of these regionally patterned populations (dorsal, ventral and caudalized) were further modulated, matured and characterized in subsequent Figs (3–8).

Naïve PSC differentiated to dorsal forebrain neurons. Confirming the dorsal forebrain progenitor identity seen by immunocytochemistry (Otx2+, Pax6+, Nestin+, Figs 2H–I and 3C,D), we observed elevated transcript levels of *Pax6* and the cortical lineage marker *Emx2*[25], by day 7 (Fig. 3B). These progenitors were driven to a post-mitotic fate by the removal of NPC morphogens and growth factors (LDN193189 and FGF2), in conjunction with the addition of the Notch pathway small molecule inhibitor DAPT[26], and pro-neuronal survival trophins including BDNF, GDNF and Ascorbic Acid (Fig. 3A). Following 4 days of maturation (day 11), the emergence of the neuronal cytoskeletal protein TUJ1, with the intermediate cortical progenitor marker Tbr2, were seen (Fig. 3E). These results mirror cortical developmental where transient Tbr2 expression follows Pax6 expression before radial glial cells commit to specific laminar layers[27]. With extended culturing in maturation

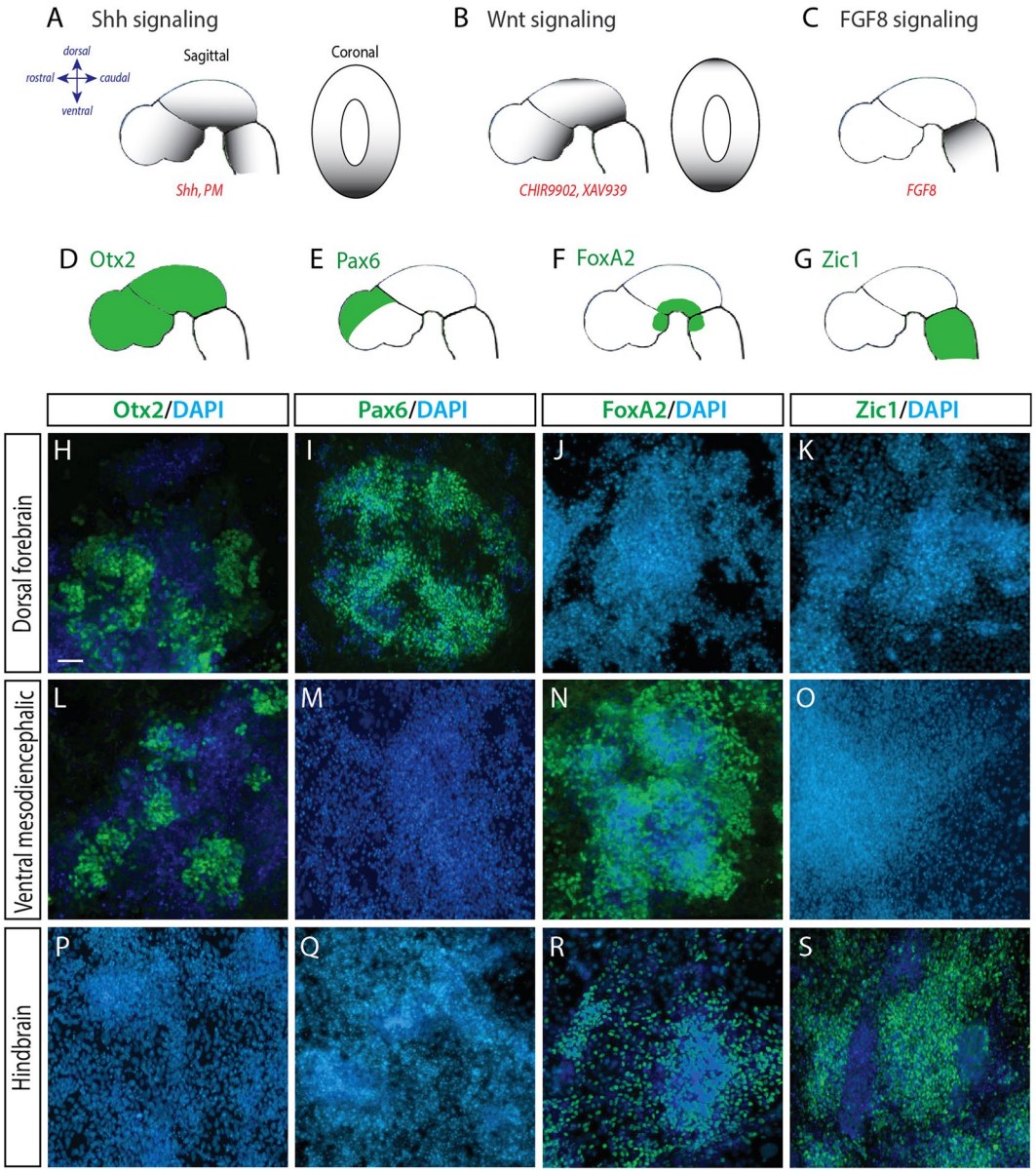

Figure 2. Modulation of bi-directional morphogen gradients generates regionally specified neural progenitors. Developing embryo schematics illustrating morphogen gradients (grey shading) and the utilized protein/small moleulces (red) employed to modulate (**A**) Shh, (**B**) Wnts and (**C**) FGF8. Schematic illustrations of the embryo (sagittal plane) depicting expression of key transcription factors (**D**) Otx2, (**E**) Pax6, (**F**) FoxA2 and (**G**) Zic1, used to identify rostral forebrain-midbrain, dorsal forebrain, ventral, and caudal hindbrain progenitors, respectively. (**H**–**K**) Representative photomicrographs of naïve mESC differentiated under default neural conditions to generate dorsal forebrain progenitors, expressing Otx2 and Pax6, but lacking FoxA2 and Zic1 expression. (**L**–**O**) Naïve mESC differentiated towards ventralised mesodiencephalic and (**P**–**S**) hindbrain progenitor fates, showing appropriate Otx2, Pax6, FoxA2 and Zic1 expression indicative of regional specification. Scale bar = 50 um.

conditions, increased numbers of Tuj1+ post-mitotic neurons were observed and co-expressed the mature cortical laminar layer markers Tbr1 (Fig. 3F) and Ctip2 (Fig. 3G). Importantly, we were able to demonstrate the ability to robustly reproduce these findings, also differentiating naïve ground state iPSCs to a dorsal forebrain fate (Supplementary Figure 1).

Naïve PSC differentiated to ventral forebrain neurons. While modulation of the Shh signaling was shown to impact default dorsal forebrain identity of PSC, resulting in acquisition of ventral neural tube fate (Fig. 2), minimal assessment of the directed differentiation and resultant progenitors/neurons was performed. Here we importantly demonstrate that ventralized cultures maintained the robust downregulation of Oct4 and upregulation of the NPC identity marker Nestin (Fig. 4B,C,F). As anticipated, ventral signals induced the loss

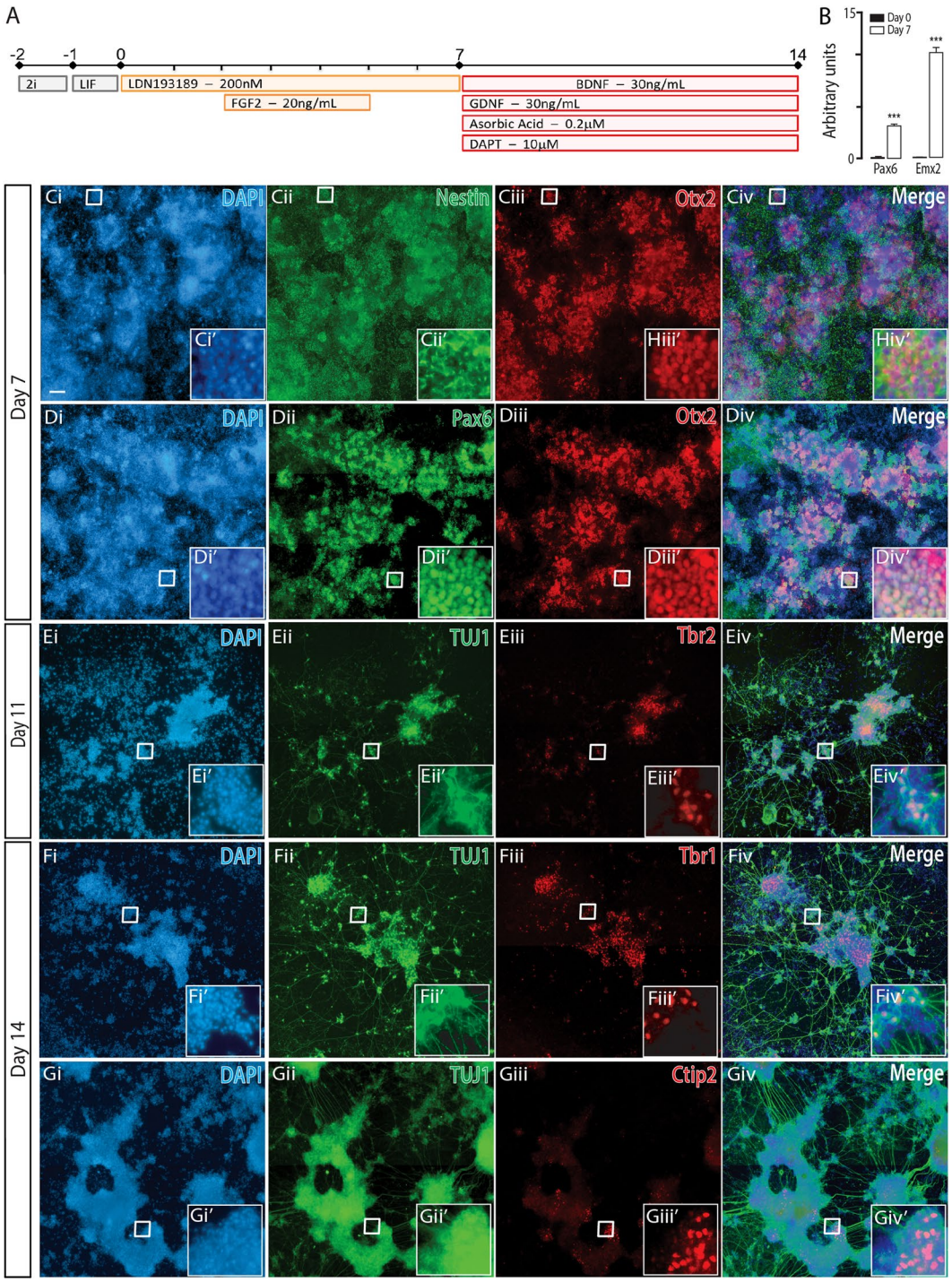

Figure 3. Naïve mESC, differentiated to a dorsal forebrain fate, show appropriate regional and temporal specification (**A**) Neural differentiation protocol detailing morphogens and small molecules employed to generate dorsal forebrain progenitors and neurons from naïve PSCs. (**B**) Quantification of transcriptional expression of dorsal forebrain indicative genes *Pax6* and *Emx2* in undifferentiated (day 0, black bar) and day 7 differentiated cultures (white bar). (**C**,**D**) Representative micrographs depicting expression of Nestin, Otx2 and Pax6 in dorsal forebrain progenitors at day7. (**E**) Maturing dorsal forebrain neurons, expressing Tuj1, show transient Tbr2 expression at day 11, and mature dorsal forebrain markers inclusive of (**F**) Tbr1 and (**G**) Ctip2 by day 14. Images show culture overviews, while inserts show immunocytochemical labeling at the resolution of individual cells. Data (n = 4) represented as mean ± SEM, Students t-test. Scale bar = 100 um. ***$p < 0.001$.

of dorsal (Pax6) identity (Fig. 4D,F,G) and significant upregulation of the ventral neural tube marker FoxA2 (67.3 ± 2.2%, Fig. 4E,F). The ventral forebrain is the site of hypothalamus formation, and indeed hypothalamic transcripts *Nhlh2* and *Otp* were significantly up-regulated under these conditions[28,29], suggesting the adoption of

a diencephalic fate (Fig. 4G). By maturating ventral forebrain NPCs, TUJ1 post-mitotic neurons arose throughout cultures with significant GABA expression (Fig. 4I), further supporting hypothalamic-like identity. While numerous FoxA2 and TH + cells were observed by day 14, these populations showed minimal overlap, reflective of VF hypothalamic dopaminergic neurons (as opposed to FoxA2 + /TH + dopamine neurons that reside in the adjacent VM) (Fig. 4J and Supplementary Figure 2),[30].

Interestingly, these ventral forebrain cultures did not express transcription factors Nkx2.1 or Olig2 (data not shown), *in vivo* markers of the adjacent developing ganglionic eminence, GE. Early developmental studies have demonstrated that inhibition of Wnt/beta-catenin signaling is important for the up-regulation of key GE transcription factors such as *Dlx2*, *Mash1* and *Gsx2*, and suppression of pallial markers such as *Emx2*[31]. Thus, we theorized the addition of a Wnt inhibiting small molecule (XAV939) may induce the generation of GE identity. Indeed, in response to XAV, efficient Nestin+ and Otx2+ forebrain NPCs were observed (Supplementary Figure 3) in conjunction with broad expression of Nkx2.1 and Olig2 (Fig. 5B, Supplementary Figure 4), suggestive of a GE phenotype.

Continued maturation promoted widespread co-expression of TUJ1 and GABA (Fig. 5C,D and Supplementary Figure 4) that may represent lateral ganglionic eminence (LGE)-derived striatal neurons or MGE-derived interneurons. This former population can be identified by the co-expression of DARPP32+/CTIP2+ (that were not present within these cultures, Fig. 5L), and the latter, MGE neurons, confirmed by co-expression of GABA+/NKX2.1+ and NKX2.1+/OLIG2+ (Fig. 5D–E, Supplementary Figure 4). Validating these findings, transcript assessment showed significant upregulationof a raft of MGE-related NPC genes including *Nkx2.1*, *Gsx2*, *Lhx6*, *Olig2* and *Dlx2* (Fig. 5F–J), (Corbin *et al*., 2000) and upregulation with maturation of Gad67, an enzyme important in GABA synthesis for GE neurons (Fig. 5K). Of interest, in the development of this rVF protocol we have observed that earlier ventralisation of the cultures (though the administration of Shh+ PM from day 3–7) resulted in cells co-expressing DARPP32+ CTIP2+ GAD67+ (Fig. 5M) and comparatively low Nkx2.1 transcript compared to the "GE/MGE-like" populations (Fig. 5F, grey line), suggestive of a possible "LGE-like" fate (Fig. 5M). Taken together, this data indicates GE-like NPCs and neurons from ground state mPSC.

Naïve PSC differentiated to ventral midbrain neurons. During embryonic development, the isthmic organizer, at the midbrain-hindbrain boundary, secretes FGF8 and Wnts to instruct the formation of the mesencephalon[32], Fig. 2B,C, including important populations of dopaminergic neurons. To generate ventral midbrain (VM) NPCs, our caudal ventral forebrain protocol was supplemented with FGF8 (25 ng/ml) and the Wnt agonist CHIR9902 (0.3 uM). This was seen to maintain cultures rich in NPC (81 ± 4.3% Nestin+, Fig. 6C), that expressed appropriately high levels of regional identity proteins FoxA2 (70 ± 3.5%, Fig. 6E,F,H) and the forebrain-midbrain marker Otx2 (Fig. 6H,I). Further, these cultures upregulated essential VM dopaminergic transcripts *Lmx1a*, *Nurr1* and *En1* (Fig 6G)[32]. To further confirm aVM identity of these NPCs we utilized a mESC reporter line for Lmx1a (Lmx1a-eGFP); a transcription factor expressed in the roof plate and throughout the developing floor plate. In combination with Otx2 and FoxA2, the mesendiencephalic floor plate can be distinguished from roof-plate NPCs and ventral hindbrain, and was seen in differentiating cultures derived from naïve mESCs (Fig. 6I).

Ongoing maturation of the cultures to day 14, resulted in the presence of many tyrosine hydroxylase (TH – the rate-limiting enzyme in dopamine synthesis) expressing neurons (Fig. 6J,K). To differentiate between dopaminergic neurons of the caudal ventral forebrain and the ventral midbrain, we quantified TH+/FoxA2+ neurons (a population restricted to VM dopaminergic neurons). Under VM differentiation conditions, the majority (>75%) of TH+ neurons co-expressed FoxA2 (Fig. 6J,L and Supplementary Figure 5). VM dopamine neurons were characterized further using both the Lmx1a-eGFP and Pitx3-eGFP knockin reporter line that mark *bona fide* VM DAs[33]. In terminally differentiated cultures neurons co-expressing TH, Lmx1a and FoxA2 were observed (Fig. 6J), with the majority of TH+ neurons (69 ± 10.4%) co-expressing Pitx3-GFP (Fig. 6K,M). By comparison, ventral forebrain differentiation of the Pitx3-eGFP mESC reporter line saw significantly less TH+/FoxA2+ (28 + 4%, Fig. 6L), and Pitx3-GFP+/TH+ co-expressing neurons (22 ± 6%, Fig. 6N), both likely off-target populations within the VF differentiations, yet overall importantly highlight the capacity to direct naïve mPSC into ventral diencephalic or mesencephalic dopaminergic populations.

Naïve PSC differentiated to ventral hindbrain neurons. Upon successful generation of VM progenitors and neurons, we finally questioned whether stronger activation of the canonical Wnt pathway would be sufficient to driving NPCs beyond the isthmus and adopt a more caudal, hindbrain phenotype. Indeed, 5-fold higher CHIR9902 concentrations (1.5 uM), in conjunction with Shh signaling, resulted in high yields of neural progenitors (79.3 + 6.8% Nestin+), that lacked rostral (Otx2, Fig. 7Iiii) and dorsal (Pax6, Fig. 7D,F) identity markers, and showed appropriate ventralization (54.7 + 11.5% FoxA2+, Fig. 7E,F,I) at day 7. More specifically, day 7 cultures showed upregulated transcript levels of two key hindbrain genes, *Hoxa1*, crucial for the early patterning of the rhombencephalon[34] and *Zic1*, a key regulator of progenitor proliferation during early cerebellar development[35], Fig. 7G,H. Following maturation, immunocytochemical analysis at day 14 revealed the presence of numerous 5-HT+ serotonergic neurons, a population enriched throughout the hindbrain[36], (Fig. 7J, Supplementary Figure 6) as well as hindbrain Islet1+ motor neurons (Fig. 7K, Supplementary Figure 6),[37]. Taken together, these observation strongly indiciate ventral hindbrain NPC generation from naïve PSC under these ventro-caudalizing conditions.

In support of the capacity for these 5 described protocols to generate neural progenitors and neurons with relatively restricted regional identity, we compared transcript levels for genes known to be expressed within these areas in embryonic development, and their absence (or appropriately comparative levels) from other fate specified populations. Given the 'default' generation of dorsal forebrain progenitors/neurons upon Smad-induced neuralisation of PSC, gene expression within ventral and caudalised populations was compared to this DF population.

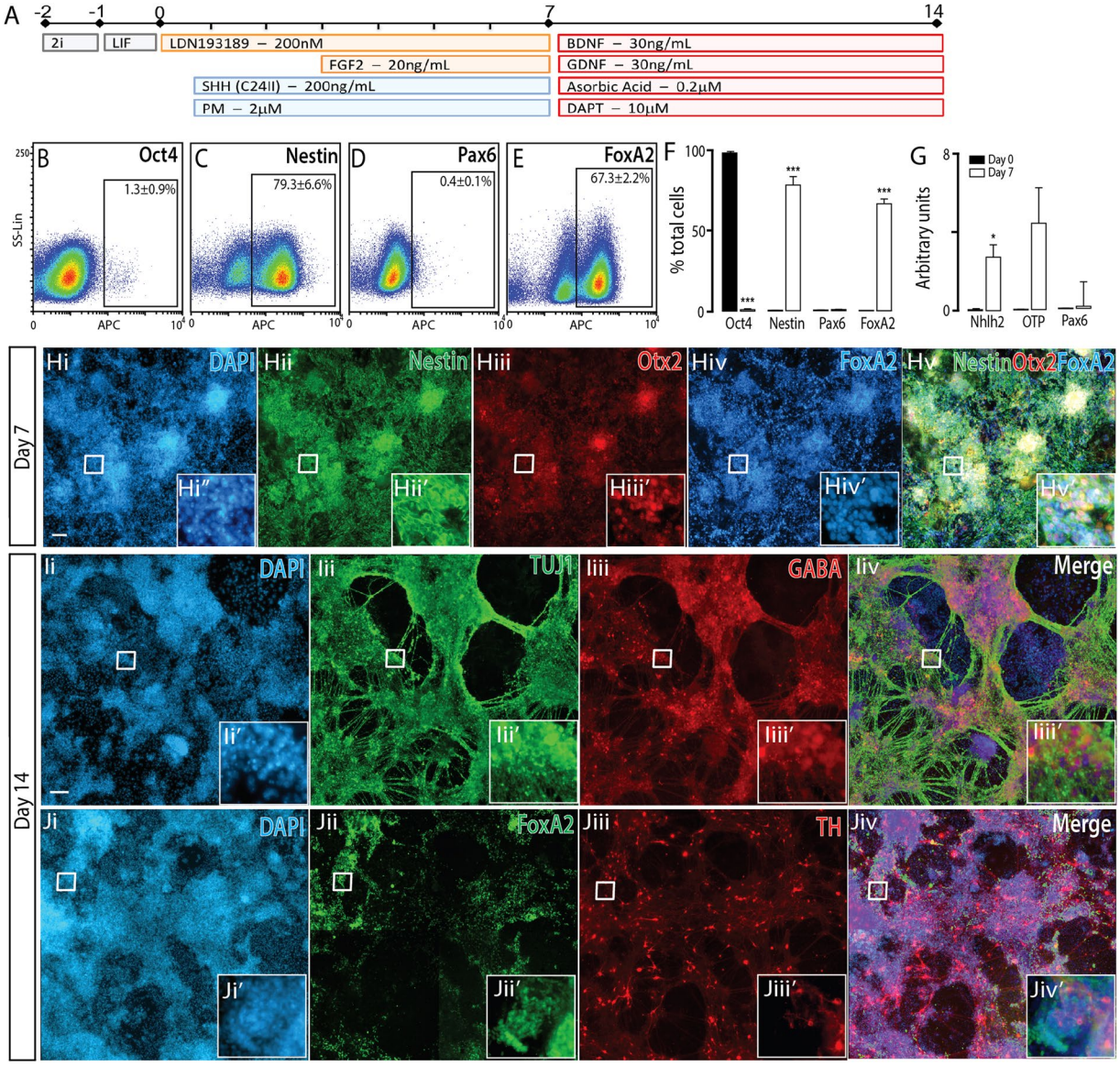

Figure 4. Naïve mESCs differentiated to a caudal ventral forebrain fate, show appropriate regional and temporal specification. (**A**) Neural differentiation protocol, detailing morphogen and small molecules employed, to generate ventral forebrain progenitors and neurons from naïve PSC. (**B**–**E**) Flow cytometry plots at day 7 and, (**F**) quantitative analysis at 0 and 7 for Oct4, Nestin, Pax6 and FoxA2, showing appropriate downregulaton of pluripotent (Oct4) and dorsal (Pax6) markers together with upregulation of neural (Nestin) and ventral (FoxA2) protein expression. (**G**) Transcriptional downregulation of *Pax6* together with the upregulation of *Nhlh2* and *OTP* suggested these cultures included neural progenitors of a ventral hypothalamic fate. (**H**) Representative photomicrographs depicting expression of Nestin, Otx2 and FoxA2 in ventral forebrain progenitors at day7. (**I**) Maturation of cultures resulted in the generation of GABA+ TUJ+ neurons, as well as FoxA2+ and TH+ neurons (showing low co-localisation), suggestive of hypothalamic neurons. Data (n = 3) represents mean ± SEM, Students t-test. Scale bar = 100 um. *$p < 0.05$, ***$p < 0.001$.

As such, we demonstrated the dorsal forebrain gene, *Pax6*, was significantly downregulated in all 4 other neural populations (Fig. 8A). Ganglinic eminence genes, *Nkx2.1* and *Gsx2*, were strongly expressed only in rostral ventral forebrain cultures (Fig. 8B,C). Within caudal ventral forebrain, inclusive of hypothalamic progenitors, *Nhlh2* was notably increased, and significantly elevated compared to more caudal VM and HB populations (Fig. 8D). *Nhlh2* however was also shown to be upregulated within the adjacent rostral VF (GE-like) cells, expression that may be explained by its known identity within subependymal neural progenitors. Reflective of *in vivo* neural development and the localization of dopaminergic subpopulations, *Lmx1a* and *TH* gene expression were elevated in caudal ventral forebrain (cVF) and VM progenitors and lowly expressed in more rostral (DF, cVF) and caudal (hindbrain) cultures (Fig. 8E,F). Finally, the rhombencephalic related genes *Hoxa1* and *Zic1* were only upregulated in HB cultures (Fig. 8G,H).

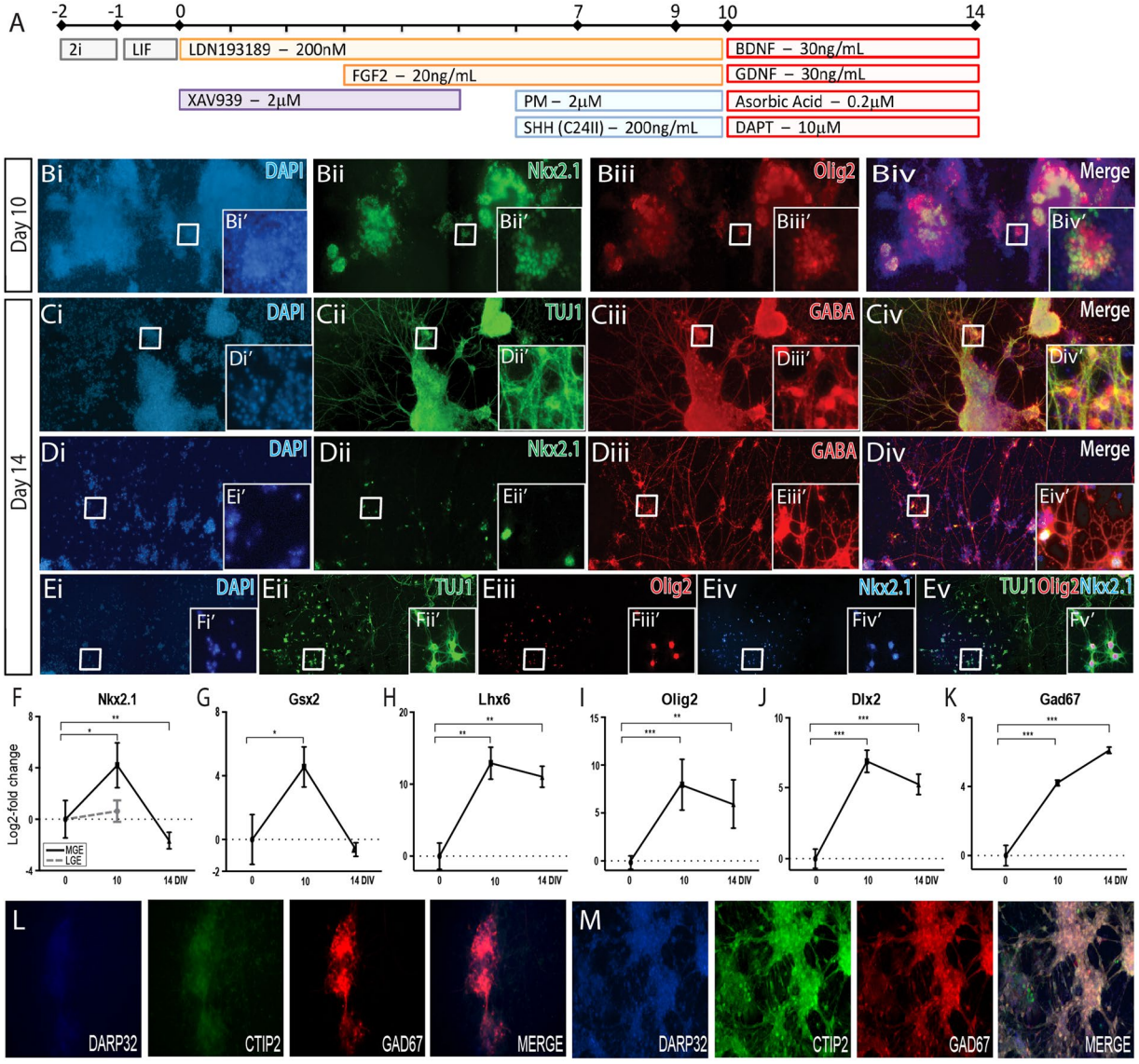

Figure 5. Naïve mESCs differentiate to rostral ventral forebrain/GE progenitors and mature GABAergic neurons. (**A**) Schematic of the neural differentiation protocol, detailing morphogen and small molecules employed, to generate medial ganglionic eminence progenitors and neurons from naïve PSCs. (**B**) Immunocytochemistry images highlighting the expression of key GE transcription factors Nkx2.1 and Olig2 within young post-mitotic cell at day 10 of differentiation. (**C**) mESCs differentiated to GE-specific neurons widely expressed TUJ1 and GABA, (**D**) with many GABA + neurons co-expressing Nkx2.1, indicative of MGE interneurons. (**E**) Numerous post-mitotic TUJ1+ neurons co-expressed the MGE markers Nkx2.1 and Olig2 by day 14. Note images (**B**–**E**) show cultures overviews, illustrating the largely homogeneous nature of the differentiations, while inserts (Bi'-Ev') show immunocytochemical labeling at the resolution of individual cells. Numerous GE-related genes showed appropriate temporal expression, including the transient upregulation of (**F**) *Nkx2.1* and (**G**) *Gsx2* as well as maintained, elevated expression of (**H**) *Lhx6*, (**I**) *Olig2* and (**J**) *Dlx2*. (**K**) *Gad67* was significantly upregulated by GE-like progenitors at day 10, with expression peaking at day 14 in mature neurons. Dashed grey line in (**F**) represents Nkx2.1 expression in "LGE-like" cultures, induced by earlier ventralization. (**L**) Reflective of an 'MGE-like' fate, rostral VF cultures appropriately expressed GAD67, but not CTIP2 or DARPP32. (**L**) In contrast, earlier ventralization of these VF progenitors resulted in cultures showing high expression of DARPP32, CTIP2 and GAD67, suggestive of a possible 'LGE-like fate. Scale bar = 100 um. Data (n = 3) represented as mean ± SD. One-way *ANOVA* with Tukey post-hoc test. *$p < 0.05$, **$p < 0.01$, ***$p < 0.001$. MGE: medial ganglionic eminience; LGE: laternal ganglionic eminence.

Significance Statement. Mouse pluripotent stem cells (PSC) provide a valuable tools in research as differentiation is rapid, cost effective and an extensive repertoire of transgenic lines contribute in our understanding of biology. However, protocols for directed differentiation of these cells has been inferior to their human counterparts. Here we demonstrate enhanced efficiency of neural differentiation by commencement from a naiive pluripotent ground-state, compared to a conventionally employed serum-dependent PSCs. Subsequently we

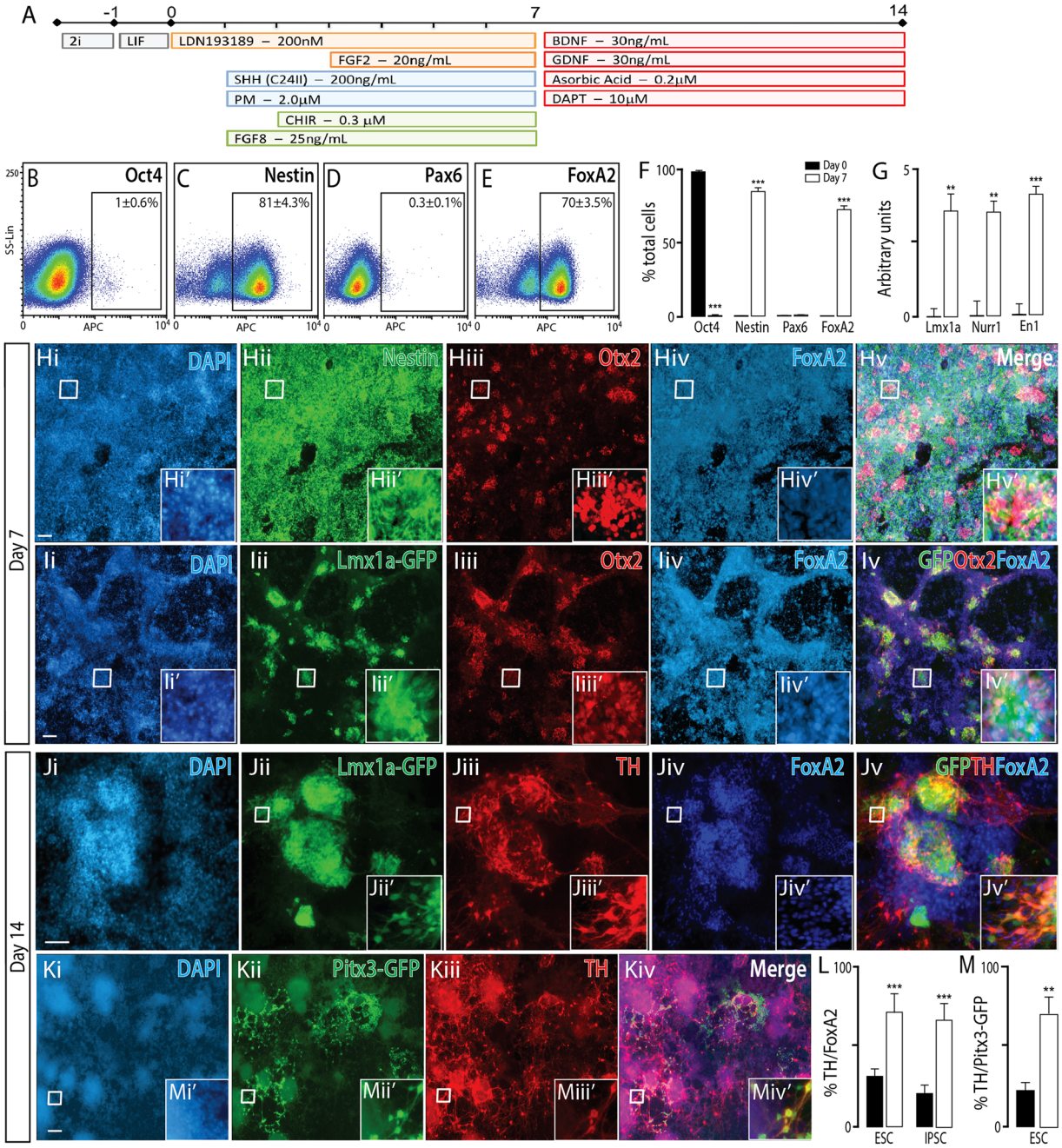

Figure 6. Naïve mESC differentiated to a ventral midbrain fate, show appropriate regional and temporal specification. (**A**) Schematic of the neural differentiation protocol, detailing morphogen and small molecules employed, to generate ventral midbrain progenitors and neurons from naïve PSC. (**B**–**E**) Flow cytometry plots at day 7 and, (**F**) quantitative analysis at day 0 and 7 for Oct4, Nestin, Pax6 and FoxA2, showing appropriate downregulaton of pluripotent (Oct4) and dorsal (Pax6) markers together with upregulation of neural (Nestin) and ventral (FoxA2) expression. (**G**) Transcriptional expression of ventral midbrain genes *Lmx1a*, *Nurr1* and *En1*. (**H**) Representative photomicrographs depicting expression of Nestin, Otx2 and FoxA2 in VM progenitors at day7. (**I**) Employment of an Lmx1a-GFP reporter line demonstrated high co-expression with Otx2 and FoxA2, indicative of ventral mesencephalic progenitors. (**J**) By day 14, these progenitors matured into VM dopaminergic neurons co-expressing the hallmark proteins Lmx1a, TH and FoxA2. (**K**) Representative images depicting Pitx3-GFP and TH expression within mature cultures, confirming ventral midbrain dopaminergic fate. (**L**) Quantification of %TH/FoxA2 neurons from VM (white) and ventral forebrain (black bars) cultures. Elevated proportions of TH+ FoxA2+ co-expressing neurons confirmed a VM dopaminergic phenotype, while FoxA2+ TH+ cells within VF cultures were indicative of off-target populations. (**M**) Quantification of TH+ / Pitx3-GFP+ neurons within ventral forebrain and ventral midbrain cultures at day 14, using the Pitx3-GFP reporter mESC line, confirmed the generation of *bona fide* VM dopaminergic neurons within VM cultures. Data represents mean ± SEM, n = 3, Students t-test. Scale bar = 100 um. **p < 0.01, ***p < 0.001.

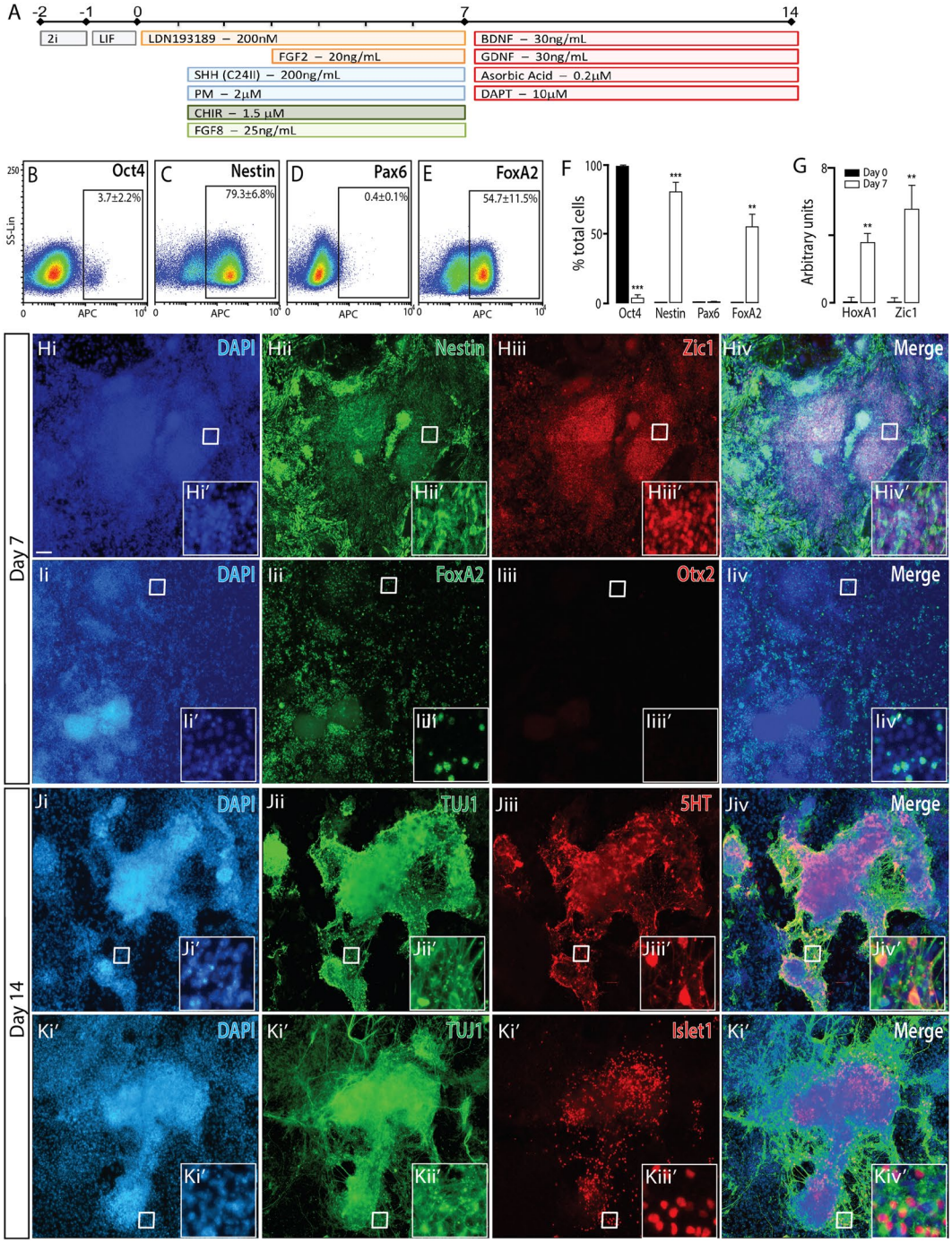

Figure 7. Naïve mESCs differentiated to a ventral hindbrain fate, show appropriate regional and temporal specification. (**A**) Schematic of the neural differentiation protocol, illustrating morphogen and small molecules employed, to generate ventral hindbrain progenitors and neurons from naïve PSCs. (**B–E**) Flow cytometry plots at day 7 and, (**F**) quantitative analysis at 0 and 7 for Oct4, Nestin, FoxA2 and Pax6, showing appropriate downregulaton of pluripotent (Oct4) and dorsal (Pax6) markers together with upregulation of neural (Nestin) and ventral (FoxA2) expression. (**G**) Transcriptional expression of hindbrain genes *Hoxa1* and *Zic1*. (**H**) Representative photomicrographs depicting expression of DAPI, Nestin and Zic1 in hindbrain progenitors at day 7. (**I**) Ventral hindbrain specification of progenitors was confirmed by the presence of ventral marker FoxA2 and absence of mesodiencephalic protein Otx2. (**J**) By day 14, hindbrain specified cultures contained serotinergic neurons immunoreactive for TUJ1 and 5HT, as well as (**K**) Islet1+ TUJ1+ neurons, indicative of motor neurons. Data represents mean ± SEM, (n = 3), Students t-test. Scale bar = 100 um. $^{**}p < 0.01$, $^{***}p < 0.001$.

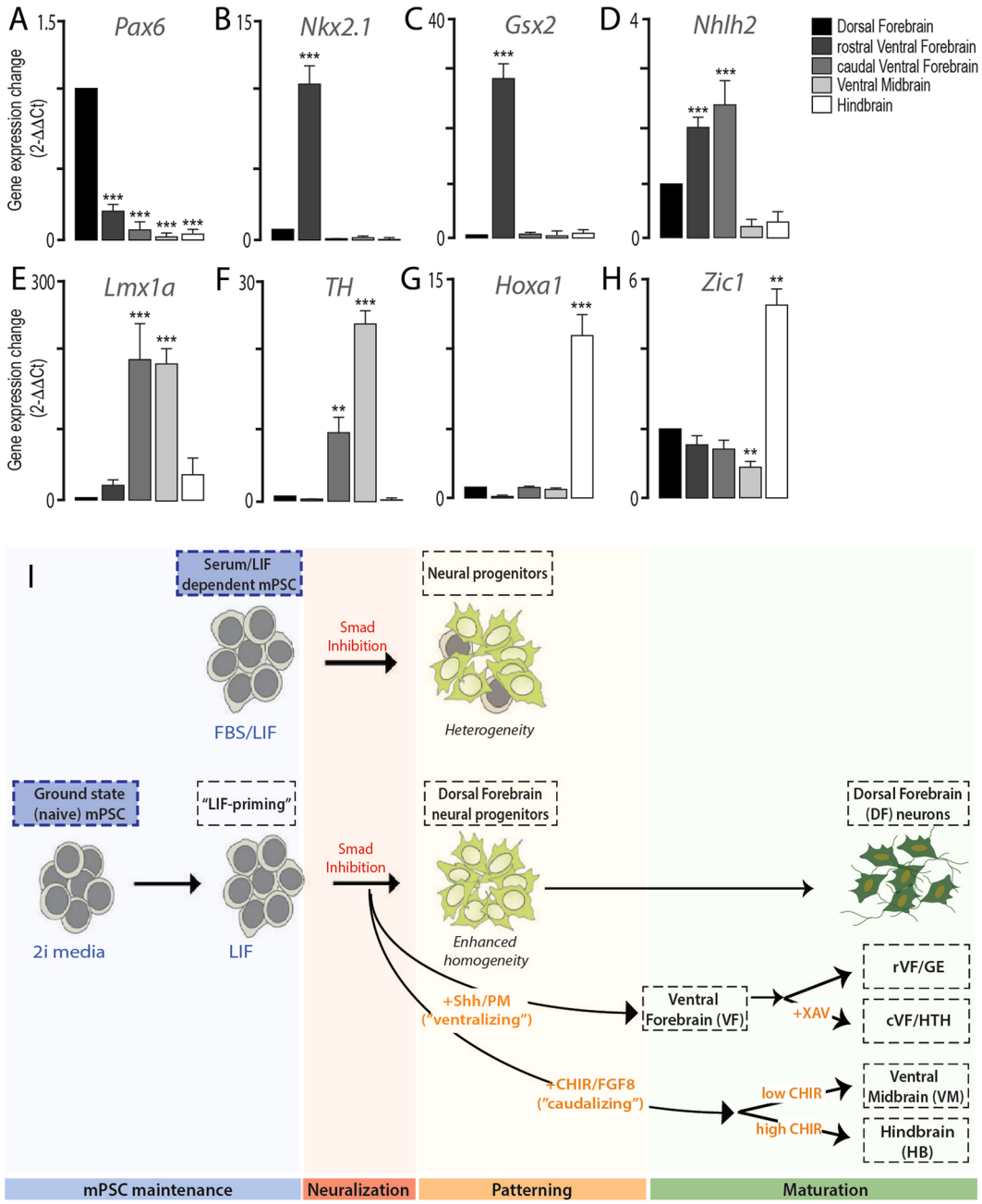

Figure 8. Transcriptional profiling of regionally distinct neural progenitor populations from mESC, and overview of differentiation. Transcriptional profiling of five neural progenitor populations, derived from naïve, ground state mESC, assessing key patterning and regionally localised genes including (**A**) *Pax6*, (**B**) *Nkx2.1*, (**C**) *Gsx2*, (**D**) *Nhlh2*, (**E**) *Lmx1a*, (**F**) *TH*, (**G**) *Hoxa1* and (**H**) *Zic1*. Upregulation of select genes within given populations confirmed specificity of the differentiations. (**I**) Schematic overview illustrating the "priming" of ground state pluripotent stem cells (blue shading), to promote homogeneneous neuralisation (pink) of mouse PSC. Subsequent patterning (orange) and maturation of cells (green), through the time and dose-dependent administration of morphogens and small molecules, resulted in the generation of regionally distinct neuronal populations including those of the dorsal forebrain (DF)/cortex, rostral and caudal ventral forebrain (rVF, cVF), ventral midbrain (VM) and hindbrain (HB).

establish novel protocols, involving early morphogen patterning of monolayer, feeder-free naïve PSC, resulting in the efficient generation of region-specific (dorsal forebrain, ventral forebrain, ventral midbrain and hindbrain) progenitors and neurons. These resultant populations will be valuble in understanding neural development, as well as disorders affecting specific neuronal populations.

Discussion

Previous studies have described the generation of region-specific neural subtypes from Serum/LIF-dependent mESCs[2,3,5,38]. While these protocols have provided means to study neural development and transplantation therapies, several limitations are associated with these protocols - namely the variability between differentiations and heterogeneity of derived cultures. Underlying these variables is the reliance on either stromal cell co-culture that introduces a variable milieu of patterning signals, the use of spontaneous embryoid bodies for uncontrolled default differentiation and/or failures to replicate developmental sequences appropriately.

By comparison, neural differentiation strategies for human PSC have advanced significantly, with numerous studies generating largely homogenous cultures of specific regional neural subtypes under rapid patterning methodologies[8–11]. While these human protocols are invaluable to the field, rodent counterparts nevertheless remain an important biological tool that in comparison possess malleable genomes and undergo rapid embryonic development. These traits facilitate cost and time effective investigations into mammalian development as well as intra-species cell transplantation studies.

We report here the development of a feeder-free directed neural differentiation system for mESCs and iPSCs along dorso-ventral and rostro-caudal axes that aligns mPSC differentiation closely with human PSC counterparts. By mimicking *in vitro* the rapid temporal signaling gradients of rodent development an array of neural lineages from the dorsal forebrain, ventral forebrain, ventral midbrain and hindbrain were formed within 14 days, Fig. 8K.

Furthermore, we describe for the first time the use of naïve mPSC as a starting material for neural differentiation, resulting in differentiated cultures of improved homogeneity and eliminated contaminant pluripotent cells (Fig. 1). Interestingly the employment of naïve mPSC required precise recapitulation of developmental sequences, involving the transition of naïve cells (reflective of pre-implantation) temporarily to a more primed (post-implantation) state, by exposure to LIF, prior to the initiation of differentiation. The use of naïve mPSC likely underlies the robust fate restriction reported here, as recent studies evaluating naïve and serum-dependent mESC have demonstrated that the former are intrinsically homogeneous at transcriptomic and epigenomic levels, while the later express a range of lineage-specific genes likely to interfere with differentiation[14,17].

Additional to the use of naïve stem cells, early patterning of mPSC reflective of embryonic development was imperative for restricted neural fate specification. Smad inhibition at the onset of differentiation forced neural specification towards the default dorsal forebrain lineage, reflected by the generation of Pax6+, Tbr2+, Emx2+ NPCs, and mirroring human PSC protocols. Following initial patterning and a week of maturation in neurotrophic factors and notch inhibitors, to induce a transition to post-mitotic neurons, dorsal forebrain progenitors differentiated into mature neurons that expressed anticipated cortical layer markers, such as Tbr1 and Ctip2. Previous mPSC protocols have reported the use of small molecule antagonists of the Sonic Hedgehog pathway to promote cortical specification from serum/LIF-dependent mESCs[5,39]. Our study found Shh inhibition was not required as evidenced by limited expression of the ventral floor-plate marker Foxa2 cells within the cultures and enrichment of dorsal cortical markers. Initiating differentiation from naïve mESC, as opposed to S/L-dependent mESCs, may underlie the improved patterning outcomes, despite a reduction in administered extrinsic signals.

Conversely, Shh agonists (Purmorphamine and recombinant Shh) were required from day 1 of differentiation to ventralize NPCs, resulting in the acquistation of a hypothalamic identity, as seen by expression of *Nhlh2* and *Otp*[40]. Of note, ventralized NPCs did not express ganglionic eminence markers such as Nkx2.1 and Olig2, suggesting that the Shh and puromorphomine concentrations used maximally activated the Shh pathway to produce the most ventral structures of the developing rostral neural tube. Following maturation, ventral forebrain NPCs developed into GABAergic neurons, a population present in the adult hypothalamus, in addition to FoxA2-TH+ dopaminergic neurons[40,41]. Interstingly, the addition of early Wnt inhibition, to reduce the extent of floorplate ventralization of the progenitors, we were able to direct cells to adopt a GE identity. These GE-like progenitors were positive for both Nkx2.1 and Olig2 and continued to develop into GABAergic neurons, a neuronal population that arises in the GE during ventral telencephalic development.

Differentiation to the ventral midbrain was also acheived from naïve mPSCs with the addition of caudalization cues supplied by FGF8 and the GSK3b inhibitor CHIR9902. This sequence of immediate neuralization, ventralization and rostrocaudal positioning closely mirrors hPSC protocols for VM differentiation[8,10,21]. Post-mitotic neurons were obtained rapidly, within 14 days of differentiation, and confirmed to be *bona fide* ventral midbrain dopamine neurons based on Lmx1a and Pitx3 expression (using our knock-in reporter line) as well as FoxA2, in addition to gene transcripts for *En1*, *Nurr1* and *Lmx1a*.

Finally, ventral hindbrain specification was attained by increased caudalisation of NPCs, using amplified canonical Wnt activation. Resultant NPCs showed evidence of hindbrain identity based upon the presence of Zic1 and lack of Otx2 immunoreactivity in conjunction with motor (Islet1) and serotonergic (5-HT) neuronal markers[36,37].

Demonstrative of the efficiency of these new protocols was the relative lack of off-target cells within each populations. Genes known from *in vivo* neural development to be to be expressed within select progenitor/neuronal populations were largely restricted within our cultures, such that dorsal identity gene *Pax6* was only expressed in dorsal forebrain cultures, yet rhombencephalic genes, *Hoxa1* and *Zic1*, were only expressed in hindbrain cultures. While the combination of restricted transcriptional gene expression as well as protein expression (and often protein co-localisation) enabled confirmation of the presence of restricted neuronal populations in some instances, we recognize that the efficiency of these differentiation protocols still contains variability, and one that is higher than comparative human PSC protocols. At one extreme >75% of naïve mESC, differentiated along a VM lineage, adopted a VM DA fate (quantitatively confirmed by TH+ Pitx3+ colocalisation) yet VF cultures were decidedly more heterogeneous (including both GABA+, TH+ FoxA2− and TH+ FoxA2+ neurons), proving challenging for defintive confirmation of neuronal identity from adjacent populations. We speculate that this, in part, is a likely consequence of the rapid differentiation of mouse PSCs compared to human counterparts that allows less time to orchestrate regional patterning and terminal signals. As such, more extensive transcriptional,

histochemical, biochemical and functional/electrophysiological profiling studies will be required in order to confirm the true efficiency of each of these described protocols.

In summary, using naïve mPSC, we describe the robust regional specification of PSC through the early manipulation of rostro-caudal and dorso-ventral morphogen gradients. These protocols, and resultant neuronal populations, may provide important tools for understanding mammalian neural development, aide in our understanding of brain-related disorders and assist in the development of new targeted therapies including cell replacement therapy.

References

1. Evans, M. J. & Kaufman, M. H. Establishment in culture of pluripotential cells from mouse embryos. *Nature* **292**, 154–156 (1981).
2. Kawasaki, H. *et al*. Induction of midbrain dopaminergic neurons from ES cells by stromal cell-derived inducing activity. *Neuron* **28**, 31–40 (2000).
3. Barberi, T. *et al*. Neural subtype specification of fertilization and nuclear transfer embryonic stem cells and application in parkinsonian mice. *Nature biotechnology* **21**, 1200–1207 (2003).
4. Ying, Q. L. & Smith, A. G. Defined conditions for neural commitment and differentiation. *Methods Enzymol* **365**, 327–341 (2003).
5. Gaspard, N. *et al*. Generation of cortical neurons from mouse embryonic stem cells. *Nat Protoc* **4**, 1454–1463, https://doi.org/10.1038/nprot.2009.157 (2009).
6. McCreedy, D. A. *et al*. A new method for generating high purity motoneurons from mouse embryonic stem cells. *Biotechnol Bioeng* **111**, 2041–2055, https://doi.org/10.1002/bit.25260 (2014).
7. Gaspard, N. & Vanderhaeghen, P. Mechanisms of neural specification from embryonic stem cells. *Curr Opin Neurobiol* **20**, 37–43, https://doi.org/10.1016/j.conb.2009.12.001 (2010).
8. Kriks, S. *et al*. Dopamine neurons derived from human ES cells efficiently engraft in animal models of Parkinson's disease. *Nature* **480**, 547–551, https://doi.org/10.1038/nature10648 (2011).
9. Shi, Y., Kirwan, P. & Livesey, F. J. Directed differentiation of human pluripotent stem cells to cerebral cortex neurons and neural networks. *Nat Protoc* **7**, 1836–1846, https://doi.org/10.1038/nprot.2012.116 (2012).
10. Kirkeby, A. *et al*. Generation of regionally specified neural progenitors and functional neurons from human embryonic stem cells under defined conditions. *Cell reports* **1**, 703–714, https://doi.org/10.1016/j.celrep.2012.04.009 (2012).
11. Qu, Q. *et al*. High-efficiency motor neuron differentiation from human pluripotent stem cells and the function of Islet-1. *Nat Commun* **5**, 3449, https://doi.org/10.1038/ncomms4449 (2014).
12. Weinberger, L., Ayyash, M., Novershtern, N. & Hanna, J. H. Dynamic stem cell states: naive to primed pluripotency in rodents and humans. *Nat Rev Mol Cell Biol* **17**, 155–169, https://doi.org/10.1038/nrm.2015.28 (2016).
13. Ying, Q. L. *et al*. The ground state of embryonic stem cell self-renewal. *Nature* **453**, 519–523, https://doi.org/10.1038/nature06968 (2008).
14. Guo, G. *et al*. Serum-Based Culture Conditions Provoke Gene Expression Variability in Mouse Embryonic Stem Cells as Revealed by Single-Cell Analysis. *Cell Rep* **14**, 956–965, https://doi.org/10.1016/j.celrep.2015.12.089 (2016).
15. Marks, H. *et al*. The transcriptional and epigenomic foundations of ground state pluripotency. *Cell* **149**, 590–604, https://doi.org/10.1016/j.cell.2012.03.026 (2012).
16. Taleahmad, S. *et al*. Proteome Analysis of Ground State Pluripotency. *Sci Rep* **5**, 17985, https://doi.org/10.1038/srep17985 (2015).
17. Kolodziejczyk, A. A. *et al*. Single Cell RNA-Sequencing of Pluripotent States Unlocks Modular Transcriptional Variation. *Cell Stem Cell* **17**, 471–485, https://doi.org/10.1016/j.stem.2015.09.011 (2015).
18. Nefzger, C. M. *et al*. Lmx1a allows context-specific isolation of progenitors of GABAergic or dopaminergic neurons during neural differentiation of embryonic stem cells. *Stem Cells* **30**, 1349–1361, https://doi.org/10.1002/stem.1105 (2012).
19. Watmuff, B., Pouton, C. W. & Haynes, J. M. *In vitro* maturation of dopaminergic neurons derived from mouse embryonic stem cells: implications for transplantation. *PLoS One* **7**, e31999, https://doi.org/10.1371/journal.pone.0031999 (2012).
20. Ye, W., Shimamura, K., Rubenstein, J. L., Hynes, M. A. & Rosenthal, A. FGF and Shh signals control dopaminergic and serotonergic cell fate in the anterior neural plate. *Cell* **93**, 755–766 (1998).
21. Niclis, J. C. *et al*. Efficiently Specified Ventral Midbrain Dopamine Neurons from Human Pluripotent Stem Cells Under Xeno-Free Conditions Restore Motor Deficits in Parkinsonian Rodents. *Stem cells translational medicine* **6**, 937–948, https://doi.org/10.5966/sctm.2016-0073 (2017).
22. Blakely, B. D. *et al*. Wnt5a regulates midbrain dopaminergic axon growth and guidance. *PLoS One* **6**, e18373 (2011).
23. Chambers, S. M. *et al*. Highly efficient neural conversion of human ES and iPS cells by dual inhibition of SMAD signaling. *Nature biotechnology* **27**, 275–280, https://doi.org/10.1038/nbt.1529 (2009).
24. Hassani, S. N., Pakzad, M., Asgari, B., Taei, A. & Baharvand, H. Suppression of transforming growth factor beta signaling promotes ground state pluripotency from single blastomeres. *Hum Reprod* **29**, 1739–1748, https://doi.org/10.1093/humrep/deu134 (2014).
25. Molyneaux, B. J., Arlotta, P., Menezes, J. R. & Macklis, J. D. Neuronal subtype specification in the cerebral cortex. *Nat Rev Neurosci* **8**, 427–437, https://doi.org/10.1038/nrn2151 (2007).
26. Borghese, L. *et al*. Inhibition of notch signaling in human embryonic stem cell-derived neural stem cells delays G1/S phase transition and accelerates neuronal differentiation *in vitro* and *in vivo*. *Stem Cells* **28**, 955–964, https://doi.org/10.1002/stem.408 (2010).
27. Englund, C. *et al*. Pax6, Tbr2, and Tbr1 are expressed sequentially by radial glia, intermediate progenitor cells, and postmitotic neurons in developing neocortex. *J Neurosci* **25**, 247–251, https://doi.org/10.1523/JNEUROSCI.2899-04.2005 (2005).
28. Wang, W. & Lufkin, T. The murine Otp homeobox gene plays an essential role in the specification of neuronal cell lineages in the developing hypothalamus. *Dev Biol* **227**, 432–449, https://doi.org/10.1006/dbio.2000.9902 (2000).
29. Vella, K. R., Burnside, A. S., Brennan, K. M. & Good, D. J. Expression of the hypothalamic transcription factor Nhlh2 is dependent on energy availability. *J Neuroendocrinol* **19**, 499–510, https://doi.org/10.1111/j.1365-2826.2007.01556.x (2007).
30. Pristera, A. *et al*. Transcription factors FOXA1 and FOXA2 maintain dopaminergic neuronal properties and control feeding behavior in adult mice. *Proceedings of the National Academy of Sciences of the United States of America* **112**, E4929–4938, https://doi.org/10.1073/pnas.1503911112 (2015).
31. Backman, M. *et al*. Effects of canonical Wnt signaling on dorso-ventral specification of the mouse telencephalon. *Dev Biol* **279**, 155–168, https://doi.org/10.1016/j.ydbio.2004.12.010 (2005).
32. Burbach, J. P., Smits, S. & Smidt, M. P. Transcription factors in the development of midbrain dopamine neurons. *Annals of the New York Academy of Sciences* **991**, 61–68 (2003).
33. Smidt, M. P. *et al*. Early developmental failure of substantia nigra dopamine neurons in mice lacking the homeodomain gene Pitx3. *Development* **131**, 1145–1155, https://doi.org/10.1242/dev.01022 (2004).
34. Barrow, J. R., Stadler, H. S. & Capecchi, M. R. Roles of Hoxa1 and Hoxa2 in patterning the early hindbrain of the mouse. *Development* **127**, 933–944 (2000).
35. Aruga, J. *et al*. Mouse Zic1 is involved in cerebellar development. *J Neurosci* **18**, 284–293 (1998).
36. Pattyn, A. *et al*. Ascl1/Mash1 is required for the development of central serotonergic neurons. *Nat Neurosci* **7**, 589–595, https://doi.org/10.1038/nn1247 (2004).

37. Pfaff, S. L., Mendelsohn, M., Stewart, C. L., Edlund, T. & Jessell, T. M. Requirement for LIM homeobox gene Isl1 in motor neuron generation reveals a motor neuron-dependent step in interneuron differentiation. *Cell* **84**, 309–320 (1996).
38. Jing, Y. *et al. In vitro* differentiation of mouse embryonic stem cells into neurons of the dorsal forebrain. *Cell Mol Neurobiol* **31**, 715–727, https://doi.org/10.1007/s10571-011-9669-2 (2011).
39. Sadegh, C. & Macklis, J. D. Established monolayer differentiation of mouse embryonic stem cells generates heterogeneous neocortical-like neurons stalled at a stage equivalent to midcorticogenesis. *J Comp Neurol* **522**, 2691–2706, https://doi.org/10.1002/cne.23576 (2014).
40. Blackshaw, S. *et al.* Molecular pathways controlling development of thalamus and hypothalamus: from neural specification to circuit formation. *J Neurosci* **30**, 14925–14930, https://doi.org/10.1523/JNEUROSCI.4499-10.2010 (2010).
41. DeMaria, J. E., Lerant, A. A. & Freeman, M. E. Prolactin activates all three populations of hypothalamic neuroendocrine dopaminergic neurons in ovariectomized rats. *Brain Res* **837**, 236–241 (1999).

Acknowledgements

This research was supported by funding from the National Health and Medical Research Council, Australia. The Florey Institute of Neuroscience and Mental Health acknowledges the support from the Victorian Government's Operational Infrastructure Support Grant. CLP was supported by a Senior Medical Research Fellowship provided by the Viertel Charitable Foundation, Australia. The authors thank Ms Mong Tien for her technical assistance.

Author Contributions

W.A.: collection and assembly of data, manuscript preparation, final approval of manuscript. J.N.: collection and assembly of data, manuscript preparation, final approval of manuscript. I.D.L.: collection and assembly of data, manuscript preparation, final approval of manuscript. C.H.: collection and assembly of data, manuscript preparation, final approval of manuscript. V.P.: collection and assembly of data, final approval of manuscript. C.B.: collection and assembly of data, final approval of manuscript. C.W.P.: supply of reagents, final approval of manuscript. J.H.: supply of reagents, final approval of manuscript. J.F.: supply of reagents, final approval of manuscript. L.H.: experimental design, final approval of manuscript. C.L.P.: financial support, collection and assembly of data, interpretation of findings, manuscript preparation, final approval of manuscript.

Additional Information

Supplementary information accompanies this paper at https://doi.org/10.1038/s41598-017-16248-x.

Competing Interests: The authors declare that they have no competing interests.

Publisher's note: Springer Nature remains neutral with regard to jurisdictional claims in published maps and institutional affiliations.

Appendix 2. Transcriptomic profiling of xenogeneic transplants: Examining human pluripotent stem cell-derived grafts in the rodent brain

Please cite this article in press as: Bye et al., Transcriptional Profiling of Xenogeneic Transplants: Examining Human Pluripotent Stem Cell-Derived Grafts in the Rodent Brain, Stem Cell Reports (2019), https://doi.org/10.1016/j.stemcr.2019.10.001

Stem Cell Reports
Article
ISSCR
OPEN ACCESS

Transcriptional Profiling of Xenogeneic Transplants: Examining Human Pluripotent Stem Cell-Derived Grafts in the Rodent Brain

Christopher R. Bye,[1,2,*] Vanessa Penna,[1,2] Isabelle R. de Luzy,[1] Carlos W. Gantner,[1] Cameron P.J. Hunt,[1] Lachlan H. Thompson,[1] and Clare L. Parish[1,*]
[1]The Florey Institute of Neuroscience and Mental Health, The University of Melbourne, Parkville, VIC, Australia
[2]Co-first author
*Correspondence: chris.bye@florey.edu.au (C.R.B.), clare.parish@florey.edu.au (C.L.P.)
https://doi.org/10.1016/j.stemcr.2019.10.001

SUMMARY

Human pluripotent stem cells are a valuable resource for transplantation, yet our ability to profile xenografts is largely limited to low-throughput immunohistochemical analysis by difficulties in readily isolating grafts for transcriptomic and/or proteomic profiling. Here, we present a simple methodology utilizing differences in the RNA sequence between species to discriminate xenograft from host gene expression (using qPCR or RNA sequencing [RNA-seq]). To demonstrate the approach, we assessed grafts of undifferentiated human stem cells and neural progenitors in the rodent brain. Xenograft-specific qPCR provided sensitive detection of proliferative cells, and identified germ layer markers and appropriate neural maturation genes across the graft types. Xenograft-specific RNA-seq enabled profiling of the complete transcriptome and an unbiased characterization of graft composition. Such xenograft-specific profiling will be crucial for pre-clinical characterization of grafts and batch-testing of therapeutic cell preparations to ensure safety and functional predictability prior to translation.

INTRODUCTION

Since the derivation of human pluripotent stem cell (hPSC) lines, there has been great hope and anticipation for the use of these cells and their derivatives in regenerative medicine. One of the most anticipated applications is their restricted fate specification to defined cellular populations for the purpose of transplantation, aimed at treating acute and chronic disorders. Some of the most advanced examples are hPSC-derived islet cells for the treatment of diabetes, retinal pigment epithelia for application in visual impairment conditions, and dopamine neurons for the replacement of those cells lost to Parkinson's disease (PD) (Trounson and McDonald, 2015).

Prior to clinical translation of hPSC-derived cells, it will be imperative that graft composition is well defined to ensure safety and functional predictability. The significance of understanding graft composition is perhaps most evidently demonstrated in hPSC-derived dopamine (DA) progenitor transplantation studies in PD models. Despite significant advancements in differentiation protocols resulting in high yields of correctly specified progenitors for grafting (Kirkeby et al., 2012; Kriks et al., 2011; Niclis et al., 2017b), following protracted graft analysis (>6 months) only a fraction of the transplant is composed of mature DA neurons (Doi et al., 2014; Kirkeby et al., 2012, 2017; Kriks et al., 2011; Niclis et al., 2017a; Samata et al., 2016). Such outcomes suggest that the small proportion of poorly specified cells present in the cultures subsequently expands following transplantation to dominate the graft. Histochemical assessment has been able to confirm that these grafts are predominantly "neural" in origin and of an appropriate regional identity (Kriks et al., 2011; Samata et al., 2016); however, due to limited antibody availability to selectively assess the human cells, as well as not knowing what to specifically look for, the identity of much of these grafts remains unknown. This raises the concern of what impact these cells may have on graft function as well as on the host.

Transcriptionally profiling grafts has been hindered by the inability to selectively isolate the graft, which is interdispersed with the host tissue. When the graft can be clearly identified, (e.g., grafts of reporter stem cell lines), careful laser-capture microdissection can reduce the level of contaminating host cells. However, laser-capture-based approaches are labor intensive, require meticulous tissue processing to maintain RNA quality, and are associated with low RNA yields. An alternative approach is isolating the grafted cells by tissue dissociation and applying fluorescent or magnetic cell-sorting strategies. This approach relies on the dissociation of post-mitotic cells and can result in poor survival. Single-cell genomic profiling of cells within the graft has also increasingly been employed to assess molecular and cellular diversity within defined populations (Etzrodt et al., 2014; La Manno et al., 2016; Tang et al., 2010). While providing an accurate assessment of the cell identity within the graft, such approaches are also onerous and sample just a fraction of the graft.

Circumventing these challenges, we develop here a method that employs a selective detection process to discriminate graft transcripts within a mixed graft-host tissue pool. This simple approach relies on identifying RNA

Please cite this article in press as: Bye et al., Transcriptional Profiling of Xenogeneic Transplants: Examining Human Pluripotent Stem Cell-Derived Grafts in the Rodent Brain, Stem Cell Reports (2019), https://doi.org/10.1016/j.stemcr.2019.10.001

sequence differences between the host and graft species to design species-specific primers for the purpose of real-time qPCR, and similarly recognizing species-specific reads for RNA sequencing (RNA-seq). The utility and rigor of these techniques are demonstrated by comparing different transplant populations of human cells in the rodent brain.

RESULTS

Design and Validation of Xenograft-Specific Primers for Real-Time qPCR

To identify xenograft-specific sequences using qPCR, we designed primers targeting regions of dissimilarity between the two species (Figure 1A). Specifically, primers targeted an RNA sequence containing a minimum of 5-bp mismatches between xenograft and host, or two mismatches within the 5 bp at the 3′ end of the primer (e.g., Ki67 and LMX1A forward primers) (Figure 1B). To confirm the specificity of the primers for xenograft transcript, we tested primers with *in vitro* pools of mouse or human cells known to express the target genes. A total of 30 primers were designed and tested (Figure 1B). Primer specificity for xenograft transcripts (over mouse) ranged from 500 to 1.0 × 10^7 times greater, with a median specify of 174,000 (Figure 1C). Using an arbitrary cutoff of 1,000 times (1,000×) greater specificity for the human pool compared with mouse, primers for 97% of genes (29/30) were deemed as specific.

With success at designing species-specific primers, as validated *in vitro*, next the feasibility of this approach *in vivo* was determined, targeted at confirming the ability to discriminate between xenograft and host transcripts. To achieve this, we analyzed transplants of human stem cells in the striatum of immune-compromised athymic mice using qPCR. The specificity of the primers for xenograft RNA were confirmed *in vivo* by measuring the ability to detect the expression of four constitutively expressed genes in grafted tissue compared with ungrafted tissue (i.e., mouse striatal tissue containing no xenograft) (Figure 1D). The four primers tested specifically detected xenograft transcripts *in vivo*, with expression in the grafted host greater than the host-only tissue for PSMB4 (10,349×), MTHFD (769×), CHAMP2A (2,775×), and HPRT1 (1,726×).

To access the capacity of species-specific primers to provide a readout of graft size, we implanted a known number of neural progenitors (10,000, 30,000, 100,000, or 300,000 cells) into the rodent brain and assessed the expression levels of housekeeping genes after 2 weeks. A xenograft-specific primer for a housekeeping gene was used to assess graft size, while a host-specific primer enabled assessment of the amount of host tissue present within the isolated tissue. Expressed as a proportion of total RNA, xenograft RNA constituted 0.8% ± 0.60% (10,000 cells), 6.5% ± 2.48% (30,000 cells), 12.8% ± 1.78% (100,000 cells), or 18.1% ± 3.31% (300,000 cells) of the RNA population (Figure 1E). The estimate of xenograft RNA showed a tight and significant correlation with the number of cells transplanted (r^2 = 0.78), demonstrating the utility of the method to rapidly estimate graft size.

Characterization of Xenografts Using Species-Specific Real-Time qPCR

To demonstrate and validate the utility of species-specific transcriptional profiling of xenografts, we compared RNA from three distinct xenografts: (1) grafts derived from undifferentiated PSCs, anticipated to contain proliferative populations and cells from all three germ layers after 1 month *in situ* (subsequently referred to as the "undifferentiated" grafts); (2) transplants of ventral midbrain (VM) neural progenitors, analyzed 1 month after implantation and anticipated to show characteristic signatures of immature neuronal progenitor neurons (subsequently referred to as "immature neuronal" grafts); and (3) grafts of VM neural progenitors, allowed to mature for 5 months *in situ* into neuronal populations inclusive of dopamine neurons (denoted "mature neuronal" grafts). In parallel, tissue was collected from separate animals for immunohistochemistry to provide verification of the gene-expression results.

Using an antibody specific for human cells (human nuclear antigen [HNA]) that enabled delineation of the graft, size and cell number were determined. Grafts of undifferentiated cells were large and expansive (7.0 ± 3.5 mm^3 containing 2.03 × 10^6 ± 0.43 × 10^6 cells), while immature neuronal grafts were small (0.43 ± 0.07 mm^3 with 0.49 × 10^5 ± 0.11 × 10^5 cells), and of moderate size following ongoing maturation (mature neuronal grafts: 2.4 ± 0.25 mm^3 containing 1.51 × 10^5 ± 0.31 × 10^5cells) (Figures 2A–2D). Transcriptional estimation of graft size, by xenograft-specific qPCR, measured the proportion of xenograft RNA at 33.0% ± 8.9% in the undifferentiated grafts, 1.8% ± 0.4% in the immature neuronal grafts, and 9.2% ± 0.9% in the mature neuronal grafts (Figure 2E), reflective of graft sizes determined histologically.

Necessary for the safe clinical translation of cell transplantation is the removal of proliferative cells prior to implantation, or their reduction to low levels shortly thereafter. Hence, in an effort to characterize graft composition, the expression of the proliferative gene *Ki67* was assessed. A large population of $Ki67^+$/HNA^+ dividing cells were identified in the undifferentiated grafts (9.5% ± 1.0%) that was significantly reduced in immature neuronal grafts (0.74% ± 0.16%) and reduced further in the mature neuronal grafts (0.28% ± 0.06%) (Figures 2A–2C and 2F). Xenograft-specific gene expression (expressed relative to

Please cite this article in press as: Bye et al., Transcriptional Profiling of Xenogeneic Transplants: Examining Human Pluripotent Stem Cell-Derived Grafts in the Rodent Brain, Stem Cell Reports (2019), https://doi.org/10.1016/j.stemcr.2019.10.001

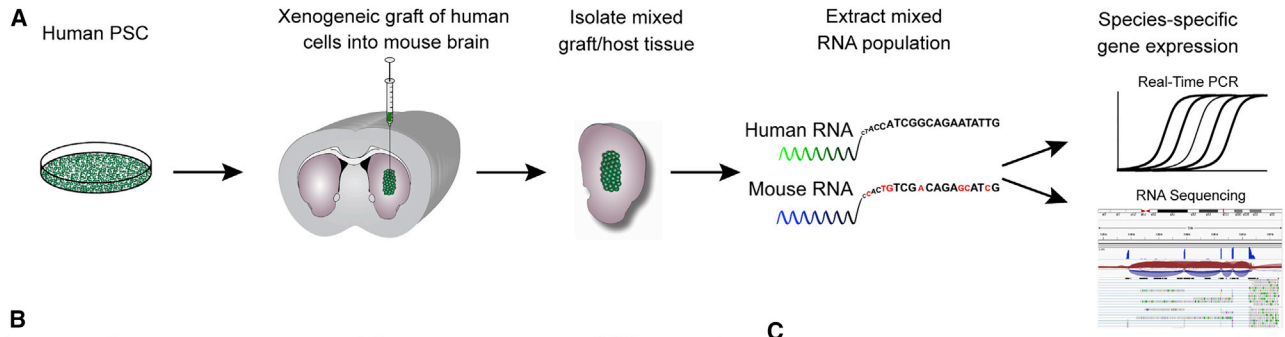

B

Gene	Forward Primer	Reverse Primer	Fold Specificity
Proliferation & Trilineage Markers			
MKi67	GCCTCCTAATACGCCTCTCA	CCTGATGGTTGAGGCTGTTC	2845005
AFP	CCCAGTTTGTTCAAGAAGCCA	ACACCCTGAAGACTGTTCATCT	9026
GATA6	AGAAGATGGAAGGGAAGGGC	GTCCTAGTCCTGGCTTCTGG	560
BRACHY	CGATCCTGGGTGTGCGTAAC	GCCGCAGTAGTAGTGCTGTT	4770
COL2A1	GCCGGTCTGCTTCTTGTAAA	GAGGGTGGGATGAATGGACA	1131652
NCAM1	TCCAGGCCAGGCAGAATATT	TCATCGTCTTCCTCTTGCTC	535304
NES	CTGGAGCAGGAGAAACAGGG	CTGAGGGAAGTCTTGGAGCC	1668361
Immature Dopaminergic Markers			
LMX1A	ATGAACCCCTACACGGCTCT	TAAGGGTGCATGTGGTCTCC	1916443
TH	GAGGCCATCATGGTAAGAGGG	CTGCCTGCGCCCAATGAAC	38699
OTX2	AGCTGCACTGAAACTTTACGA	CCAATGTCTCTTTACTGCTAGGC	2375830
EN1	AAGAAATAGCCAAGTGTCTCCA	GTCTGGCCTGGATCGCTC	3281
NEUROG2	CCCCTTTCTCTTTAACGCCG	ATGTAGAAGCAAAGGTGAAGAGA	3929
NR4A2	GGTGTCCGGGTTCCCTTC	TCCGCGTCTCTCTTCATTCA	81245
PITX3	CAGCCAACCTTAGTCCGTG	CGGAGGCTGTGAATCGTTG	4421
Mature Dopaminergic Markers			
DAT1	TTCCTCAACTCCCAGTGTGC	CCGTTCTGCTCCTTGACAAG	9027
VMAT2	ACAGCTAGTTCTCTCAAGTGTAG	GCCAACCAGATAACATGTTAACA	443938
GIRK2	TGCGGATTTCATGACGTCTC	TGGAATGAAGTGGGGAAAGATAA	31433
CALB1	TCCAACAAACTTACTGTCAGAGA	CTAGACACCAGGATATGCAGTAT	129267
SYB2	TCTGTGCCATCATCGTGGTAG	CAGGCTTGGGACACATCGAG	1514070
Non-Dopaminergic Markers			
GFAP	TCTAAGGCCGAAGAAGGGTC	TTCCTCAGCGACTAAAGGCA	26068
EAAT1	GCTGGGGAATTCACCTCGTT	CCCCATCTTGGGCTCTTCTC	506428
OLIG1	AGACCAGCTGTTTGGAGAGC	GATGCAAGGCGGTTGGTTTT	11585
MBP	GAGGCACGGATCCAAGTACC	TTGTACATGTTGCACAGCCC	2062
Guidance Cues			
IGSF8	TGCCCTGGACACCCTATTTG	GGGATCACCGTTTTCGAAGC	558036
NLGN3	CCAACTCTCTCTGTGTCCGT	GCAAAACCCAGATCAGACCTG	218913
SEMA5A	CTGGACAAGTACGACTCGGT	GGAACTGGGGATTTACAAGAAGC	288557
Housekeeping Genes			
PSMB4	TGCACTTTACAGAGGTCCAATC	CGTAGGATCCCAGCATGTCT	5235877
MTHFD1	CAGTAGTGTGATCCCCTGGC	GCCTTTATTAGTCCGCTGCC	2005
CHMP2A	AGATGAGCTGTCGAACCTCC	GCAGGTTCTTAAGCCGTTCC	428816
HPTR1	GCTGAGGATTTGGAAAGGGTG	GCTACAATGTGATGGCCTCC	2201415

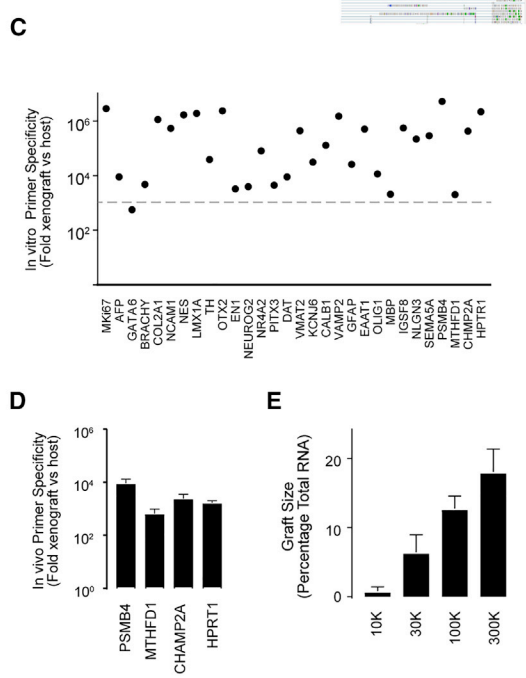

Figure 1. Design and Validation of Xenograft-Specific Primers for Real-Time qPCR

(A) Schematic of the experimental paradigm. hPSC-derived cells were transplanted into the rodent brain. Tissue containing both transplanted cells and host tissue was dissected, and the RNA isolated to produce a mixed-species RNA pool. Xenograft gene expression was discriminated from the host using species-specific primers for qPCR, or by RNA-seq to profile the entire genome.

(B) Table of human xenograft-specific primers designed for the present study. Nucleotide bases shown in red correspond to mismatches between the human and mouse RNA sequence, and underlined bases represent the presence of insertions or deletions.

(C) Graph of the specificity of xenograft-specific primers for human transcript relative to rodent host transcript *in vitro* showing an average specificity of 5,000 times that of the host (also represented numerically as "fold specificity" in B). An arbitrary cutoff of 1,000-fold (gray line) represents an ideal specificity threshold, with 96% of primers designed in this study exceeding this threshold.

(D) *In vivo* specificity of xenograft-specific primers for four constitutively expressed transcripts, showing an average specificity of ~4,000 times greater in the transplanted compared with untransplanted host.

(E) Estimation of xenograft size using a xenograft-specific primer, PSMB4, showed a significant correlation ($r^2 = 0.78$) with actual number of cells implanted into the host.

Data in (D) and (E) represent mean ± SEM, n = 4 grafts/group.

the undifferentiated grafts) showed that Ki67 expression in the immature grafts was reduced to 0.11 ± 0.02-fold, and to 0.05 ± 0.01-fold in mature grafts (Figure 2G), corresponding closely to the cell counts, and highlighting the capacity for xenograft-specific qPCR to detect rare cell populations.

Please cite this article in press as: Bye et al., Transcriptional Profiling of Xenogeneic Transplants: Examining Human Pluripotent Stem Cell-Derived Grafts in the Rodent Brain, Stem Cell Reports (2019), https://doi.org/10.1016/j.stemcr.2019.10.001

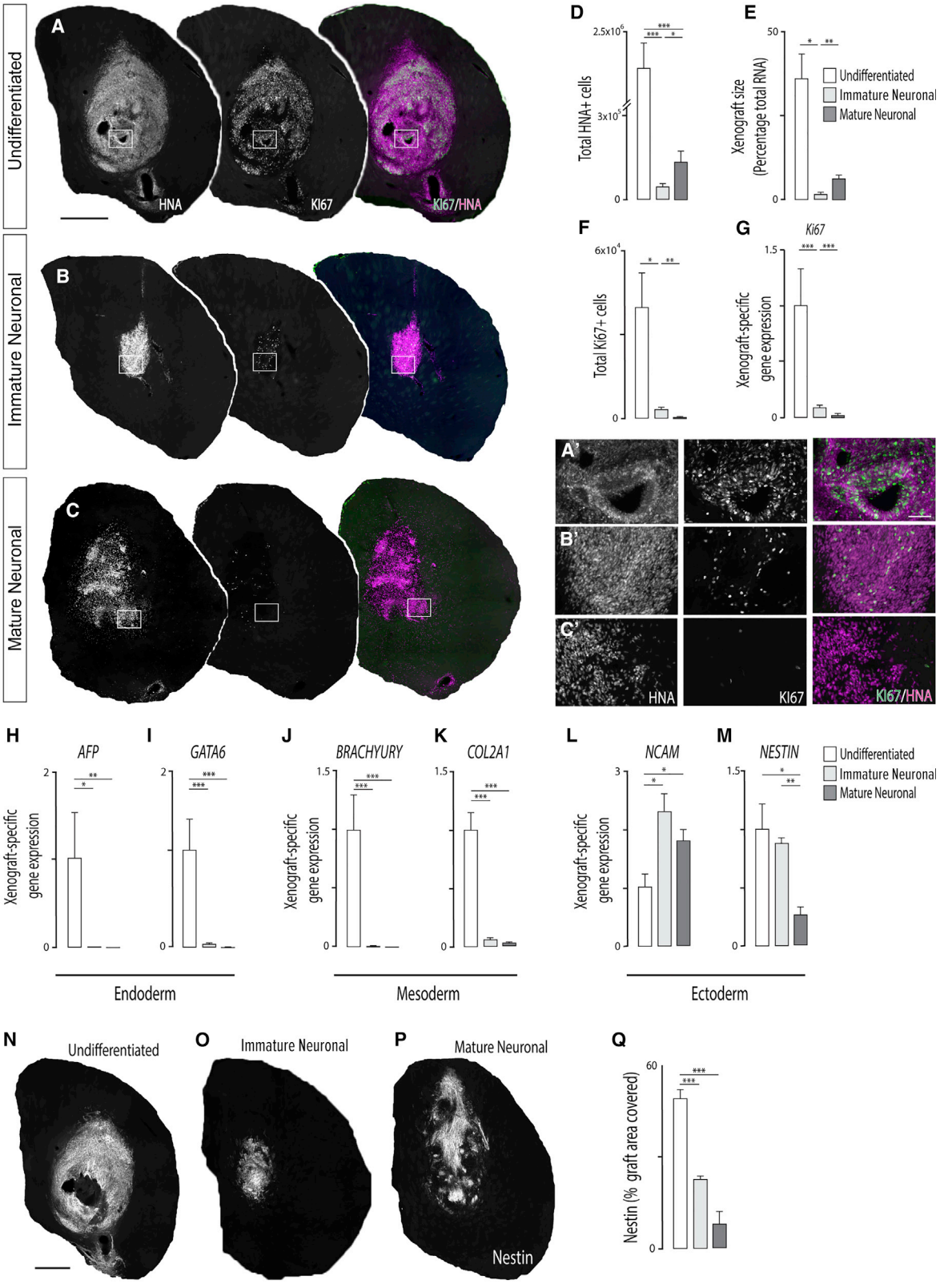

(legend on next page)

The capacity of the technique to detect different cellular populations within a graft was demonstrated using primers targeted against genes restricted to defined germ layers (endoderm, mesoderm, and ectoderm) (Tsankov et al., 2015; D'Antonio et al., 2017). Unsurprisingly, endoderm (AFP and GATA6) and mesoderm (Brachyury and Collagen2A type 1, COL2A1) genes were lowly expressed in the immature and mature neuronal grafts (Figures 2H–2K). In contrast, expression of the ectoderm marker neural cell adhesion marker (NCAM) was elevated in the immature and mature neuronal grafts (2.25 ± 0.39 and 1.58 ± 0.38, respectively) (Figure 2L). The neuroectodermal stem cell marker, Nestin, expressed in the immature neuronal grafts, was reduced in the mature graft, reflective of downregulation of the gene during neuronal maturation as observed in development (Wiese et al., 2004) (Figure 2M) and confirmed by Nestin immunohistochemistry (Figures 2N–2Q). Greater differences in neuroectodermal gene expression between the undifferentiated and neuronal fate-restricted grafts (immature neuronal and mature neuronal) were not observed, largely due to the preferential default neural fate acquisition of PSCs (Munoz-Sanjuan and Brivanlou, 2002).

Next, the sensitivity of the approach to detect more subtle changes present between immature neuronal and mature neuronal grafts was assessed. Immunohistochemistry against GFP (to identify the LMX1A-GFP$^+$ cells) and TH (tyrosine hydroxylase) identified immature VM neural progenitors and mature dopaminergic neurons, respectively (Figures 3A–3C). Counts revealed that 21% ± 4% of cells in the undifferentiated grafts expressed GFP, a proportion that was enriched in the immature neuronal grafts (82% ± 1%) and maintained in the mature neuronal grafts (76% ± 4%) (Figure 3D). Xenograft-specific gene expression showed that LMX1A was increased 32.7 ± 1.7-fold in the immature neuronal grafts, and reduced 17.2 ± 2.3-fold in the mature neuronal grafts (Figure 3E), commensurate with the cell counts and in accordance with the previously described downregulation of the gene in maturing midbrain dopamine neurons during development. Counts of the mature dopaminergic marker TH identified 0.3% ± 0.04% cells in the undifferentiated grafts (TH$^+$/HNA$^+$), significantly increased in the immature neuronal grafts (4.4% ± 1.5%), and further increased in the mature neuronal grafts (7.2% ± 0.9%) (Figure 3F). Xenograft-specific gene-expression analysis supported the increase in TH with expression 8- and 12-fold greater in the immature and mature neuronal grafts, respectively, compared with those of undifferentiated cells (Figure 3G).

To demonstrate the utility of the approach to rapidly and comprehensively profile graft composition, we assessed nine additional genes anticipated to be expressed predominantly in neural specified grafts. Four genes expressed within VM neural progenitors included the midbrain-hindbrain restrictive gene Engrailed-1 (EN1), forebrain-midbrain gene OTX2, dopaminergic precursor Nurr1 (NR4A2), and pro-survival gene PITX3 (Figures 3H–3K). As expected, in comparison with undifferentiated grafts, upregulation of OTX2 (3-fold) and NR4A2 (16-fold) were observed in the immature neuronal grafts (rich in dopaminergic progenitors) but not the more mature (dopaminergic neuronal) grafts, reflective of the transient expression of these genes in embryonic development (Niclis et al., 2017b). PITX3 was upregulated in both the immature and mature neuronal grafts compared with the undifferentiated grafts. Surprisingly, EN1 was downregulated in the neuronal grafts, a result that likely reflects its many roles in early development inclusive of embryonic segmentation and limb formation. The five mature neuronal genes examined included G-protein-regulated inward-rectifier potassium channel 2 (GIRK2/KCNJ6) and Calbindin-1 (CALB1), markers of mature midbrain dopamine neuron subpopulations; dopamine transporter (DAT/SLC6A3) and vesicular monoamine transporter 2 (VMAT2/SLC18A2), both responsible for dopamine recycling; and vesicle-associated membrane protein Synaptobrevin

Figure 2. *In Vivo* Validation of a Xenograft Profile Using Species-Specific qPCR

(A–C) Representative micrograph depicting a graft of undifferentiated hPSCs 1 month after implantation (A), an immature neuronal graft at 1 month (B), and a mature neuronal graft at 5 months (C). Human nuclear antigen (HNA) labeled all human donor cells within the host, while Ki67 labeled proliferative cells.

(D and E) Quantification of HNA$^+$ cells within the grafts (D) closely mirrored the proportion of human-specific transcript (as a percentage of total transcript) (E).

(F and G) Quantification of Ki67$^+$ proliferative cells, significantly elevated in grafts of undifferentiated hPSC (F), reflected RNA transcript levels of the gene (G).

(H–M) Trilineage specification of cells within grafts of undifferentiated hPSCs was demonstrated by high transcript expression of endoderm (AFP, GATA6), mesoderm (BRACHYURY, COL2A1), and ectoderm (NCAM, NESTIN) genes. Appropriately, neural progenitor grafts (immature and mature neuronal grafts) contained only neuroectodermal gene expression.

(N–P) Representative images of NESTIN-immunoreactive cells.

(Q) Comparative levels of Nestin transcript were validated by the proportion of the graft showing NESTIN immunoreactivity.

Data in (D–G), (H–M), and (Q) represent mean ± SEM, one-way ANOVA, n = 5 grafts/group. Scale bars, 500 μm (A–C, N–P) and 100 μm (A′–C′).

Please cite this article in press as: Bye et al., Transcriptional Profiling of Xenogeneic Transplants: Examining Human Pluripotent Stem Cell-Derived Grafts in the Rodent Brain, Stem Cell Reports (2019), https://doi.org/10.1016/j.stemcr.2019.10.001

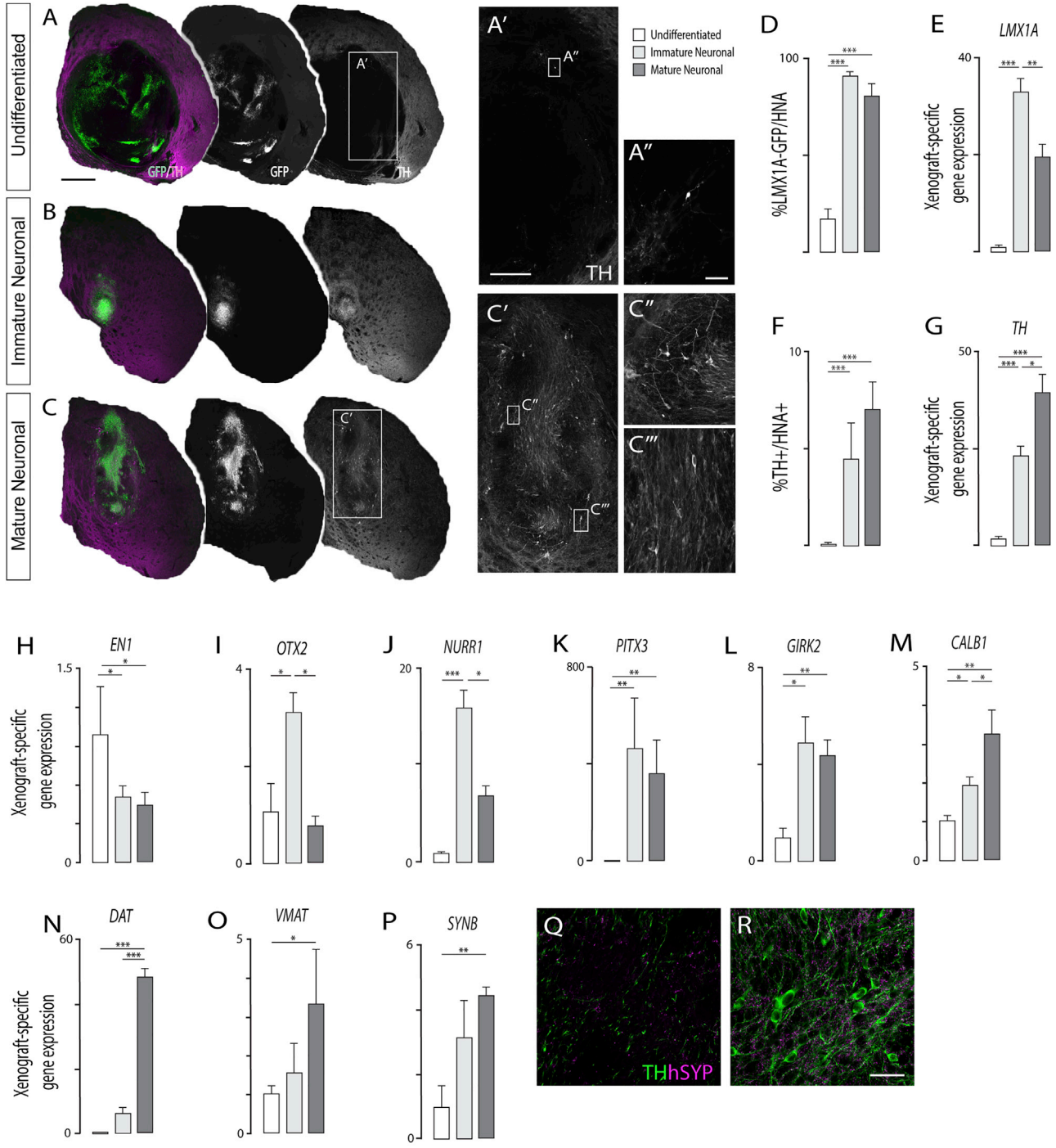

Figure 3. Validation of Midbrain Dopaminergic Identity of Xenografts Using qPCR

(A–C) Representative images from an undifferentiated hPSC (A), immature neuronal (B), and mature neuronal (C) graft depicting immunohistochemical expression of the early VM progenitor protein LMX1A (using an LMX1A-GFP reporter cell line) and mature dopamine neuron protein tyrosine hydroxylase (TH).

(D and E) Neural specification of the cells prior to transplantation (to a VM dopaminergic identity) (D) resulted in a significant increase in LMX1A-labeled cells that could be validated by species-specific LMX1A expression (E).

(F and G) Similarly, TH cell counts significantly increased within ongoing maturation of the neuronal grafts (F) compared with undifferentiated cell grafts (G), results that were validated by TH qPCR.

(legend continued on next page)

2 (SYNB/VAMP2), a mature presynaptic protein (Figures 3L–3P). Both GIRK2 and CALB1 were significantly increased in the immature and mature neuronal grafts. Not surprisingly, synaptic protein and transmitter associated genes DAT (49-fold), VMAT, and SYB2 showed significantly elevated expression in mature neuronal grafts compared with undifferentiated and immature neuronal grafts. The increased synaptic integration of the mature neuronal grafts was supported by increased histochemical labeling for human synaptophysin in mature (Figure 3R) compared with immature neuronal grafts (Figure 3Q).

Unbiased Characterization of Xenograft Composition and Identification of Transcriptional Changes Using RNA-Seq

Expanding on our species-specific transcript profiling approach, we sought to demonstrate the capacity for high throughput gene expression profiling using RNA-seq. Unlike qPCR, RNA-seq enables unbiased characterization of graft composition, confirming both known/anticipated gene expression and the presence of previously unidentifiable cell populations. RNA-seq can also provide new insight into gene expression, including recognition of mechanistic pathways contributing to graft function. Mixed-species cDNA libraries were prepared from the three graft types and subjected to paired-end, 75-bp sequencing to a target depth of approximately 20 million human reads (using the estimation of percentage xenograft RNA described in Figure 2E). A rapid and computationally efficient analysis pipeline was then established and implemented on the freely available Galaxy platform to make it accessible without specialist bioinformatics infrastructure or expertise. Reads were first mapped against the human genome, with only concordant (successfully aligned) reads subsequently mapped to the mouse genome. To minimize the risk of incorrectly specified reads, we adopted a high-stringency approach whereby all human reads found to also map to the mouse genome were discarded. The retained reads were designated as unique to the human genome, and therefore originated from the xenograft. An average of 94.4% ± 1.5% of reads were identified as unique to the human genome under these criteria across the three graft groups (Figure 4A). An average of 5.6% ± 1.5% of reads aligned to both human and mouse genome and were therefore discarded from analysis. These discarded reads mapped to 327 genes (defined as having an average of >10 reads) and showed no enrichment for any gene ontology category or pathway. Visual analysis of the ten most highly expressed genes from this list (Figures S2A–S2H) showed that the reads did not provide broad coverage across genes, aligning only to isolated fragments in both exonic and intergenic regions. The reads did not map preferentially to highly conserved regions or repeat elements, and displayed profiles consistent with originating from mouse RNA (significant mismatches to human genome, not overlapping with human-specific reads).

Taking advantage of the variation in graft size across the experimental groups, an estimate of the percentage of xenograft RNA required in the host tissue to provide a sufficient level of unique reads for analysis was assessed. Samples in which human RNA constituted just 2.5% of the total RNA (human RNA + mouse RNA) provided 86% reads unique to the human transcript using our high-stringency approach. This specificity increased exponentially such that with 6.7% human RNA, greater than 95% of the reads was classified as uniquely human, while grafts containing 35% human RNA yielded 99% unique reads (Figure 4B). Overall these results demonstrate that the analysis pipeline provided an efficient yield of species-specific reads from within a graft-host pool of tissue/RNA, including when the graft size was limited.

To determine whether the identified xenograft-specific reads were consistent with xenograft gene expression, we assembled transcripts for analysis. Examination of the global gene-expression profile by principal component analysis showed that the grafts clustered tightly as three distinct populations corresponding to the three grafted cell types (Figure 4C). A dissimilarity matrix and unsupervised clustering also showed the highest similarity between the replicates of each group, with immature neuronal and mature neuronal grafts the most closely related graft types (Figure 4D). Combined, these findings show that at a global expression level the xenograft-specific RNA-seq provided a highly specific expression profile consistent with the expected graft relationships.

To demonstrate the ability to use RNA-seq data to investigate known and unknown genes, we conducted xenograft-specific differential expression analysis (Figure 4E). A total of 11,010 differentially expressed genes were identified between the undifferentiated and

(H–P) Graft expression of early VM neural progenitor transgenes as revealed by species-specific qPCR primers for EN1 (H), OTX2 (I), NURR1 (J), PITX3 (K), as well as mature dopaminergic neuronal genes GIRK2 (L), CALB (M), DAT (N), VMAT (O), and SYNB (P).

(Q and R) Immunohistochemical labeling against TH (green) and human synaptophysin (hSYP, magenta) in immature (Q) and mature (R) neuronal grafts.

Data in (D–G) and (H–P) represent mean ± SEM, one-way ANOVA, n = 5 grafts/group. Scale bars, 500 μm (A–C), 200 μm (A and C′), and 50 μm (A″, C″, C‴, Q, and R).

Please cite this article in press as: Bye et al., Transcriptional Profiling of Xenogeneic Transplants: Examining Human Pluripotent Stem Cell-Derived Grafts in the Rodent Brain, Stem Cell Reports (2019), https://doi.org/10.1016/j.stemcr.2019.10.001

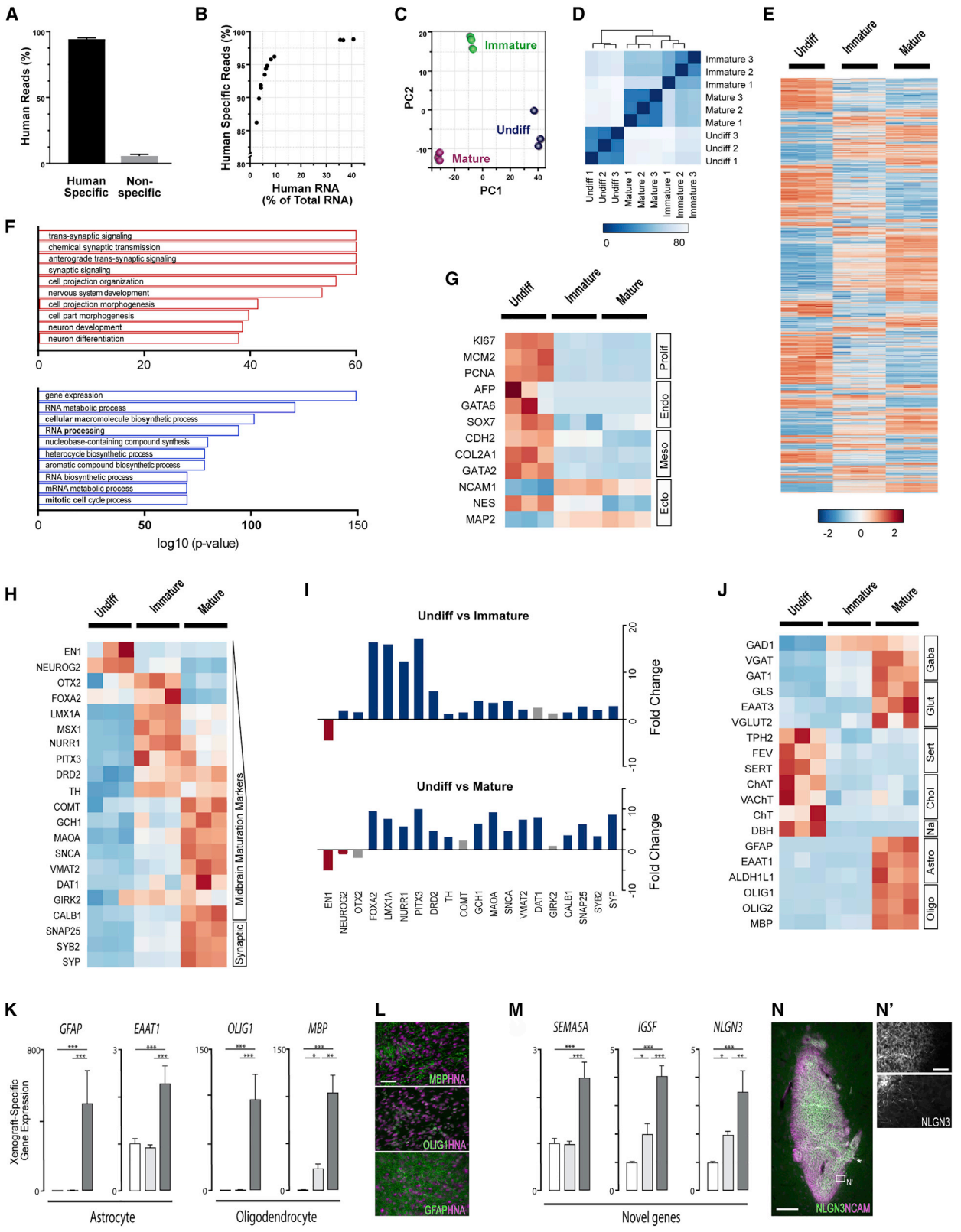

(legend on next page)

immature neuronal grafts (Table S1) and 12,449 genes between the undifferentiated and mature neuronal grafts (Table S2). Enriched gene ontology categories between undifferentiated and immature neuronal grafts identified upregulation of genes associated with synaptic signaling, axonal plasticity, and neural development, while RNA expression/processing and regulation of cell-cycle genes were downregulated (Figure 4F). Analysis of genes at this comparison identified 233 transcription factors potentially involved in the development of mature dopaminergic populations (Table S3), and 751 genes coding for axon guidance cues and receptors (Table S4), including several associated with the classical axon guidance superfamilies (Figure S3A). Many of the identified guidance cues have previously been implicated in dopamine axonal plasticity in rodents, but not yet in humans. These results provide an expansive list of targets for the potential modulation of cell populations or axon growth and plasticity in the maturation and integration of neuronal grafts.

The utility of the RNA-seq data to provide an unbiased characterization of the xenograft composition was first confirmed by assessment of known genes. Reflective of qPCR observations, Ki67 was highly expressed in the undifferentiated grafts (Figure 2G). Two additional pro-proliferation genes, DNA replication licensing factor MCM2 and proliferative cell nuclear antigen, were similarly upregulated (Figure 4G). Expression of three markers of an endodermal, mesodermal, and ectodermal lineage were all shown to be highly expressed in the undifferentiated cell group. In accordance with qPCR findings, endodermal and mesodermal genes were downregulated in the immature and mature neuronal grafts, while ectodermal markers remained expressed or were downregulated with ongoing graft maturation, reflective of neural development. Further validating the approach, numerous vascular-associated genes, such as essential hematopoietic transcription factor TAL1 and vasculogenesis gene FLT1, were upregulated in the undifferentiated PSC grafts (i.e., teratomas) but not neural progenitor grafts, and could be validated by qPCR (Figure S4).

Genes of known association with dopamine development and function showed increased expression in immature and mature neuronal grafts compared with the undifferentiated. Expression levels were represented as a heatmap (Figure 4H) and graphed as fold change for each of the comparisons between the graft types (Figure 4I). Markers of dopamine progenitors NEUROG2, FOXA2, OTX2, and LMX1A were most highly expressed in the immature neuronal grafts. NR4A2, PITX3, TH, and DRD2 were maintained at high levels in the both immature and mature neuronal grafts, while the mature genes GCH1, MAOA, SNCA (α-synuclein), VMAT2/SLC18A2, and DAT1/SLC6A3 were expressed most highly in the mature neuronal grafts. Confirming graft maturation, synaptic markers SNAP25 (Synaptosome Associated Protein 25), Synaptobrevin2 (SYNB/VAMP2), and SYP (Synaptophysin) were all significantly upregulated in the immature neuronal grafts, with even greater fold changes in the mature neuronal grafts (Figure 4I).

Figure 4. Unbiased Characterization of Xenograft Composition and Identification of Transcriptional Changes Using RNA-Seq

(A) Graph showing that 94.4% of the RNA-seq reads were uniquely mapped to the human genome (xenograft-specific) compared with 5.6% mapping to both human and host (ambiguous origin).

(B) Graph of the percentage of xenograft-specific reads compared with the size of the xenograft, showing that xenografts contributing $\geq$2.5% of the total RNA provide greater than 86% uniquely identified xenograft reads.

(C) Principal component analysis comparing the global gene-expression profile of each xenograft revealed the samples clustered into three distinct groups corresponding to the three graft types.

(D) A dissimilarity matrix of the global RNA profile correlation and unsupervised clustering showed the highest similarity between the replicates of each group.

(E) Heatmap of xenograft-specific gene expression.

(F) Graph of enriched gene ontology categories between undifferentiated and immature neuronal grafts.

(G) Heatmap of markers of germ layer lineages across the different graft types.

(H and I) Heatmap (H) and fold change (I) in gene expression for early and late VM dopaminergic neuron markers across the three graft types.

(J) Heatmap of non-dopaminergic neural cell type markers across the three graft types.

(K) Real-time qPCR verification of the expression of astrocyte (GFAP, EAAT1) and oligodendrocyte (OLIG1, MBP) genes.

(L and M) Representative immunohistochemistry (L) confirmed the presence of astrocytes and oligodendrocytes in the mature grafts. RNA-seq (M) identified a number of previously unidentified genes expressed in the mature neuronal grafts that could be verified by qPCR (SEMA5A, IGSF8, NLGN3).

(N) Immunohistochemical staining against NLGN3 (green) and human-specific NCAM confirmed the presence of this plasticity-associated gene within the mature neuronal grafts.

Data represent mean ± SEM, one-way ANOVA. (A–J) n = 3 grafts/group, (K and M) n = 5 grafts/group. Scale bars, 50 μm (L and N′) and 250 μm (N).

With less than 5% of VM neural progenitor grafts consisting of dopamine neurons, and yet little knowledge of the identity of the remaining >95% of cells, the dataset was screened for markers of other neural (non-dopaminergic) cell populations in the three grafted cell groups (Figure 4J). GABAergic (GAD1, VGAT/SLC32A1, GAT-1/SLC6A1) and glutamatergic (GLS, EAAT2/SLC1A2, VGlut2/SLC17A6) related genes were found to be expressed in the mature neuronal grafts, suggestive of the presence of these neuronal populations, while low expression of serotoninergic (TPH2, FEV, SERT/SLC6A4), cholinergic (ChAT, VAChT/SLC18A3, Ch/TSLC5A7), and noradrenergic (DBH) relative to undifferentiated grafts inferred that few of these neuronal populations were present within midbrain-differentiated grafts. Strikingly, non-neuronal cell types showed unexpectedly high expression within mature grafts, including astrocyte-associated genes GFAP, GLAST/SCL1A3, and ALDH1L1 as well as oligodendrocyte genes OLIG1, OLIG2, and MBP (Figure 4J). Xenograft-specific qPCR profiling and immunohistochemistry for the astrocyte markers GFAP and EAAT1/SLC1A3 as well as oligodendrocyte markers OLIG1 and MBP confirmed the presence of these cell populations in the mature grafts (Figures 4K and 4L). Retrospective assessment of matured VM progenitor grafts from four previous grafting studies performed in the laboratory validated and confirmed the significant proportions of these glial populations within grafts (data not shown). The identification of non-target cell types in the mature grafts demonstrates the utility of using xenograft-specific profiling to screen a broad range of phenotypic markers and cell populations.

Finally, the dataset was utilized to detect unique candidate genes that may participate in the maturation and plasticity of human PSC-derived VM progenitor grafts. We identified and examined three genes that show significantly elevated expression within the mature neuronal graft: SEMA5a (Semaphorin 5A), IGSF8 (Immunoglobulin superfamily member 8), and NGLN3 (Neuroligin 3). Each of these genes were confirmed by qPCR (Figure 4M) and NGLN3 further validated by immunohistochemistry, showing punctate expression throughout the graft and evident along graft-derived axonal fibers (Figures 4N and 4N′). A lack of reliable commercially available antibodies against Semaphorin A5 and IGSF8 prevented confirmation of expression at the protein level. These findings provide the first efforts and evidence for identifying the true composition of VM neural progenitor grafts and highlight the utility for this transcriptional profiling methodology in understanding graft composition. In the present context, the identification of new genes involved in graft maturation may present candidate proteins for manipulation in the future, targeted at promoting graft plasticity, integration, and function.

DISCUSSION

Here, we describe an approach to transcriptionally profile xenografts by discriminating the graft species RNA from host. The technique is designed to allow standardization and characterization of graft composition. The method is simple to implement, requires minimal experience, and is highly reproducible. The rapid design of primers and large quantity of RNA generated allows a greatly enhanced number of genes to be measured in a relatively short time frame, enabling a more thorough characterization of grafts inclusive of proteins/genes that are currently difficult to discriminate. When combined with RNA-seq, the technique provides an unbiased means to screen graft composition, investigate key questions pertaining to their function, and provide insight into strategies to enhance grafting outcomes.

Within this study we demonstrated the utility of this technique by analyzing three distinct human grafts within the rodent brain: grafts derived from undifferentiated hPSCs, grafts of immature neural progenitors, and grafts of neural progenitors left to mature *in situ* over several months. Xenograft-specific qPCR and RNA-seq were both demonstrated to accurately and efficiency discriminate xenograft gene expression from host. In addition, to cross-validate these qPCR and RNA-seq outcomes, we confirmed findings by immunohistochemistry, where antibodies were available, with quantification across the three methodologies generating highly correlated results.

Validated both *in vitro* and *in vivo*, the specificity of xenograft-specific (human) qPCR primers designed for the 30 genes examined in the present study showed 1,000- to >1,000,000-fold increased expression over the mouse host. As such, the technique allowed the presence of a xenograft to be confirmed and provided an estimate of the graft size. The proportion of xenograft RNA in individual pools of both graft and host tissue correlated with pre-determined cell numbers, while cell counts in experimental groups quantified in parallel using immunohistochemistry also closely matched these estimates, as did the proportion of xenograft RNA estimated by RNA-seq. The technique was also able to accurately detect both large- and small-scale changes in graft cell populations, such as the expression of germ layer lineage-specific markers in undifferentiated cell grafts, compared with the more subtle changes between immature and mature neuronal grafts.

A key advantage of this transcriptional profiling approach is the ease of tissue and RNA isolation, allowing standardization across laboratories and by separate operators. Here, grafts were placed into the striatum as it provided an easily identifiable structure for gross tissue dissection, yet gratfs could be transplanted in any location.

Following gross tissue dissection, RNA was readily isolated using a standard column-based protocol. The large amount of tissue ensured that the RNA extraction was robust against the effects of RNA loss or degradation and allowed the RNA quality and quantity to be analyzed using the commonly available nanodrop spectrophotometer. The mixed-species RNA population could then be directly interrogated with PCR or RNA-seq, making the process easily achievable for most laboratories without necessary expertise in microdissection, single-cell sorting, or RNA handling. To make the RNA-seq analysis methods employed here accessible without specialist bioinformatics experience or infrastructure, we implemented the analysis pipeline in the freely available Galaxy web platform (www.usegalaxy.org/), which provides point-and-click access to all the required bioinformatics tools (Afgan et al., 2018).

Analysis of graft composition is often hindered by the availability of reliable antibodies, or the presence of a protein of interest in both the graft and host tissue, thereby preventing the ability to discriminate the graft. This latter challenge is especially relevant when cells migrate and intersperse within host tissues or, in the context of neural transplants, when axons innervating regions distal to the site of implantation cannot be accurately separated. Xenograft-specific qPCR can readily detect any gene of interest in a graft, irrespective of the expression in the host or localization of the cell within surrounding tissues. As evidence, here we successfully designed primers against NURR1/NR4A2, EN1, and PITX3, examples where antibodies are unavailable or unreliable. Primers were also designed against genes expressed in both the graft and host tissue for which human-specific antibodies are not available, including broadly expressed neural (Nestin and GFAP), dopamine-specific (TH, DAT1/SLC6A3 and VMAT2/SLC18A2), and synaptic genes (SYB2/VAMP2). Added to this was the ability to detect rare events within transplants, such as proliferative Ki67 cells. Importantly, validity of the species-specific qPCR technique was demonstrated by similarities in gene-expression levels and cell counts within the grafts.

The inability to easily apply high-throughput gene or protein analysis to xenografts has been a major impediment to understanding graft integration and to identifying targets to enhance survival, maturation, and plasticity that may affect overall graft function. Xenograft-specific RNA-seq provides an easily accessible tool for the interrogation of the entire transcriptome of the transplant, allowing the investigation of previously unknown genes and pathways active in the graft. Importantly, the RNA-seq data also contain host-specific reads, thereby providing the means to examine interactions between the host tissue and the xenograft. Here, we have described the ability of xenograft-specific profiling to characterize graft composition. The ability to measure all the expressed genes in the graft allows an unbiased assessment and the ability to rapidly screen a range of cell phenotypes. No prior assumptions are required (as with antibody selection or qPCR primer design). The capture of all genes allows an expanded examination of markers, providing a thorough analysis of the target cell populations. The advantage of an unbiased and thorough coverage of phenotypic markers was exemplified here by the surprising expression of astrocyte and oligodendrocyte transcripts within grafts derived from fluorescence-activated cell sorting (FACS)-sorted VM neural progenitors. The presence of these cell types predominantly in mature grafts highlights the importance of long-term transplantation to accurately access the efficiency of differentiation protocols. The presence of small pools of poorly specified cells can expand to become a significant component of the graft at therapeutically relevant time frames, yet are not easily detected *in vitro*. These cell types are difficult to detect using conventional approaches, as host astrocyte and oligodendrocyte cells can migrate to infiltrate the graft and can only be directly detected using transgenic reporters. As the use of transgenic reporters is not feasible in a clinical setting, xenograft-specific profiling may present the only approach for pre-clinical testing of cell-differentiation protocols and cell batch verification prior to transplantation in patients. This is especially relevant in light of the two recently commenced clinical trials (Cyranoski, 2018; Barker et al., 2017) that adopt similar differentiation protocols to the one used here for the generation of midbrain dopamine neurons in the treatment of PD.

Finally, we demonstrated the utility of the species-specific RNA-seq approach in identifying previously unidentified genes within grafts. Here, we identified the expression of Nlgn3, Sema5A, and IGSF8 within mature neuronal grafts (compared with immature). These proteins have previously been implicated in axonal and synaptic plasticity (Bariselli et al., 2018; Kantor et al., 2004) or shown to be expressed on dopaminergic progenitors (Bye et al., 2015), but their roles in dopaminergic graft maturation remains to be explored. With previous work showing that hPSC-derived dopamine neurons show inferior plasticity to grafts derived from fetal tissue, identification of such genes may present new targets for modulating axonal growth and graft integration.

While we highlight the many benefits of whole tissue xenograft-specific transcriptomics, we also acknowledge the limitations. Unlike in single-cell sequencing, the transcript levels of individual cells are not captured individually. This restricts the classification of complex cell populations in the graft, with the xenograft-specific expression profile reflecting expression over the entire graft and unable to identify how many cells express a given gene or the level of expression within each cell. The approaches described here are thus highly complementary. One also recognizes that while RNA-seq profiling of the grafts is highly sensitive

and informative, it can also be expensive, especially when attempting to detect low numbers of grafted cells.

In summary, we describe an alternative approach to profiling xenografts. While demonstrated in the context of PSC-derived dopamine grafts for cell therapy in PD, this technique holds promise for profiling all xenografts, both within and outside the brain.

EXPERIMENTAL PROCEDURES

Cell Culture, Differentiation, and Sorting

Mouse RNA, containing mixed cell populations, inclusive of naive PSCs through to maturing cells from all germline lineages (ecto-, meso-, and endoderm), was obtained by pooling together undifferentiated mouse PSCs (E14TG2a obtained from ATCC, USA), whole mouse embryos (embryonic day 9.5 [E9.5] and E12.5), and maturing VM progenitors isolated from E10.5, E12.5, E14.5, and postnatal day 1 pups.

Human RNA, containing mixed cell populations, was generated by pooling undifferentiated human PSCs together with embryoid bodies (consisting of all germ layers), and varying maturation stages of VM neural progenitors and mature dopamine neurons (derived from differentiated human embryonic stem cells, as described below).

The H9 human embryonic stem cell line, expressing a green fluorescent reporter under the LMX1A promoter (H9 LMX1A-GFP), was cultured as previously described (Niclis et al., 2017b). Maintenance of pluripotency, prior to transplantation, was confirmed by morphology and the co-expression of OCT4 and SOX2 (Figures S1A–S1D). Undifferentiated hPSCs for transplantation were isolated by Accutase treatment and resuspended at 10,000 cells/μL.

To obtain a pool of purified neural progenitors of known origin, we differentiated PSCs to a VM fate as previously described (Niclis et al., 2017b), with correctly specified cells isolated by FACS for the GFP reporter gene, LMX1A. At 21 days *in vitro*, differentiating cultures were dissociated in Accutase to a single-cell suspension and FACS performed on a MoFlo cell sorter (Beckman Coulter). The generation of neural progenitors (of VM identity) was verified by co-expression of OTX2, FOXA2, and LMX1A (LMX1A-GFP$^+$) (Figures S1E–S1I). As previously described, >95% of GFP$^+$ cells co-expressed the ventral floorplate marker FOXA2 and forebrain-midbrain marker OTX2 (Niclis et al., 2017b), indicating that isolation of this GFP fraction (>80% of cells, Figure S1J) could enrich for correctly specified VM progenitors from the heterogeneous differentiated cultures by FACS. The FACS-isolated cell fraction was resuspended at 100,000 cells/μL in maturation medium and stored on ice until the time of implantation.

Cell Transplantation

All animal procedures were approved by The Florey Institute of Neuroscience and Mental Health Animal Ethics committee. Surgeries were performed on 30 athymic (Foxn1nu) nude mice under 2% isofluorane anesthesia. One microliter of cells was stereotaxically injected into the brains at the following coordinates, relative to bregma, as previously described (Kauhausen et al., 2013): 0.5 mm anterior, 2.1 mm lateral, and 3.2 mm below the surface of the dura. Transplant groups (n = 10/group) included: (1) undifferentiated hPSCs implanted for a period of 1 month; (2) VM progenitors, implanted for 1 month; and (3) VM progenitors, implanted for 6 months.

Tissue Processing and Histochemistry

After the prescribed period of graft survival (1 or 6 months), a subset of animals (n = 5/group) were killed by an overdose of sodium pentobarbitone (100 mg/kg), and transcardially perfused with 4% paraformaldehyde and cryosectioned. Immunohistochemistry was performed on fixed cell cultures or brain sections as previously described (Somaa et al., 2017). Primary antibodies and dilutions were as follows: 4′,6-diamidino-2-phenylindole (DAPI, 1 μg/mL; Sigma Aldrich), goat anti-FOXA2 (1:200; Santa Cruz Biotechnology), chicken anti-GFP (1:1,000; Abcam), rabbit anti-GFAP (1:800; DAKO), mouse anti-HNA (1:300; Millipore), rabbit anti-Ki67 (1:1,000; Thermo Fisher), mouse anti-NESTIN (1:200; Millipore), mouse anti-Neuroligin 3 (Nlgn3, 1:100; Synaptic Systems), mouse anti-OCT4 (1:100; Santa Cruz), rabbit anti-Olig1 (1:200; Millipore), rabbit anti-OTX2 (1:4,000; Millipore), mouse anti-PSA-NCAM (1:200; Santa Cruz), goat anti-SOX2 (1:200; R&D), mouse anti-synaptophysin (hSYP, 1:1,000; Enzo Life Sciences), sheep anti-TH (1:800; Pelfreeze), rabbit anti-TH (1:1,000; Pelfreeze). For quantification of HNA$^+$, Ki67$^+$, GFP$^+$, and TH$^+$ cells, images were captured at 20× magnification using a Zeiss Axio Observer Z.1 epifluorescence microscope. The density of Nestin labeling (percentage of immunoreactive pixels) was assessed from captured images and analyzed using ImageJ software.

RNA Isolation and Real-Time qPCR

The remaining animals (n = 5/group) were killed, the brains removed, and the striatum (containing the transplant) dissected from surrounding tissues and snap frozen. Tissue was homogenized using a TissueLyser LT (Qiagen) and total RNA extracted using the RNeasy Mini Kit (Qiagen). RNA yield and integrity were assessed using a Nanodrop One spectrophotometer (ThermoFisher Scientific) and confirmed using a Qubit (Thermo Fisher Scientific) and Tapestation (Agilent). The RNA was analyzed by qPCR or RNA-seq (Figure 1A).

Species-specific primers were designed using Primer3 (Untergasser et al., 2012), aimed at containing a minimum of 5-bp mismatches between graft and host, or two mismatches in the 5 bp at the 3′ end between species. Primers were targeted manually to regions of dissimilarity (identified by blasting paralog genes) or using Primer-BLAST and selecting both the xenograft and host species (*Homo sapiens* and *Mus musculus*, respectively in the present context) under organism in the "Primer Pair Specificity Checking Parameters." This identified primers specific only to the xenograft species (i.e., human). All xenograft-specific primers used in this study are listed in Figure 1B. Lineage-specific genes were selected from established markers used in the characterization of embryoid bodies (Tsankov et al., 2015; D'Antonio et al., 2017), and genes associated with vascular/endothelial cell differentiation identified from the MGI Gene Ontology Browser and Park et al. (2013). Genes were selected for confirmation with xenograft-specific qPCR based on showing highly significant upregulation in undifferentiated/teratoma grafts compared with neural progenitor grafts.

First-strand reverse transcription of 500 ng of RNA into cDNA was conducted using the SuperScript VILO cDNA Synthesis Kit (Invitrogen) according to the manufacturer's recommendations. Real-time qPCR was carried out on 25 ng of cDNA using the SYBR GreenER qPCR SuperMix Universal (Invitrogen) and run on a Rotor-Gene 6000 (Qiagen). To control for the size of the xenograft, we identified a xenograft-specific reference (housekeeping) gene. PSMB4, MTHFD1, CHAMP2A, and HPRT1 were tested and PSMB4 selected as the optimal housekeeping gene due to its high specificity and stable expression across the three graft types (Figure S1K). All qPCR data were analyzed using the ΔΔCt method (Pfaffl, 2001), using the xenograft-specific reference gene and expressed relative to the undifferentiated grafts. Five independent biological replicates were analyzed per group.

RNA Sequencing

cDNA libraries (containing graft and host RNA) were prepared using the TruSeq stranded mRNA sample preparation kit (Illumina). For sequencing, the final cDNA concentration of each sample was adjusted to generate a target of 20 million xenograft-specific reads using the percentage xenograft RNA calculated from the qPCR data. Note that due to the low percentage of xenograft RNA in the Immature neuronal grafts, 5.5 million reads were targeted. Libraries were subjected to paired-end, 75-bp sequencing on an Illumina HiSeq 2000 platform (Illumina) with three independent biological replicates analyzed per group.

Analysis was conducted on the Galaxy web platform (Afgan et al., 2018) using the Galaxy Australia server, and using Bioconductor (Huber et al., 2015) in the statistical analysis environment R (https://www.R-project.org/). Alignment to the human genome (Hg38) was performed using HISAT2 (2.0.3.3). Paired concordant reads were then mapped against the mouse reference genome (mm10). Under our high-stringency approach, all reads that aligned to both the human and mouse genome were discarded, accounting for an average of 5% of human reads.

Read counts for each gene were generated using HTSeq-count (0.6.1) on union mode (Anders et al., 2015). Differential expression analysis and principal component analysis were conducted with DeSeq2 (2.11.38) (Love et al., 2014). Expression heatmaps and unsupervised clustering were performed on log-transformed row-scaled expression values using the gplots package in R (Pfaffl, 2001). Gene ontology enrichment analysis on biological process was performed using the DAVID gene ontology browser (Huang da et al., 2009). Lists of human transcription factors and axon guidance cues and receptors were sourced from the HumanTFDB (Hu et al., 2019) and the KEGG PATHWAY Database (Kanehisa et al., 2017) (hsa04360, *Homo sapiens* axon guidance), respectively. The RNA-seq data generated from this study has been deposited in NCBI's Gene Expression Omnibus and are accessible through series accession number GEO: GSE126804.

Statistical Analysis

All data are presented as mean ± SEM. Statistical tests employed (inclusive of one-way ANOVA and Student's t tests) are stated in the figure legends. Alpha levels of $p < 0.05$ were considered significant with all statistical analysis performed using GraphPad Prism: *$p < 0.05$, **$p < 0.01$, and ***$p < 0.001$.

SUPPLEMENTAL INFORMATION

Supplemental Information can be found online at https://doi.org/10.1016/j.stemcr.2019.10.001.

AUTHOR CONTRIBUTIONS

C.L.P. and C.R.B. conceived the study and wrote the manuscript; C.R.B., V.P., I.R.L., C.W.G., C.P.J.H., L.H.T., and C.L.P performed the experiments; C.L.P. provided reagents; C.L.P. provided the funding.

ACKNOWLEDGMENTS

The authors thank Professor Alicia Oshlack, Dr. Jessica Kauhausen, Ms. Mong Tien, and Ms. Brianna Xuerub for their expert technical assistance, and acknowledge the support of the flow cytometry facility at the Melbourne Brain Centre and the MCRI/VCGS Sequencing Service and Development Platform. We thank Vinicius R.M. Carneiro for his assistance in software development to screen transcript homology. V.P. and I.R.d.L. were supported by The University of Melbourne International Scholarships, Australia. C.W.G. is supported by an Australian Postgraduate Award. C.L.P. was supported by a Senior Medical Research Fellowship provided by the Viertel Charitable Foundation, Australia. This research was funded by the National Health and Medical Research Council Australia project grant APP1102704 and Stem Cells Australia. The Florey Institute of Neuroscience and Mental Health acknowledges strong support from the Victorian Government and in particular the funding from the Operational Infrastructure Support Grant.

Received: April 17, 2019
Revised: October 1, 2019
Accepted: October 1, 2019
Published: October 31, 2019

REFERENCES

Afgan, E., Baker, D., Batut, B., van den Beek, M., Bouvier, D., Cech, M., Chilton, J., Clements, D., Coraor, N., Grüning, B.A., et al. (2018). The Galaxy platform for accessible, reproducible and collaborative biomedical analyses: 2018 update. Nucleic Acids Res. *46*, W537–W544.

Anders, S., Pyl, P.T., and Huber, W. (2015). HTSeq—a Python framework to work with high-throughput sequencing data. Bioinformatics *31*, 166–169.

Bariselli, S., Hornberg, H., Prevost-Solie, C., Musardo, S., Hatstatt-Burkle, L., Scheiffele, P., and Bellone, C. (2018). Role of VTA dopamine neurons and neuroligin 3 in sociability traits related to nonfamiliar conspecific interaction. Nat. Commun. *9*, 3173.

Barker, R.A., Parmar, M., Studer, L., and Takahashi, J. (2017). Human trials of stem cell-derived dopamine neurons for Parkinson's disease: dawn of a new era. Cell Stem Cell *21*, 569–573.

Bye, C.R., Jonsson, M.E., Bjorklund, A., Parish, C.L., and Thompson, L.H. (2015). Transcriptome analysis reveals transmembrane targets on transplantable midbrain dopamine progenitors. Proc. Natl. Acad. Sci. U S A *112*, E1946–E1955.

Cyranoski, D. (2018). 'Reprogrammed' stem cells implanted into patient with Parkinson's disease. Nat. News https://doi.org/10.1038/d41586-018-07407-9.

D'Antonio, M., Woodruff, G., Nathanson, J.L., D'Antonio-Chronowska, A., Arias, A., Matsui, H., Williams, R., Herrera, C., Reyna, S.M., Yeo, G.W., et al. (2017). High-throughput and cost-effective characterization of induced pluripotent stem cells. Stem Cell Reports *8*, 1101–1111.

Doi, D., Samata, B., Katsukawa, M., Kikuchi, T., Morizane, A., Ono, Y., Sekiguchi, K., Nakagawa, M., Parmar, M., and Takahashi, J. (2014). Isolation of human induced pluripotent stem cell-derived dopaminergic progenitors by cell sorting for successful transplantation. Stem Cell Reports *2*, 337–350.

Etzrodt, M., Endele, M., and Schroeder, T. (2014). Quantitative single-cell approaches to stem cell research. Cell Stem Cell *15*, 546–558.

Hu, H., Miao, Y.R., Jia, L.H., Yu, Q.Y., Zhang, Q., and Guo, A.Y. (2019). AnimalTFDB 3.0: a comprehensive resource for annotation and prediction of animal transcription factors. Nucleic Acids Res. *47*, D33–D38.

Huang da, W., Sherman, B.T., and Lempicki, R.A. (2009). Systematic and integrative analysis of large gene lists using DAVID bioinformatics resources. Nat. Protoc. *4*, 44–57.

Huber, W., Carey, V.J., Gentleman, R., Anders, S., Carlson, M., Carvalho, B.S., Bravo, H.C., Davis, S., Gatto, L., Girke, T., et al. (2015). Orchestrating high-throughput genomic analysis with Bioconductor. Nat. Methods *12*, 115–121.

Kanehisa, M., Furumichi, M., Tanabe, M., Sato, Y., and Morishima, K. (2017). KEGG: new perspectives on genomes, pathways, diseases and drugs. Nucleic Acids Res. *45*, D353–D361.

Kantor, D.B., Chivatakarn, O., Peer, K.L., Oster, S.F., Inatani, M., Hansen, M.J., Flanagan, J.G., Yamaguchi, Y., Sretavan, D.W., Giger, R.J., et al. (2004). Semaphorin 5A is a bifunctional axon guidance cue regulated by heparan and chondroitin sulfate proteoglycans. Neuron *44*, 961–975.

Kauhausen, J., Thompson, L.H., and Parish, C.L. (2013). Cell intrinsic and extrinsic factors contribute to enhance neural circuit reconstruction following transplantation in Parkinsonian mice. J. Physiol. *591*, 77–91.

Kirkeby, A., Grealish, S., Wolf, D.A., Nelander, J., Wood, J., Lundblad, M., Lindvall, O., and Parmar, M. (2012). Generation of regionally specified neural progenitors and functional neurons from human embryonic stem cells under defined conditions. Cell Rep. *1*, 703–714.

Kirkeby, A., Nolbrant, S., Tiklova, K., Heuer, A., Kee, N., Cardoso, T., Ottosson, D.R., Lelos, M.J., Rifes, P., Dunnett, S.B., et al. (2017). Predictive markers guide differentiation to improve graft outcome in clinical translation of hESC-based therapy for Parkinson's disease. Cell Stem Cell *20*, 135–148.

Kriks, S., Shim, J.W., Piao, J., Ganat, Y.M., Wakeman, D.R., Xie, Z., Carrillo-Reid, L., Auyeung, G., Antonacci, C., Buch, A., et al. (2011). Dopamine neurons derived from human ES cells efficiently engraft in animal models of Parkinson's disease. Nature *480*, 547–551.

La Manno, G., Gyllborg, D., Codeluppi, S., Nishimura, K., Salto, C., Zeisel, A., Borm, L.E., Stott, S.R.W., Toledo, E.M., Villaescusa, J.C., et al. (2016). Molecular diversity of midbrain development in mouse, human, and stem cells. Cell *167*, 566–580.e19.

Love, M.I., Huber, W., and Anders, S. (2014). Moderated estimation of fold change and dispersion for RNA-seq data with DESeq2. Genome Biol. *15*, 550.

Munoz-Sanjuan, I., and Brivanlou, A.H. (2002). Neural induction, the default model and embryonic stem cells. Nat. Rev. Neurosci. *3*, 271–280.

Niclis, J.C., Gantner, C.W., Hunt, C.P.J., Kauhausen, J.A., Durnall, J.C., Haynes, J.M., Pouton, C.W., Parish, C.L., and Thompson, L.H. (2017a). A PITX3-EGFP reporter line reveals connectivity of dopamine and non-dopamine neuronal subtypes in grafts generated from human embryonic stem cells. Stem Cell Reports *9*, 868–882.

Niclis, J.C., Gantner, C.W., Alsanie, W.F., McDougall, S.J., Bye, C.R., Elefanty, A.G., Stanley, E.G., Haynes, J.M., Pouton, C.W., Thompson, L.H., et al. (2017b). Efficiently specified ventral midbrain dopamine neurons from human pluripotent stem cells under xeno-free conditions restore motor deficits in parkinsonian rodents. Stem Cell Transl. Med. *6*, 937–948.

Park, C., Kim, T.M., and Malik, A.B. (2013). Transcriptional regulation of endothelial cell and vascular development. Circ. Res. *112*, 1380–1400.

Pfaffl, M.W. (2001). A new mathematical model for relative quantification in real-time RT-PCR. Nucleic Acids Res. *29*, e45.

Samata, B., Doi, D., Nishimura, K., Kikuchi, T., Watanabe, A., Sakamoto, Y., Kakuta, J., Ono, Y., and Takahashi, J. (2016). Purification of functional human ES and iPSC-derived midbrain dopaminergic progenitors using LRTM1. Nat. Commun. *7*, 13097.

Somaa, F.A., Wang, T.Y., Niclis, J.C., Bruggeman, K.F., Kauhausen, J.A., Guo, H., McDougall, S., Williams, R.J., Nisbet, D.R., Thompson, L.H., et al. (2017). Peptide-based scaffolds support human cortical progenitor graft integration to reduce atrophy and promote functional repair in a model of stroke. Cell Rep. *20*, 1964–1977.

Tang, F., Barbacioru, C., Bao, S., Lee, C., Nordman, E., Wang, X., Lao, K., and Surani, M.A. (2010). Tracing the derivation of embryonic stem cells from the inner cell mass by single-cell RNA-Seq analysis. Cell Stem Cell *6*, 468–478.

Trounson, A., and McDonald, C. (2015). Stem cell therapies in clinical trials: progress and challenges. Cell Stem Cell *17*, 11–22.

Tsankov, A.M., Akopian, V., Pop, R., Chetty, S., Gifford, C.A., Daheron, L., Tsankova, N.M., and Meissner, A. (2015). A qPCR ScoreCard quantifies the differentiation potential of human pluripotent stem cells. Nat. Biotechnol. *33*, 1182–1192.

Untergasser, A., Cutcutache, I., Koressaar, T., Ye, J., Faircloth, B.C., Remm, M., and Rozen, S.G. (2012). Primer3—new capabilities and interfaces. Nucleic Acids Res. *40*, e115.

Wiese, C., Rolletschek, A., Kania, G., Blyszczuk, P., Tarasov, K.V., Tarasova, Y., Wersto, R.P., Boheler, K.R., and Wobus, A.M. (2004). Nestin expression—a property of multi-lineage progenitor cells? Cell. Mol. Life Sci. *61*, 2510–2522.

Appendix 3. Viral delivery of GDNF promotes functional integration of human stem cell grafts in Parkinson's disease

Article

Cell Stem Cell

Viral Delivery of GDNF Promotes Functional Integration of Human Stem Cell Grafts in Parkinson's Disease

Graphical Abstract

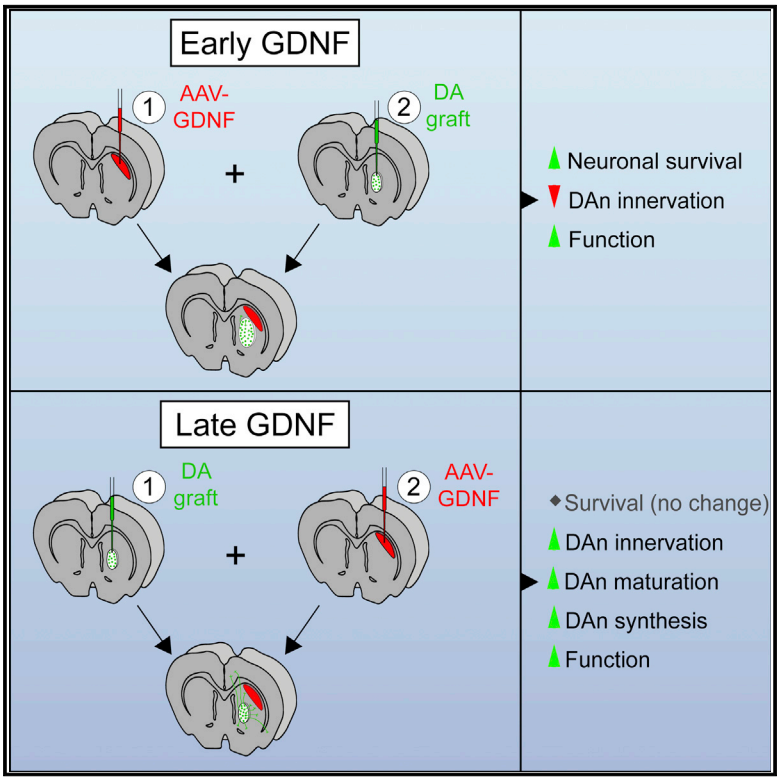

Highlights

- DAn grafting into a GDNF-rich host aids pan-neuronal survival but impedes plasticity
- Delaying graft exposure to GDNF increases DAn maturation, plasticity, and function
- GDNF promotes functional integration of DAn grafts via MAPK signaling
- Modulating the host environment can improve the integration of human neural grafts

Authors

Carlos W. Gantner, Isabelle R. de Luzy, Jessica A. Kauhausen, ..., Deniz Kirik, Lachlan H. Thompson, Clare L. Parish

Correspondence

clare.parish@florey.edu.au

In Brief

Gantner et al. provide preclinical evidence that the timely overexpression of glial cell-derived neurotrophic factor (GDNF) within the host brain can promote the maturation, plasticity, and functional integration of human stem cell-derived dopamine grafts in a rodent model of Parkinson's disease.

Gantner et al., 2020, Cell Stem Cell *26*, 1–16
April 2, 2020
https://doi.org/10.1016/j.stem.2020.01.010

CellPress

Please cite this article in press as: Gantner et al., Viral Delivery of GDNF Promotes Functional Integration of Human Stem Cell Grafts in Parkinson's Disease, Cell Stem Cell (2020), https://doi.org/10.1016/j.stem.2020.01.010

Cell Stem Cell
Article

Viral Delivery of GDNF Promotes Functional Integration of Human Stem Cell Grafts in Parkinson's Disease

Carlos W. Gantner,[1] Isabelle R. de Luzy,[1] Jessica A. Kauhausen,[1] Niamh Moriarty,[1] Jonathan C. Niclis,[1] Christopher R. Bye,[1] Vanessa Penna,[1] Cameron P.J. Hunt,[1] Charlotte M. Ermine,[1] Colin W. Pouton,[2] Deniz Kirik,[3] Lachlan H. Thompson,[1] and Clare L. Parish[1,4,*]

[1]Florey Institute of Neuroscience and Mental Health, Parkville, VIC 3052, Australia
[2]Monash Institute of Pharmaceutical Sciences, Monash University, Parkville, VIC 3052, Australia
[3]Brain Repair and Imaging in Neural Systems (B.R.A.I.N.S) Unit, Department of Experimental Medical Science, Lund University, Lund 221 00, Sweden
[4]Lead Contact
*Correspondence: clare.parish@florey.edu.au
https://doi.org/10.1016/j.stem.2020.01.010

SUMMARY

Dopaminergic neurons (DAns), generated from human pluripotent stem cells (hPSCs), are capable of functionally integrating following transplantation and have recently advanced to clinical trials for Parkinson's disease (PD). However, pre-clinical studies have highlighted the low proportion of DAns within hPSC-derived grafts and their inferior plasticity compared to fetal tissue. Here, we examined whether delivery of a developmentally critical protein, glial cell line-derived neurotrophic factor (GDNF), could improve graft outcomes. We tracked the response of DAns implanted into either a GDNF-rich environment or after a delay in exposure. Early GDNF promoted survival and plasticity of non-DAns, leading to enhanced motor recovery in PD rats. Delayed exposure to GDNF promoted functional recovery through increases in DAn specification, DAn plasticity, and DA metabolism. Transcriptional profiling revealed a role for mitogen-activated protein kinase (MAPK)-signaling downstream of GDNF. Collectively, these results demonstrate the potential of neurotrophic gene therapy strategies to improve hPSC graft outcomes.

INTRODUCTION

Clinical trials have provided evidence that human ventral midbrain (VM) dopamine (DA) progenitors, transplanted into the denervated striatum of Parkinson's disease (PD) patients, can structurally integrate, restore DA transmission, and alleviate motor symptoms (Barker et al., 2013). Hindering this therapy has been the reliance on human fetal tissue that, in addition to availability and ethical constraints, remains poorly standardized. Consequently, focus has shifted to generating replacement DA progenitors from human pluripotent stem cells (hPSC), including embryonic stem cells (ESCs) and induced pluripotent stem cells (IPSCs), that are capable of generating derivatives of all three germ layers *in vitro*, including DA progenitors. Employing highly standardized procedures, recent years have seen rapid advancements in protocols for the generation of bona fide VM DA neurons from both human embryonic stem cells (hESCs) and IPSCs (Kirkeby et al., 2012; Kriks et al., 2011; Niclis et al., 2017a).

Following transplantation, hPSC-derived DA progenitors are capable of maturing into DA neurons, adopting appropriate target acquisition and restoring gross motor deficits (Grealish et al., 2014; Niclis et al., 2017b). However, overall proportions of DA neurons within the grafts remain low. In part, this likely reflects the poor survival of these cells during and immediately following transplantation, as reported for fetal tissue grafts (Castilho et al., 2000; Olanow et al., 1996). In addition, transplanted hESC-derived DA neurons show inferior axonal growth compared to human fetal VM donor tissue. Related, Grealish et al., (2014), employing a human-specific neural cell adhesion molecule and tyrosine hydroxylase (TH) co-immunoreactivity to selectively compare graft-derived DA axons from hESC-derived and human fetal donor grafts, demonstrated reduced innervation of host A9-target tissue (dorsolateral and dorsomedial striatum) from the ESC-derived grafts. Such observations suggest that greater efforts to promote survival and axonal plasticity of hPSC-derived DA neurons following transplantation are required to improve outcomes after grafting and make this therapy clinically competitive.

Unlike the developing brain that contains a cocktail of neurotrophic and morphogenic proteins that influence survival, differentiation, and axonal connectivity, the adult brain is a notably less permissive environment for the survival and integration of transplanted progenitors, with many developmental cues down-regulated or absent. First identified for its role in the survival and plasticity of embryonic midbrain DA neurons in culture (Lin et al., 1993), glial cell line-derived neurotrophic factor (GDNF) has been shown to increase the survival, plasticity, and metabolism of DA neurons in pre-clinical and clinical studies for PD (for reviews, see Björklund et al., 1997; Kirik et al., 2017; Thompson and Björklund, 2012). Recombinant GDNF protein has also been used to promote the survival of DA progenitors within fetal donor

preparations prior to transplantation (Rosenblad et al., 1996), with studies in rodents and non-human primates demonstrating the benefits of prolonged delivery into the host tissue (via infusion) (Ahn et al., 2005; Johansson et al., 1995; Sinclair et al., 1996; Yurek, 1998) or injection of viral vectors) (Elsworth et al., 2008; Georgievska et al., 2004; Kauhausen et al., 2013; Redmond et al., 2009; Thompson et al., 2009; Wakeman et al., 2014; Winkler et al., 2006) for promoting survival, plasticity, and functionally appropriate integration of DA-rich fetal VM tissue grafts.

Here, we have assessed the impact of long-term GDNF overexpression on hPSC-derived VM DA progenitor grafts. We showed that exposure of the graft to GDNF had a significant impact on survival, plasticity, and functional integration and notably that the timing of exposure was an important variable. Using a recombinant adeno-associated viral (AAV) vector to overexpress GDNF in the denervated host striatum, we showed that transplanting hESC-derived DA progenitors directly into a GDNF-rich environment promoted survival yet impacted on the capacity of the graft to innervate the host striatum. In contrast, exposure of the DA progenitors to GDNF several weeks after implantation had no effect on survival but positively impacted on DA neuron maturation, innervation of DA-relevant targets, and functional outcomes. With hPSC therapies rapidly moving toward the clinic, these findings have important implications for promoting survival, plasticity, integration, and thereby function of hPSC-derived DA grafts, targeted at restoring DA transmission in PD patients.

RESULTS

Validation of DA Differentiation, GDNF Expression, and GDNF-Induced Motor Recovery

Midbrain DA neurons were differentiated from an hESC line expressing enhanced GFP under the PITX3 promoter (PITX3-GFP) using a recent, clinically relevant xenogeneic-free protocol (Figure 1A) (Niclis et al., 2017a). Enrichment of DA progenitors was confirmed by $OTX2^+/FOXA2^+$ co-expression at 15 days *in vitro* (DIV) (Figure 1B), with limited PITX2, PAX6, or $BARHL1^+$ cells (indicative of unintended lateral or rostral midbrain contaminants) (Figure 1C). While progenitors were isolated at 20 DIV for transplantation, parallel cultures, extended to 25 DIV, confirmed the ability of the cells to generate bona fide VM DA neurons, displaying high proportions of GFP (PITX3), TH, and FOXA2 co-expression (Figure 1E). qPCR analysis of maturing DA progenitors *in vitro* confirmed upregulation of early and late DA determinant genes LMX1A and TH, respectively, and the canonical GDNF receptor, GFRα1 (Figure 1D). Maintenance of Ret expression within VM progenitors (also expressed on hPSCs) (Kriks et al., 2011), was confirmed by real-time PCR (Figure S1), indicating the VM progenitors were capable of responding to GDNF at the time of transplantation. Long-term stable expression of AAV5-GDNF (Figures 1F and S2) and the control AAV5-mCherry (Figure S3B) were observed at 6 months within the host striatum, as well as along the ipsilateral striatonigral tract, using GDNF and RFP immunohistochemistry, respectively.

Rats receiving 6-OHDA lesions alone (6-OHDA), lesion + AAV-GDNF (GDNF), lesion + PITX3-GFP VM DA progenitor transplants (graft), or lesion + combined AAV-GDNF and PITX3-GFP VM DA graft (graft + GDNF) underwent a battery of motor tests prior to grafting and at 16 and 24 weeks post-transplantation (Figure 1G). All rats included in the study showed an amphetamine-induced rotational asymmetry of >5 rotations/min pre-transplantation, that was stable for 24 weeks in the 6-OHDA lesion control group (Figure 1H). As expected, in the absence of a cell graft, GDNF did not reverse rotational behavior (Figure 1H, red line). In contrast, rats receiving a graft with or without GDNF showed complete recovery by 24 weeks (Figure 1H, green and blue lines). In the cylinder test (an assessment of spontaneous motor asymmetry), motor dysfunction was reflected as a decrease in weight-bearing contralateral paw touches following lesioning (Figure 1I). Recovery was only observed in the graft + GDNF group at 24 weeks (Figure 1I).

Transplantation of PSC-Derived DA Precursors into a GDNF-Overexpressing Environment Promotes Graft Survival but Disrupts Axonal Targeting

At 24 weeks after transplantation, all animals (±GDNF) displayed surviving grafts, as confirmed by GFP expression (Figures 2A and 2B). Importantly, we found no gross evidence of aberrant graft growth. This was supported by extremely few $Ki67^+$ cells within the grafts at 24 weeks, suggesting that the *in vitro* differentiation and subsequent maturation of the pluripotent stem cell-derived progenitors *in situ* was sufficient to deplete proliferative pools. In all animals the GFP^+ grafts were predominantly confined to the striatum. The validity of PITX3-eGFP as an accurate marker of DA neurons was confirmed by co-expression with the rate-limiting enzyme in DA synthesis, TH, (Figures S3C and S4Ai, S4Aii, S4Bi, and S4Bii and using confocal microscopy), with >85% of cells co-expressing TH^+ and GFP^+. GFP^+ neurons commonly clustered at the periphery of the graft with significant GFP^- areas within the graft core (Figures 2A and 2B), as previously observed for both fetal and PSC-derived VM grafts. Volumetric analysis confirmed that GDNF significantly increased graft size at 6 months (graft: 7.04 ± 0.96 mm^3 and graft + GDNF: 13.33 ± 1.72 mm^3) (Figure 2C). Both GFP^+ (graft: 5,268 ± 654; graft + GDNF: 9,476 ± 1,462) and TH^+ (graft: 4,092 ± 602; graft + GDNF: 7,986 ± 1375) neuron numbers commensurately increased with graft volume in the presence of GDNF, such that DA cell density was unchanged (Figures 2D and 2E), indicating that GDNF promoted survival but not DA differentiation. As an index of GDNF-induced maturation of the graft, assessment of the proportion of GFP^+ (PITX3) cells that co-expressed TH revealed a subtle but not significant increase (cells: 79.29% ± 9.0%, cells + GDNF: 91.5% ± 7.3%, $p = 0.3$, data not shown). Interestingly, the total GFP^- population also increased concomitantly, suggesting that GDNF also influenced non-DA cells within the grafts (Figure 2F). Note, AAV-mCherry had no impact on motor function (data not shown) or the neural composition of the graft (inclusive of TH^+HNA^+ neurons, $NeuN^+HNA^+$ neurons, APC^+HNA^+ mature oligodendrocyte, and $GFAP^+$ astrocyte density) (Figures S3D–S3G), compared to grafts of cells alone and were not further analyzed.

To assess the competence of transplanted DA progenitors to mature into correctly specified A9 or A10 DA subtypes, we assessed calbindin (CALB) or GIRK2 immunoreactivity within GFP^+ DA neurons (Figures 2H and 2I). Specification of $GFP^+/GIRK2^+$ or $GFP^+/CALB^+$ was constant regardless of GDNF

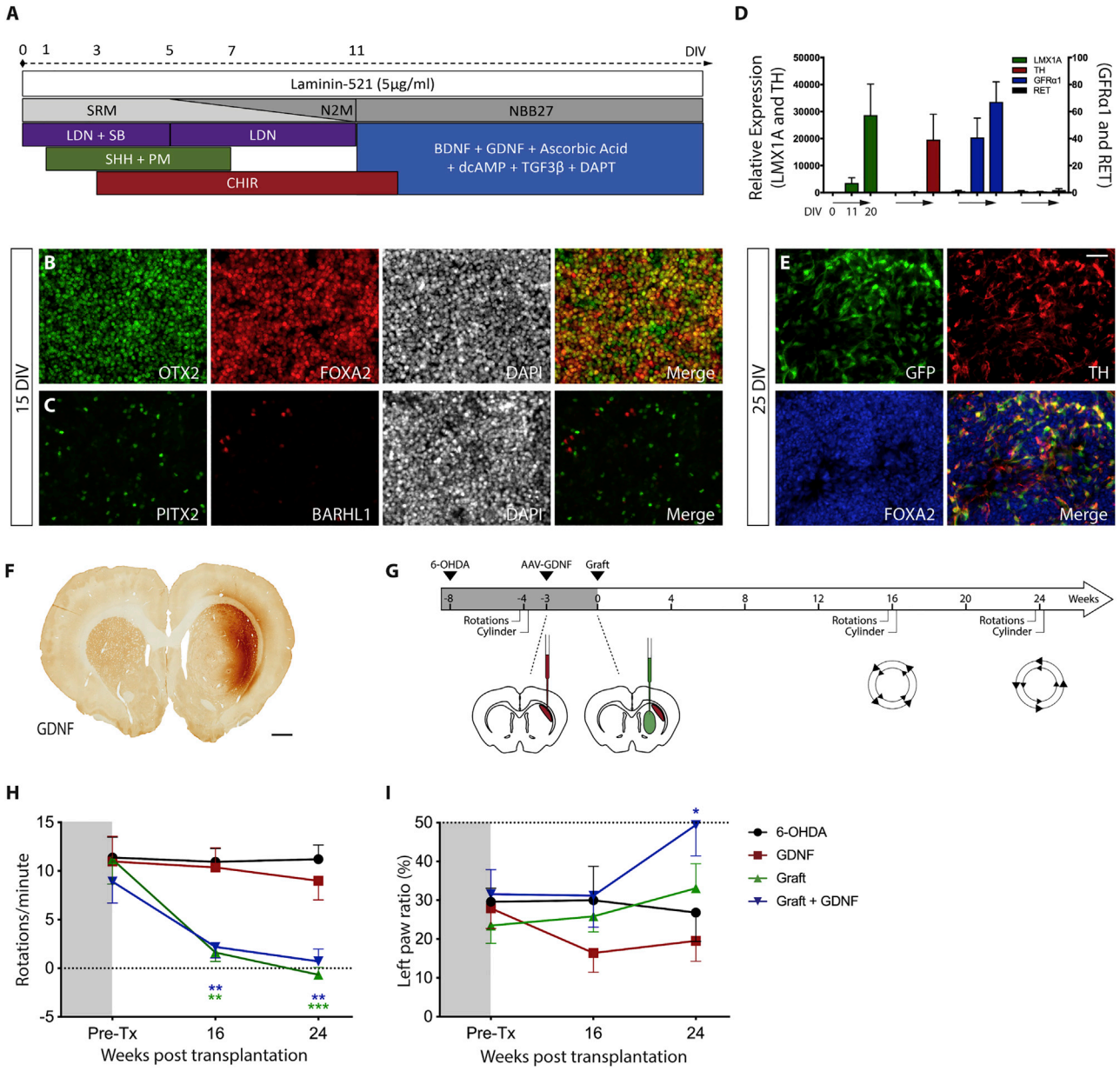

Figure 1. Exposure of hESC-Derived DA Transplants to GDNF, from the Time of Implantation, Improved Motor Deficits in Parkinsonian Rats

(A) Differentiation protocol for hESCs into VM progenitors, suitable for transplantation.

(B) Photomicrographs showing high OTX2 and FOXA2 co-expression within progenitors at 15 DIV.

(C) Low numbers of PITX2$^+$ and BARHL1$^+$ cells, indicative of off-target rostral progenitor populations, validated efficiency of the VM differentiation.

(D) Graph showing mRNA levels of the pluripotency marker OCT4, VM progenitor/neuron markers (LMX1A, NURR1, TH), and GDNF receptors (RET, GFRα1) during differentiation, relative to undifferentiated human ESCs. Values normalized to HPRT1 expression. n = 3 independent cultures, mean ± SEM.

(E) Validation of VM differentiation into DA neurons, as confirmed by PITX3-GFP, TH, and FOXA2 expression at 25 DIV.

(F) Coronal section of the rat brain illustrating sustained GDNF expression 6 months after intrastriatal injection of AAV-GDNF.

(G) Schematic summary of *in vivo* study.

(H) All grafted animals showed complete reversal of amphetamine-induced rotations at 24 weeks.

(I) Correction of forelimb asymmetry in the cylinder test was only observed in rats receiving grafts in the presence of GDNF. Scale bars, 50 µm (B, C, and E); 1 mm (F). Lesion, n = 11 rats; GDNF, n = 7; graft, n = 7, and graft + GDNF, n = 7. Two-way ANOVA compared to 6-OHDA with Dunnett's correction for multiple comparisons. Data presented as mean ± SEM.

expression. In contrast the percentage of GFP$^+$/GIRK2$^+$/CALB$^+$ co-expressing neurons significantly increased in Graft + GDNF compared to graft animals (21.17% ± 0.97% and 41.23% ± 6.24%, respectively), such that only 16% of grafted GFP$^+$ cells failed to adopt the A9/A10 fate in the presence of GDNF, compared to 31% of GFP$^+$ cells in the absence of GDNF

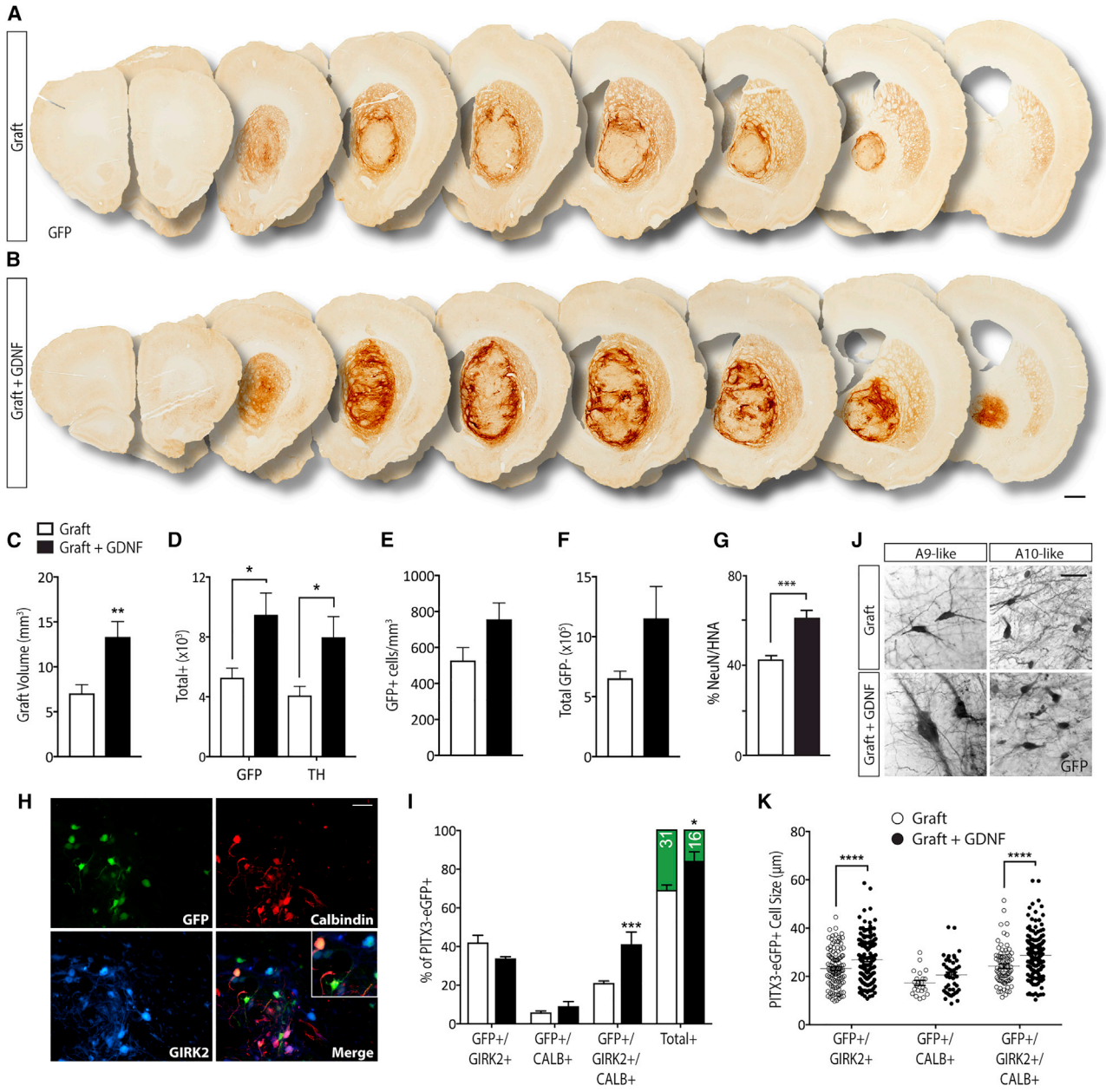

Figure 2. Implantation of hPSC-Derived DA Progenitors into a GDNF-Rich Environment Promotes Graft Survival

(A and B) Photomontage illustrating a representative hPSC-derived VM progenitor graft in the absence (A) and presence (B) of AAV-GDNF, showing PITX3-GFP expression.

(C) Assessment of graft volume showed significantly larger grafts in the presence of GDNF.

(D and E) GFP^+ and TH^+ cell numbers commensurately increases with volume in animals receiving transplants in the presence of GDNF (D) resulting in unchanged GFP^+ cell density (E).

(F) GDNF exposure also increased the number of GFP^- cells within grafts.

(G) Cell + GDNF grafts showed enhanced maturation, as revealed by the increased proportion of $NeuN^+$ neurons.

(H and I) Representative image showing GFP (PITX3) cells co-expressing GIRK2 and/or calbindin (CALB), indicative of A9-like and A10-like VM DA neurons (H) and their relative contribution (I). Note, green bar represents % of GFP^+ cells that are neither $GIRK2^+$ or $CALB^+$.

(J) Representative images of A9-like (large, angled soma) or A10-like cells (small, circular soma) ± GDNF.

(K) GFP/GIRK co-expressing neurons were significantly larger in the presence of GDNF suggestive of increased maturation.

Scale bars, 1 mm (A and B); 50 μm (H and I). All data expressed as mean ± SEM, Student's t test (n = 7/group).

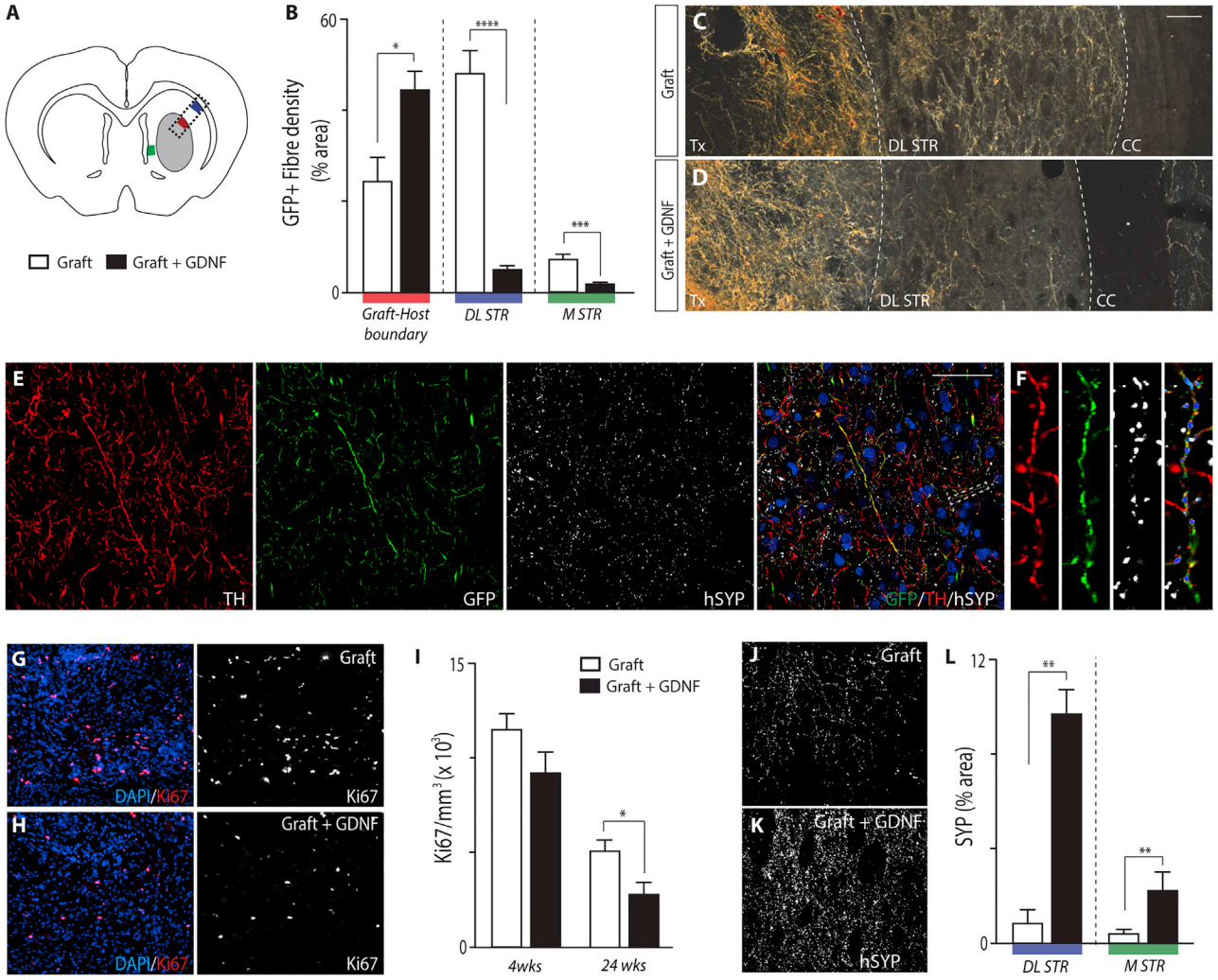

Figure 3. Early Exposure of hPSC-Derived DA Transplants to GDNF Impedes Axonal Sprouting and Integration into the Host Brain

(A) Schematic showing sampling sites for estimates of graft-derived fiber density at the graft-host border (red) and within dorsolateral (blue) and medial (green) striatum. Dotted line demarcates region of interest depicted in (C) and (D).

(B) Transplants in the presence of GDNF showed increased GFP$^+$ DA innervation density at the graft border, but significant reduction in their capacity to innervate the host striatum. Data represent mean ± SEM, Student's t test (n = 5–6 grafts/group).

(C and D) Representative photomicrographs illustrating the increase in graft-derived GFP$^+$ innervation within the transplant, and decreased striatal innervation in animals receiving grafts in the presence (D), compared to absence (C), of GDNF. Tx, transplant; DL STR, dorsolateral striatum; CC, corpus callosum. Scale bar, 100 μm.

(Eand F) Transplants were capable of forming DA synaptic connections within the host striatum, confirmed by TH$^+$, GFP$^+$, and hSYP co-labeling within the representative Graft + GDNF brain. (F) Zoom of highlighted DA fiber highlighting hSYP puncta. Scale bar, 50 μm (E).

(G and H) Photomicrographs of Ki67$^+$ proliferative cells within a graft, and in the presence of GDNF.

(I) The increase in graft size, observed in the presence of GDNF, was not due to an increase in proliferation as seen by Ki67$^+$ analysis at 4 and 24 weeks post-transplantation.

(J–L) Representative images and quantitative assessment of hSYP puncta within the host striatum animals receiving a VM graft in the absence (J) and presence (K) of GDNF. GDNF increased hSYP puncta density within the striatum, indicative of synaptic maturation and integration of the graft. All data expressed as mean ± SEM, Student's t test (n = 5–6 grafts/group).

(Figure 2I, green bar). In addition, GIRK2-expressing cells within the grafts (GFP$^+$/GIRK2$^+$ and GFP$^+$/GIRK$^+$/CALB$^+$) were significantly hypertrophied in the presence of GDNF (Figures 2J and 2K), findings that collectively suggest GDNF promoted the maturation of DA neurons.

The integration of grafted DA neurons into the host tissue was assessed using GFP innervation density at the graft-host boundary, as well as within the dorsolateral striatum (DL STR), the target region for the A9 DA neurons responsible for motor function, and the medial striatum (Figure 3A). Reflective of the increase in GFP$^+$ cells, GFP$^+$ fiber density at the graft-host boundary was significantly increased in the presence of GDNF (graft: 24.34% ± 5.17%; graft + GDNF: 44.05% ± 10.65% area covered by GFP$^+$ pixels) (Figures 3B–3D). Surprisingly, GFP$^+$ innervation density

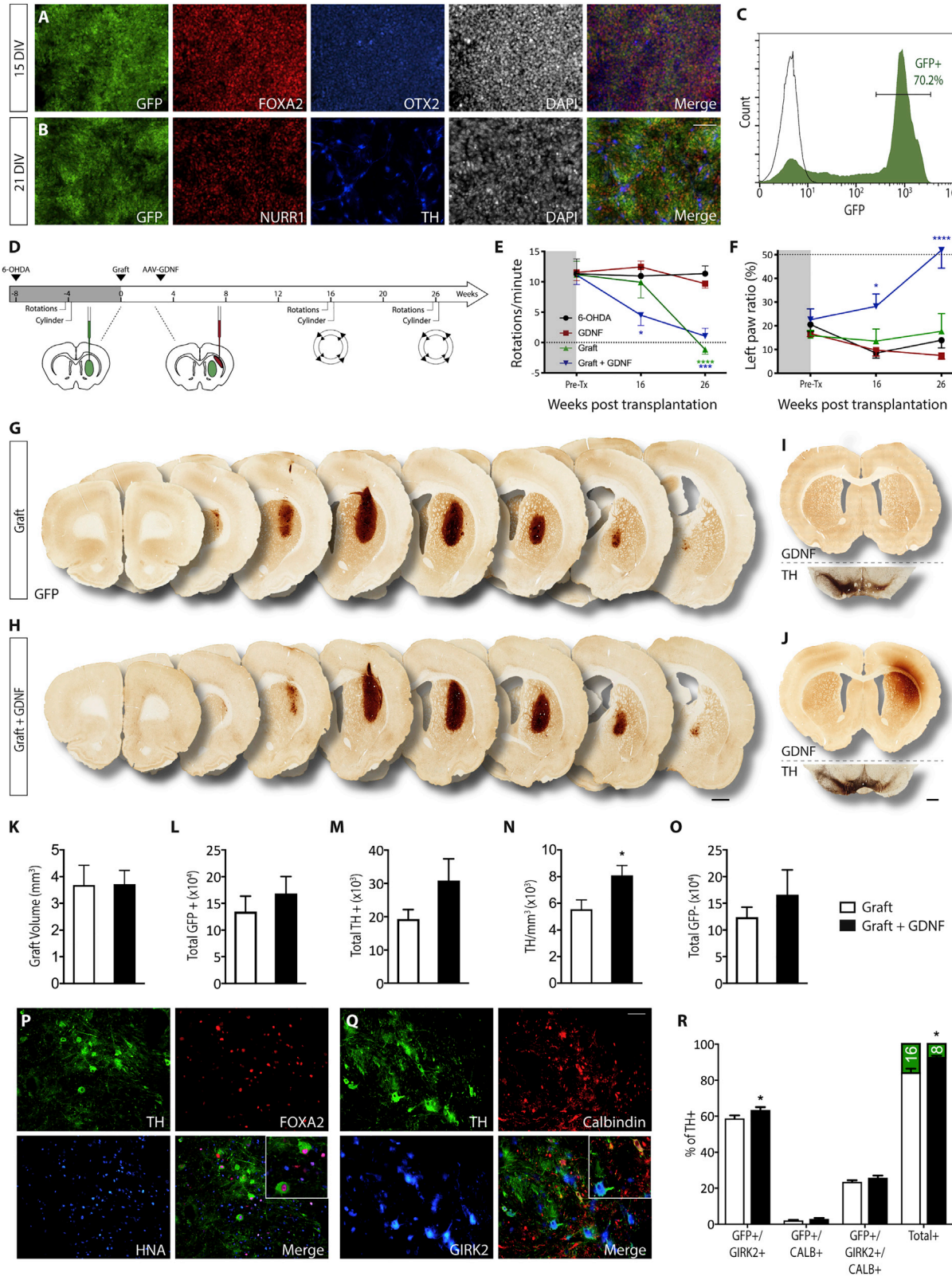

(legend on next page)

within the DL STR was significantly diminished in the presence of GDNF (graft: 47.25% ± 5.39%; graft + GDNF: 4.8% ± 0.93%). To determine whether the reduced innervation was a consequence of excessive GDNF levels, we assessed GFP^+ fiber density within the medial striatum (M STR), where protein levels were notably lower (Figure S2A). Similar to the DL STR, GFP^+ fiber density was significantly reduced (Figure 3B). Despite poor host innervation from grafts in the presence of GDNF, those GFP^+ fibers within the DL STR remained capable of forming synapses, as revealed by the presence of human-specific synaptophysin (hSYP) immunoreactivity along GFP^+ fibers (Figures 3E and 3F).

The surprising reduction in DA innervation of the host striatum by grafted cells exposed to GDNF led us to delve further into understanding the means by which these transplants improved motor function. Assessment of $KI67^+$ proliferative progenitors within grafts at 4 and 24 weeks revealed a progressive and significant decrease (Figures 3G–3I), indicating the pro-maturation (and not proliferative) effect of GDNF. Confirming these maturation findings, the density of $NeuN^+$ cells within GDNF-exposed grafts was significantly increased (cells: 41.6% ± 1.9% $NeuN^+HNA^+$ cells, and cells + GDNF: 58.0% ± 3.0%) (Figure 2G). Total $5HT^+$ serotonergic neurons, a neuronal population capable of influencing motor function and contributing to graft-induced dyskinesia (Carlsson et al., 2007; Hagell et al., 2002), were also significantly elevated 3-fold in GDNF-exposed grafts ($5HT^+HNA^+$ cells: 502 ± 11 and cells + GDNF: 1,420 ± 206). Other neuronal populations (including $GAD67^+$ $GABA^+$, DBH^+, and $ChAT^+$) were notably sparse and not different between graft and graft + GDNF. Reflective of the increased neuronal maturation, the density of graft-derived human synaptophysin ($hSYP^+$) synapses were also more abundant in the presence of GDNF, within both the dorsolateral (graft: 1.24% ± 0.52%; graft + GDNF: 8.52% ± 1.69% $hSYP^+$ area) and medial striatum (Figures 3J–3L). These data suggest that while GDNF induced graft maturation and synaptogenesis, effects were also observed in non-DA neurons, inclusive of undesirable serotonergic cells that have the capacity to influence motor functions.

Delayed GDNF Delivery Promotes Recovery of Motor Function without Increasing Cell Survival

Because the DA neurons only accounted for a fraction of the graft - a common observation for hPSC-derived VM progenitor grafts - and the delivery of GDNF prior to cell transplantation negatively impacted on the ability of the grafted DA neurons innervate the host striatum, we next looked to employ two major refinements to a subsequent study. First, we employed an LMX1A-eGFP reporter ESC line to enable selective isolation of VM progenitors, recently demonstrated to provide a 3-fold enrichment of DA neurons within grafts (de Luzy et al., 2019). Second, we altered the timing of GDNF delivery to 3 weeks after transplantation, such that the grafts were exposed to GDNF after a period that would influence survival, addressing instead the capacity for GDNF to modulate axonal plasticity. These modifications were deemed an advancement of the study and not intended for comparative assessment of grafts exposed to GDNF from the outset.

As previously reported (Niclis et al., 2017a), we confirmed the ability of the LMX1A-eGFP H9 hESC line to differentiate into VM progenitors, with >85% of cells co-expressing GFP, OTX2, and $FOXA2^+$ at 15DIV (Figure 4A). On the day of transplantation, cultures yielded a high proportion $GFP^+/NURR1^+$ progenitors (Figure 4B) that could be fluorescence-activated cell sorting (FACS)-purified (>70% $eGFP^+$) (Figure 4C) and transplanted.

Rotation and cylinder tests were conducted periodically before and after grafting to validate the functionality of LMX1A-GFP-derived DA transplants ± GDNF (Figure 4D). 6-OHDA-induced motor deficits were again stable for 26 weeks in 6-OHDA lesion control animals (±GDNF) (Figure 4E). Complete abolishment of rotational asymmetry was observed 26 weeks in animals receiving transplants (±GDNF), however, recovery was notably accelerated in grafted animals receiving GDNF (Figure 4E). In the cylinder test, only animals receiving combined graft and GDNF treatment showed significant improvement in contralateral forepaw use

Figure 4. Delayed Exposure of hPSC-Derived DA Grafts to GDNF Enhances Functional Recovery in Parkinsonian Rats, Independent of Cell Survival

(A and B) Differentiation of LMX1A-eGFP hESC into VM progenitors was confirmed by the high co-expression of GFP, FOXA2, and OTX2 by 15 DIV (A) as well as GFP, NURR1, and TH at the time of transplantation (21 DIV) (B).

(C) FACS plot illustrating the isolation of LMX1A-eGFP expressing VM progenitors from differentiating cultures at 21 DIV for transplantation.

(D) Schematic overview of the study design.

(E and F) All grafted animals showed restoration of rotational asymmetry at 26 weeks after grafting (E), yet only rats receiving transplants in the presence of GDNF showed significant improvements in the use of the impaired (left) paw in the cylinder test (F). Two-way ANOVA compared to 6-OHDA with Dunnett's correction for multiple comparisons.

(G and H) Photomontage illustrating a representative overview of a VM progenitor transplant in the absence (G) and presence of AAV-GDNF (H). Grafts were immunostained for GFP to identify LMX1A-eGFP expressing cell deposits.

(I) Coronal section illustrating the absence of GDNF expression in the adult striatum, and reduction in TH-immunoreactivity (TH-ir) in the lesioned midbrain of the rat brain depicted in (G).

(J) GDNF immunohistochemistry confirmed targeted, long-term delivery of the AAV-GDNF into the DL STR and overlying cortex. TH immunohistochemistry confirmed MFB DA lesioning. Images are from the same brain depicted in (H).

(K–N) Graphs highlighting that delayed GDNF delivery had no significant effect on graft volume (K), the survival of GFP^+ DA progenitors (L), or TH^+ DA neurons (M) but has a modest effect on TH^+ cell density (N). Student's t test (n = 5–6 grafts/group).

(O) GDNF also had no effect on the total number of non-DA (HNA^+/TH^-) cells within grafts.

(P) The ability of $LMX1A^+$ grafted progenitors within the graft to mature into DA neurons was confirmed by the co-expression of TH, FOXA2, and HNA.

(Q) High proportions of transplanted TH^+ DA neurons co-expressed GIRK2 and/or CALB, indicative of A9 and A10-like specification.

(R) Quantification of TH^+ neurons that co-express GIRK2 and/or CALB.

Scale bars, 50 μm (A, B, P, and Q), 1 mm (G and H). Groups: lesion, n = 9; GDNF, n = 8; graft, n = 7; graft + GDNF, n = 7. (E-F) Two-way ANOVA against 6-OHDA with Dunnett's correction for multiple comparisons (E and F), Student's t test (K–O and R). All data expressed as mean ± SEM.

(graft + GDNF: 51.94% ± 7.66%; graft: 17.72% ± 7.40%; GDNF alone: 7.49% ± 1.51%) (Figure 4F).

At 26 weeks post-transplantation, surviving grafts, identified as dense GFP immunoreactive deposits, were observed in all animals (Figures 4G and 4H). Sustained GDNF expression, restricted to the DL STR and overlying cortex, was confirmed only in animals that received AAV-GDNF (Figures 4I and 4J). 6-OHDA lesions consistently ablated TH^+ neurons within the substantia nigra, while leaving ventral tegmental area DA neurons relatively spared (Figures 4I and 4J). Co-expression of TH, FOXA2, and human nuclear antigen (HNA) confirmed that $LMX1A^+$ grafts were be rich in midbrain DA neurons (Figure 4P). As anticipated, quantitative assessment revealed no difference in graft volume (Figure 4K), GFP^+ cells (Figure 4L), or TH^+ DA neuron number between the two groups (graft: 19,810 ± 2,828; graft + GDNF: 30,381 ± 6,513, p = 0.153) (Figure 4M), highlighting the absence of a cell survival effect. However, total yields of TH^+ DA neurons within both graft and graft + GDNF were substantially elevated following sorting, accounting for an estimated 10% of total cells within the transplant (TH^+/HNA^+). The high proportion of DA neurons within the graft could be most evidently seen by comparative assessment of PSA-NCAM (total graft), GFP (VM progenitors and DA neurons), and TH^+ (DA neurons) (Figure S3), reflecting the efficacy of the selective isolation and transplantation of appropriately patterned VM-specific $LMX1A\text{-}GFP^+$ progenitors. Graft exposure to GDNF had a modest but significant impact on TH^+ density (cells + GDNF: 8,095 ± 730/mm^3; cells: 5,555 ± 699/mm^3) (Figure 4N). Assessment of the non-DA fraction of the graft (TH^-/HNA^+ cells) revealed no change in cell number, indicative of the absence of a GDNF effect on survival and/or proliferation (Figure 4O). No difference was observed in the proportion of $NeuN^+/HNA^+$ neurons, APC^+/HNA^+ oligodendrocytes, or $GFAP^+$ astrocyte density within cell or cell + GDNF grafts (data not shown). Furthermore, $5HT^+$ neurons were notably sparse, as previously observed (de Luzy et al., 2019)—a positive consequence of $LMX1A^+$ progenitor selection prior to grafting.

Co-expression of TH, together with GIRK2 and/or CALB, again confirmed the ability of DA neurons within the grafts to mature into subtype specific populations with similar proportions in the presence or absence of GDNF (Figures 4Q and 4R). Small but significant increases in the overall proportion of total GIRK2 and/or CALB-specified DA neurons were seen in animals receiving GDNF (graft: 84.44% ± 1.96%; graft + GDNF: 92.24% ± 1.41%), indicative of improved and/or accelerated maturation of the grafts (Figure 4R).

Delayed Delivery of GDNF Modulates Appropriate Innervation of the Host Targets from Human Stem Cell-Derived DA Neurons

Given the robust number of TH^+ neurons present within the grafts, we next assessed DA innervation within key target nuclei of the VM DA system. As GFP (LMX1A) was not selectively indicative of DA identity, TH^- immunoreactivity was used to quantify innervation density. Important for the quantitative assessment of TH^+ DA fibers emanating from the graft was the need to confirm robust ablation of the host DA system within the ipsilateral striatum and overlying cortex, as observed in 6-OHDA lesioned animals (Figure 5A). In contrast, notable TH immunoreactivity was observed along the rostrocaudal axis ipsilateral to the graft in animals that received transplants (±GDNF) (Figures 5B and 5C). Delayed exposure of the graft to GDNF resulted in significant increases in TH^+ fiber density within multiple intra- and extra-striatal nuclei, including the overlying cingulate cortex (cing. CTX), perirhinal cortex (peri. CTX), DL STR, and ventrolateral striatum (VL STR) (Figures 5B–5D).

Acute upregulation of the intermediate early response gene, c-Fos, in medium spiny neurons (MSN) of the striatum following amphetamine administration has been shown to be modulated by DA release and subsequent receptor activity, thereby providing an indirect measure of DA signaling (Cenci et al., 1992). To facilitate c-Fos analysis, animals were injected with d-amphetamine 1 h prior to perfusion. $c\text{-}Fos^+$ activation was validated in MSNs by $CTIP2^+/DARPP\text{-}32^+$ co-expression (Figure 5E), with quantitative assessments performed within the medial, dorsolateral, and ventrolateral striatum (Figures 5F–5H and S5). As anticipated, 6-OHDA lesioning reduced c-Fos expression within both the dorsolateral and ventrolateral striatum, in comparison to the contralateral hemisphere and intact control animals (Figures 5F–5H, S4C, and S4D). Lesioning had no effect on $c\text{-}Fos^+$ cells in the medial striatum (Figure 5F). Grafts (±GDNF) increased $c\text{-}Fos^+$ density along the rostrocaudal axis of the DL STR, an effect particularly pronounced immediately caudal to the site of graft implantation, and not significantly different to the intact control animals (Figure 5G). Within the ventrolateral striatum, only grafts in the presence of GDNF showed a significant increase in c-Fos expression relative to the lesion controls (Figure 5H) that was not significantly different to the intact brain. Within the caudal regions of the ventrolateral striatum (0.5 to 1.5 mm caudal to bregma), density of $cFos^+$ was significantly elevated in animals receiving grafts in the presence of GDNF (Figure S5D).

GDNF Restores Dopamine Levels and Modulates Graft-Specific Gene Expression

We next investigated the effect of GDNF on gene expression and DA metabolism within the graft. A cohort of mice were transplanted with FACS-purified $LMX1A^+$ DA progenitors (±AAV-GDNF 3 weeks after transplantation), with tissue isolated at 6 months for either transcriptional profiling or high-performance liquid chromatography (HPLC) (Figures 6A and 6B). Mice were confirmed to have comparable, viable grafts at 6 months to those observed in rats (Figure S6A). To identify gene changes within the graft, we performed species-specific RNA sequencing (RNA-seq) analysis on host striatal tissue, containing the VM grafts ± GDNF, using previously described methods (Bye et al., 2019). Whole genome hierarchical analysis revealed distinct differences in gene expression between the two graft groups, with 240 genes significantly upregulated and 58 genes downregulated in the graft + GDNF compared to graft alone (false discovery rate (FDR) < 0.05) (Figures 6C and 6D). GDNF-upregulated genes were associated with gene ontology biological processes including cell-cell signaling, synaptic signaling, cell communication, and secretion (Figure 6E).

Selective analysis of the upregulated genes revealed many with known roles in DA development and homeostasis such as TH, SLC18A2/VMAT, DDC/AADC, and ALDH1A2 (Figure 6F). The non-canonical Notch ligand DLK1, known to influence VM

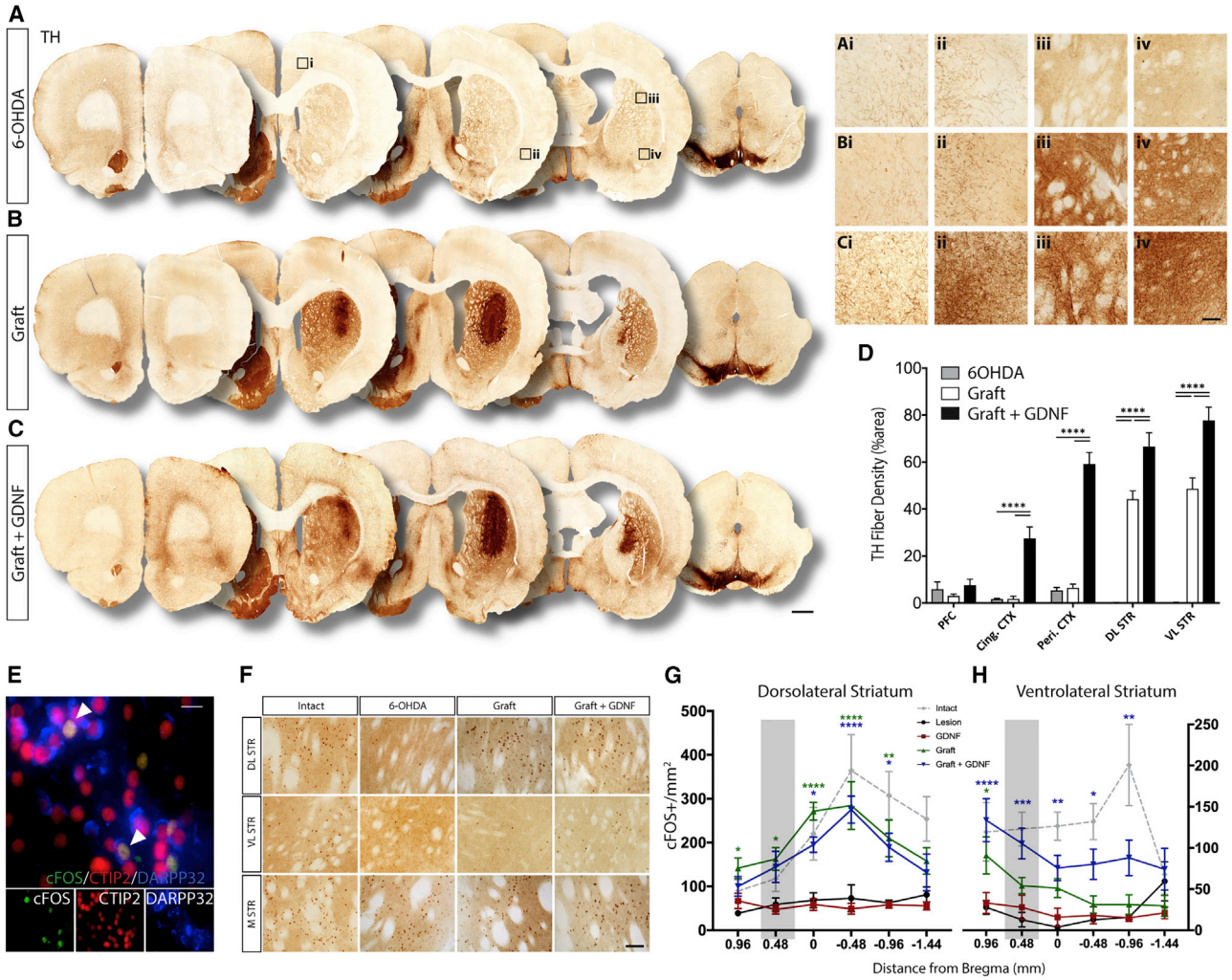

Figure 5. Delayed Exposure of the VM Graft to GDNF Promoted Dopaminergic Innervation of the Host Tissue, Activation of Striatal Neurons, and Upregulated Dopamine Biosynthesis

(A–C) Photomontages illustrating the density of TH^+ fibers within the rat brain following 6-OHDA lesioning (A) and after VM progenitor grafts in the absence (B) and presence of AAV-GDNF (C). (Ai–Civ) High power images from (A–C) illustrating the density of TH^+ fibers in the motor cortex (Ai-Ci), (Aii–Cii) perirhinal cortex, (Aiii–Ciii) DL STR, and (Aiv–Civ) ventrolateral striatum. Scale bar, 1 mm (A–C); 100 μm (insets).

(D) Quantification of TH fiber density within the host tissue of 6-OHDA lesioned rats with and without cell grafts and AAV-GDNF. Two-way ANOVA, Tukey correction for multiple comparisons. n = 7–9 rats/group.

(E) Activation of host striatal neurons was confirmed by co-expression of c-Fos, CTIP, and DARPP-32. Scale bar, 40 μm.

(F) Representative photomicrographs of $c\text{-}FOS^+$ cells within the striatum of Intact and 6-OHDA lesioned rats ± grafts ± AAV-GDNF.

(G) Quantification of $c\text{-}Fos^+$ cells within the host brain revealed significant increases in activated cells in the DL STR of grafted animals, irrespective of GDNF expression.

(H) Rats receiving grafts in the presence of GDNF showed significant increases in cFos activation in the ventrolateral striatum. Data represent mean ± SEM. Two-way ANOVA against 6-OHDA, Dunnett's correction for multiple comparisons. Intact, n = 6; lesion, n = 9; GDNF, n = 8; graft, n = 7; graft + GDNF, n = 7. Gray bar represents the site of transplantation (0.5 mm rostral of bregma). All data expressed as mean ± SEM.

Abbreviations: PFC, prefrontal cortex; cing. CTX, cingulate cortex; peri. CTX, perirhinal cortex; DL STR, dorsolateral striatum; VL STR, ventrolateral striatum.

DA neurogenesis and DAT expression during development (Jacobs et al., 2009; Surmacz et al., 2012) and be regulated by GDNF (Christophersen et al., 2007) was also upregulated, in accordance with its recent identification as a predictive marker of positive hPSC-derived DA graft outcomes (TH^+ cell number and innervation density) (Kikuchi et al., 2017; Kirkeby et al., 2017). Supporting the influence of GDNF on graft plasticity and motor function, upregulation of numerous synaptic (SYTL5, SYT12), axon guidance (BDNF, EPHA2, SEM3E), and adhesion (LAMC2, ITGA11/10/3) genes were also observed (Figure 6G).

Several upregulated genes identified by RNA-seq were verified by qPCR, using human-specific primers to target the graft, and not host, transcript (Figure S5C). These RNA-seq/qPCR findings provide detailed transcriptional profiling of hPSC-derived grafts following extrinsic modulation, providing insight into the underlying genetic changes that drive the functional

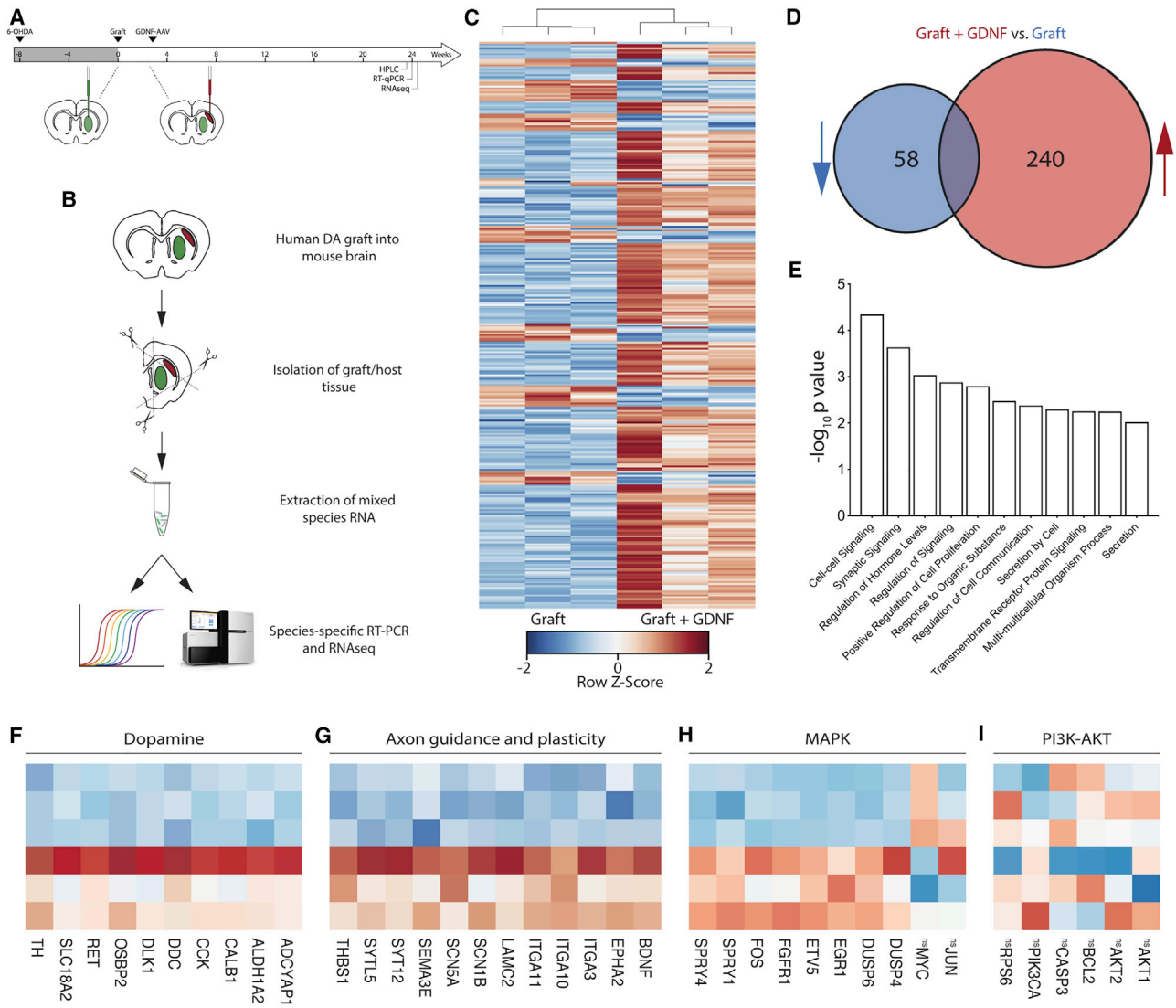

Figure 6. Transcriptional Profiling of VM Grafts in the Presence and Absence of GDNF Identified Known and Unknown DA Homeostatic, Synaptogenesis, and Axonal Plasticity-Related Genes

(A) Schematic overview of experiments designed to probe transcriptomic and DA metabolic changes in grafts exposed to GDNF.

(B) RNA was isolated from grafted mice (±GDNF) and analyzed by both real-time qPCR and RNA-seq.

(C) Unbiased hierarchical clustering analysis of gene expression changes in graft and graft + GDNF tissue samples, (n = 3/group).

(E) Gene ontology analysis clustering of upregulated genes in grafts exposed to GDNF. Note: "ns" preceding gene names indicates those "not significantly" changed.

(F–I) Heatmap of selected genes related to dopamine (F), axon guidance and plasticity (G), MAPK signaling (H), and PI3K-AKT signaling (I).

integration of DA-enriched grafts. Such profiling analysis also provide new insight into graft responses. By way of example, we show cholecystokinin (CCK), a neuropeptide known for modulating DA release within midbrain DA pathways, including in fetal VM transplants (Wang et al., 1994), was significantly upregulated in response to GDNF (Figures 6F and S6D). To confirm this, we examined the expression and localization of CCK protein, and show 2-fold more CCK^{+} neurons in GDNF-treated grafts, with 34.6% co-expressing TH, suggesting that GDNF regulates CCK expression and potentially modulates DA transmission within the grafted brain. Although CCK cell counts were low, this likely reflects the challenges in visualizing this population at a protein level, noting that the peptide is rapidly translocated to the nerve terminal (Agersnap et al., 2016). With CCK expressed within most midbrain DA neurons (Hökfelt et al., 1980), further studies involving blocking of axonal transport will be required to reveal the true impact of GDNF of this population. Protein-protein interaction network analysis of differentially expressed genes demonstrated the upregulation of genes associated with neural development, synaptic transmission, adhesion, and GDNF activity, further confirming our observations within maturing DA grafts (Figure S7).

We additionally assessed genes associated with downstream GDNF signaling. Within DA neurons, GDNF/GFRα1 binding

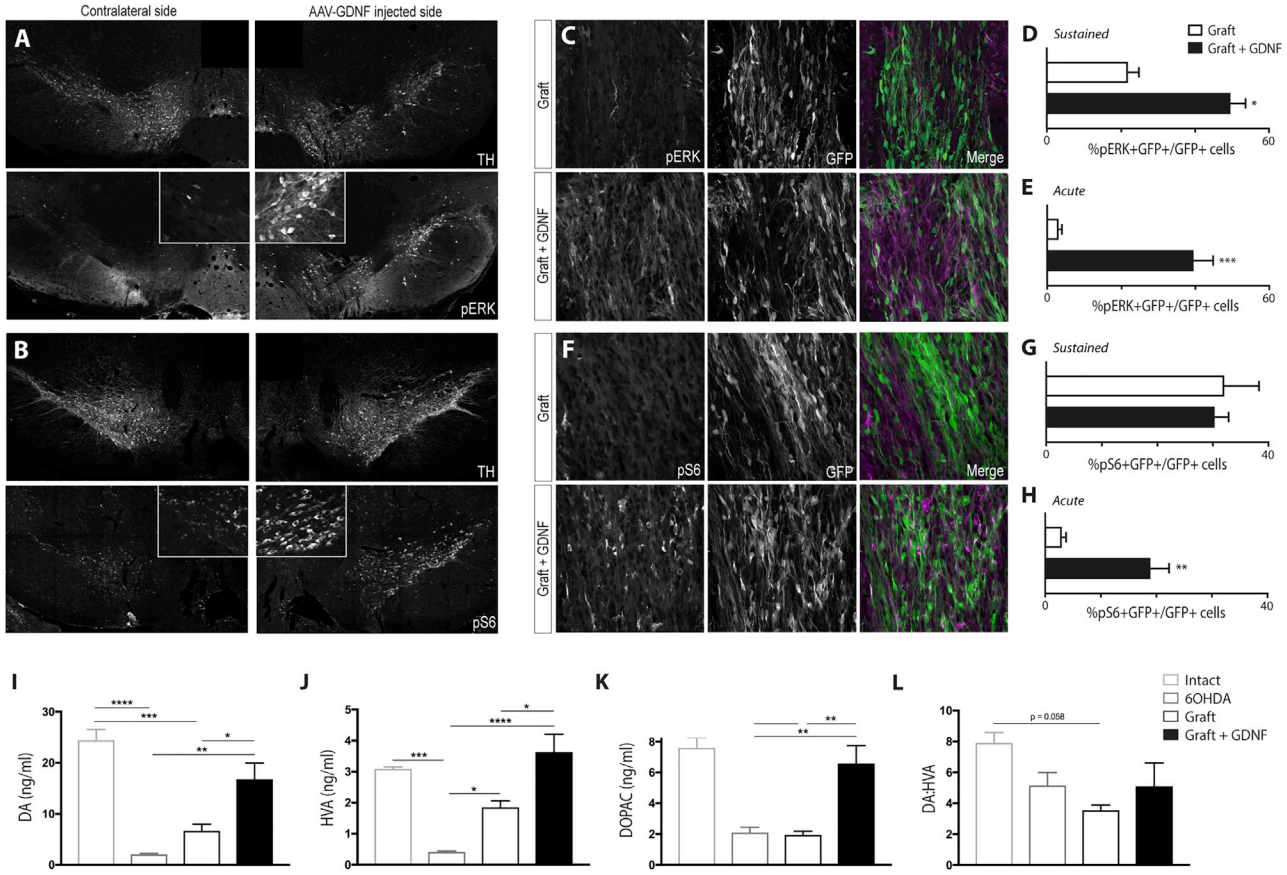

Figure 7. GDNF Overexpression Temporally Regulates Downstream pERK and pS6 Signaling in Grafted Dopamine Neurons

(A and B) Assessment of the host midbrain (ipsilateral and contralateral to the AAV-GDNF intrastriatal delivery) verifying the capacity to measure changes in (A) pERK and (B) pS6 within DA neurons.

(C) Representative images showing pERK co-localized with GFP$^+$ (PITX3) DA cells in grafts in the absence or presence of "Acute" GDNF exposure.

(D and E) Proportion of GFP$^+$ DA neurons co-expressing pERK after "Sustained" (D) and "Acute" (E) exposure to AAV-delivered GDNF.

(F) Representative images showing pS6 co-localized in GFP$^+$ DA cells within grafts in the absence or presence of "Acute" GDNF exposure.

(G and H) Proportion of GFP$^+$ DA neurons co-expressing pS6 after "Sustained" (G) and "Acute" (H) exposure to AAV-delivered GDNF.

(I–K) HPLC confirmed a significant reduction in DA (I) and DA metabolites, HVA (J), and DOPAC (K) in the striatum of lesioned (compared to intact) mice, an effect that could be partially restored by hESC-derived DA grafts and fully restored when transplants were exposed to GDNF.

(L) Reflective of commensurate changes in DA and it's metabolites, dopamine turnover (DA:HVA) remained unchanged across lesion and grafted animals. Data represent mean ± SEM, n = 4–6 mice/group (D, E, G, H, and I–L); Student's t test (D, E, G, and H); one-way ANOVA with Tukey correction for multiple comparisons (I–L). All data expressed as mean ± SEM.

triggers signaling via a complex with the receptor tyrosine kinase Ret, which in turn modulates downstream PI3K-AKT and mitogen-activated protein kinase (MAPK)-ERK pathways that activate transcription of genes involved in survival and/or plasticity (Kramer and Liss, 2015). In addition to significantly elevated Ret expression (Figure 6F), we observed upregulation of a number of MAPK-associated genes with known roles in plasticity, including EGR1 and SPRY1 (predictive genes recently linked to high DA neuron yields within in grafts) (Kirkeby et al., 2017), but no change in MAPK-associated genes linked to cell migration and proliferation (JUN, MYC) (Figure 6H). In contrast, genes associated with the PI3K-AKT pathway (e.g., AKT1, AKT2, and PIK3CA) were not significantly changed (Figure 6I), suggesting that GDNF mediates the plasticity of human DA neurons via the MAPK-ERK, and not PI3K-AKT, pathway.

These findings were confirmed by assessing the expression of phosphorylated ribosomal protein S6 (pS6), an indicator of the upstream activation of the neuroprotective pathway Akt/mTOR pathway, as well as phosphorylated ERK (pERK), specifically in graft-derived (PITX3$^-$GFP$^+$) DA neurons. Assessment of the host midbrain (ipsilateral and contralateral to the AAV-GDNF intrastriatal delivery) verified the capacity to measure changes in pERK and pS6, as revealed by increased labeling within TH$^+$ neurons (Figures 7A and 7B). Confirming the transcriptional findings, a significant increase in the proportion of DA neurons co-expressing pERK (%pERK$^+$GFP$^+$/total GFP$^+$) was observed in grafts exposed to GDNF (cells: 21% ± 5%; cells + GDNF: 48% ± 6%), yet no change was observed the proportion of pS6-immunoreactive DA neurons (Figures 7D and 7G).

Recognizing that assessment of PI3K-AKT and MAPK-ERK was performed on grafts that had been exposed for many

months to GDNF, and the potential for modulation of downstream target genes over time, we performed an additional cohort of transplantation (±"late GDNF") to assess acute responsiveness of the grafts, within days of exposure, to GDNF protein. Consistent with transcriptional and protein changes in response to sustained GDNF exposure, acute exposure to GDNF induced a 10-fold increase in pERK-expressing DA neurons, compared to non-GDNF exposed grafts (Figures 7C and 7E). Acute GDNF exposure also significantly increased the proportion of DA neurons co-expressing pS6 (Figures 7F and 7H), suggestive of early dual GDNF roles in survival and plasticity, with ongoing contributions to graft plasticity at protracted periods after transplantation.

Finally, we utilized HPLC to demonstrate elevated striatal DA metabolism in animals receiving grafts in the presence of GDNF. Importantly, a >90% reduction in striatal DA levels in 6-OHDA lesioned animals confirmed ablation of the host midbrain DA system, (6-OHDA: 2.0 ± 0.2 pmol/mg of wet tissue; intact: 24.4 ± 2.2 pmol/mg) (Figure 6J), as previously reported (Parish et al., 2008). Reflective of the improvement in rotational asymmetry, grafts in the absence or presence of GDNF showed significant elevations in DA levels (6.7 ± 1.3 pmol/mg and 16.8 ± 3.1 pmol/mg, respectively) (Figure 6J), as well as the DA metabolites HVA (1.9 ± 0.2 pmol/mg and 3.6 ± 0.6 pmol/mg) and DOPAC (1.9 ± 0.3 pmol/mg and 6.6 ± 1.1 pmol/mg), compared to 6-OHDA lesion alone (HVA: 0.4 ± 0.03 pmol/mg; DOPAC: 2.1 ± 0.3 pmol/mg) (Figures 6K and 6L). However, only in the presence of GDNF were DA, DA metabolites, and overall DA metabolism (ratio of DA to HVA) restored to levels not significantly different from the intact brain, reflective of restoration of DA biosynthesis and function in these animals (Figures 6J–6M). These increases in DA levels seen in graft tissue exposed to GDNF was supported by elevated expression of genes associated with DA synthesis gene, including TH and AADC (Figures 6F and S5C).

DISCUSSION

This study highlights the impact of modulating the host environment to impact on the survival and plasticity of hPSC-derived DA transplants in the Parkinsonian brain. Employment of unique GFP-expressing stem cell reporter lines enabled precise tracking of the DA contribution to the grafts (PITX3-eGFP), as well as a 10-fold enrichment of DA neurons (by FACS isolation LMX1A-GFP progenitors) within the transplants. Utilizing these tools, we were able to demonstrate that the timing of onset for sustained GDNF delivery directly impacted on the mechanisms by which improvements in functional recovery occurred. Although all grafted animals showed restoration of amphetamine-induced motor asymmetry, reflective of the relatively low number of DA neurons required for correction of this gross motor deficit, examination of non-pharmacologically induced sensorimotor tasks revealed distinct benefits of sustained GDNF expression.

We demonstrate that transplantation of hPSC-derived VM progenitors into an already GDNF-enriched environment promoted graft survival, yet without selectivity for the DA population. More noteworthy, however, was the negative impact early exposure to GDNF had on the capacity of the graft to innervate the host tissue, such that the majority of graft-derived DA fiber growth was restricted to the graft core. In these grafts, we demonstrate increased neuronal differentiation and striatal innervation from non-DA neurons, inclusive of 5HT neurons, that likely contribute to the functional recovery observed, together with the increased TH^+ DA neuron maturation (GIRK/CALB specification). Further studies, such as selective silencing of DA cells within grafts, will be required to elucidate the relative contribution of TH^+ DA neuron verses other neuronal populations to behavioral responses. In contrast, delaying exposure of the graft to GDNF had no impact on cell survival, yet significantly increased graft-derived DA re-innervation of the host tissue, elevated striatal DA levels (to levels not different from the intact brain), and consequently, enhanced activation of postsynaptic striatal medium spiny neurons.

We demonstrate that these effects are mediated through acute PI3K-AKT and sustained MAPK signaling, downstream of GDNF-receptor activation. Interestingly, while increased activation of striatal neurons (the primary output of the transplanted DA neurons) was shown in the DL STR of animals receiving grafts in the absence and presence of GDNF, only in the presence of GDNF was cFos activation observed in the ventrolateral striatum, a region of the basal ganglia previously shown to underpin changes in more complex sensorimotor tasks following lesioning and DA transplantation (Chang et al., 1999; Mandel et al., 1990) and supported by findings in patient fetal grafting studies (Piccini et al., 2005). The importance of these findings is significant in light of former clinical trials where an estimated 15% of patients developed graft-induced dyskinesia, a phenomenon speculated to be, in part, the consequence of incomplete and uneven striatal DA re-innervation (Carlsson et al., 2006; Hagell et al., 2002).

A major contributor to the functional capacity of VM DA grafts is the relative contribution of A9 neurons (Grealish et al., 2010). Previous studies have described differential effects of GDNF on DA subpopulations, such that A10, but not A9 neurons, are protected into adulthood against apoptosis, resulting in increased cortical, but not striatal innervation (Borgal et al., 2007; Kholodilov et al., 2004), while others demonstrate survival of A9, but not A10 DA neurons in response to GDNF (Nosheny et al., 2006). Here, we report ~70% of TH^+ cells within the graft adopted an A9- or A10-like identity, with the majority of these fate-specified cells expressing GIRK2 (alone or in combination with CALB), while relatively few TH^+ cells express CALB alone. Such proportions reflect A9 and A10 contributions within the human ventral midbrain (Reyes et al., 2012). Surprisingly, in response to GDNF, a significant increase in $GIRK2^+$ cells was observed and accompanied by increased soma size, suggestive of a role for GDNF in the maturation of human DA neurons, an effect that may contribute to improvements in complex motor tasks.

In addition to the effects on survival and plasticity of DA neurons, GDNF has been shown to influence DA biosynthesis through the regulation of *TH* gene expression, a response dependent on *Ret* (Xiao et al., 2002). Unlike rodent studies where sustained GDNF induces downregulation of *TH* mRNA, a compensatory response to increased DA levels from the graft resulting in impaired graft function (Georgievska et al., 2004; Winkler et al., 2006), non-human primate studies have reported maintained increases in TH^+ cells and fiber density (Elsworth

et al., 2008; Eslamboli et al., 2005; Kordower et al., 2000). In alignment with non-human primates, we observed increases in TH^+ cells and TH^+ fibers (dependent on the time of GDNF delivery) that was accompanied by significant upregulation of *TH* mRNA. We also detected elevated levels of *AADC*, the enzyme required for the conversion of L-DOPA into DA, as well as CCK, a neuropeptide capable of modulating striatal DA levels, suggesting that GDNF is capable of regulating DA synthesis and release at multiple levels. These observations were supported by increased DA synthesis to levels not significantly different from the intact brain. Noting previous observations that developing rather than mature DA neurons are most responsive to GDNF (Elsworth et al., 2008), the elevated enzyme (*TH* and *AADC*) transcript levels observed here likely reflect ongoing graft maturation, an unsurprising observation in light of the duration of human development as well as the protracted time for integration of hPSC and fetal DA grafts in pre-clinical and clinical trials to date (Niclis et al., 2017b; Piccini et al., 2000). In this regard, extended studies, involving graft assessment at time points when human DA neurons have reached functional maturity and no longer require GDNF, will be needed to determine the effects of sustained GDNF on these transcript levels, resultant DA biosynthesis, and motor function.

During development, GDNF expression is tightly regulated, with protein levels downregulated in the adult brain beyond critical periods of cell survival and target acquisition (Kirik et al., 2017). Consequently, it is probable and likely that closer attention to the duration of expression may be required when employing gene therapy approaches targeted at promoting neuroprotection and/or plasticity. Further studies may also be required to determine whether sustained GDNF expression may result in increased aberrant innervation of target tissue that results in unregulated synaptic neurotransmission and/or increased innervation of off-targets, as a consequence of suboptimal gene therapy targeting. The dual effects of early and late GDNF on grafted DA neurons suggest that the desired therapeutic approach may involve phasic exposure to GDNF. With the recent demonstration of inducible expression vectors, for the temporal control of GDNF in the intact brain (Akhtar et al., 2018), this presents a feasible consideration for the future.

Added to requirements for temporal regulation is the need for greater control over gene therapy-associated protein dose. Here, we report targeted injection of 1.8×10^9 genomic copies of the AAV-GDNF into the striatum of rats. Although histochemical analysis confirmed protein expression, resulting in anticipated and positive impacts on graft survival and plasticity, knowledge of absolute protein levels here remained unknown. Previous reports have demonstrated that it is in fact possible to overdose the system and impart effects on other neuronal populations (Elsworth et al., 2008) as well as negatively regulate DA levels (Winkler et al., 2006), such that lower chronic doses may be more beneficial. Graft-derived DA innervation within the DL STR of GDNF-treated animals was reduced compared to non-GDNF animals and similarly observed within the medial striatum, where GDNF proteins levels were notably lower, suggesting that within the current context, the presence or absence of the protein, rather than concentration, had the greatest impact on plasticity. Related to this, and dependent on the desired requirement, studies have demonstrated that significantly lower concentrations of GDNF are required to enhance survival, compared to promoting axonal growth and plasticity. In this regard, several regulatory elements are now being tested to control the level of GDNF expression, as well as fine tune duration, that may be necessary for the optimization of GDNF gene therapy (Kirik et al., 2017).

In addition to the support of DA grafts, GDNF gene therapy may provide the supplementary advantage of protecting residual host DA neurons within the VM that are undergoing persistent degeneration. Similar to previous reports (Elsworth et al., 2008; Kauhausen et al., 2013; Thompson et al., 2009), and evidenced here, viral delivery of GDNF within the striatum also resulted in transport and transduction of cells within the midbrain, resulting in activation of downstream MAPK and PI3K-AKT signaling. Although mature DA neurons have been suggested to be less responsive to GDNF than immature DA progenitors/neurons, studies have provided evidence of improved survival in the adult brain, resulting in a number of clinical trials using GDNF (infusion and viral delivery), as well as the closely associated protein neurturin, targeted at slowing disease progression (Kirik et al., 2017; Rangasamy et al., 2010).

The combined approach of cell and gene therapy in neural repair is becoming increasingly recognized for clinical application. Studies have already demonstrated delayed disease progression using human neural progenitors engineered to overexpress GDNF in models of PD (Behrstock et al., 2006), with these approaches also confirmed to be safe in a Phase 1/2a clinical trial targeting motor neuron survival in ALS (NCT02943850, 2017). Here, we demonstrate the benefit of enriching for correctly specified DA progenitors, enabling enhanced predictability of graft outcomes, and importantly their responsiveness to targeted GDNF gene therapy. Irrespective of whether reporter lines or alternative cell sorting strategies are adopted in the future for clinical application, the impetus remains for multifaceted approaches inclusive of enriching for VM progenitors as well as the implementation of inducible GDNF transgene delivery systems.

In summary, we provide a conclusive body of evidence for the many benefits of GDNF gene therapy to improve the functionality of hPSC-derived DA neural transplants in rodent models of PD. Dependent of timing of gene delivery, we report that GDNF increases graft survival, plasticity/sprouting of DA fibers, DA innervation of host target nuclei, increased activation of striatal neurons, and elevated DA metabolism (associated with changes in regulatory synthesis gene expression). These findings suggest that a dual therapeutic approach, involving cell transplantation and targeted gene therapy, to address the shortcoming of poor survival and plasticity of human DA neurons, may have significant implications for the translation of pluripotent stem cell-based therapies into the clinic for the treatment of PD.

STAR★METHODS

Detailed methods are provided in the online version of this paper and include the following:

- KEY RESOURCES TABLE
- LEAD CONTACT AND MATERIALS AVAILABILITY

SUPPLEMENTAL INFORMATION

Supplemental Information can be found online at https://doi.org/10.1016/j.stem.2020.01.010.

ACKNOWLEDGMENTS

The authors thank Mong Tien and Davor Stanic for expert technical assistance, thank Björn Anzelius for production of the AAV vectors, and acknowledge the support of the flow cytometry facility at the Melbourne Brain Centre, Parkville, Australia. C.L.P. was supported by a National Health and Medical Research Council Australia (NHMRC) Senior Research Fellowship. C.W.G. was supported by an Australian Postgraduate Award. This work was supported by an NHMRC Australia project grant (APP1102704 to C.L.P.), Stem Cells Australia (to C.L.P.), and the Swedish Research Council (2012-2586 to D.K.). The Florey Institute of Neuroscience and Mental Health acknowledges the strong support from the Victorian Government and in particular the funding from the Operational Infrastructure Support Grant.

AUTHOR CONTRIBUTIONS

C.L.P. and C.W.G. conceived the experiments and wrote the manuscript. C.W.G., I.R.d.L., J.C.N., V.P., C.P.H., N.M., J.A.K., C.R.B., C.M.E., L.H.T., and C.L.P. performed the experiments. C.W.P., D.K., L.H.T., and C.L.P. provided reagents and expertise. C.L.P. and D.K. provided the funding.

DECLARATION OF INTERESTS

The authors declare no competing interests.

Received: May 20, 2019
Revised: October 31, 2019
Accepted: January 16, 2020
Published: February 13, 2020

REFERENCES

Agersnap, M., Zhang, M.D., Harkany, T., Hökfelt, T., and Rehfeld, J.F. (2016). Nonsulfated cholecystokinins in cerebral neurons. Neuropeptides *60*, 37–44.

Ahn, Y.H., Bensadoun, J.C., Aebischer, P., Zurn, A.D., Seiger, A., Björklund, A., Lindvall, O., Wahlberg, L., Brundin, P., and Kaminski Schierle, G.S. (2005). Increased fiber outgrowth from xeno-transplanted human embryonic dopaminergic neurons with co-implants of polymer-encapsulated genetically modified cells releasing glial cell line-derived neurotrophic factor. Brain Res. Bull. *66*, 135–142.

Akhtar, A.A., Gowing, G., Kobritz, N., Savinoff, S.E., Garcia, L., Saxon, D., Cho, N., Kim, G., Tom, C.M., Park, H., et al. (2018). Inducible Expression of GDNF in Transplanted iPSC-Derived Neural Progenitor Cells. Stem Cell Reports *10*, 1696–1704.

Barker, R.A., Barrett, J., Mason, S.L., and Björklund, A. (2013). Fetal dopaminergic transplantation trials and the future of neural grafting in Parkinson's disease. Lancet Neurol. *12*, 84–91.

Behrstock, S., Ebert, A., McHugh, J., Vosberg, S., Moore, J., Schneider, B., Capowski, E., Hei, D., Kordower, J., Aebischer, P., and Svendsen, C.N. (2006). Human neural progenitors deliver glial cell line-derived neurotrophic factor to parkinsonian rodents and aged primates. Gene Ther. *13*, 379–388.

Björklund, A., Rosenblad, C., Winkler, C., and Kirik, D. (1997). Studies on neuroprotective and regenerative effects of GDNF in a partial lesion model of Parkinson's disease. Neurobiol. Dis. *4*, 186–200.

Borgal, L., Hong, M., Sadi, D., and Mendez, I. (2007). Differential effects of glial cell line-derived neurotrophic factor on A9 and A10 dopamine neuron survival in vitro. Neuroscience *147*, 712–719.

Bye, C.R., Penna, V., de Luzy, I.R., Gantner, C.W., Hunt, C.P.J., Thompson, L.H., and Parish, C.L. (2019). Transcriptional profiling of xenogeneic transplants: examining human pluripotent stem cell-derived grafts in the rodent brain. Stem Cell Reports *13*, 877–890.

Carlsson, T., Winkler, C., Lundblad, M., Cenci, M.A., Björklund, A., and Kirik, D. (2006). Graft placement and uneven pattern of reinnervation in the striatum is important for development of graft-induced dyskinesia. Neurobiol. Dis. *21*, 657–668.

Carlsson, T., Carta, M., Winkler, C., Björklund, A., and Kirik, D. (2007). Serotonin neuron transplants exacerbate L-DOPA-induced dyskinesias in a rat model of Parkinson's disease. J. Neurosci. *27*, 8011–8022.

Castilho, R.F., Hansson, O., and Brundin, P. (2000). Improving the survival of grafted embryonic dopamine neurons in rodent models of Parkinson's disease. Prog. Brain Res. *127*, 203–231.

Cenci, M.A., Kalén, P., Mandel, R.J., Wictorin, K., and Björklund, A. (1992). Dopaminergic transplants normalize amphetamine- and apomorphine-induced Fos expression in the 6-hydroxydopamine-lesioned striatum. Neuroscience *46*, 943–957.

Chang, J.W., Wachtel, S.R., Young, D., and Kang, U.J. (1999). Biochemical and anatomical characterization of forepaw adjusting steps in rat models of Parkinson's disease: studies on medial forebrain bundle and striatal lesions. Neuroscience *88*, 617–628.

Christophersen, N.S., Grønborg, M., Petersen, T.N., Fjord-Larsen, L., Jørgensen, J.R., Juliusson, B., Blom, N., Rosenblad, C., and Brundin, P. (2007). Midbrain expression of Delta-like 1 homologue is regulated by GDNF and is associated with dopaminergic differentiation. Exp. Neurol. *204*, 791–801.

de Luzy, I.R., Niclis, J.C., Gantner, C.W., Kauhausen, J.A., Pouton, C.W., Hunt, C.P.J., Thompson, L.H., and Parish, C.L. (2019). Isolation of LMX1a ventral midbrain progenitors improves the safety and predictability of human pluripotent stem cell-derived neural transplants in Parkinsonian Disease. J. Neurosci. *39*, 9521–9531.

Elsworth, J.D., Redmond, D.E., Jr., Leranth, C., Bjugstad, K.B., Sladek, J.R., Jr., Collier, T.J., Foti, S.B., Samulski, R.J., Vives, K.P., and Roth, R.H. (2008). AAV2-mediated gene transfer of GDNF to the striatum of MPTP monkeys enhances the survival and outgrowth of co-implanted fetal dopamine neurons. Exp. Neurol. *211*, 252–258.

Eslamboli, A., Georgievska, B., Ridley, R.M., Baker, H.F., Muzyczka, N., Burger, C., Mandel, R.J., Annett, L., and Kirik, D. (2005). Continuous low-level glial cell line-derived neurotrophic factor delivery using recombinant adeno-associated viral vectors provides neuroprotection and induces behavioral recovery in a primate model of Parkinson's disease. J. Neurosci. *25*, 769–777.

Frey, P. (1983). Cholecystokinin octapeptide levels in rat brain are changed after subchronic neuroleptic treatment. Eur. J. Pharmacol. *95*, 87–92.

Georgievska, B., Carlsson, T., Lacar, B., Winkler, C., and Kirik, D. (2004). Dissociation between short-term increased graft survival and long-term functional improvements in Parkinsonian rats overexpressing glial cell line-derived neurotrophic factor. Eur. J. Neurosci. *20*, 3121–3130.

Grealish, S., Jönsson, M.E., Li, M., Kirik, D., Björklund, A., and Thompson, L.H. (2010). The A9 dopamine neuron component in grafts of ventral mesencephalon is an important determinant for recovery of motor function in a rat model of Parkinson's disease. Brain *133*, 482–495.

Grealish, S., Diguet, E., Kirkeby, A., Mattsson, B., Heuer, A., Bramoulle, Y., Van Camp, N., Perrier, A.L., Hantraye, P., Björklund, A., and Parmar, M. (2014). Human ESC-derived dopamine neurons show similar preclinical efficacy and

potency to fetal neurons when grafted in a rat model of Parkinson's disease. Cell Stem Cell *15*, 653–665.

Hagell, P., Piccini, P., Björklund, A., Brundin, P., Rehncrona, S., Widner, H., Crabb, L., Pavese, N., Oertel, W.H., Quinn, N., et al. (2002). Dyskinesias following neural transplantation in Parkinson's disease. Nat. Neurosci. *5*, 627–628.

Hökfelt, T., Rehfeld, J.F., Skirboll, L., Ivemark, B., Goldstein, M., and Markey, K. (1980). Evidence for coexistence of dopamine and CCK in meso-limbic neurones. Nature *285*, 476–478.

Jacobs, F.M., van der Linden, A.J., Wang, Y., von Oerthel, L., Sul, H.S., Burbach, J.P., and Smidt, M.P. (2009). Identification of Dlk1, Ptpru and Klhl1 as novel Nurr1 target genes in meso-diencephalic dopamine neurons. Development *136*, 2363–2373.

Johansson, M., Friedemann, M., Hoffer, B., and Strömberg, I. (1995). Effects of glial cell line-derived neurotrophic factor on developing and mature ventral mesencephalic grafts in oculo. Exp. Neurol. *134*, 25–34.

Kauhausen, J., Thompson, L.H., and Parish, C.L. (2013). Cell intrinsic and extrinsic factors contribute to enhance neural circuit reconstruction following transplantation in Parkinsonian mice. J. Physiol. *591*, 77–91.

Kholodilov, N., Yarygina, O., Oo, T.F., Zhang, H., Sulzer, D., Dauer, W., and Burke, R.E. (2004). Regulation of the development of mesencephalic dopaminergic systems by the selective expression of glial cell line-derived neurotrophic factor in their targets. J. Neurosci. *24*, 3136–3146.

Kikuchi, T., Morizane, A., Doi, D., Magotani, H., Onoe, H., Hayashi, T., Mizuma, H., Takara, S., Takahashi, R., Inoue, H., et al. (2017). Human iPS cell-derived dopaminergic neurons function in a primate Parkinson's disease model. Nature *548*, 592–596.

Kirik, D., Cederfjäll, E., Halliday, G., and Petersén, Å. (2017). Gene therapy for Parkinson's disease: Disease modification by GDNF family of ligands. Neurobiol. Dis. *97* (Pt B), 179–188.

Kirkeby, A., Grealish, S., Wolf, D.A., Nelander, J., Wood, J., Lundblad, M., Lindvall, O., and Parmar, M. (2012). Generation of regionally specified neural progenitors and functional neurons from human embryonic stem cells under defined conditions. Cell Rep. *1*, 703–714.

Kirkeby, A., Nolbrant, S., Tiklova, K., Heuer, A., Kee, N., Cardoso, T., Ottosson, D.R., Lelos, M.J., Rifes, P., Dunnett, S.B., et al. (2017). Predictive Markers Guide Differentiation to Improve Graft Outcome in Clinical Translation of hESC-Based Therapy for Parkinson's Disease. Cell Stem Cell *20*, 135–148.

Kordower, J.H., Emborg, M.E., Bloch, J., Ma, S.Y., Chu, Y., Leventhal, L., McBride, J., Chen, E.Y., Palfi, S., Roitberg, B.Z., et al. (2000). Neurodegeneration prevented by lentiviral vector delivery of GDNF in primate models of Parkinson's disease. Science *290*, 767–773.

Kramer, E.R., and Liss, B. (2015). GDNF-Ret signaling in midbrain dopaminergic neurons and its implication for Parkinson disease. FEBS Lett. *589* (24 Pt A), 3760–3772.

Kriks, S., Shim, J.W., Piao, J., Ganat, Y.M., Wakeman, D.R., Xie, Z., Carrillo-Reid, L., Auyeung, G., Antonacci, C., Buch, A., et al. (2011). Dopamine neurons derived from human ES cells efficiently engraft in animal models of Parkinson's disease. Nature *480*, 547–551.

Lin, L.F., Doherty, D.H., Lile, J.D., Bektesh, S., and Collins, F. (1993). GDNF: a glial cell line-derived neurotrophic factor for midbrain dopaminergic neurons. Science *260*, 1130–1132.

Mandel, R.J., Brundin, P., and Björklund, A. (1990). The Importance of Graft Placement and Task Complexity for Transplant-Induced Recovery of Simple and Complex Sensorimotor Deficits in Dopamine Denervated Rats. Eur. J. Neurosci. *2*, 888–894.

Nefzger, C.M., Su, C.T., Fabb, S.A., Hartley, B.J., Beh, S.J., Zeng, W.R., Haynes, J.M., and Pouton, C.W. (2012). Lmx1a allows context-specific isolation of progenitors of GABAergic or dopaminergic neurons during neural differentiation of embryonic stem cells. Stem Cells *30*, 1349–1361.

Niclis, J.C., Gantner, C.W., Alsanie, W.F., McDougall, S.J., Bye, C.R., Elefanty, A.G., Stanley, E.G., Haynes, J.M., Pouton, C.W., Thompson, L.H., and Parish, C.L. (2017a). Efficiently Specified Ventral Midbrain Dopamine Neurons from Human Pluripotent Stem Cells Under Xeno-Free Conditions Restore Motor Deficits in Parkinsonian Rodents. Stem Cells Transl. Med. *6*, 937–948.

Niclis, J.C., Gantner, C.W., Hunt, C.P.J., Kauhausen, J.A., Durnall, J.C., Haynes, J.M., Pouton, C.W., Parish, C.L., and Thompson, L.H. (2017b). A PITX3-EGFP Reporter Line Reveals Connectivity of Dopamine and Non-dopamine Neuronal Subtypes in Grafts Generated from Human Embryonic Stem Cells. Stem Cell Reports *9*, 868–882.

Nosheny, R.L., Bachis, A., Aden, S.A., De Bernardi, M.A., and Mocchetti, I. (2006). Intrastriatal administration of human immunodeficiency virus-1 glycoprotein 120 reduces glial cell-line derived neurotrophic factor levels and causes apoptosis in the substantia nigra. J. Neurobiol. *66*, 1311–1321.

Olanow, C.W., Kordower, J.H., and Freeman, T.B. (1996). Fetal nigral transplantation as a therapy for Parkinson's disease. Trends Neurosci. *19*, 102–109.

Parish, C.L., Castelo-Branco, G., Rawal, N., Tonnesen, J., Sorensen, A.T., Salto, C., Kokaia, M., Lindvall, O., and Arenas, E. (2008). Wnt5a-treated midbrain neural stem cells improve dopamine cell replacement therapy in parkinsonian mice. J. Clin. Invest. *118*, 149–160.

Piccini, P., Lindvall, O., Björklund, A., Brundin, P., Hagell, P., Ceravolo, R., Oertel, W., Quinn, N., Samuel, M., Rehncrona, S., et al. (2000). Delayed recovery of movement-related cortical function in Parkinson's disease after striatal dopaminergic grafts. Ann. Neurol. *48*, 689–695.

Piccini, P., Pavese, N., Hagell, P., Reimer, J., Björklund, A., Oertel, W.H., Quinn, N.P., Brooks, D.J., and Lindvall, O. (2005). Factors affecting the clinical outcome after neural transplantation in Parkinson's disease. Brain *128*, 2977–2986.

Rangasamy, S.B., Soderstrom, K., Bakay, R.A., and Kordower, J.H. (2010). Neurotrophic factor therapy for Parkinson's disease. Prog. Brain Res. *184*, 237–264.

Redmond, D.E., Jr., Elsworth, J.D., Roth, R.H., Leranth, C., Collier, T.J., Blanchard, B., Bjugstad, K.B., Samulski, R.J., Aebischer, P., and Sladek, J.R., Jr. (2009). Embryonic substantia nigra grafts in the mesencephalon send neurites to the host striatum in non-human primate after overexpression of GDNF. J. Comp. Neurol. *515*, 31–40.

Reyes, S., Fu, Y., Double, K., Thompson, L., Kirik, D., Paxinos, G., and Halliday, G.M. (2012). GIRK2 expression in dopamine neurons of the substantia nigra and ventral tegmental area. J. Comp. Neurol. *520*, 2591–2607.

Rosenblad, C., Martinez-Serrano, A., and Björklund, A. (1996). Glial cell line-derived neurotrophic factor increases survival, growth and function of intrastriatal fetal nigral dopaminergic grafts. Neuroscience *75*, 979–985.

Sinclair, S.R., Svendsen, C.N., Torres, E.M., Martin, D., Fawcett, J.W., and Dunnett, S.B. (1996). GDNF enhances dopaminergic cell survival and fibre outgrowth in embryonic nigral grafts. Neuroreport *7*, 2547–2552.

Surmacz, B., Noisa, P., Risner-Janiczek, J.R., Hui, K., Ungless, M., Cui, W., and Li, M. (2012). DLK1 promotes neurogenesis of human and mouse pluripotent stem cell-derived neural progenitors via modulating Notch and BMP signalling. Stem Cell Rev Rep *8*, 459–471.

Szklarczyk, D., Morris, J.H., Cook, H., Kuhn, M., Wyder, S., Simonovic, M., Santos, A., Doncheva, N.T., Roth, A., Bork, P., et al. (2017). The STRING database in 2017: quality-controlled protein-protein association networks, made broadly accessible. Nucleic Acids Res. *45* (D1), D362–D368.

Thompson, L., and Björklund, A. (2012). Survival, differentiation, and connectivity of ventral mesencephalic dopamine neurons following transplantation. Prog. Brain Res. *200*, 61–95.

Thompson, L.H., Grealish, S., Kirik, D., and Björklund, A. (2009). Reconstruction of the nigrostriatal dopamine pathway in the adult mouse brain. Eur. J. Neurosci. *30*, 625–638.

Wakeman, D.R., Redmond, D.E., Jr., Dodiya, H.B., Sladek, J.R., Jr., Leranth, C., Teng, Y.D., Samulski, R.J., and Snyder, E.Y. (2014). Human neural stem cells survive long term in the midbrain of dopamine-depleted monkeys after GDNF overexpression and project neurites toward an appropriate target. Stem Cells Transl. Med. *3*, 692–701.

Wang, Y., Perng, S.L., Lin, J.C., and Tsao, W.L. (1994). Cholecystokinin facilitates methamphetamine-induced dopamine overflow in rat striatum and fetal ventral mesencephalic grafts. Exp. Neurol. *130*, 279–287.

Watmuff, B., Hartley, B.J., Hunt, C.P., Fabb, S.A., Pouton, C.W., and Haynes, J.M. (2015). Human pluripotent stem cell derived midbrain PITX3(eGFP/w)

neurons: a versatile tool for pharmacological screening and neurodegenerative modeling. Front. Cell. Neurosci. *9*, 104.

Winkler, C., Georgievska, B., Carlsson, T., Lacar, B., and Kirik, D. (2006). Continuous exposure to glial cell line-derived neurotrophic factor to mature dopaminergic transplants impairs the graft's ability to improve spontaneous motor behavior in parkinsonian rats. Neuroscience *141*, 521–531.

Xiao, H., Hirata, Y., Isobe, K., and Kiuchi, K. (2002). Glial cell line-derived neurotrophic factor up-regulates the expression of tyrosine hydroxylase gene in human neuroblastoma cell lines. J. Neurochem. *82*, 801–808.

Yurek, D.M. (1998). Glial cell line-derived neurotrophic factor improves survival of dopaminergic neurons in transplants of fetal ventral mesencephalic tissue. Exp. Neurol. *153*, 195–202.

STAR★METHODS

KEY RESOURCES TABLE

REAGENT or RESOURCE	SOURCE	IDENTIFIER
Antibodies		
Mouse monoclonal anti-adenomatous polyposis coli, CC1 (APC)	Abcam	Cat# ab16794, RRID:AB_443473
Rabbit polyclonal anti-Barhl1	Novus Biologicals	Cat# NBP1-86513, RRID:AB_11034569
Mouse monoclonal anti-Calbindin-C28K	Swant	Cat# 300, RRID:AB_10000347
Rabbit anti-Cholecystokinin	P. Frey; Frey, 1983	N/A
Goat polyclonal anti-cFOS	Santa Cruz Biotechnology	Cat# sc-52, RRID:AB_2106783
Rat monoclonal anti-Ctip2	Abcam	Cat# ab18465, RRID:AB_2064130
DAPI	Sigma-Aldrich	Cat# D8417
Rabbit polyclonal anti-Darpp32	Millipore	Cat# AB10518, RRID:AB_10807019
Goat polyclonal anti-Foxa2	Santa Cruz Biotechnology	Cat# sc-6554, RRID:AB_2262810
Goat polyclonal anti-GDNF	R&D Systems	Cat# AB-212-NA, RRID:AB_354287
Chicken polyclonal anti-GFP	Abcam	Cat# ab13970, RRID:AB_300798
Rabbit polyclonal ant-GFP	Abcam	Cat# ab290, RRID:AB_303395)
Rabbit polyclonal anti-Girk2 (Kir3.2)	Alomone Labs	Cat# APC-006, RRID:AB_2040115
Mouse monoclonal anti-Human nuclear antigen	Millipore	Cat# MAB1281, RRID:AB_94090
Mouse monoclonal anti-NeuN	Millipore	Cat# MAB377, RRID:AB_2298772
Rabbit polyclonal anti-Nurr1	Santa Cruz Biotechnology	Cat# sc-990, RRID:AB_2298676
Rabbit polyclonal anti-Otx2	Millipore	Cat# AB9566, RRID:AB_2157186
Goat polyclonal anti-Otx2	R&D Systems	Cat# AF1979, RRID:AB_2157172
Rabbit monoclonal anti-Phospho-p44/42 MAPK	Cell Signaling Technology	Cat# 4370, RRID:AB_2315112
Sheep polyclonal anti-Pitx2	R&D Systems	Cat# AF7388, RRID:AB_11128639
Rabbit polyclonal anti-Phospho-S6 (pS6)	Cell Signaling Technology	Cat# 2211, RRID:AB_331679
Mouse monoclonal anti-Ncam (Eric1)	Santa Cruz Biotechnology	Cat# sc-106, RRID:AB_627128
Rabbit polyclonal anti-RFP	Rockland	Cat# 600-401-379, RRID:AB_2209751
Mouse monoclonal anti-Synaptophysin	Enzo Life Sciences	Cat# ADI-905-782, RRID:AB_10617740
Rabbit polyclonal anti-TH	Pel-Freez Biologicals	Cat# P40101-0, RRID:AB_461064
Sheep polyclonal anti-TH	Pel-Freez Biologicals	Cat# P60101-0, RRID:AB_461070
Rabbit polyclonal anti-5HT	ImmunoStar	Cat# 20080, RRID:AB_572263
Bacterial and Virus Strains		
AAV5-CBAp-hGDNF-235	Gift from D. Kirik	N/A
AAV5-CBA-mCherry-243	Gift from D. Kirik	N/A
Chemicals, Peptides, and Recombinant Proteins		
Accutase	Innovative Cell Technologies	Cat# AT104
Ascorbic acid	Sigma-Aldrich	Cat# A4403
Brain-derived neurotrophic factor	R&D Systems	Cat# 248-BDB
CHIR99021	Miltenyi Biotech	Cat# 130-103-926
D-amphetamine sulfate	Tocris Bioscience	Cat# 2813
Dibutyryl cAMP	Tocris Bioscience	Cat# 1141
Glial cell line-derived neurotrophic factor	R&D Systems	Cat# 212-GD
Laminin-521	BioLamina	Cat# LN521
LDN193189	Miltenyi Biotech	Cat# 130-103-925
mTeSR1	StemCell Technologies	Cat# 85880

(*Continued on next page*)

Continued

REAGENT or RESOURCE	SOURCE	IDENTIFIER
N-[N-(3,5-Difluorophenacetyl)-L-alanyl]-S-phenylglycine t-butyl ester (DAPT)	Sigma-Aldrich	Cat# D5942
Purmorphamine	Miltenyi Biotech	Cat# 130-104-465
ReLeSR	StemCell Technologies	Cat# 05873
SB431542	R&D Systems	Cat# 1614
SHH C25II	R&D Systems	Cat# 464-SH
TGFβ3	Peprotech	Cat# 100-36E
Y27632 (ROCK inhibitor)	Tocris Bioscience	Cat# 1254
Critical Commercial Assays		
MycoAlert™ Mycoplasma Detection Kit	Lonza	Cat# LT07-218
RNeasy Mini Kit	QIAGEN	Cat# 74104
SuperScript™ VILO™ cDNA Synthesis Kit	Invitrogen	Cat# 11754050
SYBR GreenER™ qPCR SuperMix Universal Kit	Invitrogen	Cat# 11762100
TruSeq Stranded mRNA Library Prep Kit	Illumina	Cat# RS-122-2101
Deposited Data		
RNA-seq dataset	accession number GEO: GSE143136	NCBI's Gene Expression Omnibus
Experimental Models: Cell Lines		
H9 PITX3-GFP human embryonic stem cells	Colin Pouton Laboratory; Watmuff et al., 2015	N/A
H9 LMX1A-GFP human embryonic stem cells	Colin Pouton Laboratory; Nefzger et al., 2012	N/A
Experimental Models: Organisms/Strains		
Mouse: BALB/c-Foxn1^{nu}/Arc	Animal Resources Centre	Cat# BCNU
Rat: CBH-^{rnu}/Arc	Animal Resources Centre	Cat# CBHNU
Oligonucleotides		
See Table S1 for list of RT-qPCR primers	N/A	N/A
Software and Algorithms		
ImageJ (Fiji) version 2.0.0	NIH	RRID:SCR_003070, https://imagej.net/Fiji
Graphpad Prism version 7	Graphpad	RRID:SCR_002798), https://www.graphpad.com
Zeiss Zen Pro	Zeiss	RRID:SCR_013672, https://www.zeiss.com/microscopy/int/products/microscope-software/zen.html
FlowJo version 10.4	Becton, Dickinson and Company	RRID:SCR_008520, https://www.flowjo.com/
STRING version 11	STRING consortium	https://string-db.org/cgi/input.pl
Adobe Photoshop CC	Adobe	RRID:SCR_014199, https://www.adobe.com/products/photoshop.html
Adobe Illustrator CC	Adobe	RRID:SCR_010279, https://www.adobe.com/products/illustrator.html

LEAD CONTACT AND MATERIALS AVAILABILITY

Further information and requests for resources and reagents should be directed to and will be fulfilled by the Lead Contact, Clare Parish (clare.parish@florey.edu.au). This study did not generate new unique reagents.

EXPERIMENTAL MODEL AND SUBJECT DETAILS

Rodents

All animal procedures adhered to the Australian National Health and Medical Research Council's (NHMRC) Code of Practice for the Use of Animals in Research and were approved by the Florey Institute of Neuroscience and Mental Health animal ethics committee. Animals were group housed in individually ventilated cages on a 12:12-hour light/dark cycle with *ad libitum* access to food and water. Due to the xenogeneic transplantation of human cells into rodents, adult athymic (CBH^{rnu}) nude rats and athymic ($Foxn1^{nu}$) nude mice were used. Male and female rodents were 8-12 weeks of age at the commencement of the study and were utilized and grouped irrespective of their gender. Animals were test- and drug-naive prior to commencement of the study (i.e., 6-OHDA lesioning).

Human embryonic stem cells

The female human embryonic stem cell (hESC) reporter lines, H9 PITX3-eGFP and H9 LMX1A-eGFP, were cultured in T25 flasks coated with 5 μg/ml Laminin-521 (BioLamina) in mTeSR1 medium (StemCell Technologies) at 37°C and 5% CO_2. Media was changed everyday. When cultures reached 70%–80% confluency they were passaged for further culture by incubation in ReLeSR (StemCell Technologies) for 5 minutes at room temperature. ReLeSR was removed, cells were washed once in PBS−/− and then detached by a sharp tap of the flask and/or direct pipetting until the cells were small clumps (~5-50 cells). Clumps were pelleted without centrifugation, directly added to fresh mTeSR medium and immediately seeded into a new Laminin-521 coated flask.

METHOD DETAILS

Human ESC culture

For VM differentiation, hPSC cultures at 70%–80% confluence were dissociated by the addition of Accutase (Innovative Cell Technologies) for 5 minutes at 37°C, gently pipetted to a single cell solution and counted on a haemocytometer. 375,000 cells/cm2 were seeded in fresh mTeSR1 media supplemented with 10 μM Y27632 (ROCKi). 24 hours later, neural induction was achieved by dual SMAD inhibition using LDN193189 (200 nM, 0–11 days *in vitro*, DIV; Stemgent) and SB431542 (10 mM, 0–5DIV; R&D Systems). Ventral midbrain patterning was simultaneously achieved by supplementation of the media with sonic hedgehog (200 ng/mL, 1-7DIV; R&D Systems), purmorphamine (2 mM, 1–7DIV; Stemgent) and CHIR99021 (3 mM, 3–13DIV; Miltenyi Biotech). From 11DIV, cultures were matured in the presence of brain-derived neurotrophic factor (BDNF, 20ng/ml, R&D Systems), glial cell line-derived neurotrophic factor (GDNF, 20ng/ml, R&D Systems), recombinant human transforming growth factor type b3 (TGFb3, 1ng/ml, Peprotech), ascorbic acid (200nM, SigmaAldrich), dibutyryl cAMP (0.05mM, Tocris) and DAPT (10μM, Sigma-Aldrich). At 20 DIV cultures enriched with ventral midbrain progenitors were dissociated using Accutase (Innovative Cell Technologies) in preparation for transplantation.

Surgical procedures

Surgeries were performed on 78 athymic (CBH^{rnu}) nude rats and 26 athymic ($Foxn1^{nu}$) nude mice under 2%–5% isofluorane anesthesia. Rats received unilateral injections (3.5ul) of 6-OHDA (3.5 μg/μl free base dissolved in a solution of 0.2 mg/ml L-ascorbic acid in 0.9% w/v NaCl) into the medial forebrain bundle (MFB, 3.4mm posterior, and 1.3mm lateral to bregma, and 6.8mm below the dura surface) using a 10 mL Hamilton syringe fitted with a glass capillary. In mice, 6OHDA (1.5μl, 1.6 μg/μl) was injected into the substantia nigra (3.0mm posterior, 1.2mm lateral to bregma, and 4.2mm below the dura surface). A subset of animals received an injection of the adeno-associated viral vector carrying GDNF under the chicken β-actin promoter (AAV-GDNF, 0.25 μl; $7.2e^{12}$ gc/ml) or a control virus, expressing mCherry fluorescent protein (AAV-mCherry, 0.25 μl; $4.1e^{12}$ gc/ml) into the dorsolateral striatum (Rats: 0.5mm rostral, 3.5mm lateral to Bregma and 3.6mm below the surface of the brain; Mice: 1mm rostral, 2mm lateral to Bregma and 2.9mm below the surface of the brain). Human PSC-derived DA progenitors were transplanted into the denervated striatum (1 μl; 100,000 cells/μl) (Rats: 0.5mm anterior, 2.5mm lateral to Bregma and 4.0mm below the dura surface; Mice: 0.5mm anterior, 2.5mm lateral, 4.0mm ventral).

Study I - Transplantation of progenitors into a GDNF-overexpressing environment

AAV-GDNF (or AAV-mCherry as control) was injected into rats 5 weeks after 6-OHDA lesioning. After a further 3 weeks, these animals were implanted with VM progenitors differentiated from the H9 PITX3-eGFP human ESC line (100,000 cells in 1ul). *Study II – Delayed exposure of the transplant to GDNF*: Eight weeks following 6-OHDA lesioning, rats and mice received implants of 100,000 FACS isolated GFP-expressing VM progenitors. For FACS isolation of GFP+ progenitors, differentiated VM cultures from the H9 LMX1A-GFP hPSC line were filtered using a 70 μm cell strainer and re-suspended at $3x10^6$ cells/ml in HBSS-Ca^{2+}-Mg2+ containing 1% BSA, 0.05% DNase and 1mM EDTA. The GFP+ cell fraction was separated using a FACS Diva flow cytometer (100 μm nozzle at 22PSI, MoFlo XDP, Becton Dickinson) after initial filtering for cell debris and doublets as well as the dead cell (7-aminoactionomycin-D labeled) fraction. The detection threshold for GFP was established using differentiated VM cultures from (a non-reporter) H9 hPSC. Purity in the GFP+ populations was found to be > 99% based in reanalysis of the separated fraction. The cells were collected in HBSS-Ca^{2+}-Mg2+ containing 1% fetal bovine serum (FBS), pelleted by centrifugation and immediately re-suspended at $1x10^6$ cells/ul, in preparation for transplantation (de Luzy et al., 2019). Three weeks later AAV-GDNF was injected into the host striatum. *Study III – Acute assessment of grafts' responsiveness to GDNF:* 6OHDA lesioned mice received grafts of 100,000 VM progenitors differentiated from the H9 PITX3-eGFP human ESC line, to enable specific tracking of graft-derived (GFP+) DA cells. Three weeks

later AAV-GDNF was injected into the host striatum. A subset of animals confirmed expression of the GDNF transgene (by GDNF histochemistry) after 10 days, but not earlier, and hence control and AAV-GDNF animals were killed at day 14, enabling assessment of grafts after acute(~4day) expose to GDNF.

Behavioral Analysis

Four weeks after lesioning, unilateral DA function was assessed using the amphetamine-induced rotation and cylinder tests, with re-testing performed at various intervals following transplantation. In brief, *Amphetamine rotations*: net rotations over 60 minutes were analyzed 10 minutes after intraperitoneal injection of D-amphetamine sulfate (5mg/kg; Tocris Bioscience). *Cylinder test*: animals were placed within a clear glass cylinder (20cm diameter) and two observers recorded 20 weight-bearing forepaw wall contacts over three consecutive days. Data is presented as left paw ratio: (Left/(Left + Right))*100. Upon completion of initial testing 4 weeks post-lesioning, animals displaying a functional deficit (> 300 rotations in 60 min) were ranked in order of the percentage rotational asymmetry and evenly distributed across the four treatment groups (Lesion, Lesion+GDNF, Lesion+Graft, Lesion+Graft+GDNF). The behavioral testing and allocation to (4) treatment groups was performed on 2 cohorts of rats, for Study I and Study II, described above.

Immunohistochemistry

Animals received intraperitoneal D-amphetamine sulfate (5mg/kg) one hours prior to receiving an overdose of sodium pentobarbitone (100mg/kg) followed by transcardial perfusion with Tryode solution followed by 4% paraformaldehyde. Brains were coronally or horizontally sectioned (40 μm; 12 series) on a freezing microtome (Leica).

Immunohistochemistry was performed on free-floating sections from adult rats and mice. The tissue was

incubated overnight with primary antibodies diluted in 0.1 m PBS containing 5% normal serum and 0.25% Triton X-100 (Amresco, USA). Primary antibodies and dilutions are shown in the Key Resources Table.

Detection of the primary–secondary antibody complexes was through peroxidase driven precipitation of di-amino-benzidine (DAB), or conjugation of a fluorophore. Secondary antibodies generated in donkey were applied for 2 h at room temperature at a dilution of 1:400 for fluorescent detection using 488, 549 or 649 conjugated anti-mouse, anti-chicken, anti-rabbit, antisheep or anti-goat (Jackson ImmunoResearch). Chromogenic detection of antibody-DAB complex was carried out using biotin conjugated donkey anti-rabbit (1:500, 2 h; Jackson ImmunoResearch) followed by peroxidase conjugated streptavidin (1 h, Vectastain ABC kit, Vector laboratories) and incubation with DAB (0.5mg/ml, 5min), which was precipitated by addition of 1% w/v H2O2 . Fluorescently labeled sections were coverslipped with fluorescent mounting media (Dako) and chromogenic labeled sections dehydrated in alcohol and xylene and coverslipped with DePeX mounting media (BDH Chemicals, UK).

Gene Expression Analysis

For transcriptional profiling, the ipsilateral striatal hemisphere containing the LMX1A-GFP transplant was dissected from mice 6 months after transplantation. The tissue was lysed using a TissueLyser LT (QIAGEN) and total RNA extracted using the RNeasy Mini Kit (QIAGEN). RNA yield and integrity were assessed using a Nanodrop One spectrophotometer (ThermoFisher Scientific) and confirmed using a Qubit (Thermo Fisher Scientific) and Tapestation (Agilent). The RNA was analyzed by RNA-seq (illumina). Alignment against the human genome was conducted to select only human specific sequences for analysis. GO enrichment analysis (biological process) was performed using the DAVID gene ontology browser, protein-protein interactions were probed using STRING (https://string-db.org/cgi/input.pl) (Szklarczyk et al., 2017). A number of genes showing significant change in expression (between Graft and Graft + GDNF) were validated using quantitative real time PCR (qPCR, ABI7700 sequence detection system, Applied Biosystems, Foster City, CA), using the comparative ΔΔCT method. To selectively assess these gene expression changes in the graft and not host tissue, quantitative PCR (qPCR) primers were designed against regions containing nucleotide base-pair differences between the mouse and human gene. Primers were validated for their selectivity on control mouse (no expression) and human (gene expression) tissue, prior to testing on grafted samples. See Table S1 for a list of primers.

Real time PCR, to validate GDNF receptor expression, was performed on undifferentiated PSCs (0 DIV) and differentiated VM progenitors (11, 20 and 25 DIV). The amplicon sizes for GFRa1 and RET were 133 and 122 bp, respectively. In brief, 10ul of the amplified product was loaded per lane and electrophoretically separated using a 3.5% agarose gel at 80V for 55 min.

HPLC

Using reverse phase liquid chromatography with electrochemical detection, dopamine and its metabolites, 3,4-Dihydroxyphenylacetic acid (DOPAC) and homovanillic acid (HVA), levels were measure from mouse striatal tissue 6 months after the transplantation of LMX1A-GFP VM progenitors, in the absence and presence of GDNF. For tissue preparation, the striatal tissue was dissected out on a chilled plate, weighed, and placed in 200 μL 0.4 M perchloric acid ($HClO_4$) containing 0.05% sodium metabisulphite ($Na_2S_2O_5$) and 0.01% disodium EDTA. The sample tissue was homogenized, cellular and vesicular membranes disrupted using a sonicator and finally stored at −80°C. On the day of analysis, all samples were centrifuged at 10,000 rpm for 10 minutes, and filtered through min-ispin filters for additional 3 minutes at 10,000 rpm before being injected into the HPLC. For each sample, 5 μL was injected by a cooled autosampler (SIL 20A, Shimadzu, Rydalmere, NSW, Australia) and Shimadzu LC-AT pump on to a reverse-phase C18 column (4.6mm diameter, 150mm length; CHROMPACK, Croydon, UK) coupled with an electrochemical detector (Decade II, Antec Leyden, Rydalmere, NSW, Australia). The mobile phase, (KH_2PO_4, 70mM; EDTA di-sodium salt, 0.5 mM; octane-sulphonic acid, sodium salt,

8mM; with 17% HPLC grade methanol, pH 3) was delivered at a flow rate of 500 mL min^{-1}). Data was expressed as pmol/ml of DA, DOPAC or HVA and dopamine turnover determined by the ratio of DA to HVA.

QUANTIFICATION AND STATISTICAL ANALYSIS

Fluorescence images were captured on a Zeiss Axio ObserverZ.1 upright epifluorescence or Zeiss LSM 780 confocal microscope. Bright and darkfield images, including multi-tiled images, were taken on a Leica DM6000 upright microscope, and where necessary, images stitched using Zen (Zeiss) or LAS (Leica) software. Grafts were delineated by human PSA-NCAM expression and volume extrapolated using Cavalieri's principle. For GFP, TH and cFOS+ quantification, all positive cells were counted from brightfield images and corrected for series number. For GIRK2 and Calbindin quantification, dopamine neurons were first identified using TH immunoreactivity from confocal images. For fiber density assessment, 10 z stack sections (1μm per section) were obtained and compressed. TH+ fibers were isolated on color inverted images using the 'color range' tool on Photoshop (Adobe). Data is expressed as percentage of immunoreactive pixels. All areas were captured in triplicate with conserved settings. Sampling for fiber density and cFOS labeled neurons was performed in the medial (AP: 0.0, ML: −1.8 and DV: −5.1), dorsolateral (AP: 0.0, ML: −3.8 and DV: −3.9) and ventrolateral (AP: 0.0, ML: −4.0 and DV: −6.9) striatum of rats, (from sections 1 mm anterior to 1.5mm posterior to Bregma).

Note, all behavior testing and histological assessments were performed with the researcher blinded to the experimental group.

All data are presented as mean ± SEM. Statistical tests employed (inclusive of one- and two-way ANOVA and Student's t tests) and number of independent culture replicates or animals/group are stated in figure legends. Alpha levels of $p < 0.05$, $^{**}p < 0.01$, $^{***}p < 0.001$ and $^{****}p < 0.0001$.

DATA AND CODE AVAILABILITY

The RNA-seq data generated from this study has been deposited in NCBI's Gene Expression Omnibus and are accessible through series accession number GEO: GSE143136.

Appendix 4. Prolonged GDNF presentation from tissue-specific hydrogels improves the functional integration of human neural grafts in a rodent model of Parkinson's Disease

Prolonged GDNF presentation from tissue-specific hydrogels improves the functional integration of human neural grafts in a rodent model of Parkinson's Disease

Vanessa Penna[1*], Carlos C.W. Gantner[1*], Yi Wang[2], Charlotte Ermine[1], Niamh Moriarty[1], Cameron P. Hunt[1], Isabelle R. de Luzy[1], Ben *** [3], Richard Williams [3], Lachlan H. Thompson[1], David R. Nisbet[2], Clare L. Parish[1†]

[1] The Florey Institute of Neuroscience and Mental Health, The University of Melbourne, Parkville, Victoria, Australia, 3052. [2] Laboratory of Advanced Materials, Research School of Engineering, The Australian National University, Canberra, Australia, 2601. [3] Centre for Molecular and Medical Research, School of Medicine, Deakin University, Warun Ponds, VIC 3216, Australia

* Equal contribution
†Author for correspondence: Clare Parish, clare.parish@florey.edu.au

Running title: Functionalised hydrogels support dopamine grafts in PD

Key Words: stem cells, transplantation, dopamine, Parkinson's Disease, biomaterials, self-assembling peptide, hydrogel, laminin, glial cell-derived neurotrophic factor, GDNF.

Acknowledgements

The authors thank Mong Tien and Brianna Xuerub for their expert technical assistance and acknowledge the support of the flow cytometry facility at the Melbourne Brain Centre. VP and IDL were supported by The University of Melbourne International Scholarships, Australia. CG is supported by an Australian Postgraduate Award. DRN was supported by a NHMRC Dementia Research Leadership Fellowship (APP1135687). CP was supported by a Senior Research Fellowship provided by the National Health and Medical Research Council Australia. This research was funded by the National Health and Medical Research Council Australia project grant APP11599265, APP1144996 and Stem Cells Australia. The Florey Institute of Neuroscience and Mental Health acknowledges the strong support from the Victorian Government and in particular the funding from the Operational Infrastructure Support Grant. Access to the facilities of the Centre for Advanced Microscopy (CAM) with funding through the Australian Microscopy and Microanalysis Research Facility (AMMRF) is gratefully acknowledged. This research was undertaken on the small angle X-Ray Scattering beamline at the Australian Synchrotron, part of Australian Nuclear Science and Technology Organisation.

ABSTRACT

The survival and subsequent synaptic integration of transplanted dopaminergic (DA) progenitors are essential for ameliorating motor symptoms in Parkinson's Disease (PD). However, human pluripotent stem cell-derived (hPSC) DA progenitors are exposed to numerous stressors prior to, and during implantation that together result in poor survival. Additionally, hPSC-derived grafts show axonal plasticity below that of the intact brain, and notably inferior to fetal tissue grafts. These observations suggest that a more conducive environment, akin to the developing brain, may support hPSC-DA progenitors and improve graft outcomes. Here, we employed a tissue-specific, self-assembling peptide (SAP) hydrogel to support DA progenitor grafts. The biomimetic hydrogel presented a laminin epitope and could be loaded with glial cell-derived neurotrophic factor (GDNF) via shear gel-solution transition, to sustain delivery. SAP hydrogels were biocompatible with DA progenitor transplantation and biased A9 neuron specification (51% increase). Sustained GDNF delivery induced a 2.7-fold increase in DA neuron survival and enhanced graft plasticity. The improvements resulted in restoration of motor deficits at 6 months. Taken together, these findings highlight the therapeutic benefit of employing customised tissue-specific hydrogels to improve the standardisation, predictability and functional efficacy of human PSC transplants for PD.

INTRODUCTION

Clinical trials have provided proof of principle that the transplantation of new dopamine (DA) neurons into the striatum of Parkinson's disease (PD) patients can survive, integrate and restore motor function (Barker et al., 2016). Demonstrated using fetal tissue, these trials were hindered by challenges of standardisation, ethics and availability, and more recent efforts have focused on pluripotent stem cells (PSC) as a viable source of DA neurons. Current differentiation protocols yield correctly specified ventral midbrain (VM) progenitors that, when implanted into animal model of PD, are capable of functionally integrating (Kirkeby et al., 2012; Kriks et al., 2011; Niclis et al., 2017a), with similar efficacy to human fetal tissue (Grealish et al., 2014). These exciting observations have resulted in the recent commencement of multiple clinical trials (Barker et al., 2017).

The number of DA neurons that survive in a graft is recognized as the most decisive factor in governing whether a transplant is successful in ameliorating symptoms, yet cell survival remains a major challenge for the field. Preclinical and clinical studies report cell survival rates ranging from 1-20% for fetal tissue grafts (Castilho et al., 2000; Hagell and Brundin, 2001), and average dopamine neuron yields of <5% for human PSC-derived DA progenitor grafts (Doi et al., 2014; Kirkeby et al., 2012; Kriks et al., 2011; Niclis et al., 2017b; Samata et al., 2016). During transplantation cells undergo a series of physical traumas that render them susceptible to cell death including their detachment from underlying culture matrices, the shear forces exerted during injection into the brain and the adult host brain – an environment devoid of trophic cues (Castilho et al., 2000; Moriarty et al., 2018b).

Another major deciding factor in the functional efficiency of these grafts is their capacity to integrate into existing host circuitry, with evidence highlighting the necessity for synaptic connectivity between A9 DA neurons in the graft and host striatal neurons (Grealish et al., 2010). While the requirement for this specific synaptic integration is known, the level of reinnervation of the host tissue by fetal derived grafts remains well below that of the intact brain – a phenomena that has been termed the 'ceiling effect'(Kirik et al., 2001). This is likely underpinned by the absence of trophic cues in the adult brain, that are normally present during development when DA neurons are born and direct target-specific axogenesis *in situ*. In addition, more recent studies have observed that human PSC-derived DA transplants show significantly poorer striatal innervation than their human VM fetal counterparts (Grealish et al., 2014). The recognition that the establishment of correct neural circuitry during development requires a tightly orchestrated physical and trophic environment, suggests that greater attention to the host milieu is required to promote survival, plasticity and integration of human PSC-derived DA neurons.

A number of efforts to inhibit cell death cascades and deliver trophic proteins have been investigated to influence the survival and plasticity of grafts. However surprisingly little attention has been paid to the extracellular matrix environment, despite its importance in providing both physical and chemical support for cells, including DA neurons (Alsanie et al., 2017; Bye et al., 2019; Zhang et al., 2017). Such observations highlight an opportunity to engineer protective and cell-instructive microenvironments for neural grafts, that can concomitantly act as programmable protein delivery vectors - see reviews (Bruggeman et al., 2019; Jendelova et al., 2016). Recently, polymer hydrogels, functionalised with glial cell-derived neurotrophic factor (GDNF), were shown to improve the survival and integration of DA neurons within rodent fetal tissue grafts in models of PD (Moriarty et al., 2017; Moriarty et al., 2018b; Wang et al., 2016). In parallel work, an advanced neural tissue-specific laminin-based hydrogel was shown to improve the survival, maturation and functional integration of human PSC-derived cortical progenitor grafts in stroke models, (Somaa et al., 2017), a response that could be enhanced through sustained delivery of brain derived neurotrophic factor from the hydrogel (Nisbet et al., 2018). Such observations raise the question whether similar neural tissue-specific biomaterials, functionalised with GDNF might overcome many of the challenges currently hindering human PSC-derived VM progenitor grafts in PD.

We have recently demonstrated that long-term viral overexpression of GDNF can support hPSC-DA progenitor grafts (Gantner et al., 2020). However, unrestricted GDNF can impede graft plasticity (Gantner et al., 2020) and has been shown in rodent models to downregulate DA-associated genes after prolonged exposure (ref from GDNF paper). Here we show evidence that a tissue-specific laminin-

based hydrogel is capable of sustained GDNF release and in combination with DA progenitor transplantation can ameliorate motor deficits in PD rats. SAP hydrogels modulate behavioural recovery through increasing DA survival, A9 specification, and plasticity. These findings highlight the potential therapeutic benefit of customised hydrogels to support human PSC-derived neural transplants in brain repair.

MATERIALS & METHODS

Self-assembling peptide hydrogel preparation

A tissue specific self-assembling peptide for the brain's major ECM protein - laminin - was fabricated using solid phase peptide synthesis, as previously described (Rodriguez et al., 2013). The laminin-based epitope synthesized had the sequence isoleucine-lysine-valine-alanine-valine (IKVAV), a fragment of the a1 chain of the protein. To ensure self-assembly under physiological conditions, two aspartate residues were incorporated at the N-terminus of the peptide to lower the pH at which spontaneous assembly occurred. Gelation was initiated using a well-established pH switch, as previously described, to yield a 20mg/ml stock (Nisbet et al., 2018). The final hydrogels were made by mixing at a 1:1 ratio with magnesium and calcium-free HBSS ± cells. Following gelation, rheology was conducted to confirm a modulus similar to the rat brain (Rodriguez et al., 2013; Somaa et al., 2017). Fourier transform infrared (FTIR), circular dichroism (CD) spectroscopy, and transmission electron microscopy verified synthesis and structure of the desired nanofibrillar structure (Rodriguez et al., 2013). The resultant hydrogels could be reversed to an aqueous state by application of shear force (achieved via repeated titration or vortexing), such that the gel disassembled into a liquid solution. Reversal of the gel into a liquid state enabled incorporation and homogeneous distribution of GDNF recombinant protein into the polymer. We refer to this incorporation of the functional protein into the polymer as shear loading or shear containment. Shear reversal of the gel also enabled incorporation of cells into the aqueous polymer solution for efficient delivery into the brain.

Assessment of GDNF release, and function, from SAP hydrogel

To assess the release kinetics of GDNF from the scaffold, GDNF (100 ng, R&D Systems) was loaded into the SAP (50 μL) by reverse shearing of the gel to an aqueous state prior to casting the gel into a well of a 96-well plate. PBS (200 μL) was added to the well and incubated at 37 °C. The supernatant was collected at pre-determined intervals over a 4-week period. All supernantant samples were stored at -20 °C until the time of analysis. The GDNF levels (protein unfolding and cumulative release) was quantified by enzyme linked immunosorbent assay (ELISA), using previously described methods (Wang et al., 2014; Wang et al., 2016). Release profiles were performed in triplicate wells for each time point and, repeated on 3 independent experiments.

Small angle X-ray scattering (SAXS) was performed using the beamline at the Australian Synchrotron. Hydrogel samples were prepared, as per above, two days before testing and stored in Eppendorf vials. Prior to exposure, PBS backgrounds were loaded into 1.5 mm glass capillaries. Two 5-second exposures were taken for each sample background on two different camera lengths: 900 mm and 7000 mm. PBS backgrounds were then removed from the capillaries and replaced with hydrogel samples. Four 5-second exposures were taken for each sample on the two different camera lengths. Data analysis was performed using ScatterBrain, with averages taken for each sample on each camera length and relevant backgrounds subtracted. Data for each sample for the two different camera lengths were then combined using IgorPro.

The functionality of the GDNF released from the hydrogels was confirmed using previously described methods (Nisbet et al., 2018). As above, GDNF was shear-loaded into SAP, cast into a 48 well plate and 100ul of media added. Conditioned media (shGDNF-CM) was collected after 12 hours and applied to primary ventral midbrain neurons for comparison to untreated cultures as well as those treated directly with recombinant GDNF protein (soluble GDNF, sGDNF, 20ng/ml). Primary VM cultures were performed and assayed as previously described (Blakely et al., 2011). In brief, VM tissue was microdissected from the brains of embryonic day 11.5 (E11.5) embryos that were obtained from time-mated mice expressing GFP under the tyrosine hydroxylase promotor. VM tissue was dissociated using

0.05% trypsin and 0.1% DNase, subsequently blocked using 10% serum, and the cells resuspended in N2 media. Cells were seeded at a density of 125,000 cells/well in 48 well plates (coated with PDL/laminin). After 72 hours, cultures were fixed with 4% paraformaldehyde and TH+ neuron number and neurite length were assessed.

Ventral midbrain specification of human pluripotent stem cells

The H9 human embryonic stem cell (hESC) reporter line expressing GFP under the LMX1A promotor (LMX1A-eGFP) was expanded and differentiated to a ventral midbrain progenitor identity as previously described (Niclis et al., 2017a). In brief, the cell line, confirmed to be karyotypically normal and routinely tested for absence of mycoplasma, was cultured on laminin 521 (BioLamina) in mTeSR1 (StemCell Technologies) supplemented with 0.4% penicillin-streptomycin (Life Technologies). To promote neural induction, cells were exposed to dual SMAD inhibition using LDN193189 (200nM, Stemgent; from 0-11 days in vitro, DIV) and SB431532 (10µM, R&D Systems; 0-5DIV). Ventral patterning was achieved by addition of sonic hedgehog (C25II, 100ng/ml, R&D Systems; 1-7DIV) and purmorphamine (2µM, Stemgent; 1-7DIV), and the cells caudalised to a midbrain identity by Wnt activation using CHIR99021 (3µM, Miltenyi Biotech; 3-13DIV). Regional identity of the differentiating cells was confirmed at 11DIV. At 21 DIV cultures were dissociated using Accutase (Life Technologies) and correctly specified ventral midbrain progenitors isolated by fluorescent activated cell sorting (FACS) based upon expression of LMX1A-eGFP, using previously described methods (de Luzy et al., 2019).

Surgical Procedures

All animal procedures were conducted in agreement with the Australian National Health and Medical Research Council's published Code of Practice for the Use of Animals in Research, and experiments approved by The Florey Institute of Neuroscience and Mental Health Animal Ethics committee. Animals were group housed in individually ventilated cages with low irritant bedding on a 12:12-hour light/dark cycle with *ad libitum* access to food and water. Surgeries were performed on 55 athymic (CBHrnu) nude rats under 2% isofluorane anaesthesia. Rats received unilateral 6-OHDA (3.5µl, 3.2 µg/µl) lesions of the medial forebrain bundle at the following stereotaxic co-ordinates: 3.4mm caudal, 1.4mm lateral to bregma, and 6.8mm below the surface of the dura. Human ESC-derived LMX1A-eGFP expressing VM progenitors were transplanted into the denervated striatum (1 µl; 100,000 cells/ µl) at the following co-ordinates: 0.5mm anterior, 2.5mm lateral to Bregma and 4.0mm below the dura.

Treatment groups were as follows: Lesion, Lesion + LMX1A-eGFP+ VM progenitors (subsequently referred to as 'Cells'), Lesion + Cells+ DDIKVAV SAP (referred to as 'Cells + SAP'), Lesion + Cells + soluble GDNF ('Cells + GDNF'), and Lesion + Cells + SAP shear loaded with GDNF (Cells + SAP-GDNF), n=7-11 rats per group. GDNF was delivered (mixed with cells or shear loaded into the IKVAV polymer) at a final concentration of 1ug/injection. A total of 150,000 cells were injected per animal, delivered within the IKVAV polymer (at a final concentration of 10mg/ml) or HBSS media. All animals received a final injection volume of 2µl.

Behavioural testing

Behavioural assessment of motor impairment was performed 3 weeks after unilateral 6OHDA lesioning using the amphetamine-induced rotation and adjusted stepping tests, as previously described (Niclis et al., 2017a; Somaa et al., 2017). In brief, for rotational testing, net rotations over 60 minutes were analysed 10 minutes after intraperitoneal injection of D-amphetamine sulfate (5mg/kg; Tocris Bioscience). Animals displaying a functional deficit (>300 rotations/hr), indicative of extensive unilateral ablation of the midbrain dopamine pathway, were included in the study. The 33 rats reaching criteria were ranked in order of the percentage rotational asymmetry and evenly distributed across the 5 treatment groups. For the cylinder test, rats were placed within a clear glass cylinder and the first 20 forepaw touches recorded over three consecutive days. Data was presented as left paw ratio (Left/(Left + Right)) × 100. Behavioural testing was repeated at 24weeks post-transplantation. Note, the delivery of GDNF or SAP into 6OHDA lesioned rats, in the absence of cell grafts, had no impact on motor performance, with stable motor deficits observed at 24 weeks, indistinguishable from Lesion only animals (data not shown). Beyond motor assessment, these animals were not further analysed in the present study.

Tissue Processing & immunohistochemistry

At 24 weeks post-implantation animals all animals received an acute injection of D-amphetamine sulfate (5mg/kg) prior to an overdose of sodium pentobarbitone (100 mg/kg). Animals were transcardially perfused with 4% paraformaldehyde and the brains processed for immunohistochemistry as previously described (Somaa et al., 2017). Primary antibodies and dilution factors were as follows: mouse anti-CD11b (1:100, Serotec), goat anti-cFos (1:1000, Santa Cruz), goat anti-FOXA2 (1:200, Santa Cruz), rabbit anti-GFAP (1:200, DAKO), chicken anti-GFP (1:1,000; Abcam), rabbit anti-GFP (1:20,000; Abcam), mouse anti-human nuclear antigen (HNA, 1:300, Millipore), mouse anti PSA-NCAM (1:200, Santa Cruz), mouse anti-Nestin (1:200, Millipore), mouse anti-NeuN (1:100; R&D Systems), rabbit anti-OTX2 (1:4000; Millipore), mouse anti-synaptophysin (1:1000, human specific, Enzo Life Sciences), anti-rat endothelial cell antigen-1 (RECA-1, 1:500, Serotec), rabbit anti-TH (1:500, Pel-Freeze), sheep anti-TH (1:800, Pelfreeze). Secondary antibodies for (i) direct detection were used at a dilution of 1:200—DyLight 488, 549 or 649 conjugated donkey anti-mouse, anti-chicken or anti-rabbit (Jackson ImmunoResearch); and (ii) indirect with streptavidin-biotin amplification—biotin conjugated donkey anti-rabbit (1:500; Jackson ImmunoResearch) followed by peroxidase conjugated streptavidin (Vectastain ABC kit, Vector laboratories), or 649 conjugated streptavidin (1:200; Jackson ImmunoResearch). Total cells *in vitro*, and *in vivo* were visualized with 4', 6-diamidino-2-phenylindole (DAPI, 1:5000, Sigma-Aldrich). All fluorescent images were captured using a Zeiss Axio Observer.Z1 epifluorescence or Zeiss confocal microscope system. Bright and dark-field images were obtained using a Leica DM6000 upright microscope.

Total number of HNA+, TH+, GIRK2+, CALBINDIN+ as well as density of NeuN+ and cFOS+ cells were counted from images captured at 20X magnification. The density of graft-derived PSA-NCAM labelling (%immunoreactive pixels) within the dorsolateral striatum (the midbrain DA forebrain target that underpins gross motor function) was assessed from images captured at 20X magnification and analysed using ImageJ software. Density of human specific synaptophysin (expressed as % immunoreactive voxels) as well as % TH+ punta co-expressing hSYP (indicative of graft-derived DA synapses) was assessed from confocal captured images at 20X and analysed using iMaris software (Bitplane, USA).

The immunological response of the host brain to the implantation of the Cells and/or the SAP scaffold (including the presence of GDNF) was assessed at predetermined sites lateral to the graft-host border (delineated according to GFP labelling), as depicted in ***Figure 3A***. The area covered by GFAP or CD11b immunoreactivity was expressed as a percentage of the total pixels, as previously described (Rodriguez et al., 2014). RECA-1+ and CD34+ immunostaining was employed to identify specific host and host + graft-derived blood vessels within the graft and host tissue. Vessel density (expressed as the percentage total area covered by staining), within graft and host tissue, was estimated using previously described methods (Somaa et al., 2017).

Statistical Analysis

All data are presented as mean $\pm$ SEM. Statistical tests employed (inclusive of one-way ANOVA and student t-tests) are stated in figure legends. Alpha levels of $p<0.05$ were considered significant with all statistical analysis performed using GraphPad Prism. *$p < 0.05$, **$p < 0.01$, ***$p < 0.001$ and ****$p < 0.0001$.

RESULTS

Tissue-specific scaffolds deliver functional GDNF to promote DA survival and plasticity *in vitro*

The current study examined the capacity of GDNF functionalised scaffolds to support human pluripotent stem cell-derived VM progenitor grafts in a rat model of Parkinson's disease, ***Figure 1A***. For this purpose, we engineered a laminin-inspired hydrogel, capable of mimicking the structural and functional attributes of the brain's native extracellular matrix. The hydrogel was synthesised by the self-assembly of the specific peptide sequence, isoleucine-lysine-valine-alanine-valine (IKVAV), encoding for an epitope for the binding domain of laminin - a major ECM protein required for cell attachment, proliferation, differentiation and plasticity (Matson and Stupp, 2012). To enable assembly under

physiological conditions (pH 7.4), two aspartate residues were added to the N-terminus of the peptide to adjust the pKa, resulting in a final peptide sequence, DDIKVAV (***Figure 1B***). Aromatic fluorenylmethloxy carbonyl (Fmoc) moieties were used to protect the amino-terminus, which during self-assembly also provide shared electrons π-π interactions, creating the backbone structure (shown in red ***Figure 1B***). The individual peptides interacted through hydrogen bonds to form secondary β-sheets that were confirmed by fourier transform infrared (FTIR) and circular dichroism (CD), ***Figure 1C-D***. Through a combination of amphiphilic organisation, π-π interactions and the β sheet folding, hollow nanotubes were formed. These nanotubes interacted to create hydrated bundles (***Figure 1B***), forming the matrix of the hydrogel, and could be visualised by transmission electron microscopy (***Figure 1E***). Appropriate for *in vivo* delivery and the support of implanted neural progenitors, the resultant gels (at 10 mg/ml) had a storage and loss modulus similar to the rat brain (SAP hydrogel: G' ~ 0.6kPa, G" ~ 0.1kPa; Rat brain: 0.3-1.1kPa (Weickenmeier et al., 2018)), ***Figure 1F***. Note, shear-loading of the SAP hydrogel with GDNF had no impact on the assembly or mechanical properties of the gels (***Figure 1C,D,F***).

Structural differences between the Fmoc-DDIKVAV and the hydrogel loaded with GDNF were further confirmed through the use of SAXS. The application of SAXS to the hydrogel with shear-contained GDNF (Figure 1*** *– pic to come*) revealed differences in the scattering of electrons by each sample, indicating structural differences between the two systems. These structures were distinct from the Fmoc-DDIKVAV, highlighting the successful incorporation of GDNF on the surface of the peptide fibril without significant changes to the underlying macrostructure.

Importantly, we confirmed the stability and functionality of GDNF released from the SAP hydrogels *in vitro*, prior to *in vivo* delivery. Surprisingly, recombinant GDNF protein added directly to the culture media, rapidly unfolded/degraded, with just 20% of the protein present after 15 minutes, and less than 3% at 24 hours, ***Figure 1G***. In contrast, shear entrapment of the protein within the hydrogel resulted in an initial burst release within the first 15 minutes, likely the consequence of poorly entrapped GDNF rapidly leaking from the hydrogel prior to reforming, that was followed by a delayed and sustained release from 7-14 days, ***Figure 1H-I***. To confirm the functionality of the GDNF protein released from the SAP hydrogels, prior to *in vivo* testing, we treated VM primary cultures, isolated from the developing embryo and rich in DA progenitors, with soluble recombinant GDNF protein (sGDNF) or conditioned media collected from GDNF shear loaded SAP gels (shGDNF-CM). As anticipated, sGDNF treatment resulted in a significant increase in the survival of TH+ DA neurons in culture (%TH+/DAPI, ***Figure 1J,L-N)***, as well as TH+ neurite length (***Figure 1K,O-Q***), effects that were mimicked, although notably more modest, by treatment of the cultures with shGDNF-CM (***Figure 1J-Q***).

DA progenitors were differentiated from LMX1A-eGFP human embryonic stem cells using an established xenogeneic-free protocol (Niclis et al., 2017a). Appropriate and efficient VM fate specification of the cells in culture was validated at 11DIV by the co-expression of floor-plate marker FOXA2, forebrain-midbrain transcription factor OTX2 and neural progenitor marker NESTIN – present in >85% of cells (***Figure 1R-S***). At the time of transplantation (21DIV), >75% of cells expressed the early intrinsic determinant transgene LMX1A (LMX1A-eGFP+, ***Figure1T-U***), a population that could be readily isolated by FACS (***Figure 1V***), for the purpose of VM DA neuron enrichment in grafts, as previously described (de Luzy et al., 2019).

GDNF-Functionalized scaffolds promote functional recovery and increased graft survival in Parkinsonian rats

Behavioural testing, for asymmetric motor function in unilaterally 6OHDA lesioned rats, was performed four weeks after 6OHDA lesioning (pre-transplantation, Pre-Tx) and repeated at 24 weeks after grafting, (***Figure 2A***). All animals receiving a cell graft showed significant correction of amphetamine-induced rotational asymmetry, whilst ungrafted animals displayed a persistent stable motor deficit (***Figure 2B***). In the stepping task, used to assess spontaneous motor function, all animals prior to transplantation showed a deficit in the contralateral forepaw use (~10% use of the impaired contralateral, compared to the unimpaired ipsilateral paw). Only animals receiving DA grafts in the

presence of GDNF-functionalised SAP scaffold (black bars), showed a significant improvement in limb use 24wks after grafting, ***Figure 2C***.

In support of the observed improvement in rotational asymmetry, at 24 weeks after transplantation all animals displayed surviving grafts, predominantly confined to the striatum, as revealed by staining against the human specific neural cell adhesion protein, PSA-NCAM, ***Figure 2D-G***. No evident tissue overgrowths were observed in any grafts, indicative that the implanted progenitors were sufficiently fate restricted in vitro prior to implantation. Volumetric assessment of the PSA-NCAM+ graft revealed that grafts in the presence of the GDNF-functionalised SAP hydrogel (Cells + SAP-shGDNF) were significantly larger (2-fold) than cells in the absence or presence of SAP or sGDNF alone, ***Figure 2H***. Total cells within the grafts, quantified using human nuclear antigen (HNA) immunolabeling, showed no significant difference between Cells, Cells+sGDNF or Cells + SAP, indicating that the presence of the biomaterial had no impact on the overall survival of cells, nor their distribution (i.e. the hydrogel did not impede the migration and distribution of cells within the graft core). Commensurate with the increase in graft volume, cell grafts in the presence of the GDNF functionalised scaffold showed a concomitant increase (1.9-fold) in HNA+ cells, but no change in density, ***Figure 2I-J***.

Tissue specific scaffolds show in vivo biocompatibility and are vascularised by host-derived endothelia

Necessary for understanding the potential utility of this biomaterial approach for cell delivery was an assessment of the biocompatibility of the implanted scaffolds. We have previously demonstrated the persistence of these SAP-based hydrogels up to 9 months after implantation (Somaa et al., 2017). Therefore, we next assessed the presence of markers against reactive astrocytes (GFAP) and microglia (CD11b) 6 months after implantation. Compared to cell grafts alone (Cells), neither the presence of unfunctionalized or GDNF-functionalised SAP increased the inflammatory response, with GFAP and CD11b cell density not significant different across treatment groups, measured at either the graft-host interface (Field of View 1, FOV1, ***Supplementary Figure 3A-G***), or more protracted distances away from the graft core (data not shown). As the death of DA progenitors occurs acutely during preparation of the tissue/cell suspension, or within days of implantation (Castilho et al., 2000), in a separate cohort of animals the density of GFAP immunoreactive astrocytes was assessed 2 weeks post-implantation. Similar to assessment at 6 months, the presence of the biomaterial imparted no inflammatory response above that observed in animals implanted with Cells alone (***Supplementary Figure 1H-J***).

Necessary for the survival of cells within large grafts is their juxtaposition to a vascular supply. Staining for RECA1+, to identify endothelial cells lining the vasculature, as well as GFP to demarcate the graft, revealed the presence of a vascular network within the grafts, ***Supplementary Figure 2A-F***. In comparison to the host brain, RECA1+ vessels were significantly less dense, with no difference between grafted groups (***Supplementary Figure 2H***), indicating that neither the biomaterial nor the GDNF influenced vascularisation of the graft. Similar to previous observations of large human PSC-derived neural grafts (Somaa et al., 2017), the RECA1+ cells were GFP- (***Supplementary Figure 2G*** *– pic to come*), indicative of the recruitment endothelial progenitors from the host tissue – an unsurprising observation in light of the *in vitro* neural fate restriction of the cells, and selection of LMX1A-eGFP neural progenitors, prior to implantation.

Functionalized scaffolds promote survival of DA neurons and bias A9-specification

The function of PSC-derived VM neural progenitor graft is underpinned by their capacity to form mature, tyrosine hydroxylase (TH) expressing DA neurons. NeuN+/HNA+ co-immunoreactivity revealed that approximately a third of the cells within all grafts adopted a mature neuronal phenotype, irrespective of the presence of the hydrogel or GDNF protein, ***Figure 3A-C***. In contrast, while the acute delivery of GDNF or presence of the IKVAV SAP hydrogel alone had no impact on TH+ cell number, grafts in the presence of the functionalized SAP scaffold, sustaining GDNF delivery (Cells + SAP-shGDNF), showed a 2.7-fold increase in TH+ cells ***Figure 3D-H***. This increase in DA neurons within the graft, was over and above the increase in graft volume, with TH+ cell density notably elevated (Cells: 8.2 $\pm$ 1.4 TH+/mm^3, Cells+SAP-shGDNF: 11.7 $\pm$ 1.9 TH+/mm^3), ***Figure 3I***.

The presence of the hydrogel and/or GDNF had no impact on the capacity of the TH+ neurons within the grafts to acquire a mature fate, with >75% of all TH+ cells within the grafts showing GIRK2+ and/or Calbindin (CALB+) co-localisation, indicative of A9 and A10-like SN and VTA DA neurons. More detailed assessment of A9 and A10-like identity, however, revealed a significant shift in TH+GIRK2+ A9 fated cells in the presence of the SAP hydrogel (Cells: 1,727 $\pm$ 114; Cells + SAP: 2,878 $\pm$ 157; Cells + sGDNF: 2,609 $\pm$ 148; Cells + SAP-sh-GDNF: 7,014 $\pm$ 592). This increase in A9 fate acquisition was at the expense of A10-like identity, with a reciprocal decrease in CALB+TH+ cells (Cells: 750 $\pm$ 32; Cells + SAP: 349 $\pm$ 80; Cells + sGDNF, 637 $\pm$ 63; Cells + SAP-sh-GDNF: 1618 $\pm$ 157 TH+CALB+ cells), ***Figure 3J,L***. Assessment of proportion of TH+ cells acquiring A9 or A10 fate revealed that this fate shift was specific to the presence of the SAP hydrogel, and not additive effects of sustained GDNF, as both Cells + SAP and Cells + SAP-shGDNF showed a significant increase in the proportion of GIRK2+ cells (43% and 38%, respectively), compared to grafts of Cells alone (28%), yet were not significantly different from each other, ***Figure 3K,M***.

Functionalized scaffolds support the integration of hPSC-derived VM graft

Finally, the capacity of the grafted neurons to innervate the host striatum was assessed. Underpinning improvements in spontaneous motor function, only grafts in the presence of GDNF-functionalised scaffolds (Cells + SAP-shGDNF) showed a significant increase in density of graft-derived human PSA-NCAM+ fibers, ***Figure 4A,D***. Surprisingly, no difference in the density of graft-derived human synaptophsin was observed, indicating that neither the presence of the hydrogel or GDNF influenced synaptic maturity of the grafts at large (***Figure 4B***). As NCAM and hSYP labelled all graft derived fibres and synapses, a more selective assessment of DA synapses (TH+hSYP+) was performed, specifically within the dorsolateral striatum - the target site for A9 DA neurons responsible for motor function. The synergy of the SAP hydrogel and sustained GDNF resulted in a significant (24%) increase in the percentage of TH+ puncta colocalised with hSYP, compared to Cells alone (***Figure 4C,F-G***).

DISCUSSION

Biomaterials have the capacity to significantly improve cell transplantation for neural repair. Examined most extensively in their neural capacity to support cell transplants after stroke (see review – (Bruggeman et al., 2019; Jendelova et al., 2016), more recently functionalised natural and synthetic polymers, capable of recapitulating structural and biochemical elements of the extracellular matrix, have been shown to promote the survival, differentiation and functional integration of rodent fetal tissue grafts in models of PD (Moriarty et al., 2018a; Moriarty et al., 2017; Rodriguez et al., 2018; Wang et al., 2016). With human PSC rapidly advancing towards the clinic for cell replacement therapy in PD patients there is an evident need to understand how biomaterials may also support and improve these graft outcomes. Recent efforts, utilising functionalised hyaluronic acid hydrogels, have attempted to support hPSC-derived DA progenitors/neurons during transplantation, yet showed notably small grafts with limited integration into the host tissue and functionality below standard levels, effects likely underpinned by the mature state of the implanted cells (Adil et al., 2018; Adil et al., 2017). Here, we fabricated a shear-reversible neural tissue-specific laminin-based peptide hydrogel, capable of sustained presentation of the neurotrophic factor GDNF, to improve human PSC-derived DA graft outcomes. In animals receiving cell grafts in the presence of the GDNF-functionalised hydrogel both induced and spontaneous motor deficits were ameliorated. Underpinning these behavioural improvements were increases in graft survival, DA fate acquisition and innervation of appropriate host target nuclei.

Anoikis, a form of programmed cell death that occurs when anchorage-dependent cells are detached from their surrounding extracellular matrix, affects donor cells during their harvest from *in vitro* cultures (or dissociation of fetal tissue) as well as acutely post implantation if they fail to form local adhesions (Moriarty and Dowd, 2018). While a range of soft hydrogels that gel *in situ*, have been trialled to protect cells against shear forces during implantation and rebuild de novo tissue where necessary, their remains a requirement for engineered scaffolds to provide cell adhesive matrix *in situ* (Newland et al., 2015). In this regard, the employed self-assembling peptide-based (SAP) hydrogels, presenting a cell adhesive epitope (IKVAV) for laminin provided a tissue-specific biomimetic of the native neural ECM. *In vitro*, this functional epitope has been reported to promote neuronal adhesion and survival

with greater efficiency than laminin protein itself, due to the high density of signals presented to the surface (Silva et al., 2004). *In vivo*, IKVAV-presenting SAP hydrogels have been shown to promote the survival of human PSC-derived cortical progenitors (Nisbet et al., 2018; Somaa et al., 2017), yet surprisingly had no impact on the survival of the present VM progenitors grafts. Consequently, further study into region-sepcific ECM differences may aid design of future hydrogels. In addition to their adhesive properties, ECM proteins (including laminins) also contribute to stem cell maintenance, differentiation and plasticity (Theocharidis et al., 2014), roles that have been confirmed using IKVAV peptides for cultured neural progenitors and transplanted cortical progenitors (Nisbet et al., 2018; Somaa et al., 2017). Within the present findings, IKVAV SAP hydrogels had no impact on the maturation of VM progenitors into postmitotic NeuN+ neurons or acquisition of TH+ DA identity within grafts, yet importantly biased GIRK2+TH+ specification, at the expense of CALB+TH+ A10-like DA neurons. Likely underpinning these disparate outcomes is the complexity of the laminin family of proteins. Laminins are heterotrimeric proteins that contain α-, β-, and γ-chains, with the employed nomenclature describing the chains present (e.g. laminin-521 comprising of an α5, β2, and a γ1 subunit) – with a total of 15 laminin trimers identified to date. Interestingly, recent success in the directed differentiation of human PSC into VM DA progenitors/neurons has been underpinned by the culturing of cells on laminin substrates, with 4 specific laminins recognised in this capacity (Lam-111, Lam-421, Lam-511 and Lam-521). With hPSC-DA differentiation protocols varying between research groups, differing success for the different laminins have been observed, indicating that identification of the necessary and optimal subunits remains to be determined and/or the existence of redundant roles. Added to this, recent deep-sequencing analysis of laminin subchain expression within the developing ventral midbrain has revealed the presence of α1, α4, α5, β1, β2 and γ1, and enriched mRNA for Lam-111, -411, -421, -511 and -521 (Zhang et al., 2017). Furthermore, culturing of rodent midbrain primary neurons on Lam521 promoted survival of DA neurons (by suppressing the cell death associated protein, PTEN), and promoted DA differentiation (by increasing expression of genes critical for VM DA identity, inclusive of LMX1A and PITX3), superior to other VM present laminins (Zhang et al., 2017).

In the present study, the employed peptide sequence IKVAV (Ile-Lys-Val-Ala-Val) is derived from the α1 subchain, one of the most potent laminin subunits influencing adhesion, differentiation and plasticity. Whilst IKVAV/ α1 appeared to have no effect on survival or DA differentiation in the current context, the increase in A9 specification provides the first evidence, to our knowledge, of selectively enriching for this subpopulation DA neurons within human PSC-derived grafts. Recognising the importance of this population for alleviating motor symptoms (Grealish et al., 2010), may provide means for implanting fewer cells with more targeted function. Future efforts, exploring additional α subunits, such as α5, as well as inclusion of β and γ subchains epitopes, within composite peptide gels, that mimic naturally occurring, or artificially engineered laminins may further enhance graft outcomes according to aforementioned mechanisms for VM progenitors, as observed *in vitro*.

Growth factor deprivation of progenitors isolated from the developing embryo or *in vitro* cultures is a major contributor to cell death during acute graft integration. Such observations justified a large body of work into the re-introduction of GDNF into the adult brain to support dopamine progenitor grafts (Farrell and Barker, 2012). In addition to the impact on graft survival, GDNF is involved in DA plasticity and maturation. In the present study, acute delivery of GDNF failed to influence survival or plasticity, a likely consequence of insufficient dose and/or duration of delivery, noting that former studies showing the benefit of recombinant protein delivery in vivo used repeated doses over weeks (Rosenblad et al., 1996), or continual infusion (Yurek, 1998). In more recent years, viral delivery approaches have been employed to sustain GDNF level – targeted at slowing PD progression (Kirik et al., 2017) and supporting grafts (Farrell and Barker, 2012; Kauhausen et al., 2013) Gantner et al!!!!!!. However, a key challenge of this approach is the inability to silence the transgene after graft integration, which can result in aberrant axonal growth and downregulation of DA-associated genes in host and hPSC-derived DA grafts (Gantner et al., 2020; Winkler et al., 2006). In support of fetal tissue graft studies (Moriarty et al., 2017; Wang et al., 2016), we show prolonged delivery of GDNF from IKVAV-SAP promotes the survival and plasticity of human PSC-derived VM progenitor grafts. *In vitro* we showed an initial burst release of GDNF, followed by a delayed and sustained delivery beyond 28 days, with this biphasic delivery likely underpinning initial progenitor survival, and subsequent integration. The modest, but significant, effects on graft plasticity suggest that higher concentrations of GDNF,

and/or the incorporation of other DA axonal growth promoting proteins, such as Wnt5a (Blakely et al., 2011; Parish et al., 2008), may enhance graft plasticity and functional integration.

Vascularisation of solid tissue grafts is critical for their survival, yet surprisingly little attention has been paid to the vessel network within fetal or human PSC-derived VM progenitor grafts. We provide here the first characterisation of blood vessels within grafts, showing the presence of organised host-derived (HNA-) endothelial cells. Similar to observations that the presence of the biomaterial did not impede the capacity of transplanted cells to migrate within the host tissue (unchanged cell density within the graft core) nor extend axonal projections into the surrounding striatal target tissue, host-derived endothelial cells were capable of infiltrating into the graft core. The density of the vessel network across all graft conditions was significantly less than the host tissue, suggesting that delivery of additional trophic cues such as BDNF, VEGF and/or erythropoietin, targeted at promoting angiogenesis, may improve graft outcomes - as has been observed following SAP-sustained delivery of BDNF for human PSC-derived neural grafts in stroke (Nisbet et al., 2018).

Taken together, these findings provide the first substantiated evidence for a functionalised, tissue-specific hydrogel to improve the survival, differentiation and integration of human PSC-derived DA progenitor grafts in an animal model of PD. These findings highlight that additional efforts, incorporating functionalised biomaterials to influence the donor cells and host tissue should be considered as the field moves towards the clinic. Here we present findings for a laminin α1 subchain peptide hydrogel presenting GDNF, providing the impetus for greater attention to ECM-related and growth factor related strategies. Further studies targeting additional/alternative proteins for neuroprotection, plasticity and even vascularisation, are necessary to ensure maximal functional benefits can be obtained from grafted progenitors – targeted not only for cell replacement therapy in PD, but other conditions where cell transplantation presents a therapeutically viable option.

References

Adil, M.M., Rao, A.T., Ramadoss, G.N., Chernavsky, N.E., Kulkarni, R.U., Miller, E.W., Kumar, S., and Schaffer, D.V. (2018). Dopaminergic Neurons Transplanted Using Cell-Instructive Biomaterials Alleviate Parkinsonism in Rodents. Advanced Functional Materials *28*.

Adil, M.M., Vazin, T., Ananthanarayanan, B., Rodrigues, G.M.C., Rao, A.T., Kulkarni, R.U., Miller, E.W., Kumar, S., and Schaffer, D.V. (2017). Engineered hydrogels increase the post-transplantation survival of encapsulated hESC-derived midbrain dopaminergic neurons. Biomaterials *136*, 1-11.

Alsanie, W.F., Penna, V., Schachner, M., Thompson, L.H., and Parish, C.L. (2017). Homophilic binding of the neural cell adhesion molecule CHL1 regulates development of ventral midbrain dopaminergic pathways. Scientific reports *7*, 9368.

Barker, R.A., Parmar, M., Kirkeby, A., Bjorklund, A., Thompson, L., and Brundin, P. (2016). Are Stem Cell-Based Therapies for Parkinson's Disease Ready for the Clinic in 2016? J Parkinsons Dis *6*, 57-63.

Barker, R.A., Parmar, M., Studer, L., and Takahashi, J. (2017). Human Trials of Stem Cell-Derived Dopamine Neurons for Parkinson's Disease: Dawn of a New Era. Cell stem cell *21*, 569-573.

Blakely, B.D., Bye, C.R., Fernando, C.V., Horne, M.K., Macheda, M.L., Stacker, S.A., Arenas, E., and Parish, C.L. (2011). Wnt5a regulates midbrain dopaminergic axon growth and guidance. PLoS One *6*, e18373.

Bruggeman, K.F., Moriarty, N., Dowd, E., Nisbet, D.R., and Parish, C.L. (2019). Harnessing stem cells and biomaterials to promote neural repair. Br J Pharmacol *176*, 355-368.

Bye, C.R., Alsanie, W., Parish, C.L., and Thompson, L.H. (2019). Modulation of Semaphorin Signalling and Axon Growth by the Cell Adhesion Molecule ALCAM through a Trans-Heterophilic Interaction in Midbrain Dopamine Neurons. J Neurosci *In Press*.

Castilho, R.F., Hansson, O., and Brundin, P. (2000). Improving the survival of grafted embryonic dopamine neurons in rodent models of Parkinson's disease. Progress in brain research *127*, 203-231.

de Luzy, I.R., Niclis, J.C., Gantner, C.W., Kauhausen, J.A., Pouton, C.W., Hunt, C.P.J., Thompson, L.H., and Parish, C.L. (2019). Isolation of LMX1a ventral midbrain progenitors improves the safety and predictability of human pluripotent stem cell-derived neural transplants in Parkinsonian Disease J Neurosci.

Doi, D., Samata, B., Katsukawa, M., Kikuchi, T., Morizane, A., Ono, Y., Sekiguchi, K., Nakagawa, M., Parmar, M., and Takahashi, J. (2014). Isolation of human induced pluripotent stem cell-derived dopaminergic progenitors by cell sorting for successful transplantation. Stem Cell Reports *2*, 337-350.

Farrell, K., and Barker, R.A. (2012). Stem cells and regenerative therapies for Parkinson's disease. Degener Neurol Neuromuscul Dis *2*, 79-92.

Gantner, C.W., Kauhausen, J.A., de Luzy, I.R., Niclis, J.C., Penna, V., Hunt, C.P., Bye, C.R., Ermine, C.M., Pouton, C.W., Thompson, L.H.*, et al.* (2020). Viral delivery of GDNF promotes functional integration of human stem cell grafts in Parkinson’s disase. Cell stem cell.

Grealish, S., Diguet, E., Kirkeby, A., Mattsson, B., Heuer, A., Bramoulle, Y., Van Camp, N., Perrier, A.L., Hantraye, P., Bjorklund, A.*, et al.* (2014). Human ESC-derived dopamine neurons show similar preclinical efficacy and potency to fetal neurons when grafted in a rat model of Parkinson's disease. Cell stem cell *15*, 653-665.

Grealish, S., Jonsson, M.E., Li, M., Kirik, D., Bjorklund, A., and Thompson, L.H. (2010). The A9 dopamine neuron component in grafts of ventral mesencephalon is an important determinant for recovery of motor function in a rat model of Parkinson's disease. Brain *133*, 482-495.

Hagell, P., and Brundin, P. (2001). Cell survival and clinical outcome following intrastriatal transplantation in Parkinson disease. J Neuropathol Exp Neurol *60*, 741-752.

Jendelova, P., Kubinova, S., Sandvig, I., Erceg, S., Sandvig, A., and Sykova, E. (2016). Current developments in cell- and biomaterial-based approaches for stroke repair. Expert Opin Biol Ther *16*, 43-56.

Kauhausen, J., Thompson, L.H., and Parish, C.L. (2013). Cell intrinsic and extrinsic factors contribute to enhance neural circuit reconstruction following transplantation in Parkinsonian mice. The Journal of physiology *591*, 77-91.

Kirik, D., Cederfjall, E., Halliday, G., and Petersen, A. (2017). Gene therapy for Parkinson's disease: Disease modification by GDNF family of ligands. Neurobiology of disease *97*, 179-188.

Kirik, D., Winkler, C., and Bjorklund, A. (2001). Growth and functional efficacy of intrastriatal nigral transplants depend on the extent of nigrostriatal degeneration. J Neurosci *21*, 2889-2896.

Kirkeby, A., Grealish, S., Wolf, D.A., Nelander, J., Wood, J., Lundblad, M., Lindvall, O., and Parmar, M. (2012). Generation of regionally specified neural progenitors and functional neurons from human embryonic stem cells under defined conditions. Cell reports *1*, 703-714.

Kriks, S., Shim, J.W., Piao, J., Ganat, Y.M., Wakeman, D.R., Xie, Z., Carrillo-Reid, L., Auyeung, G., Antonacci, C., Buch, A.*, et al.* (2011). Dopamine neurons derived from human ES cells efficiently engraft in animal models of Parkinson's disease. Nature *480*, 547-551.

Matson, J.B., and Stupp, S.I. (2012). Self-assembling peptide scaffolds for regenerative medicine. Chem Commun (Camb) *48*, 26-33.

Moriarty, N., Cabre, S., Alamilla, V., Pandit, A., and Dowd, E. (2018a). Encapsulation of young donor age dopaminergic grafts in a GDNF-loaded collagen hydrogel further increases their survival, re-innervation and functional efficacy after intra-striatal transplantation in hemi-Parkinsonian rats. Eur J Neurosci.

Moriarty, N., and Dowd, E. (2018). Brain repair for Parkinson's disease: is the answer in the matrix? Neural regeneration research *13*, 1187-1188.

Moriarty, N., Pandit, A., and Dowd, E. (2017). Encapsulation of primary dopaminergic neurons in a GDNF-loaded collagen hydrogel increases their survival, re-innervation and function after intra-striatal transplantation. Scientific reports *7*, 16033.

Moriarty, N., Parish, C.L., and Dowd, E. (2018b). Primary tissue for cellular brain repair in Parkinson's disease: Promise, problems and the potential of biomaterials. Eur J Neurosci.

Newland, B., Welzel, P.B., Newland, H., Renneberg, C., Kolar, P., Tsurkan, M., Rosser, A., Freudenberg, U., and Werner, C. (2015). Tackling Cell Transplantation Anoikis: An Injectable, Shape Memory Cryogel Microcarrier Platform Material for Stem Cell and Neuronal Cell Growth. Small *11*, 5047-5053.

Niclis, J.C., Gantner, C.W., Alsanie, W.F., McDougall, S.J., Bye, C.R., Elefanty, A.G., Stanley, E.G., Haynes, J.M., Pouton, C.W., Thompson, L.H.*, et al.* (2017a). Efficiently Specified Ventral Midbrain Dopamine Neurons from Human Pluripotent Stem Cells Under Xeno-Free Conditions Restore Motor Deficits in Parkinsonian Rodents. Stem cells translational medicine *6*, 937-948.

Niclis, J.C., Gantner, C.W., Hunt, C.P.J., Kauhausen, J.A., Durnall, J.C., Haynes, J.M., Pouton, C.W., Parish, C.L., and Thompson, L.H. (2017b). A PITX3-EGFP Reporter Line Reveals Connectivity of Dopamine and Non-dopamine Neuronal Subtypes in Grafts Generated from Human Embryonic Stem Cells. Stem Cell Reports *9*, 868-882.

Nisbet, D.R., Wang, T.Y., Bruggeman, K.F., Niclis, J.C., Somaa, F.A., Penna, V., Hunt, C.P., Wang, Y., Kauhausen, J.A., Williams, R.J.*, et al.* (2018). Shear containment of BDNF within molecular hydrogels promote human stem cell engraftment and post-infarction remodeling in stroke. Advanced Biosystems *2*, 1-13.

Parish, C.L., Castelo-Branco, G., Rawal, N., Tonnesen, J., Sorensen, A.T., Salto, C., Kokaia, M., Lindvall, O., and Arenas, E. (2008). Wnt5a-treated midbrain neural stem cells improve dopamine cell replacement therapy in parkinsonian mice. The Journal of clinical investigation *118*, 149-160.

Rodriguez, A.L., Bruggeman, K.F., Wang, Y., Wang, T.Y., Williams, R.J., Parish, C.L., and Nisbet, D.R. (2018). Using minimalist self-assembling peptides as hierarchical scaffolds to stabilise growth factors and promote stem cell integration in the injured brain. Journal of tissue engineering and regenerative medicine *12*, e1571-e1579.

Rodriguez, A.L., Parish, C.L., Nisbet, D.R., and Williams, R.J. (2013). Tuning the amino acid sequence of minimalist peptides to present biological signals via charge neutralised self assembly. Soft Matter *9*, 3915-3919.

Rodriguez, A.L., Wang, T.Y., Bruggeman, K.F., Horgan, C.C., Li, R., Williams, R.J., Parish, C.L., and Nisbet, D.R. (2014). In vivo assessment of grafted cortical neural progenitor cells and host response to functionalized self-assembling peptide hydrogels and the implications for tissue repair. J Mater Chem B *2*, 7771-7778.

Rosenblad, C., Martinez-Serrano, A., and Bjorklund, A. (1996). Glial cell line-derived neurotrophic factor increases survival, growth and function of intrastriatal fetal nigral dopaminergic grafts. Neuroscience *75*, 979-985.

Samata, B., Doi, D., Nishimura, K., Kikuchi, T., Watanabe, A., Sakamoto, Y., Kakuta, J., Ono, Y., and Takahashi, J. (2016). Purification of functional human ES and iPSC-derived midbrain dopaminergic progenitors using LRTM1. Nature communications *7*, 13097.

Silva, G.A., Czeisler, C., Niece, K.L., Beniash, E., Harrington, D.A., Kessler, J.A., and Stupp, S.I. (2004). Selective differentiation of neural progenitor cells by high-epitope density nanofibers. Science *303*, 1352-1355.

Somaa, F.A., Wang, T.Y., Niclis, J.C., Bruggeman, K.F., Kauhausen, J.A., Guo, H., McDougall, S., Williams, R.J., Nisbet, D.R., Thompson, L.H.*, et al.* (2017). Peptide-Based Scaffolds Support Human Cortical Progenitor Graft Integration to Reduce Atrophy and Promote Functional Repair in a Model of Stroke. Cell reports *20*, 1964-1977.

Theocharidis, U., Long, K., ffrench-Constant, C., and Faissner, A. (2014). Regulation of the neural stem cell compartment by extracellular matrix constituents. Progress in brain research *214*, 3-28.

Wang, T.Y., Bruggeman, K.A., Sheean, R.K., Turner, B.J., Nisbet, D.R., and Parish, C.L. (2014). Characterization of the stability and bio-functionality of tethered proteins on bioengineered scaffolds: implications for stem cell biology and tissue repair. J Biol Chem *289*, 15044-15051.

Wang, T.Y., Bruggeman, K.F., Kauhausen, J.A., Rodriguez, A.L., Nisbet, D.R., and Parish, C.L. (2016). Functionalized composite scaffolds improve the engraftment of transplanted dopaminergic progenitors in a mouse model of Parkinson's disease. Biomaterials *74*, 89-98.

Weickenmeier, J., Kurt, M., Ozkaya, E., de Rooij, R., Ovaert, T.C., Ehman, R.L., Butts Pauly, K., and Kuhl, E. (2018). Brain stiffens post mortem. J Mech Behav Biomed Mater *84*, 88-98.

Winkler, C., Georgievska, B., Carlsson, T., Lacar, B., and Kirik, D. (2006). Continuous exposure to glial cell line-derived neurotrophic factor to mature dopaminergic transplants impairs the graft's ability to improve spontaneous motor behavior in parkinsonian rats. Neuroscience *141*, 521-531.

Yurek, D.M. (1998). Glial cell line-derived neurotrophic factor improves survival of dopaminergic neurons in transplants of fetal ventral mesencephalic tissue. Experimental neurology *153*, 195-202.

Zhang, D., Yang, S., Toledo, E.M., Gyllborg, D., Salto, C., Carlos Villaescusa, J., and Arenas, E. (2017). Niche-derived laminin-511 promotes midbrain dopaminergic neuron survival and differentiation through YAP. Sci Signal *10*.

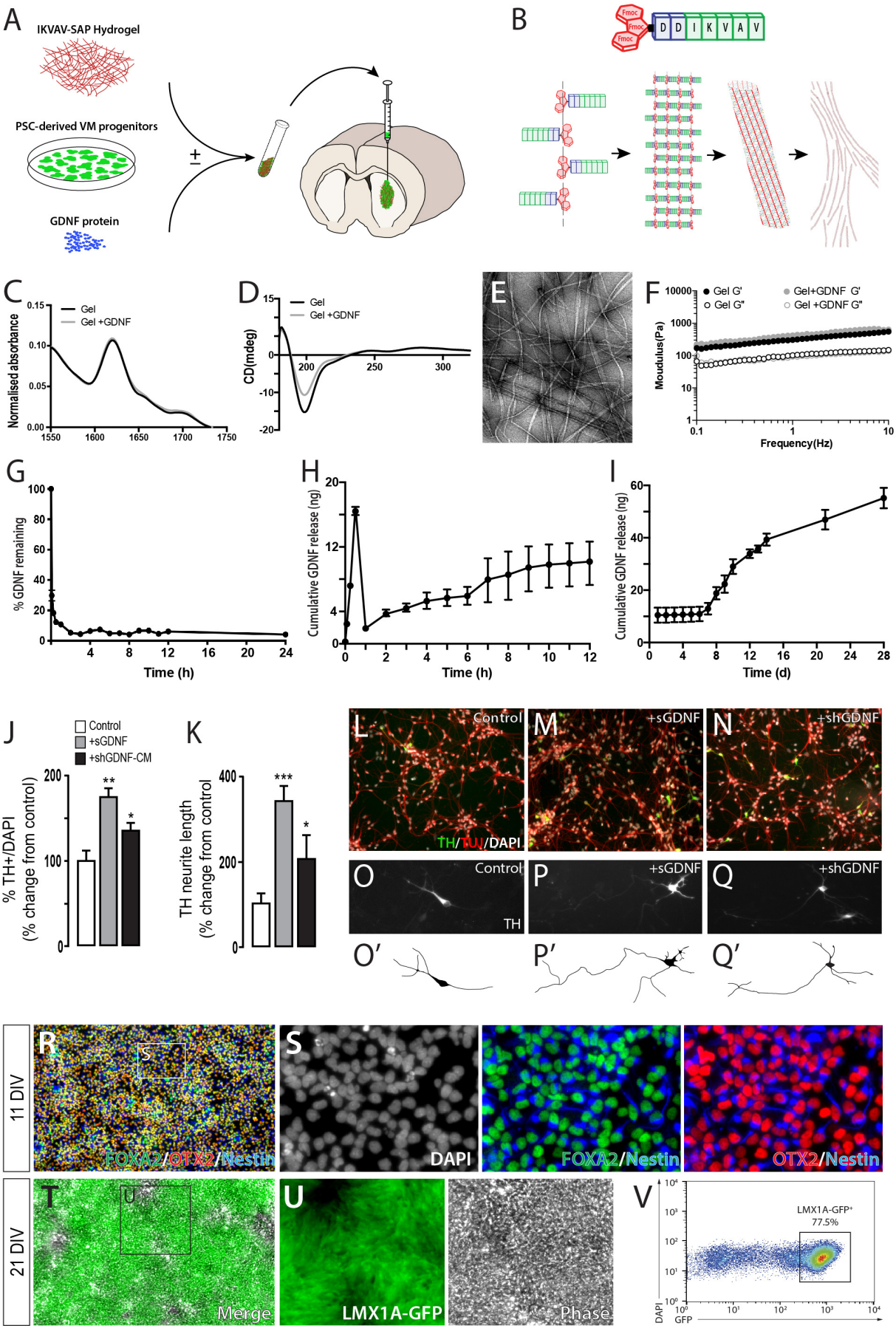
A
IKVAV-SAP Hydrogel
PSC-derived VM progenitors
GDNF protein
B
Fmoc
D D I K V A V
C
Gel
Gel +GDNF
Normalised absorbance
D
CD(mdeg)
E
F
Gel G'
Gel G"
Gel+GDNF G'
Gel +GDNF G"
Moudulus(Pa)
Frequency(Hz)
G
% GDNF remaining
Time (h)
H
Cumulative GDNF release (ng)
Time (h)
I
Cumulative GDNF release (ng)
Time (d)
J
Control
+sGDNF
+shGDNF-CM
% TH+/DAPI
(% change from control)
K
TH neurite length
(% change from control)
L
Control
TH/TUJ/DAPI
M
+sGDNF
N
+shGDNF
O
Control
TH
P
+sGDNF
Q
+shGDNF
O'
P'
Q'
11 DIV
R
S
FOXA2/OTX2/Nestin
DAPI
FOXA2/Nestin
OTX2/Nestin
21 DIV
T
U
Merge
LMX1A-GFP
Phase
V
LMX1A-GFP+
77.5%
DAPI
GFP

Figure 1. Generation of SAP hydrogel biomaterial and hESC-derived VM progenitors suitable for transplantation. (A) Schematic of *in vivo* study design. (B) Schematic peptide structure showing its self-assembly, leading to a naturally nanofiber structure (combination of amphiphilic organisation, π-π interactions and the β sheet folding forming the nanofibrils). (C) Peptide interaction through hydrogen bonds forming and secondary β sheets were confirmed by Fourier transform infrared (FTIR) of amide I region showing characteristic peak for β sheets with an observable carbamate peak. (D) The stable formation of a dominant assembly, confirmed by circular dichroism spectroscopy, showing transition peak at 220 nm. (E) Electron microscopy confirmed the appropriate assembly of Hydrogel nanofibrils. (F) Storage and loss modulus of the hydrogel. (G) Soluble GDNF in media was rapidly degraded (>90% degradation within 2hrs). (H-I) Shear entrapment of GDNF within the hydrogel resulted in an initial burst release (within 15 mins), followed by a delayed and sustained release, observed over 28 days. (J-K) VM primary cultures treated with soluble recombinant GDNF protein (sGDNF) and with conditioned media collected from SAP hydrogels shear loaded with GDNF (shGDNF-CM), confirming GDNF functionality – as revealed by increased TH+ cells and longer neurites. (L-Q) Representative pictures from VM primary culture with and without sGDNF or shGDNF-CM. (R-S) VM fate specification of human PSCs at 11DIV confirmed by the co-expression of FOXA2, OTX2 and NESTIN. (T-U) Expression of the early intrinsic determinant transgene, LMX1A, at the time of transplantation (21DIV). (V) Use of an LMX1A-eGFP reporter human PSC cell line enabled isolation of correctly specified VM progenitors, by FACS isolation, prior to transplantation. Data represents Mean +SEM. Figure J-K, n=3 independent cultures. * $p<0.05$, ** $p< 0.01$, *** $p<0.001$.

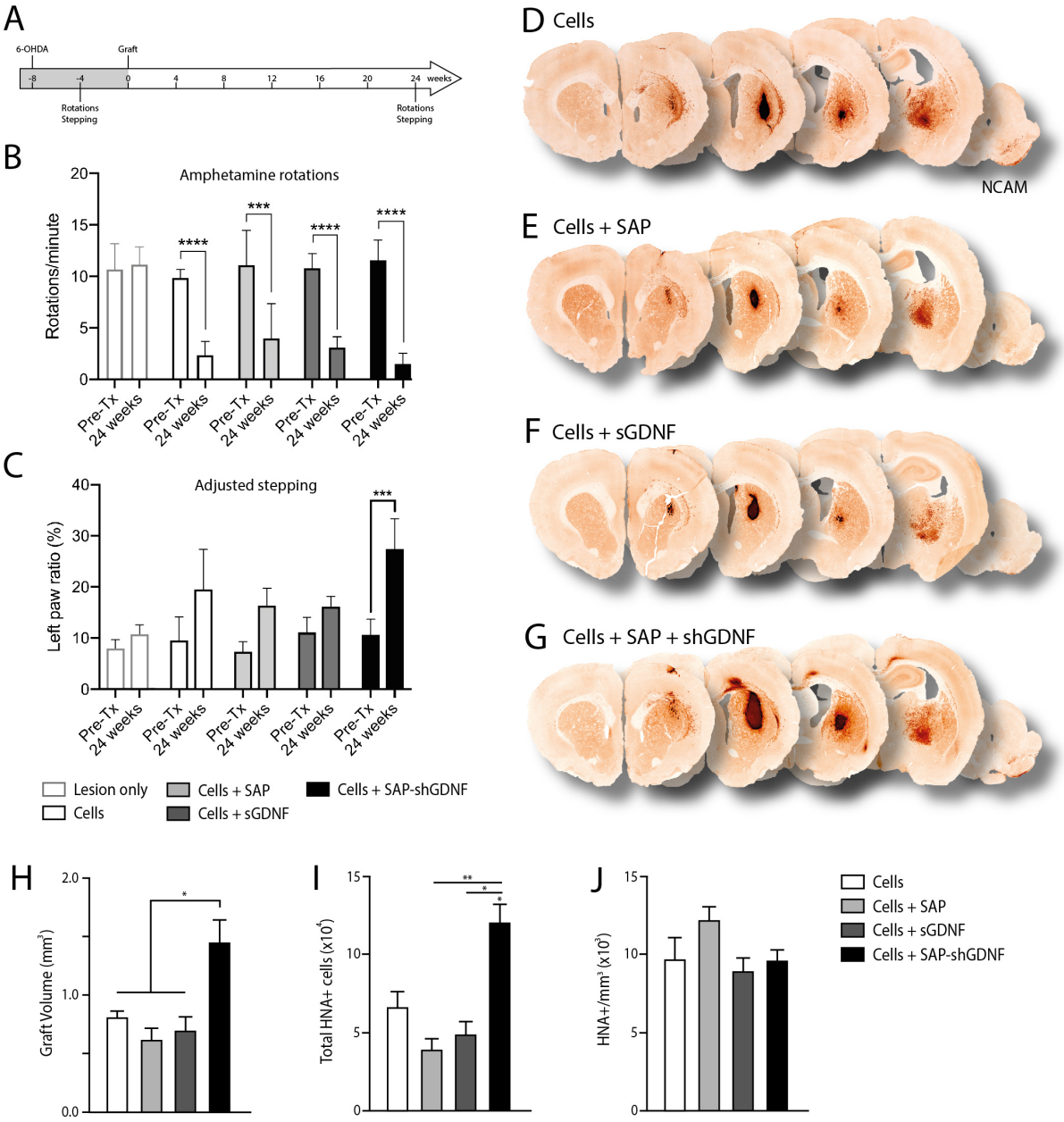

Figure 2. Implantation of human ESC-derived VM progenitors together with a GDNF functionalised tissue-specific scaffold improves motor function in Parkinsonian rats. (A) Schematic overview of in vivo study design. (B) All animals receiving a human PSC-derived VM progenitor cell graft showed significant correction of amphetamine-induced rotational asymmetry. (C) Only animals receiving cell graft in the presence of the GDNF-functionalised SAP scaffold displayed a significant recovery in the adjusted stepping task at 24 weeks after grafting. (D-G) Representative photomicrographs of DA grafts confirmed graft survival as shown by PSA-NCAM staining after 24 weeks. (H) Graft volumetric assessment by PSA-NCAM labelling revealed that grafts in the presence of the GDNF-functionalised SAP hydrogel were significantly larger compared to the other graft groups. (I) A concomitant increase in the total number of HNA+ cells was observed in the Cells + SAP-shGDNFP group. (J) SAP hydrogels did not alter the density of grafted cells after 24 weeks. Data represents Mean +SEM, n=6-7 Grafts/group. * $p<0.05$.

Figure 2

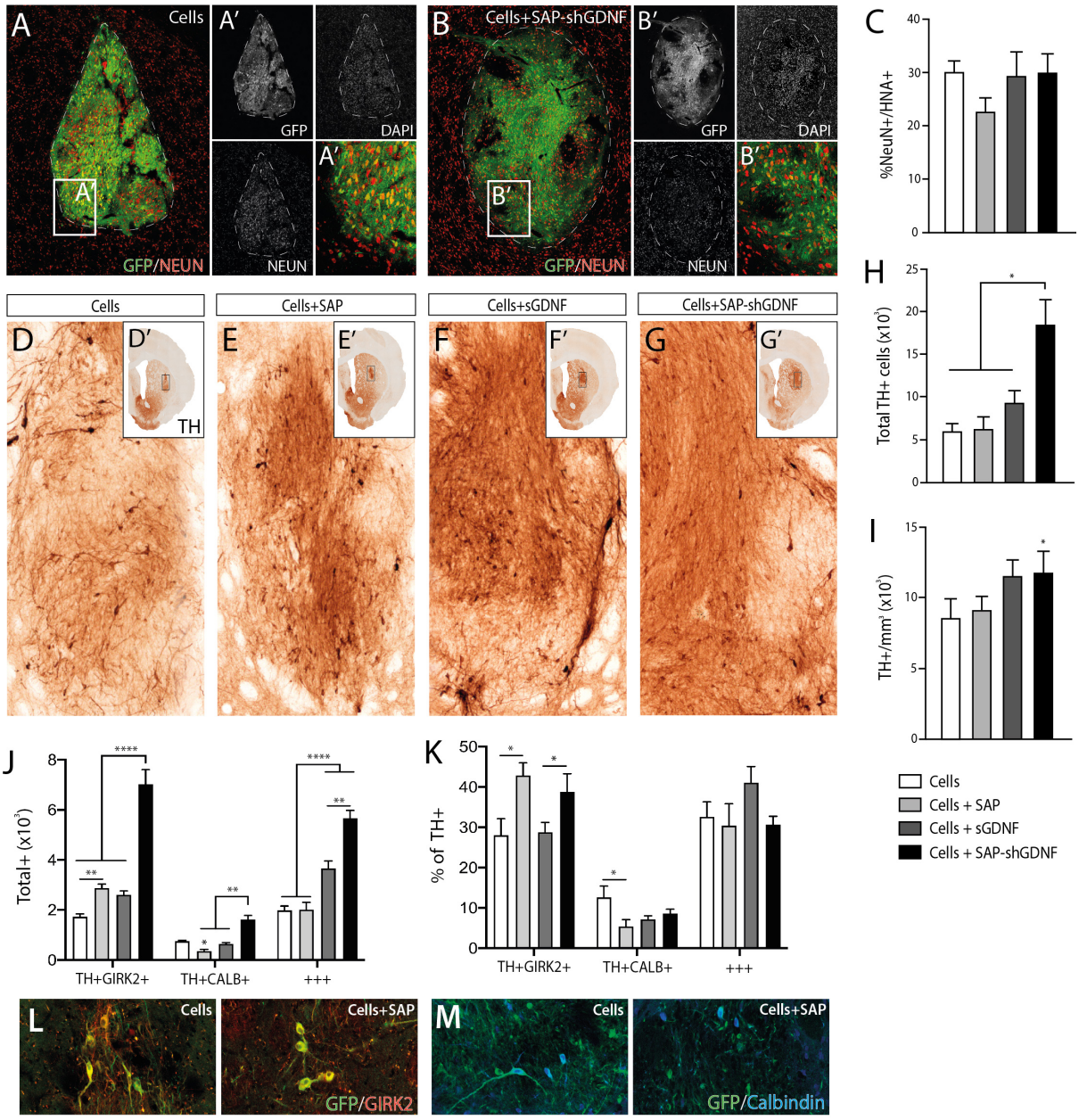

Figure 3. Functionalized scaffolds increase graft size, DA neuron yield and bias A9-specification. (A-B) Representative pictures of NeuN+/HNA+ co-expression in a graft of (A) Cells alone and (B) Cells+SAP-shGDNF. (C) Approximately a third of the cells within all grafts adopted a mature neuronal phenotype, irrespective of the presence of the biomaterial and/or GDNF. (D-G) Representative photomicrographs of TH+ cells within grafts, at 24 weeks, showing that grafts in the presence of a GDNF functionalized SAP scaffold had increased TH+ cells. (H) Quantification of TH+ cells within the graft and (I) density of TH+ cells. (J) Grafts in the presence of a GDNF-functionalized SAP scaffold showed an increase in TH+/GIRK2+, TH+/CALB+ and TH+/GIRK2+/CALB+ cells, indicative of DA graft survival. (K) Expressed as a proportion of TH+ cells, only grafts in the presence of the tissue-specific IKVAV SAP hydrogel showed a significant increase in the percentage of TH+/GIRK2+ (A9-like DA neurons), at the expense of TH+/CALB+ (A10). (L-M) Representative photomicrographs of GIRK2, Calbinidn (CALB+) and TH+ cells within a Cells- and Cells+SAP graft. Data represents Mean +SEM, n=6-7 Grafts/group. * $p<0.05$, ** $p<0.01$, **** $p<0.0001$.

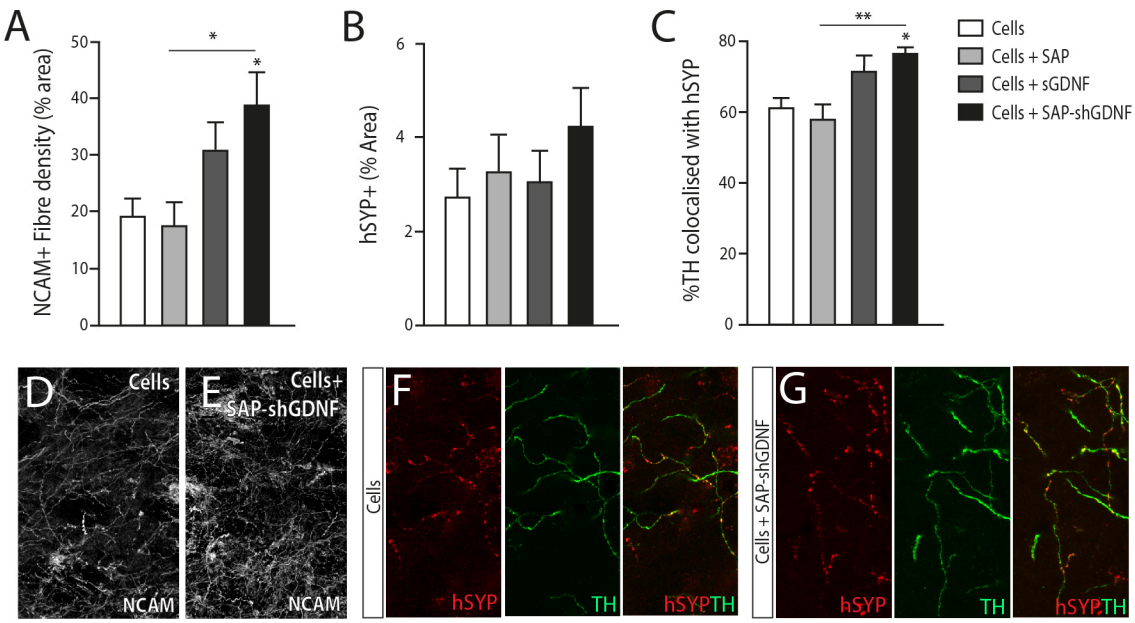

Figure 4. GDNF Functionalised hydrogels enhance graft plasticity and dopaminergic synapse formation. (A) Quantification of graft-derived human NCAM fiber density and (B) human synaptophysin (hSYP) within the host striatum. (C) Quantitative assessment of the proportion of TH-immunoreactive puncta co-localised with hSYP within the host striatum, indicating that GDNF functionalized scaffolds promoted maturation of DA synapses. (D) Representative images of NCAM-labeled graft fibers within the striatum of an animal grafted with cells alone, or cells+ SAP-shGDNF. (F) Photomicrographs showing hSYP and TH labeling (plus merged images) taken from the host striatum of a rat grafted with Cells and, (G) Cells + SAP-shGDNF, noting the increased density of co-localised puncta in the present of the functionalized scaffold. Data represents Mean +SEM, n=5-6 Grafts/group. * $p<0.05$, ** $p<0.01$.

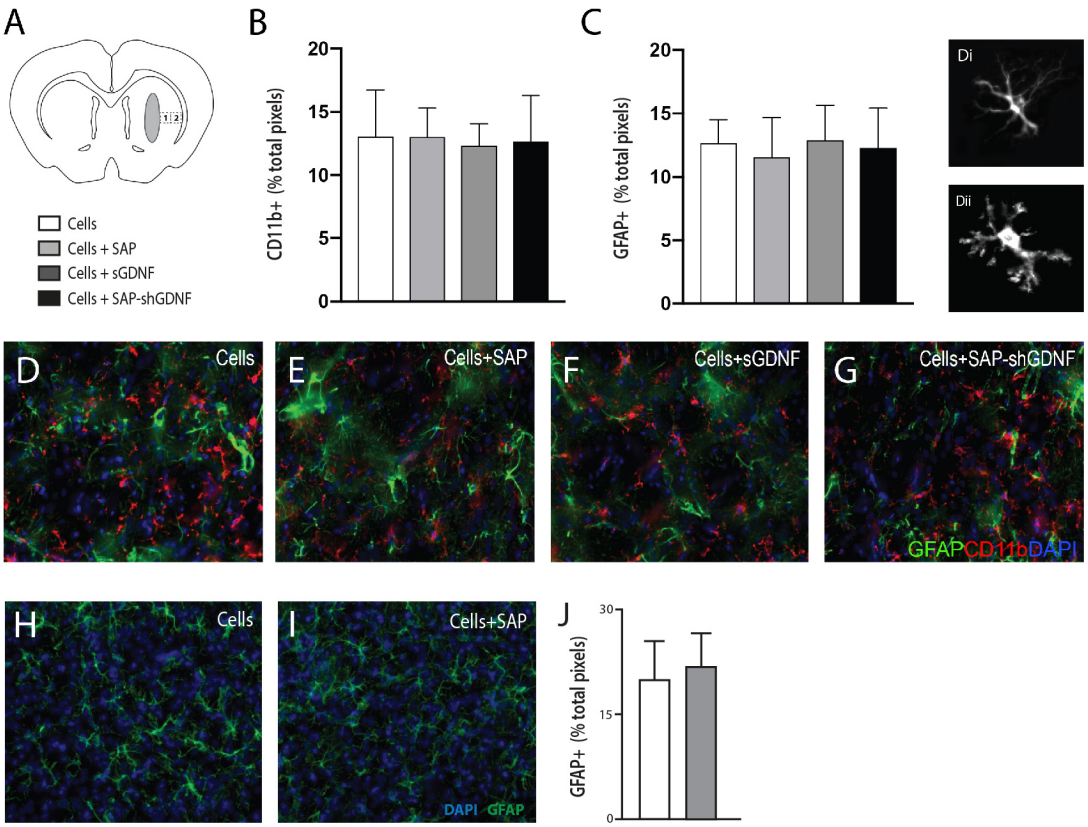

Supplementary Figure 1. Tissue specific scaffolds show in vivo biocompatibility. (A) Schematic figure showing the regions of sampling of GFAP and CD11b density – at the graft-host boundary (field of view 1, FOV1) and a more distal site away from the graft border (FOV2). (B-C) Assessment of immunoreactive markers against microglial - Cd11b (B), and reactive astrocytes – GFAP (C), at 24 weeks after implantation, showing no difference in inflammatory response across the groups. (D-G) Representative picture of GFAP (green) and Cd11b (red) among the groups, at 24 weeks. (D) Cells, (E) Cells+SAP, (F) Cells+sGDNF, (G) Cells+SAP-shGDNF. (H-I) Representative images of GFAP staining within FOV1 showing comparable GFAP+ immunoreactivity within (H) Cells and (I) Cells+SAP implanted animals, acutely (2 weeks) after implantation. (J) Quantification of GFAP+ density adjacent ot the graft. Data represents Mean +SEM, (B-C) n=6-7, (J) n=4/group.

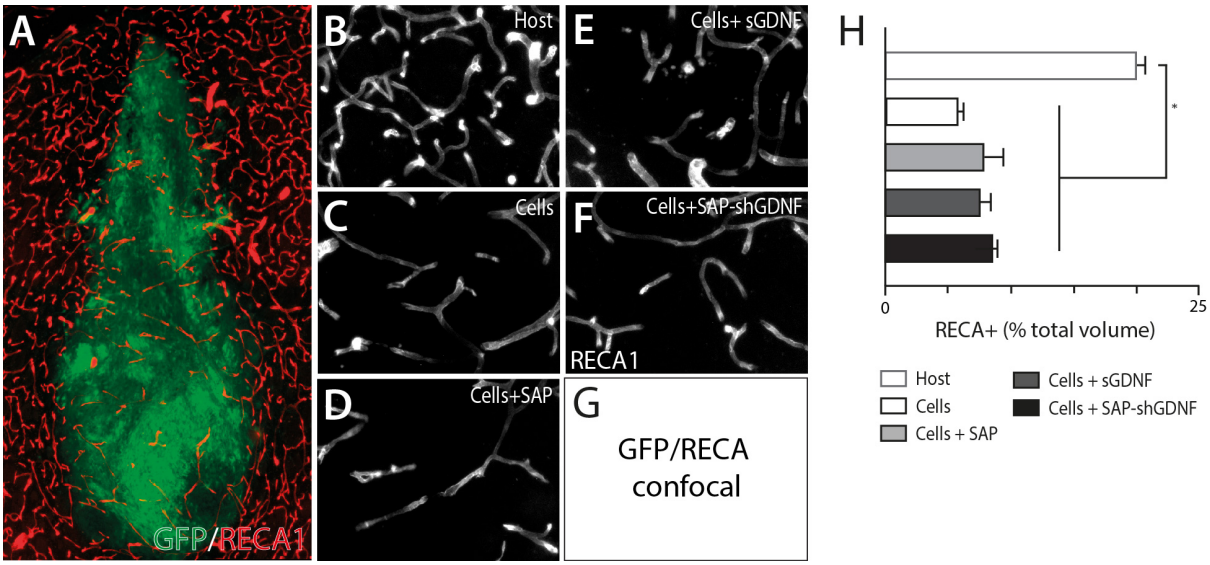

Supplementary Figure 2. Human PSC-derived VM progenitor grafts show modest vascularization that was not influenced by the presence of GDNF and/or the SAP hydrogel. (A) Representative overview of a graft illustrating RECA1 + staining against endothelial cells, revealing the presence of a vascular network within the grafts. (B) The vascular network was visibly denser in the host, compared to the (C-F) grafts. (G) Quantitative analysis showed no difference in vascularization between grafted groups, indicating that neither the biomaterial nor the GDNF influenced vascularization. Data represents Mean +SEM, n=5-7 Grafts/group. * $p<0.05$.